De l'interaction entre banquise, lumière et phytoplancton arctique

Marion Lebrun

Sorbonne Université

École doctorale : "129 - Science de l'environnement"

LOCEAN/NEMO R&D

De l'interaction entre banquise, lumière et phytoplancton arctique

Par Marion Lebrun

Thèse de doctorat d'océanographie physique

Dirigée par Gurvan Madec et Martin Vancoppenolle

Présentée et soutenue publiquement le 13/12/2019

Devant un jury composé de :

M. Damien Cardinal	(LOCEAN, Paris)	Président du jury
M. Marcel Babin	(Takuvik Joint International Laboratory, Québec)	Rapporteur
M. David Salas Y Mélia	(CNRM-Météo France Toulouse)	Rapporteur
M. Laurent Bopp	(LMD, Paris)	Examinateur
Mme Camille Lique	(Ifremer, Brest)	Examinateur
M. Roland Séférian	(CNRM-Météo France Toulouse)	Examinateur
M. Gurvan Madec	**(LOCEAN, Paris)**	**Directeur de thèse**
M. Martin Vancoppenolle	**(LOCEAN, Paris)**	**Co-directeur de thèse**

Remerciements

Dans bon nombre de manuscrits, j'ai pu lire dans la partie remerciement à quel point la thèse avait fait « grandir » ses auteurs. Je pense qu'on ne peut saisir ce concept qu'une fois arrivé au bout de sa thèse et qu'on prend le temps de regarder en arrière.

Pendant ces trois ans, je n'ai cessé d'essayer d'imaginer une conversation avec mon moi du passé. Je lui racontais toutes les belles aventures que j'accomplissait au fur et à mesure de l'avancée de mon doctorat et elle me regardait des étoiles plein les yeux osant à peine croire à ces histoires. Effectivement, cette thèse a été une magnifique aventure avec ses hauts, ses bas aussi, mais qui m'a fait grandir plus que ce que je pouvais me l'imaginer. Et comme aime à le dire Monkey D Luffy, une aventure ne se fait pas sans « nakama » (compagnons en japonais). Et bien, j'ai pour ma part de nombreux nakama à remercier pour cette aventure !

Il est de coutume de commencer par remercier les membres du jury de thèse pour leur retour et leur conseil au sujet du travail accompli ces dernières années. Cependant, à l'heure où j'écris ces lignes, aucun membre du jury n'a encore reçu mon manuscrit. Je ne peux pour le moment que les remercier d'avoir accepté de prendre part à mon aventure, ainsi que de me céder de leur temps et de leur expertise dans les mois à venir.

Chaque membre du jury a intégré mon aventure à des moments différents. David Salas Y Mélia et Roland Séférian, par exemple, l'ont rejointe lorsque je n'étais encore qu'un bébé : lors de mon stage de master 1. Avec Matthieu Chevallier, ils m'ont aidé à faire mes premiers pas dans la recherche. Ils m'ont aussi transmis la passion pour les régions polaires, pour la banquise, pour la modélisation. Pour tout cela, je les remercie.

Laurent Bopp a suivi ma thèse avec l'ensemble du comité de thèse composé aussi d'Olivier Aumont, de Roland Séférian (encore !), et de Jean Baptiste Sallée. Je les remercie tous pour leur temps, leur patience et leurs conseils. Grâce à eux, les réunions du comité étaient pleines d'intenses discussions scientifiques, de vin et de pâté !

Marcel Babin a aussi rejoint l'équipage au cours de la thèse, malgré un océan d'écart. Son intérêt pour mon sujet de recherche et ses nombreux conseils distillés au fil des diverses réunions et conférences où nous nous sommes rencontrés m'ont aidé à m'améliorer tout au long de ses trois années. Merci pour tout cela.

Je remerci aussi Damien Cardinal et Camille Lique, qui ont généreusement accepté de me donner de leur temps et de leur connaissance pour m'aider encore à grandir dans cette thèse.

Je garde évidemment les deux derniers membres de ce jury pour la fin :

Gurvan, je réalise, en fouillant dans mes souvenirs, à quel point nos discussions étaient riches scientifiquement, même lorsqu'il ne s'agissait pas de ma thèse. Ton enthousiasme pour mon travail et mes résultats m'ont beaucoup aidée à m'affirmer. A nos premières discussions, je n'osais pas trop prendre la parole, de peur de dire des bêtises. Mais tu as su me laisser ma place, et me faire gagner confiance en moi. Tu as été une grande source de conseils qui m'ont permis de m'améliorer tout au long de ma thèse. Merci pour tout.

Martin, tu m'accompagnes, depuis le master 2, dans ma découverte de la recherche. Toi, plus que quiconque m'a transmis les enseignements qui font de moi la presque chercheuse que je suis. Plus que ton temps, tu m'as aussi partagé ta patience, ta curiosité, ton plaisir pour la recherche… toutes ses choses qui m'encouragent aujourd'hui à continuer dans cette voie. Tu m'as toujours traitée comme une collègue et jamais comme juste une étudiante. Cela m'a beaucoup aidée à gagner confiance en moi et aussi à gagner en autonomie. Enfin durant cette thèse, tu m'as permis de réaliser bon nombre de rêves d'enfant : voir des ours polaires, faire ma première carotte de banquise, manger des ramens au Japon. Pour tout ça et sûrement pour plein d'autres choses que j'oublie, Merci !

Merci évidemment aux membres du LOCEAN avec qui j'ai partagé ces trois ans.

Merci à l'équipe NEMO de m'avoir fait une petite place et plus particulièrement à Julie qui m'a apportée énormément de soutien tout au long de cette thèse. Tu as toujours trouvé les mots justes pour me rassurer et remotiver quand j'en avais besoin, merci !

Merci aussi à l'ensemble du service administratif du laboratoire. Vous avez souvent acceuilli et supporté une Marion angoissée et perdue. Merci notamment à Dany, m'a presque voisine qui m'a accueillie à bras ouverts dès que j'avais un problème ou une question et qui m'a aidée dans beaucoup de situations.

Merci aussi à mes nakama de couloir et de cantine : Anne Cécile, Katia, Lucie, Marylou, Yona, Sara, Clément, Yann, Felix, Anda, Damien, Nicolas… J'ai souvent fait l'ours pendant ces trois ans, merci de ne pas m'en avoir tenu rigueur et de m'avoir souvent sorti de ma caverne !

J'ai eu beaucoup trop de co-bureaux durant ces trois ans, aussi j'aimerais seulement remercier celui qui est resté le plus longtemps : Moïse. Merci pour ta joie même dans les moments difficiles, merci aussi pour tes conseils et tes leçons d'informatique.

Merci aussi à tous mes nakama rencontrés en meeting et conférences qui ont dû supporter mon stress chronique : Daniela, Gwenaëlle, Vanessa, Christophe, Itsuka, EunYae, Raphaël, Emiliano, Eric, Letizia, Giulia, Marie, et tous les autres. Merci à tous ceux qui ont participé à l'école d'été Sentinelle Nord avec qui j'ai passé dix jours merveilleux et tellement formateurs et encore tous ceux que j'ai rencontrés lors des réunions Green Edge ou encore au lac Saroma!

Enfin, sortons un peu du monde du travail pour remercier mes derniers nakama.

Merci à Mathias qui a été d'un incroyable soutien tout le long de ses trois ans. Cette dernière année, tu as supporté mes états d'âme et mes angoisses sans broncher, tu m'as soutenue, réconfortée, remotivée, alors que tu avais, toi aussi une thèse à gérer. Merci d'avoir été et d'être toujours là à chaque instant !

Merci enfin à ma famille, mon père, ma mère et mes deux soeurs. Merci d'avoir pris du plaisir à suivre mon aventure, merci de m'avoir soutenu dans les moments difficiles, me faisant prendre les bonnes décisions au moment ou j'avais terriblement besoin de conseils. Merci de me montrer combien vous êtes tous fiers de moi et aussi de me vanner suffisamment pour que je ne prenne pas la grosse tête !

J'ai sans doute oublié beaucoup du monde. Aussi je réserve ses dernières lignes aux oubliés. Merci aussi à vous d'avoir fait parti de l'aventure !

Sommaire

Introduction

En 2015, un an avant le début de cette thèse, avait lieu, à Paris, la COP21 réunissant 195 pays participants, en plus de l'Union européenne. La COP21 avait pour but de trouver des accords pour limiter le réchauffement global de la planète en dessous des 2 °C. A la suite de la COP21, sortait en 2018, deux ans après le début de cette thèse, le Rapport spéciale 1.5 °C du GIEC (Groupe d'experts intergouvernemental sur l'évolution du climat). Ce rapport portait sur les impacts climatiques d'un réchauffement global de 1.5 °C par rapport au niveau préindustriel (mesuré sur la période 1850-1900) et soulignait l'urgence de réduire nos émissions de gaz à effet de serre pour limiter le réchauffement global de la planète. C'est dans ce contexte de prise de conscience d'urgence climatique que cette thèse s'est développée durant ces dernières années. D'après le rapport 1.5 du GIEC, la température globale actuelle de la planète serait supérieure d'environ 1 °C par rapport au niveau préindustriel en raison des émissions d'origines anthropiques (IPCC 2018). Selon les modèles climatiques, ce réchauffement devrait continuer dans les prochaines décennies, allant d'un réchauffement de plus de 1 °C, d'ici 2100, pour le scénario d'émission le plus optimiste (RCP2.6), à plus de 4 °C pour le scénario le plus pessimiste (RCP8.5 ; IPCC 2013).

Les valeurs de réchauffement relevées en Arctique sont quant à elles, deux à trois fois supérieures à la moyenne globale. On appelle ce phénomène l'amplification polaire. Cette amplification polaire est due à un certain nombre de rétroactions positives (Pithan et Mauritsen, 2014 ; Stuecker et al., 2018). Parmi les rétroactions les plus importantes, on trouve celle de la réduction de la couverture de la glace de mer (ou banquise) arctique, qui a un fort pouvoir réfléchissant et qui, en fondant, réduit la quantité de rayonnement solaire réfléchi vers

l'atmosphère et amplifie le réchauffement initial. La couverture de glace de mer arctique a perdu en moyenne 50.10^3 de km^2/an sur la période 1979-2010 (Cavalieri & Parkinson, 2012). Si la fonte de la banquise arctique est plus remarquable en été, on constate aussi un retrait de la glace de mer en hiver (Cavalieri & Parkinson, 2012 ; Massonnet et al., 2018) . En raison du réchauffement climatique, le volume de banquise arctique est réduit. On retrouve cette réduction dans l'évolution de l'étendue de banquise, mais aussi dans la réduction de son épaisseur (une réduction d'environ 65% sur la période 1975-2012 ; Lindsay & Schweiger, 2015) et de son âge (disparition d'environ 40% de la banquise la plus ancienne entre 1980-2010 ; Maslanik et al., 2011). D'après les projections des modèles du système Terre, ce retrait de la banquise arctique devrait continuer dans les prochaines décennies avec une possible disparition de la banquise d'été entre 2040 et 2060 (Massonnet et al., 2012 ; Stroeve et al., 2012).

L'étude de la réponse de la banquise arctique au changement climatique est capitale en raison de nombreux enjeux, tels que :

(i) Des enjeux géopolitiques et économiques entre les différents pays frontaliers, tels que les États-Unis, le Canada, la Russie, la Norvège et le Danemark (Fig.1). En effet, le retrait de la banquise arctique pourrait permettre l'ouverture de nombreuses routes navigables aujourd'hui bloquées par les glaces (Aksenov et al., 2017) ou encore l'accès à de nouvelles ressources (Par exemple les hydrocarbures ; Harsem et al., 2011).

(ii) Des enjeux sociétaux. En effet, les populations autochtones des régions de l'Arctique, les Inuits, sont très dépendantes de la présence de banquise sur laquelle ils se déplacent en hiver, ils chassent et pêchent … La réduction de la banquise arctique pourrait les contraindre à abandonner leur mode de vie actuel (Huntington et al., 2017).

(iii) Et enfin, des enjeux écosystémiques. En effet en Arctique de nombreuses espèces sont dépendantes de la présence de banquise, comme les ours polaires ou les mammifères marins (baleines, narvals … ; Laidre et al., 2015 ; Stern & Laidre, 2016). La banquise influence aussi grandement la croissance du phytoplancton en Arctique (Wassmann & Reigstad, 2011).

Figure 1 : Carte de L'Arctique. Les contours gris indiquent la bathymétrie (Chevallier, 2012).

Le phytoplancton désigne un ensemble d'espèce autotrophes ou mixotrophes (c'est-à-dire végétales ou semi-végétales). Le terme planctonique fait référence au caractère dérivant de ces organismes puisqu'ils vivent en suspension dans la colonne d'eau. Ces organismes sont présents

dans tous les océans. L'étude du phytoplancton et de son évolution en réponse au réchauffement climatique est cruciale pour comprendre l'impact du réchauffement climatique sur tous les écosystèmes marins, car les organismes phytoplanctoniques sont à la base de la chaine alimentaire. De plus, le phytoplancton joue un rôle considérable dans le stockage de CO_2 par les océans (Parmentier et al., 2013 ; Post et al., 2013). En Arctique, le phytoplancton est largement influencé par la banquise qui régule à la fois la quantité de lumière mais aussi de nutriments dont le phytoplancton a besoin pour se développer. En effet, les organismes purement autotrophes pratiquent la photosynthèse. C'est-à-dire qu'ils synthétisent les sucres dont ils ont besoin pour se développer à partir de CO_2 et d'énergie électromagnétique (de lumière). Sans lumière, une plante photosynthétique, comme le phytoplancton, ne peut se développer. Si aux moyennes et basses latitudes la lumière disponible à la surface de l'océan est généralement très peu limitante pour le phytoplancton, ce n'est pas le cas aux hautes latitudes, comme en Arctique. La disponibilité en lumière pour le phytoplancton des eaux arctiques est limitée d'une part par la nuit polaire ; période de plusieurs mois durant laquelle le soleil reste sous l'horizon et durant laquelle le rayonnement solaire est nul ; d'autre part par la banquise et généralement par la neige qui la recourvre ; qui atténuent une grande partie du rayonnement transmis à l'océan.

La banquise arctique influence le rayonnement transmis à l'océan et par conséquent le développement du phytoplancton. Pour comprendre la réponse du phytoplancton arctique au réchauffement climatique, il est crucial de comprendre ces interactions entre banquise, lumière et phytoplancton. L'étude de ces interactions a longtemps été limitée par le manque d'observations (que ce soit pour la lumière ou le pour le phytoplancton sous la banquise). Les modèles du système Terre sont par conséquent mal contraints pour ce qui est de la représentation du phytoplancton dans les régions englacées (Vancoppenolle et al., 2013). Depuis plusieurs années, le nombre d'observations a augmenté dans ces régions, remettant

parfois en cause des éléments considérés comme établis (par exemple la découverte d'efflorescence de phytoplancton sous la banquise ; Arrigo et al., 2012 ; Fortier et al., 2002 ; Mundy et al., 2009).

L'objectif de cette thèse est, à l'aide d'analyse d'observation in situ, de données satellites et de simulations des modèles du système Terre, de comprendre certaines des interactions entre banquise, phytoplancton et lumière. En identifiant certaines des incertitudes majeures liées à ces interactions dans les modèles du système Terre, il sera possible, à l'avenir, de mieux contraindre les modèles du système Terre quant à la croissance du phytoplancton dans la zone de glace de l'Arctique. Pour atteindre cet objectif, je me focalise sur trois aspects majeurs des interactions banquise, lumière et phytoplancton arctique. J'étudie d'abord les mécanismes d'évolution de la saisonnalité de la banquise arctique, principalement en lien avec le forçage solaire (Fig. 2a). J'analyse ensuite comment la banquise influence la transmission du rayonnement solaire à l'océan sous-jacent (Fig. 2b). Enfin, je m'intéresse aux impacts du couple banquise-lumière sur le phytoplancton Arctique (Fig. 2c).

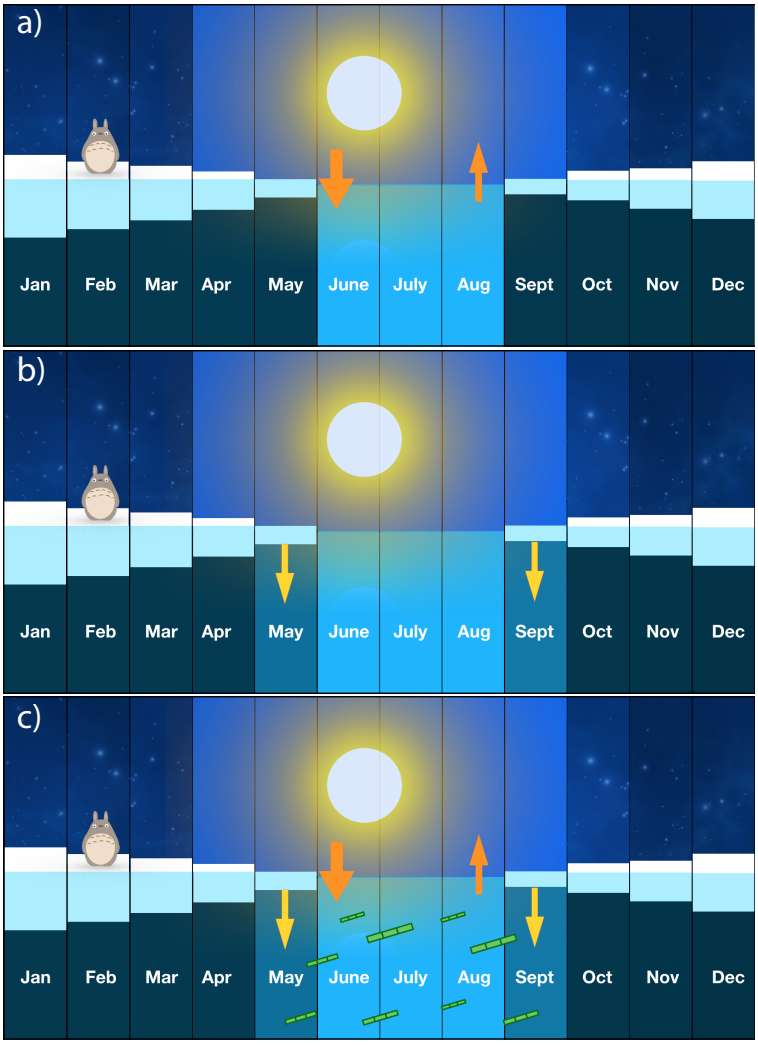

Figure 2 : Schéma illustrant les trois différentes études de cette thèse. a) mécanismes d'évolution de la saisonnalité de la glace arctique en réponse au forçage solaire ; b) impact de la banquise sur le rayonnement transmis à l'océan ; c) impact du cycle saisonnier de la lumière transmise à l'océan sur le phytoplancton arctique.

Ce manuscrit est organisé en quatre parties : un état de connaissances actuelles sur les interactions banquise, lumière et phytoplancton arctique formule les questions qui sont examinées lors de cette thèse. Il précède les trois chapitres de résultats. Les trois chapitres de résultats sont présentés sous forme d'articles scientifiques (dont l'un est publié, les deux suivants sont encore en préparation).

Le premier chapitre, publié dans *The Cryosphere* en janvier 2019 (Lebrun et al., 2019), porte sur les mécanismes d'évolution de la saisonnalité de la banquise arctique en réponse au forçage

solaire. J'étudie l'évolution présente et future de la période d'eau libre en Arctique (période durant laquelle il n'y a pas de banquise) à partir de données satellites et des projections de modèles du système Terre. Je m'interroge aussi sur les mécanismes thermodynamiques associés à cette évolution.

Le but du second chapitre est d'évaluer la représentation modélisée du transfert radiatif dans les régions englacées arctiques et de l'améliorer, tant en intensité, qu'en termes de composition spectrale à partir d'une analyse de donnée in situ. L'augmentation de la quantité de mesures d'optiques de la banquise ces dernières années (parmi lesquelles, SLOPE 2019 en Hokkaido durant laquelle j'ai pu contribuer à améliorer la base de données d'optique de la glace ; cf. annexe) permet d'avoir aujourd'hui un nouveau regard sur le transfert radiatif dans la zone de glace arctique.

Le troisième chapitre porte, quant à lui, sur l'impact de la saisonnalité de la lumière transmise à l'océan sur le phytoplancton à partir de données satellites et de simulations par des modèles du système Terre. Le but de ce chapitre est, à partir des résultats du premier et du second chapitre, de mieux diagnostiquer la saisonnalité de la lumière disponible pour le phytoplancton dans les zones de glace arctiques. Ce chapitre a aussi pour but de mieux comprendre les relations entre banquise et phytoplancton dans le modèle d'océan bleu/blanc/vert NEMO, utilisé dans les modèles français du Système Terre.

Enfin, à la suite de ces trois chapitres, je résume, dans une dernière partie, les résultats majeurs de cette thèse qui répondent aux problématiques énoncées dans la première partie. Je fais aussi l'état des différents projets en perspective de cette thèse.

Références

Aksenov, Y., Popova, E. E., Yool, A., Nurser, A. J. G., Williams, T. D., Bertino, L., & Bergh, J. (2017). On the future navigability of Arctic sea routes: High-resolution projections of the Arctic Ocean and sea ice. *Marine Policy*, *75*, 300–317. https://doi.org/10.1016/j.marpol.2015.12.027

Arrigo, K. R., Perovich, D. K., Pickart, R. S., Brown, Z. W., Dijken, G. L. van, Lowry, K. E., et al. (2012). Massive Phytoplankton Blooms Under Arctic Sea Ice. *Science*, *336*(6087), 1408–1408. https://doi.org/10.1126/science.1215065

Cavalieri, D. J., & Parkinson, C. L. (2012). Arctic sea ice variability and trends, 1979–2010. *The Cryosphere*, *6*(4), 881–889. https://doi.org/10.5194/tc-6-881-2012

Chevallier, M. (2012, December 7). *Prévisibilité saisonnière de la glace de mer de l'océan Arctique* (thesis). Paris Est. Retrieved from http://www.theses.fr/2012PEST1117

Fortier, M., Fortier, L., Michel, C., & Legendre, L. (2002). Climatic and biological forcing of vertical flux and biogenic particles under seasonal Arctic sea ice. *Marine Ecology-Progress Series*, *225*, 1–16. https://doi.org/10.3354/meps225001

Harsem, Ø., Eide, A., & Heen, K. (2011). Factors influencing future oil and gas prospects in the Arctic. *Energy Policy*, *39*(12), 8037–8045. https://doi.org/10.1016/j.enpol.2011.09.058

Huntington, H. P., Gearheard, S., Holm, L. K., Noongwook, G., Opie, M., & Sanguya, J. (2017). Sea ice is our beautiful garden: indigenous perspectives on sea ice in the Arctic. In D. N. Thomas (Ed.), *Sea Ice* (pp. 583–599). John Wiley & Sons, Ltd. https://doi.org/10.1002/9781118778371.ch25

IPCC, 2013: *Climate Change 2013: The Physical Science Basis. Contribution of Working Group I to the Fifth Assessment Report of the Intergovern- mental Panel on Climate Change* [Stocker, T.F., D. Qin, G.-K. Plattner, M. Tignor, S.K. Allen, J. Boschung, A. Nauels, Y. Xia, V. Bex and P.M. Midgley (eds.)]. Cambridge University Press, Cambridge, United Kingdom and New York, NY, USA, 1535 pp.

IPCC, 2018: *Global Warming of 1.5°C. An IPCC Special Report on the impacts of global warming of 1.5°C above pre-industrial levels and related global greenhouse gas emission pathways, in the context of strengthening the global response to the threat of climate change, sustainable development, and efforts to eradicate poverty* [Masson-Delmotte, V., P. Zhai, H.-O. Pörtner, D. Roberts, J. Skea, P.R. Shukla, A. Pirani, W. Moufouma-Okia, C. Péan, R. Pidcock, S. Connors, J.B.R. Matthews, Y. Chen, X. Zhou, M.I. Gomis, E. Lonnoy, T. Maycock, M. Tignor, and T. Water eld (eds.)]. In Press.

Laidre, K. L., Stern, H., Kovacs, K. M., Lowry, L., Moore, S. E., Regehr, E. V., et al. (2015). Arctic marine mammal population status, sea ice habitat loss, and conservation recommendations for the 21st century. *Conservation Biology*, *29*(3), 724–737. https://doi.org/10.1111/cobi.12474

Lebrun, M., Vancoppenolle, M., Madec, G., & Massonnet, F. (2019). Arctic sea-ice-free season projected to extend into autumn. *The Cryosphere*, *13*(1), 79–96. https://doi.org/10.5194/tc-13-79-2019

Lindsay, R., & Schweiger, A. (2015). Arctic sea ice thickness loss determined using subsurface, aircraft, and satellite observations. *The Cryosphere*, *9*(1), 269–283. https://doi.org/10.5194/tc-9-269-2015

Maslanik, J., Stroeve, J., Fowler, C., & Emery, W. (2011). Distribution and trends in Arctic sea ice age through spring 2011. *Geophysical Research Letters*, *38*(13), L13502. https://doi.org/10.1029/2011GL047735

Massonnet, F., Fichefet, T., Goosse, H., Bitz, C. M., Philippon-Berthier, G., Holland, M. M., & Barriat, P.-Y. (2012). Constraining projections of summer Arctic sea ice. *The*

Cryosphere, *6*(6), 1383–1394. https://doi.org/10.5194/tc-6-1383-2012

Massonnet, François, Vancoppenolle, M., Goosse, H., Docquier, D., Fichefet, T., & Blanchard-Wrigglesworth, E. (2018). Arctic sea-ice change tied to its mean state through thermodynamic processes. *Nature Climate Change*, *8*(7), 599–603. https://doi.org/10.1038/s41558-018-0204-z

Mundy, C. J., Gosselin, M., Ehn, J., Gratton, Y., Rossnagel, A., Barber, D. G., et al. (2009). Contribution of under-ice primary production to an ice-edge upwelling phytoplankton bloom in the Canadian Beaufort Sea. *Geophysical Research Letters*, *36*(17). https://doi.org/10.1029/2009GL038837

Parmentier, F.-J. W., Christensen, T. R., Sørensen, L. L., Rysgaard, S., McGuire, A. D., Miller, P. A., & Walker, D. A. (2013). The impact of lower sea-ice extent on Arctic greenhouse-gas exchange. *Nature Climate Change*, *3*(3), 195–202. https://doi.org/10.1038/nclimate1784

Pithan, F., & Mauritsen, T. (2014). Arctic amplification dominated by temperature feedbacks in contemporary climate models. *Nature Geoscience*, *7*(3), 181–184. https://doi.org/10.1038/ngeo2071

Post, E., Bhatt, U. S., Bitz, C. M., Brodie, J. F., Fulton, T. L., Hebblewhite, M., et al. (2013). Ecological consequences of sea-ice decline. *Science (New York, N.Y.)*, *341*(6145), 519–524. https://doi.org/10.1126/science.1235225

Stern, H. L., & Laidre, K. L. (2016). Sea-ice indicators of polar bear habitat. *The Cryosphere*, *10*(5), 2027–2041. https://doi.org/10.5194/tc-10-2027-2016

Stroeve, J. C., Kattsov, V., Barrett, A., Serreze, M., Pavlova, T., Holland, M., & Meier, W. N. (2012). Trends in Arctic sea ice extent from CMIP5, CMIP3 and observations. *Geophysical Research Letters*, *39*(16), L16502. https://doi.org/10.1029/2012GL052676

Stuecker, M. F., Bitz, C. M., Armour, K. C., Proistosescu, C., Kang, S. M., Xie, S.-P., et al. (2018). Polar amplification dominated by local forcing and feedbacks. *Nature Climate Change*, *8*(12), 1076–1081. https://doi.org/10.1038/s41558-018-0339-y

Vancoppenolle, M., Bopp, L., Madec, G., Dunne, J., Ilyina, T., Halloran, P. R., & Steiner, N. (2013). Future Arctic Ocean primary productivity from CMIP5 simulations: Uncertain outcome, but consistent mechanisms. *Global Biogeochemical Cycles*, *27*(3), 605–619. https://doi.org/10.1002/gbc.20055

Wassmann, P., & Reigstad, M. (2011). Future Arctic Ocean Seasonal Ice Zones and Implications for Pelagic-Benthic Coupling. *Oceanography*, *24*(3), 220–231. https://doi.org/10.5670/oceanog.2011.74

Problèmes Physiques

La zone de glace arctique subit de larges changements en réponse au réchauffement global. Ces changements ont un impact majeur sur la disponibilité en lumière pour la croissance du phytoplancton. L'étude du phytoplancton et de son évolution en réponse au réchauffement climatique est cruciale pour comprendre l'impact du réchauffement climatique sur tous les écosystèmes marins, car il est à la base de la chaîne alimentaire et il joue un rôle considérable dans le stockage de CO_2 par les océans (Parmentier et al., 2013 ; Post et al., 2013). Mieux comprendre les interactions entre banquise, lumière et phytoplancton dans la zone de banquise arctique est fondamental pour mieux caractériser l'évolution présente et future du phytoplancton arctique.

Dans cette partie, je me propose de faire l'état des connaissances à propos de l'interaction entre banquise, lumière et phytoplancton arctique en me focalisant sur trois thèmes majeurs : l'impact du rayonnement solaire sur la saisonnalité de la banquise arctique ; l'impact de la banquise sur le rayonnement transmis à la surface de l'océan et enfin l'impact du couple lumière-banquise sur le phytoplancton arctique.

La première partie pose la base thermodynamique et dynamique des cycles saisonniers de la banquise arctique. Dans la seconde partie, je me concentre sur les indicateurs de la saisonnalité de la banquise arctique et sur leur évolution. Dans la troisième partie, je m'intéresse à l'optique marine dans la zone de glace. Une dernière partie est focalisée sur les processus régissant le développement du phytoplancton dans les régions arctiques ainsi que son évolution présente et future. Je conclus avec un résumé des points clés importants et des grandes problématiques aujourd'hui non résolues.

1. Banquise et saisonnalité du climat en Arctique

1.1 Cycle solaire

Le cycle saisonnier de la banquise arctique est l'un des signaux saisonniers les plus marquants du climat de l'hémisphère Nord. La saisonnalité de la zone de glace arctique est contrôlée, au premier ordre, par le cycle solaire. Pendant l'hiver, au-dessus du cercle polaire (66,3 °N), le soleil reste sous l'horizon. Ceci est dû à l'effet combiné de l'inclinaison de l'axe de rotation de la Terre et de sa course autour du soleil. Le rayonnement solaire incident est, par conséquent, nul au-dessus du cercle polaire, pendant une partie de l'année (entre 2 et 6 mois selon la latitude). C'est ce qu'on appelle la nuit polaire. En été, pour les mêmes raisons, les jours sont plus longs. Le rayonnement solaire mensuel reçu par les hautes latitudes peut alors atteindre des valeurs bien supérieures à celles des latitudes moyennes pendant l'été (Fig. 1).

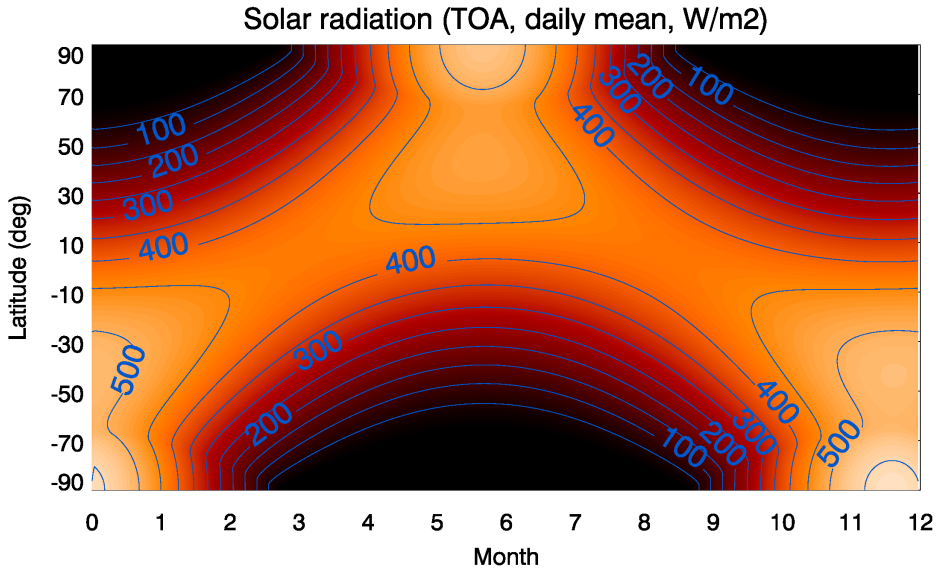

Figure 1 : Moyennes journalières du rayonnement reçu sur une surface unitaire au sommet de l'atmosphère terrestre en fonction de la latitude et de la date (en W/m^2). (Figure issue de Peixoto et Oort, 1991).

Le cycle solaire varie aussi avec la latitude : la nuit polaire est plus longue et plus sombre, la latitude augmentant. Cette grande variabilité saisonnière et spatiale à des conséquences

importantes notamment sur la thermodynamique de la banquise et de l'océan arctique, mais aussi sur la disponibilité en lumière pour les organismes photosynthétiques de l'océan Arctique.

1.2 Saisonnalité de la banquise : généralités

Les processus de fonte et de formation de la banquise témoignent de la forte variabilité saisonnière du cycle solaire, qui gouverne au premier ordre ces processus.

En hiver, pendant la nuit polaire, le rayonnement solaire étant nul, l'océan ne reçoit pas de chaleur par l'atmosphère. Au contraire, il en perd par rayonnement infrarouge (IR). Lorsque la température de l'océan atteint environ -1.8 °C, l'eau de mer gèle, formant de la glace dite « de mer » (ou banquise) qui flotte sur l'eau liquide du fait de sa faible densité à l'état solide. L'étendue (la surface de l'océan couvert par au moins 15%[1] de banquise) maximale de banquise (~15 millions de km^2) est atteinte en mars (Fig. 2 ; Fig. 3).

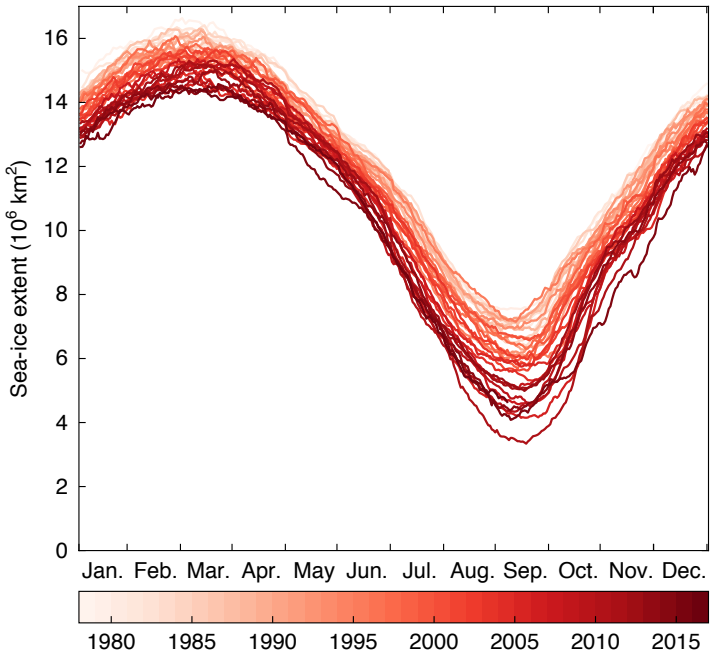

Figure 2 : Cycle saisonnier de l'étendue de glace en Arctique (en million de km^2) en fonction de l'année entre 1979 (couleurs claires) et 2017 (couleurs foncées). (Par Massonnet et al., 2018).

[1] Fait ici référence à la concentration de banquise. C'est à dire la fraction d'un domaine océanique donné, occupé par de la glace de mer (généralement exprimé en %)

En été, les fortes valeurs d'irradiance solaire réchauffent la banquise et la font fondre par la surface. La neige qui couvre la banquise (Fig. 4a) fond dans un premier temps. Puis la banquise s'affine au fur et à mesure de la saison et des mares de fonte se forment (Fig.4 b, c), jusqu'à la fonte totale de la banquise. La banquise arctique atteint son étendue minimum d'environ 6 millions de km^2 en septembre (Fig. 2). La banquise qui ne fond pas en été (Fig. 3), et qui perdure plus d'une année, est appelée banquise pérenne ou pluriannuelle. Elle s'oppose à la banquise saisonnière qui, elle, fond chaque année. Ces deux types de banquise impactent différemment la lumière transmise à la surface de l'océan, ainsi que le phytoplancton.

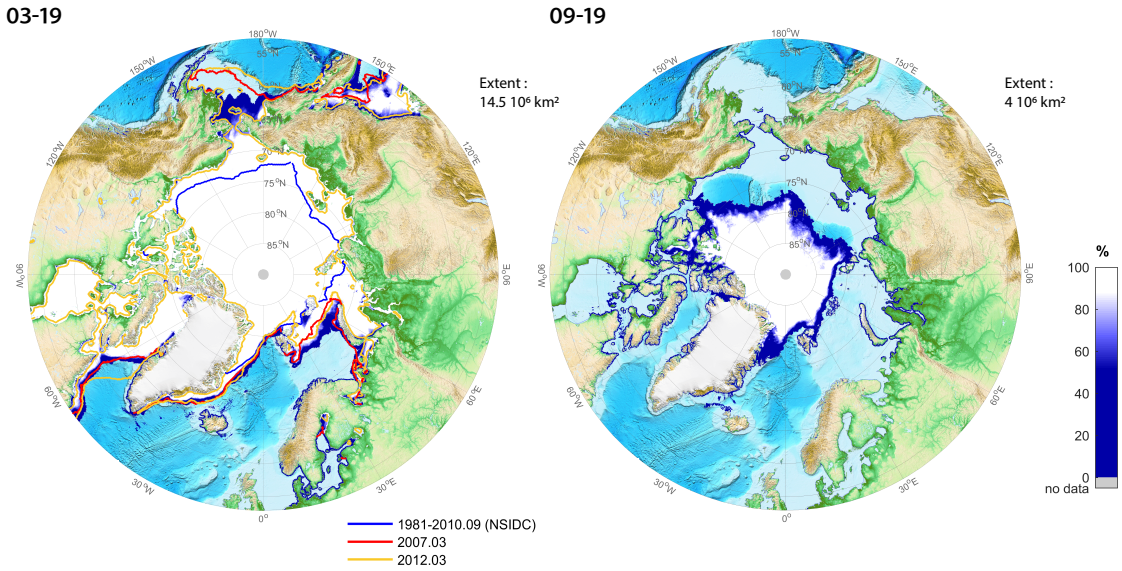

Figure 3 : Carte des concentrations de banquise mensuelle en Arctique en mars (gauche) et septembre 2019 (droite) issues des produits satellites AMSR2 (http ://data.seaiceportal.de). Sur la carte de gauche, les contours représentent le bord de glace (défini lorsque la concentration dépasse 15% de banquise) moyen pour le mois de septembre sur la période 1981-2010 (bleu) ; le bord de glace du mois de mars pour les années 2007 (rouge) et 2012 (jaune) durant lesquelles l'étendue de la banquise a atteint des minimums historiques.

La répartition spatiale de la banquise arctique suit aussi, au premier ordre, celle du cycle solaire. La concentration de banquise arctique diminue naturellement avec la latitude (Fig. 3). La distribution géographique de la glace de mer est aussi impactée par d'autres processus tels que les flux de chaleur océanique qui peuvent la faire fondre même aux relativement hautes latitudes

(par exemple, dans la région de la mer du Groenland). La dérive de la banquise peut aussi influencer sa distribution spatiale (cf. section 1.4).

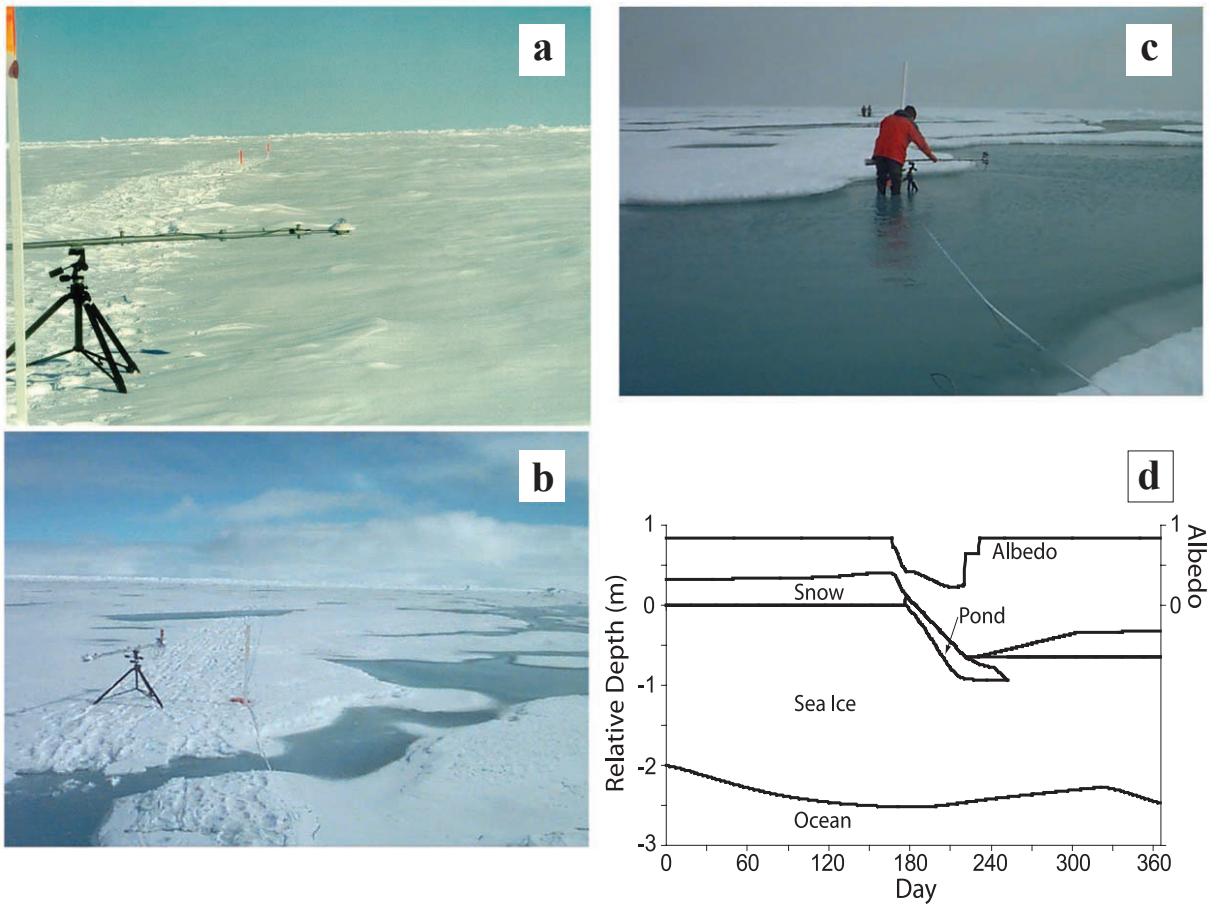

Figure 4 : photographies des différents stades de fonte de la banquise (a,b,c ; Perovich 2002) ; et schéma du cycle saisonnier de la banquise révélant la diminution de l'épaisseur de la neige et de la banquise ainsi que l'apparition des mares de fonte et l'évolution de l'albédo de surface associé (c ; Taylor et Feltham, 2004).

1.3 Thermodynamique de la banquise et rétroactions

Le cycle solaire arctique impacte la thermodynamique de la banquise qui va majoritairement gouverner sa saisonnalité. Le modèle de Semtner (1976) permet de décrire ces mécanismes à des fins d'illustration. D'après ce modèle, qui considère l'équilibre des flux de chaleur dans la banquise et qui néglige le stockage de chaleur sensible dans la glace de mer, le bilan de chaleur à la surface de la banquise s'écrit :

$$Q_{atm} = Q_c \qquad (1),$$

avec, Q_{atm} les flux de chaleur atmosphériques (rayonnement solaire, rayonnement infrarouge, flux de chaleur sensible et latente) et Q_c le flux de chaleur par conduction.

D'après la loi de Fourier, le flux de conduction Q_c s'écrit :

$$Q_c = \frac{k}{h}\Delta T \quad (2).$$

Où, k est la conductivité thermique de la glace ; h est l'épaisseur de la glace et ΔT est la différence de température entre la base et le sommet de la couche de banquise. En présence de glace de mer, les flux conductifs (~10 W/m^2) dans la glace se substituent aux flux turbulents océan-atmosphère (~100 W/m^2). Ces flux conductifs sont d'autant plus faibles que la banquise est épaisse. Cela se traduit par une forte capacité pour la banquise à isoler l'océan des échanges de chaleur avec l'atmosphère.

Le bilan de chaleur à la base s'écrit, quant à lui :

$$Q_c = Q_{oce} - \rho L.\frac{dh}{dt} \quad (3),$$

avec, Q_{oce} les flux de chaleur océaniques, ρ la densité de la glace de mer, L la chaleur latente et $\frac{dh}{dt}$ le taux de croissance de la banquise.

La croissance de la banquise est régulée par la conduction thermique. En hiver, les flux atmosphériques contribuent à refroidir la surface. La température à la base de la banquise est inférieure à la température du sommet de la couche de glace de mer. Pour se rapprocher de l'équilibre, il va y avoir une perte de chaleur de la surface vers l'atmosphère par conduction. Ceci va contribuer à faire croître la banquise.

En été, le rayonnement solaire domine les autres flux atmosphériques. La température de l'air est alors positive et supérieure à celle de la surface (qui est à 0 °C). L'énergie solaire excédentaire ne peut être compensée par la conduction dans la glace ou par l'échauffement de la glace, ce qui démarre la fonte de la banquise.

A ces processus thermodynamiques de fonte et de croissance de la banquise vont s'associer des rétroactions qui amplifient ou tempèrent ces processus. Bien qu'il existe de nombreuses

rétroactions qui affectent directement, ou indirectement, la fonte et la croissance de la banquise, je ne présente ici que les deux rétroactions majeures. La rétroaction croissance-épaisseur (Bitz & Roe, 2004) est l'une des rétroactions qui tempèrent la croissance (ou la fonte) de la banquise. En associant les équations (2) et (3) et en négligeant les flux de chaleur océaniques, le taux de croissance de la banquise peut s'écrire :

$$\frac{dh}{dt} = -\frac{1}{\rho L}.\frac{k}{h}\Delta T \qquad (4).$$

Le taux de croissance de la glace dépend de l'inverse de l'épaisseur (Stefan, 1891). Plus la glace est épaisse, moins la croissance sera efficace. Dans un scénario de réchauffement global, l'amincissement de la glace, entraîné par sa fonte, implique une augmentation de son taux de croissance. La croissance de la glace sera donc plus efficace tempérant l'impact de la fonte sur l'épaisseur (Fig. 5, branche de droite). Un autre effet de la rétroaction croissance-épaisseur est associé au couvert de neige. La neige, ayant un fort pouvoir isolant, suit la même logique que pour la banquise. Plus le couvert de neige est important, moins la croissance de la banquise sera efficace, car isolée de l'atmosphère par la neige.

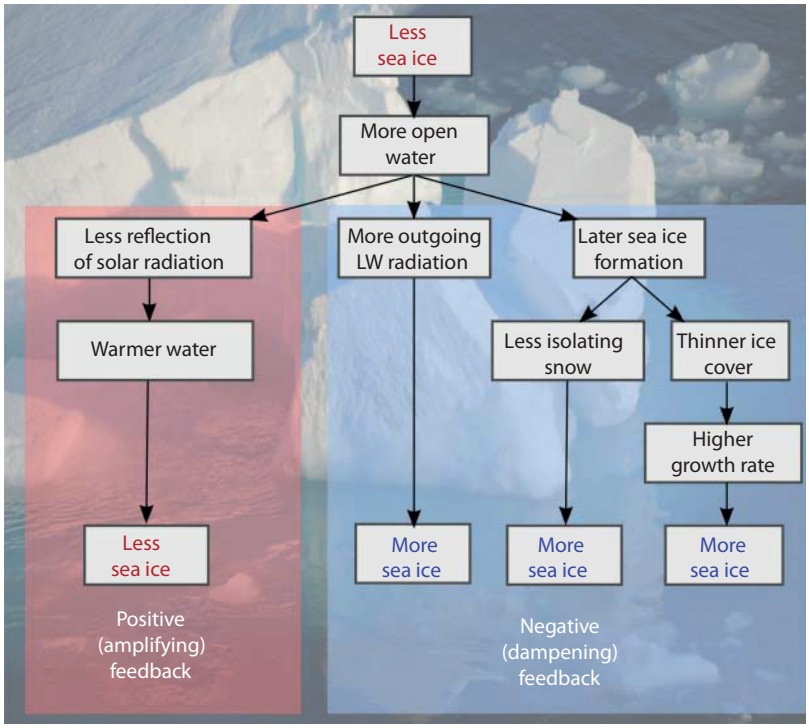

Figure 5 : Schéma représentant certaines des rétroactions majeures associées à la formation de la banquise (Notz et Bitz, 2016).

L'une des rétroactions majeures amplifiant les processus de fonte ou de croissance de la banquise, et généralement mentionnée dans la littérature, est la rétroaction glace-albédo (Fig. 5, branche de gauche). L'albédo d'un corps désigne sa capacité à refléter le rayonnement solaire. L'albédo de la glace de mer s'écrit comme le rapport entre le rayonnement solaire réfléchi par la surface de la banquise et le rayonnement solaire incident. Les premières simulations de Maykut et Untersteiner (1971) montrent que l'albédo a un impact majeur sur le bilan thermique de la banquise. En effet plus le rayonnement solaire est réfléchi par la banquise (plus son albédo est important), moins il y a d'énergie absorbée par la banquise pour la faire fondre. Au cours de la fonte de la banquise, la neige disparaît progressivement, puis la glace commence à fondre, des mares de fonte recouvrent progressivement la surface de la banquise jusqu'à la disparition complète de la glace. Toutes ces étapes vont impacter l'albédo de la surface de la banquise. Perovich (2002) décrit cinq phases, pendant la fonte de la banquise, au cours desquelles l'albédo de la surface diminue passant de 0.9 pour une banquise couverte de neige à 0.2 pour une banquise couverte de mares de fonte (Fig. 4). La diminution progressive de l'albédo pendant la fonte amplifie la fonte elle-même. Lorsque la glace a complètement fondu, l'albédo prend la valeur de l'eau de mer, bien plus faible que celle de la glace (~0.06). Une partie du rayonnement solaire absorbée est alors stockée par l'océan et peut provoquer un décalage dans la formation de la banquise l'hiver suivant (Perovich et al., 2007).

1.4 Dynamique de la banquise

La saisonnalité de la banquise arctique est pas impactée par sa thermodynamique mais aussi par la dynamique de la banquise.

Le déplacement de la banquise sur l'océan est induit à la fois par le vent et par les courants océaniques (Haas, 2016). La vitesse de déplacement de la glace de mer peut varier entre 1 et 10 km/jour (0,01 et 0,10 m/s ; Fig. 6 ; Kwok et al., 2013 ; Rampal et al., 2009). La dynamique de

la banquise peut déclencher certaines des rétroactions associées au processus de fonte et de formation de la banquise (cf section 1.3).

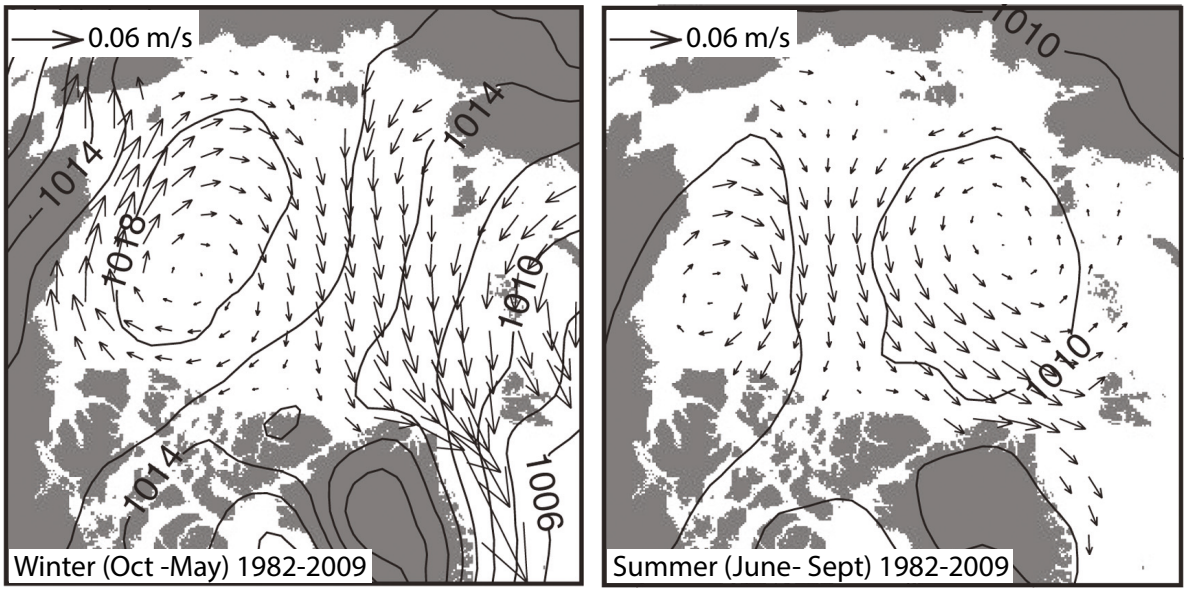

Figure 6 : Carte des vitesses moyennes de la banquise arctique obtenues par mesures satellites et issues de bouées dérivantes. Les contours représentent la pression atmosphérique (issue de Kwok et al., 2013).

Trois effets majeurs de la dérive de la glace peuvent être retenus. (i) La banquise est transportée à grande échelle, notamment à l'est du Groenland où la banquise, formée proche du pôle, est transportée vers des latitudes plus basses où elle va fondre (see Fig. 6 and Moreau et al., 2016, Fig. 2). (ii) La divergence dans la glace ouvre des chenaux d'eau libre au sein du couvert de glace, dans lesquels de la glace, peut se former en hiver (Haas, 2016 ; Notz & Bitz, 2016). Cela peut aussi renforcer drastiquement la rétroaction glace-albédo en été (Notz & Bitz, 2016). (iii) Enfin, la banquise peut subir des déformations par convergence. Les mécanismes de convergence de la glace sont moins bien connus, car complexes. La convergence peut contribuer à augmenter l'épaisseur de la banquise à petite échelle. En effet, la banquise est plutôt résistante à la compression et lors d'une convergence, la banquise va généralement se craqueler et former des crêtes de compressions (Hibler, 1979 ; Tremblay & Hakakian, 2006). Tous ces processus et notamment la dérive de la banquise et la divergence qui agissent à grande échelle vont impacter la saisonnalité de la banquise et perturber les effets thermodynamiques.

2. Indicateurs de la saisonnalité de la banquise arctique

2.1 Saisonnalité de la banquise : différentes définitions

Pour comprendre les mécanismes influençant la saisonnalité de la banquise et mieux appréhender la réponse de cette saisonnalité au réchauffement climatique, il a été nécessaire de définir des indicateurs de cette saisonnalité. Il existe différentes définitions de la saisonnalité de la banquise dans la littérature (Johnson & Eicken, 2016). Deux sont majoritairement utilisées, car relativement simples à mesurer à grande échelle par satellite.

(i) La saison de fonte (Markus et al., 2009) est décrite positive. Elle peut se mesurer par satellite à partir de la température de brillance qui présente un contraste important lorsque de l'eau est présente ou pas à la surface de la banquise. A partir d'un certain seuil de température de brillance, la glace peut être considérée comme humide, ce qui suggère que la saison de fonte a commencé. À noter qu'il existe différentes façons de décrire la saison de fonte (Markus et al., 2009 ; Stroeve et al., 2014).

(ii) La saison d'eau libre a aussi été largement étudiée ces dernières années (Parkinson, 2014 ; Stammerjohn et al., 2012 ; Stroeve et al., 2016). La saison d'eau libre est définie comme la période durant laquelle l'eau peut être considérée comme libre de glace, ou plus concrètement comme le nombre de jours durant lesquels la concentration de banquise obtenue par mesures satellites passe sous un certain seuil (Parkinson, 2014). Elle peut aussi être définie comme la période bornée par les jours de retrait et d'avancée de la banquise (date à laquelle la concentration en glace passe sous, ou dépasse, un certain seuil ; Stammerjohn et al., 2012 ; Stroeve et al., 2016).

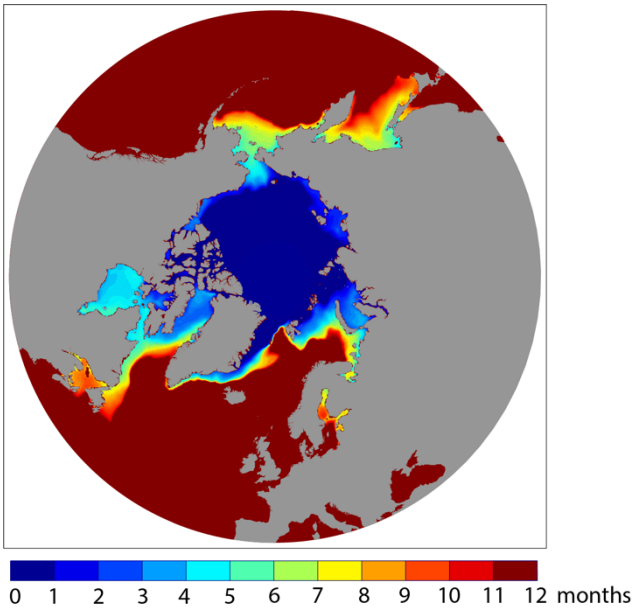

Figure 7 : Carte du nombre de mois d'eau libre moyennée sur la période 1980-2015 basée sur les concentrations de glace journalières obtenues par satellite avec un seuil à 15%. (Cf. Lebrun et al., 2019 pour méthode).

Bien que clairement différentes, et malgré les différences de définition entre les auteurs, les saisons d'eau libre et de fonte présentent des distributions spatiales similaires. La distribution spatiale de la période d'eau libre (Fig. 7) est assez similaire à celle de la concentration en banquise. Le cycle solaire dominant la saisonnalité de la banquise, la saison d'eau libre a tendance à être plus courte aux hautes latitudes. D'autres forçages, comme celui de l'océan ou de la dynamique de la banquise, interviennent dans certaines régions. La saison d'eau libre donne une information distincte de la concentration : elle indique la temporalité de la glace de mer, au contraire de la concentration qui décrit sa dimension spatiale. Il n'y pas que la distribution spatiale qui est similaire entre les différents indicateurs de saisonnalité, leur réponse au changement climatique est aussi comparable.

2.2 Réponse saisonnière au changement climatique

La réponse de la banquise au changement climatique se traduit au premier ordre par une diminution de l'étendue de glace arctique (Cavalieri & Parkinson, 2012). Cette diminution est plus marquée en été qu'en hiver (Fig. 2 ; Massonnet et al., 2018). On retrouve aussi la réponse du changement climatique dans la diminution globale de l'épaisseur de la banquise arctique (Kwok & Rothrock, 2009) ; mais aussi dans l'allongement de la période d'eau libre ou de fonte quasiment partout en Arctique (Markus et al., 2009 ; Parkinson, 2014 ; Stammerjohn et al., 2012 ; Stroeve et al., 2014 ; Stroeve et al., 2016). L'allongement de la saison d'eau libre est associé à un jour d'avancée plus tardif dans l'année et un jour de retrait plus précoce (Fig. 8 ; Stammerjohn et al., 2012 ; Stroeve et al., 2016). Le comportement du jour de retrait et d'avancée de la banquise arctique face au changement climatique est généralement associé à la rétroaction glace-albédo (Perovich et al., 2007 ; Stammerjohn et al., 2012). Lorsque la banquise se retire, une quantité d'énergie est stockée dans l'océan libre de glace. Cette quantité d'énergie doit être complètement rejetée vers l'atmosphère pour que la glace se forme à nouveau l'hiver suivant. Si la banquise se retire plus tôt, en réponse au réchauffement climatique, une quantité d'énergie supplémentaire est stockée dans l'océan. Il faut alors un temps supplémentaire pour que cette énergie soit évacuée, retardant la formation de la banquise.

D'après les projections des modèles du système Terre, l'étendue de banquise arctique devrait continuer à diminuer dans les prochaines décennies (Massonnet et al., 2012 ; Stroeve et al., 2012). Les modèles prévoient un remplacement de toute la glace pérenne en glace saisonnière entre 2040 et 2060 pour les scenarios d'émission RCP4.5 et RCP8.5 (Massonnet et al., 2012). D'après ces projections, la période d'eau libre (ou de fonte) devrait continuer d'augmenter dans les prochaines décennies (Barnhart et al., 2016). Cette augmentation de la période d'eau libre devrait être majoritairement contrôlée par la date d'avancée de la banquise (Barnhart et al., 2016 ; Wang & Overland, 2015). Néanmoins, ce signal est atténué par une forte variabilité

interannuelle. De plus, les études sur les projections des indicateurs de la saisonnalité de la banquise arctique sont encore assez rares et ne reposent, soit sur qu'un seul modèle (Barnhart et al., 2016), soit sur qu'une seule région de l'Arctique (Wang & Overland, 2015).

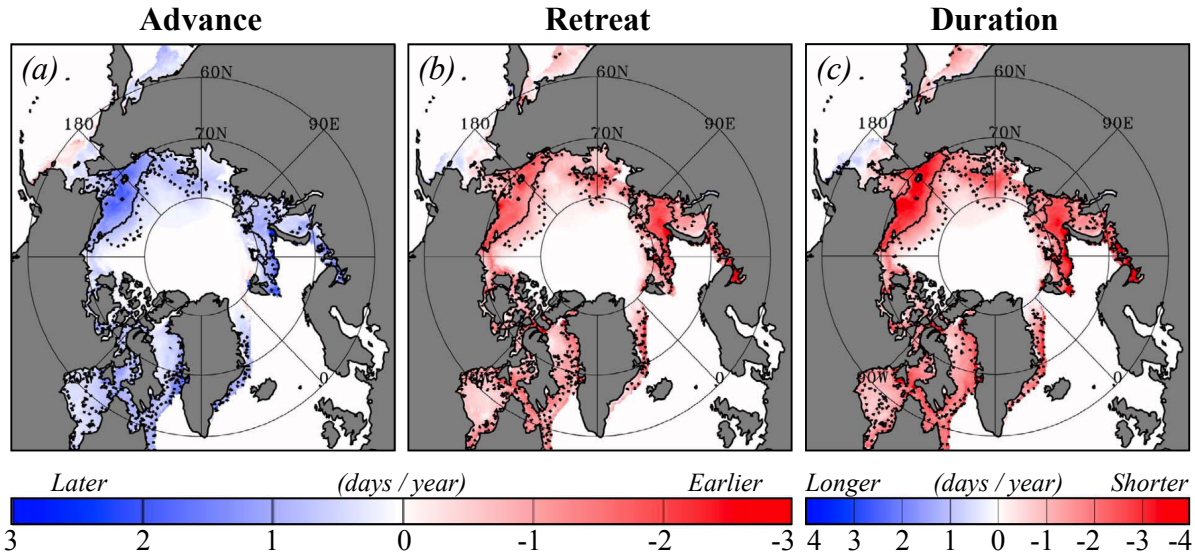

Figure 8 : tendances dans le jour d'avancée (a) et de retrait (b) de la banquise et la période d'eau libre (c) sur la période 1980-2010 basées sur les données satellites (seuil de concentration = 15% ; issue de Stammerjohn et al., 2012).

Même si la plupars des modèles s'accordent sur l'évolution future de la banquise arctique et reposent sur des processus thermodynamiques simples et bien représentés, la question sur l'avenir des périodes d'eau libre et de fonte reste encore assez peu étudiée. De plus, les mécanismes contrôlant au premier ordre l'évolution de la période d'eau libre restent encore inexpliqués.

La banquise arctique a un cycle saisonnier très marqué, influencé au premier ordre par le cycle solaire. On retrouve l'influence du cycle solaire dans l'évolution des marqueurs de saisonnalité de la banquise arctique. La présence de banquise va aussi influencer la transmission de la lumière à la surface de l'océan et altérer le cycle saisonnier de la lumière disponible pour le phytoplancton en Arctique. C'est ce que je propose d'aborder dans les paragraphes qui suivent.

3 Transfert radiatif dans la zone de glace

3.1 Propriétés optiques de la glace de mer

Si le cycle solaire joue un rôle important dans la croissance du phytoplancton arctique, la banquise, influençant la lumière disponible dans l'océan superficiel, a aussi un rôle majeur. En effet, la banquise ne transmet qu'une partie du rayonnement solaire à l'océan sous-jacent. Comme n'importe quel corps, la banquise réfléchit en partie le rayonnement solaire incident. La partie non réfléchie peut être ensuite absorbée par la banquise. Elle peut aussi être diffusée dans toutes les directions de l'espace par les cristaux qui constituent la banquise. Seule la partie qui n'est ni réfléchie, ni absorbée, ni rétrodiffusée, est transmise à la surface de l'océan (Fig. 9). La façon dont un corps interagit avec la lumière est décrite par ses propriétés optiques. Il existe deux types de propriétés optiques : les propriétés optiques inhérentes (IOP) et les propriétés optiques apparentes (AOP).

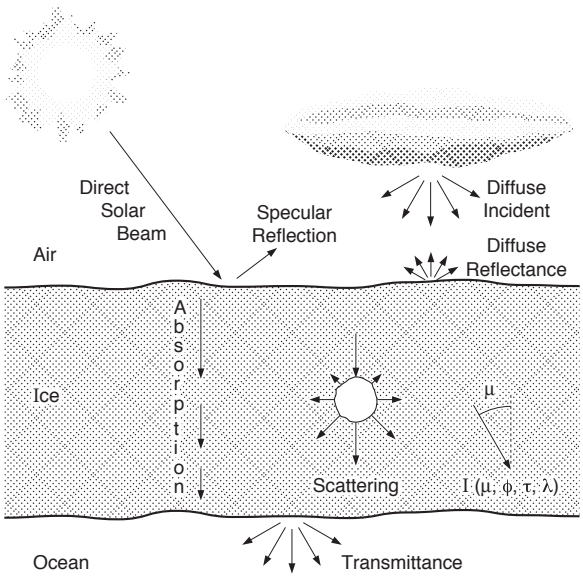

Figure 9 : Schéma du transfert radiatif dans la glace de mer (issu de Perovich et al., 1996).

Les IOP ne dépendent pas du rayonnement incident. Elles sont représentées par les coefficients d'absorption et de diffusion, l'indice de réfraction et la fonction de phase (Perovich, 1996).

Tous ces paramètres sont fortement dépendants de la microstructure du corps au travers duquel est transmise la lumière. Dans le cas de la glace de mer, il est important de noter que sa composition diffère grandement de celle de la glace pure. En effet si la glace pure est essentiellement composée d'eau à l'état solide, la glace de mer comporte aussi une phase liquide formée par les poches de saumure (Fig. 10 ; eau salée non gelée) et une phase gazeuse formée de bulles d'air emprisonnées dans la banquise (Weeks et al., 1982). Poches de saumure et bulles d'air absorbent et rétrodiffusent une grande partie du rayonnement solaire incident et contrôlent l'atténuation de la lumière au premier ordre (Perovich, 1996). Un autre exemple est celui de la neige qui est composée majoritairement de cristaux de glace orientés dans toutes les directions et de bulles d'air. Cette grande hétérogénéité favorise la diffusion (Järvinen & Leppäranta, 2011 ; Warren, 1982).

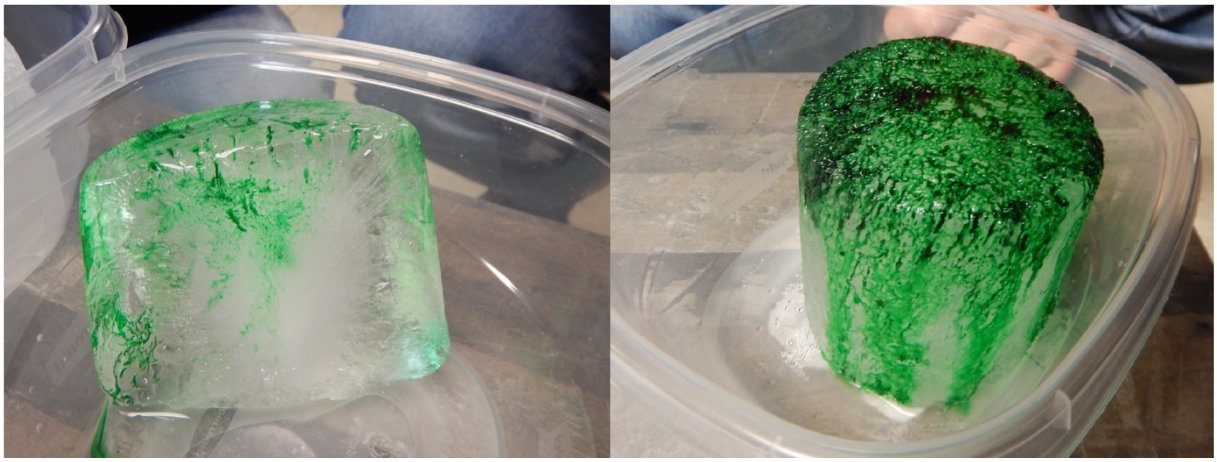

Figure 10 : Expérience mettant en évidence les différences de composition entre la glace pure et la glace de mer. L'encre met en évidence les poches de saumure dans la glace de mer. A gauche, la glace pure, à droite, la glace de mer prélevée d'une carotte. De l'encre est disposée au-dessus de chaque échantillon. A gauche, l'encre s'écoule sur l'échantillon de façon homogène. A droite, l'encre s'écoule dans les interstices de l'échantillon et une partie est retenue dans les poches de saumure accessibles (zones plus sombres).

Les AOP dépendent à la fois de la réflexion, de l'absorption et de la diffusion par la glace, mais aussi des caractéristiques du rayonnement incident telles que son intensité et son inclinaison par rapport à la surface (Perovich, 1996, Perovich, 2016). Ce sont, entre autres, l'albédo et la transmittance (rapport entre le rayonnement transmis sous la glace et le rayonnement incident).

Dans la banquise et dans la neige, les AOP sont plus simples à mesurer et mieux connues que les IOP.

Dans les modèles du Système Terre, le transfert dans la glace est représenté sur la base soit des IOP soit des AOP. On distingue deux principales représentations du transfert radiatif dans la banquise, majoritairement utilisés dans les modèles.

(i) Le premier type de représentations est basé sur l'approche dite de *Delta Eddington* (Briegleb & Light, 2007 ; Saenz & Arrigo, 2012). Cette approche est basée sur les IOP. Partant du postulat que les propriétés physiques de la glace et de la neige ne sont pas homogènes verticalement, la banquise et la neige sont divisées en plusieurs sous-couches ayant chacune leurs propriétés physiques propres (épaisseur de la couche, densité et taille des grains pour la neige et volume des poches de saumure pour la glace). Par conséquent, chacune des couches a ses propres propriétés optiques inhérentes définies empiriquement sur base d'observations : coefficient d'absorption, coefficient de diffusion et paramètre d'asymétrie (qui définit la direction du rayonnement diffusé au sein de la couche). Si cette représentation est a priori la plus complète qui existe aujourd'hui en termes de physique, elle souffre cependant de plusieurs problèmes. Tout d'abord, la microstructure y est prescrite, en particulier celle de la neige et des inclusions gazeuses dans la glace (Briegleb & Light, 2007). De plus, les mesures précises d'IOP telles que les coefficients d'absorption et de diffusion restent aujourd'hui imprécises (Perovich., 2016). Ce type de représentation dans les modèles de banquise est aussi assez complexe et coûteux en termes de temps de calcul. Enfin, il existe aujourd'hui peu d'études confrontant une telle représentation aux observations.

(ii) Le second type de représentation repose sur une spécification des propriétés apparentes en particulier l'albédo, et les coefficients d'atténuation dans la glace et dans la neige de Beer-Lambert à deux niveaux. Le premier niveau est une fine couche de surface

hautement diffusive (surface scattering layer, SSL). Le deuxième niveau correspond à l'essentiel de la glace, supposé peu diffusant, et caractérisé par un coefficient d'atténuation relativement faible. Cette représentation considère une décroissance exponentielle du rayonnement au sein de la glace en fonction d'un paramètre, κ, le coefficient d'absorption (Maykut & Untersteiner, 1971). Dans le cas d'un rayonnement incident direct (F_{sw}^{0}) seulement absorbé par la banquise, l'équation du transfert radiatif se réduit à :

$$F_{sw}^{z} = F_{sw}^{0}.e^{-\kappa z} \quad (5).$$

Où, F_{sw}^{z} est le rayonnement transmis au travers de la banquise et z l'épaisseur de la banquise (Perovich, 1996). Cette équation considère une banquise homogène verticalement et essentiellement absorbante. Pourtant la banquise réfléchit (albédo, α) et diffuse aussi une partie du rayonnement. De plus, la banquise n'est pas verticalement homogène. En surface, la SSL a une diffusion forte et une absorption élevée qui contribuent à fortement atténuer le rayonnement en surface. Pour décrire ce phénomène, on introduit le coefficient i_0 comme la fraction de rayonnement transmis au travers de la SSL. L'équation (5) devient alors (Grenfell & Maykut, 1977) :

$$F_{sw}^{z} = i_0(1-\alpha)F_{sw}^{0}.e^{-\kappa(z-h_0)} \quad (6).$$

Chacun des paramètres est défini de façon empirique en tenant compte des observations. Cette méthode est moins complexe que l'approche de Delta-Eddington mais elle présente l'inconvenient de ne pas explicitement prendre en compte l'effet de la microstructure de la glace sur le rayonnement transmis. Les nombreuses simplifications inhérentes à cette approche (par exemple l'homogénéité verticale) peuvent engendrer un certain nombre d'erreurs.

Quel que soit le type de représentation, leurs paramètres doivent être ajustés sur base de mesure d'optique de la banquise. J'aborde ces mesures dans la section suivante.

3.2 Observation de l'irradiance transmise dans la zone de glace

La microstructure de la banquise, et donc ses propriétés optiques, varient fortement dans le temps et dans l'espace. C'est à la fois vrai verticalement et horizontalement. Multiplier les observations à partir de différents types de mesures est donc fondamental.

Il existe, en effet, différents types de mesures de rayonnement transmis sous la banquise. L'un d'eux permet d'avoir une idée de l'évolution temporelle du rayonnement transmis. L'instrument est alors fixé à la banquise en dérive pendant toute une saison (Fig. 11 gauche ; Nicolaus et al., 2010). Une autre approche vise à profiler l'évolution verticale de la lumière en un point fixe (Fig. 11 centre ; Frey et al., 2011 ; Randelhoff et al., 2019). L'instrument est placé dans un trou occulté par de la neige pour prévenir toute pollution lumineuse et est lentement déplacé sur la verticale. Enfin, il est possible d'obtenir une distribution spatiale du rayonnement transmis au travers d'une parcelle de banquise à partir de l'utilisation d'un véhicule sous-marin téléguidé qui récolte l'information sur l'ensemble de la zone d'étude (Fig. 11 droite ; Katlein et al., 2015, 2017 ; Nicolaus & Katlein, 2013)

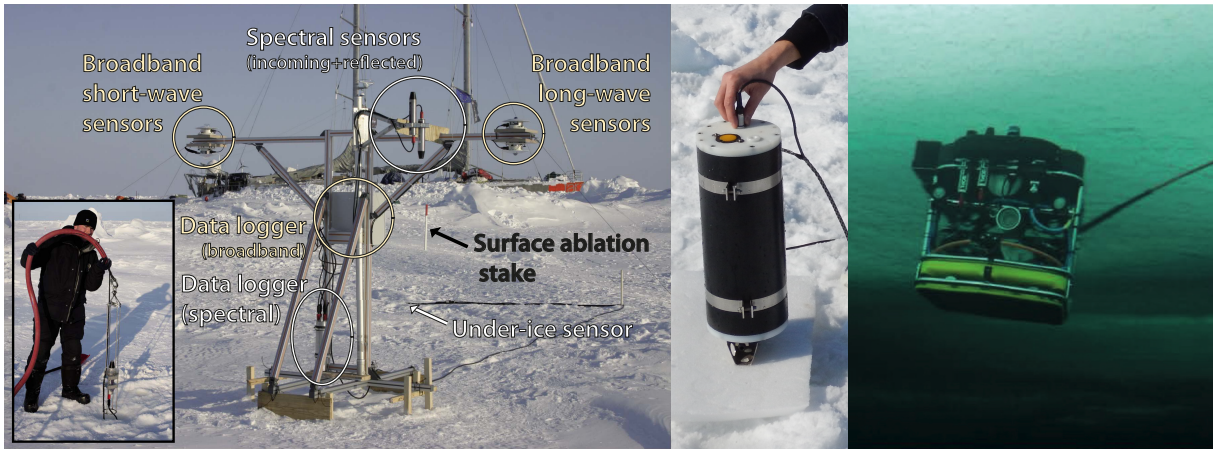

Figure 11 : Photographies de différents instruments de mesure de la lumière transmise au travers de la banquise. A gauche : l'instrument utilisé lors de la dérive transpolaire de Tara en 2007 (Nicolaus et al., 2010) ; au centre : l'instrument utilisé pour mesurer des profils de lumière sous la glace lors des campagnes au Svalbard et en Hokkaido (cf. chapitre 2). A droite un véhicule téléguidé (ROV) utilisé pour mesurer la distribution spatiale de la lumière sous la banquise (Katlein et al., 2017).

Comme la surface la banquise n'est pas homogène, la lumière transmise au travers d'une zone couverte de banquise présente généralement une large variabilité spatiale petite échelle (de l'ordre du mètre ; Fig. 12) et plus grande échelle (de l'ordre du kilomètre) notamment au moment de la fonte où banquise enneigée, banquise nue, mares de fonte et chenaux d'eau libre sont associés (Katlein et al., 2015 ; Katlein et al., 2017 ; Nicolaus et al., 2012). Chaque partie du système de banquise (neige, glace nue, mares de fonte et chenaux d'eau libre) influence différemment l'intensité du rayonnement incident ainsi que sa répartition spectrale.

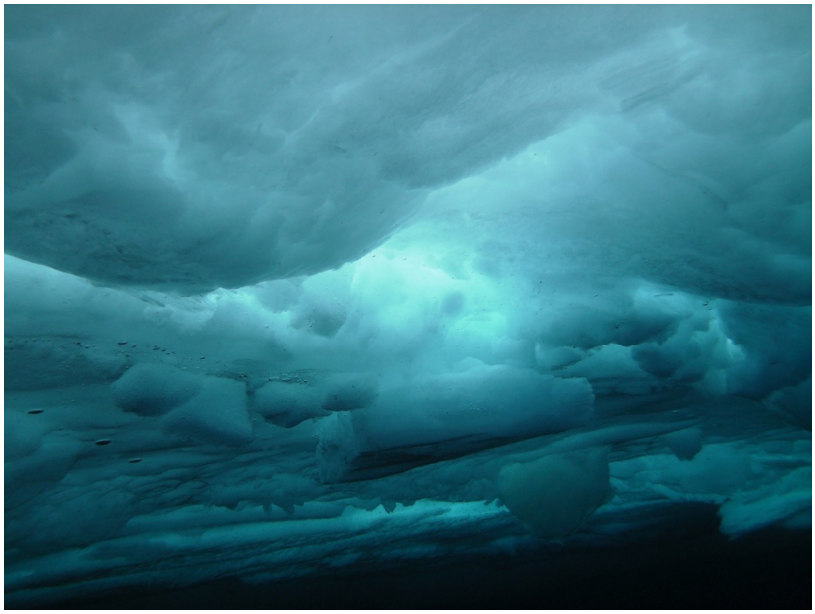

Figure 12 : Photographie prise sous la banquise lors d'une campagne en Antarctique révélant l'hétérogénéité spatiale du rayonnement transmis au travers de la banquise (crédit photo : Klaus Meiner, Australian Antarctic Division, Hobart, Tasmanie)

Si le nombre d'observations in situ sur les propriétés optiques de la banquise est aujourd'hui en augmentation, ce n'était pas le cas il y a quelques décennies. La mesure de la lumière transmise sous la glace n'est pas aisée et les campagnes sont coûteuses. Néanmoins grâce à deux campagnes en particulier (en mer de Beaufort en 1998-SHEBA ; et lors de la dérive transpolaire de Tara en 2007), un certain nombre d'informations sur les propriétés optiques de chaque composante du système de banquise a pu être obtenu.

Le rayonnement transmis mesuré dans la couche de neige est fortement atténué en raison d'un albédo élevé (0,8-0,9 ; Perovich et al., 2002) résultant d'une forte diffusion notamment dans le domaine visible (Järvinen & Leppäranta, 2011 ; Warren, 1982). La transmittance de la neige dépend de nombreux facteurs comme son épaisseur, sa densité, la taille et la forme des grains qui la composent, ou encore, la présence de particules aérosols (dont les suies ; France et al., 2012 ; Järvinen & Leppäranta, 2011 ; Marks & King, 2014 ; Warren, 1982). Cela rend l'étude des propriétés optiques de la neige assez complexe. Le rayonnement reçu sous une couche de neige est fortement atténué dans l'infrarouge (au-delà de 800 nm ; Järvinen & Leppäranta, 2011 ; Warren, 1982). La neige absorbant aussi les longueurs d'onde entre 400 et 500 nm, la neige va aussi atténuer le rayonnement dans le bleu.

La glace nue transmet quant à elle plus de lumière que la glace couverte de neige du fait d'un albédo moindre (0,6-0,7 ; Perovich et al., 2002 ; Light et al., 2008 ; Nicolaus et al., 2010) dû à l'alignement des cristaux de glace qui est globalement plus régulier. La surface de la glace présente une couche d'environ une dizaine de centimètres fortement diffusante, en raison de la présence plus importante de bulles de gaz, de saumure et de minéraux à la surface (Grenfell & Maykut, 1977 ; Light et al., 2008). Ceux-ci absorbent et diffusent la lumière, réduisant ainsi le rayonnement transmis à la surface de l'océan. A grande échelle, le rayonnement transmis par la glace nue est majoritairement contrôlé par l'épaisseur de la glace (Fig. 13 ; Katlein et al., 2015). Il peut aussi être impacté par les organismes présents dans la glace (algues de glace ; Arrigo et al., 1991). La lumière transmise à la surface de l'océan couvert de glace nue est aussi fortement atténuée à partir du proche infrarouge (au-delà de 600 nm), avec une transmittance maximum pour la glace nue autour de 500 nm, en raison de l'effet combiné de l'albédo (Nicolaus et al., 2010) et du coefficient d'extinction (Light et al., 2008).

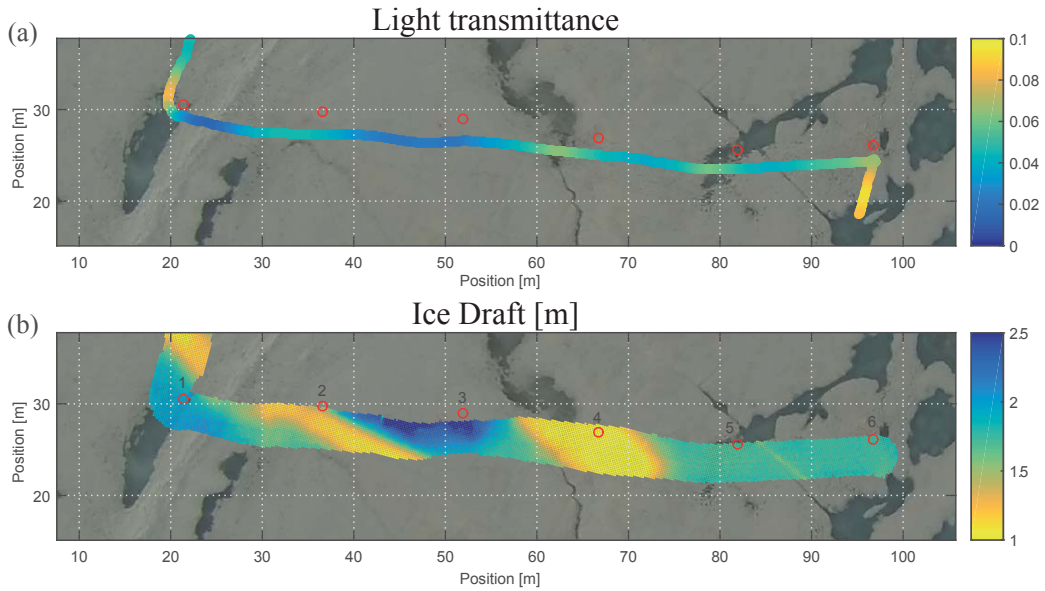

Figure 13 : Distribution spatiale de la transmittance (a) et de l'éppaisseur de la banquise (b) mesurés à partir d'un ROV réalisé sur une banquise dérivante durant la campagne du Polarstern au Nord-Est du Groenland en 2014 (Katlein et al., 2015).

Lorsque la banquise est couverte de mares de fonte, la variabilité spatiale du rayonnement transmis augmente considérablement à des échelles inférieures au kilomètre (Frey et al., 2011 ; Light et al., 2008). En effet, les mares de fonte transmettent plus de rayonnement que la glace (Fig. 13), ce qui correspond à un albédo faible (0,2-0,4 ; Perovich et al., 2002). De plus, elles diffusent la lumière de manière homogène sur la verticale, contrairement à la glace nue ou couverte de neige (Light et al., 2008). L'impact des mares de fontes sur le rayonnement transmis ne se réduit pas à la zone située directement en dessous d'elles. La diffusion horizontale du rayonnement va augmenter l'éclairement des zones à proximité, même lorsqu'elles ne sont pas couverte de mares de fonte (Frey et al., 2011). Il est alors possible d'avoir un pic d'irradiance, quelques centimètres sous une couche de glace se trouvant à proximité d'une mare de fonte (Massicotte et al., 2018).

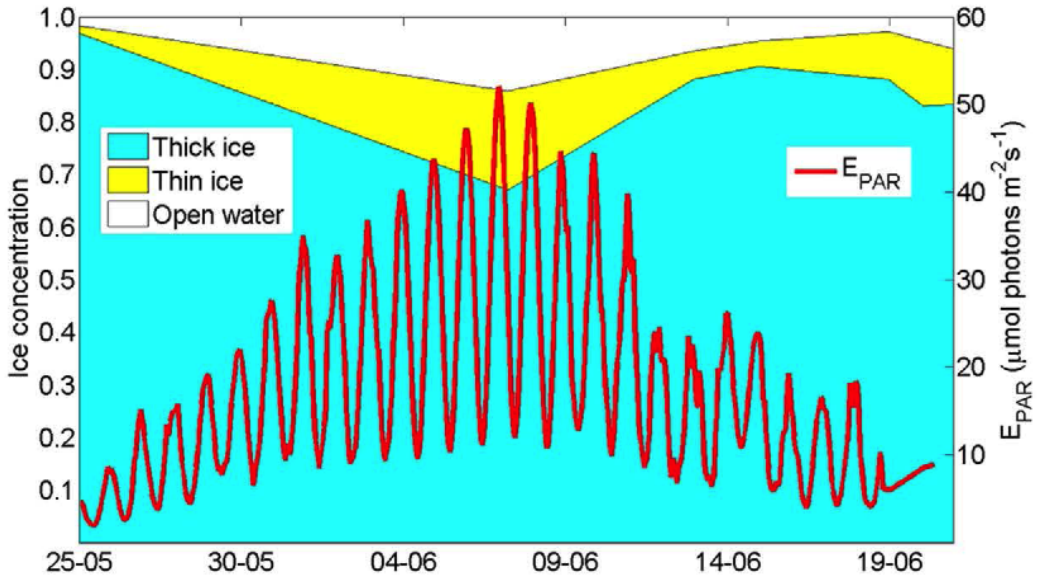

Figure 14 : Série temporelle des concentrations d'eau libre (blanc) de banquise fine (jaune) et épaisse (bleu) obtenues par mesures satellites et du rayonnement incident moyen transmis à la surface de l'océan simulé à partir du rayonnement incident mesuré en surface (E_{par} ; ligne rouge). Mesures réalisées au nord du Svalbard en juin 2015 (issue de Assmy et al., 2017).

Le même phénomène se produit à proximité des chenaux d'eau libre qui augmente fortement le rayonnement transmis dans une zone englacée (Fig. 14 ; Assmy et al., 2017).

L'étude de la transmission de la lumière dans l'eau libre est mieux documentée. La forte transmission de la lumière à la surface d'une zone d'eau libre est due à son faible albédo (~0.06 ; Payne, 1972). Une fois transmis à l'océan libre de glace, plus de la moitié du rayonnement (57%) est absorbé dans les premiers centimètres de la colonne d'eau essentiellement dans la partie infrarouge et ultra-violette du spectre lumineux. La partie visible du spectre pénètre dans l'océan, à des profondeurs qui dépendent à la fois de la longueur d'onde et de la concentration en chlorophylle (Morel, 1988). Le transfert radiatif dans les zones libres de glace étant mieux documenté, il est, par conséquent, bien représenté dans les modèles du système Terre.

3.3 L'optique de la banquise dans les modèles du système Terre

Si le rayonnement transmis dans les zones d'eaux libres est plutôt bien représenté dans les modèles du système Terre, c'est moins le cas dans la zone de glace. En effet, le peu

d’observations et la complexité de certaines composantes du problème, comme la neige ou les mares de fonte rendent la représentation du transfert radiatif dans la glace de mer difficile. Dans la plupart des modèles, la transmission du rayonnement sous la glace n'a pas été examinée en détail, elle est peu ou mal documentée. Elle fait aussi l'objet de simplifications drastiques permettant d'éviter les problèmes liés à la faible disponibilité de données observationnelles. Par exemple dans LIM, le modèle de glace de mer de l'IPSL, le rayonnement transmis sous la neige est supposé nul (Vancoppenolle et al., 2012). Cela permet de réduire la complexité et de pallier le peu d’observations. De même, les mares de fonte ne sont pas toujours représentées dans les modèles. Par conséquent, le rayonnement transmis dans les zones à forte concentration de glace est généralement très proche de zéro et est potentiellement sous-estimé. La sous-estimation du rayonnement transmis dans la zone de glace impacte non seulement la thermodynamique de l’océan, mais aussi la photosynthèse. La répartition spectrale du rayonnement sous la banquise est aussi mal représentée. Bien que cette partie soit peu documentée, le rayonnement sous la glace est réparti de la même façon en l’absence et en présence de glace (Madec et al., 2017). Pourtant, les nombreuses études sur la transmission du rayonnement a travers la banquise montrent que celle-ci influence la distribution spectrale du rayonnement. Ainsi le spectre arrivant à la surface de l’océan libre de glace est différent de celui arrivant à la surface de l’océan couvert de glace. Comme la profondeur de pénétration de la lumière de l’océan dépend notamment de sa longueur d’onde, ne pas distinguer les deux systèmes implique des erreurs potentiellement importantes sur l’éclairement dans la zone de glace.

Simuler au mieux le transfert radiatif des zones de glace est primordial notamment pour bien représenter la biogéochimie dans ces zones, puisque la lumière contrôle, au premier ordre, la croissance du phytoplancton.

4 Le phytoplancton dans la zone de glace arctique

4.1 Croissance du phytoplancton : spécificité de la zone de glace

Le phytoplancton est une algue unicellulaire, présente en grande quantité dans l'océan et qui pratique la photosynthèse. La croissance du phytoplancton est contrôlée, au premier ordre, par l'éclairement dans la colonne d'eau. Dans la majeure partie des océans, la disponibilité en lumière n'est pas limitée en surface. En profondeur, en revanche, la lumière pénètre de moins en moins et limite la croissance du phytoplancton. Pour décrire la couche d'océan qui n'est pas limitée en lumière, on parle de couche euphotique. La profondeur de la couche euphotique est généralement décrite comme la profondeur à laquelle le rayonnement transmis à l'océan atteint 1% du rayonnement en surface (Morel, 1988). Elle est de l'ordre d'une centaine de mètres dans les océans ouverts, mais peut être fortement réduite dans les eaux à forte turbidité (Sarmiento & Gruber, 2006).

Pour pratiquer la photosynthèse, le phytoplancton a aussi besoin de nutriments tels que l'azote et le phosphore présents généralement dans l'océan sous forme de nitrates (NO_3) et de phosphates (PO_4). D'autres nutriments comme le fer (Fe) voir la silice (Si) sont nécessaires pour la photosynthèse. Pour que le phytoplancton se développe, il faut qu'il y ait une quantité suffisante de nutriments en surface, dans la couche euphotique. La quantité de nutriments en surface est en partie influencée par le transport vertical qui dans certaines conditions (upwelling) peut apporter des nutriments de la subsurface vers la surface. Les nutriments peuvent aussi être apportés par transport latéral, à partir de zones riches en nutriments. Enfin, dans une moindre mesure, ils peuvent être apportés par dépôts atmosphériques. Mais ces derniers ont un impact généralement très localisé et ne contribuent pas à la répartition globale des nutriments de surface (Sarmiento & Gruber, 2006).

Enfin, la croissance du phytoplancton peut aussi être influencée par la stratification de l'océan. On peut décrire la stratification par la profondeur de la couche de mélange. Dans un océan très

stratifié, la couche de mélange est peu profonde. Le transport vertical est concentré sur une couche très fine et cela ne suffit pas à apporter les nutriments en profondeur vers la surface. La croissance du phytoplancton est alors limitée par les nutriments. Dans le cas opposé, si l'océan est faiblement stratifié, la couche de mélange est profonde et l'apport de nutriments des zones profondes vers la surface est efficace. Cependant dans une couche de mélange profonde le phytoplancton va aussi être mélangé et transporté plus en profondeur. Si la couche de mélange est plus profonde que la couche euphotique, le phytoplancton n'aura pas assez de lumière pour croître lorsqu'il sera transporté en profondeur. Sverdrup (1953) définit une profondeur idéale pour déclencher une efflorescence de phytoplancton à laquelle la base de la couche de mélange est à la même profondeur que la base de la couche euphotique.

On peut décrire la quantité de phytoplancton dans l'océan par la production primaire des océans. La production primaire est la quantité de matière organique produite par photosynthèse. Dans les océans, elle est majoritairement représentée par le phytoplancton (Behrenfeld et al., 2001). En Arctique, la production nette est d'environ 500 TgC/an en moyenne (Babin et al., 2015) contre 45 000 TgC/an dans l'océan global (Gregg et al., 2003). Les trois paramètres qui contrôlent la croissance du phytoplancton (disponibilité en lumière, en nutriments et stratification) sont largement contrôlés par la glace de mer en Arctique.

La lumière disponible en surface détermine l'épaisseur de la couche euphotique qui peut soutenir la photosynthèse si les nutriments sont suffisants. Dans la zone de glace, la faible luminosité et la présence de glace renforcent encore plus le rôle des variations d'éclairement sur la photosynthèse. En effet, dans les régions englacées arctiques, la lumière est fortement limitée, en particulier par la nuit polaire, durant laquelle l'absence de lumière rend impossible la photosynthèse, d'autre part par la banquise qui atténue fortement le rayonnement solaire transmis à la surface de l'océan (Arrigo & van Dijken, 2011 ; Assmy et al., 2017 ; Wassmann

& Reigstad, 2011). Pour cette raison, la couche euphotique dans ces régions est relativement fine.

Les nutriments sont généralement apportés en Arctique par les masses d'eaux atlantiques et Pacifique ainsi que par ruissellement, depuis les continents (Fouest et al., 2013 ; Tremblay et al., 2015). Le phytoplancton est majoritairement limité en nutriments par les nitrates (Tremblay & Gagnon, 2009). Les nutriments au voisinage de la surface de l'océan Arctique sont influencés, au premier ordre par sa stratification, elle-même influencée par la banquise (Aagaard et Carmack, 1989). En hiver, le rejet de saumure dans l'océan associé à la croissance de la banquise, entraîne un mélange des eaux de surface et diminue la stratification. La profonde couche de mélange permet de puiser des nutriments dans la couche de subsurface et de restaurer les stocks de nutriments au voisinage de la surface. En été, la fonte de la banquise injecte de l'eau douce dans l'océan ce qui augmente sa stratification. En raison de la faiblesse du mélange vertical, l'apport vertical de nutriments est très faible. Ce cycle saisonnier de la disponibilité en nutriments à la surface de l'océan est cependant très simplifié, de nombreux autres processus plus complexes interviennent sur la disponibilité en nutriment à la surface de l'océan (Tremblay et al., 2015 ; Tremblay & Gagnon, 2009).

Par conséquent, La variabilité saisonnière du phytoplancton arctique est largement influencée par le cycle saisonnier de la banquise.

4.2 Observation du phytoplancton arctique

Il existe différents moyens de mesurer l'abondance et l'activité du plancton marin. En Arctique, la mesure est gênée par la présence de glace.

L'analyse des données de couleur de l'eau, issues des satellites, informe sur la quantité de plancton présente en surface. Le phytoplancton contient des pigments comme la chlorophylle qui lui permet de pratiquer la photosynthèse. Ces pigments impactent le spectre du rayonnement

solaire réfléchi par l'océan. En étudiant comment le spectre du rayonnement solaire est impacté lorsqu'il est réfléchi par la surface de l'océan, il est possible d'avoir une information sur la concentration en chlorophylle des océans, et donc à la quantité de phytoplancton (Sarmiento & Gruber, 2006). Il existe de nombreux algorithmes pour déterminer la concentration en chlorophylle ou la production primaire à partir de la couleur de l'eau (voir par exemple Babin et al., 2015 ; Lee et al., 2015). Les données de production primaire ou de concentration en chlorophylle dérivées des mesures satellites de la couleur de l'eau permettent une étude du phytoplancton sur de larges échelles spatiales et temporelles. Les mesures in situ ne sont que ponctuelles et il est parfois difficile, voire impossible, de réaliser des mesures dans certaines zones (Hill et al., 2013 ; Matrai et al., 2013).

En Arctique, les mesures par satellite révèlent de larges valeurs de production primaire en zone d'eau libre (Fig. 15a). Ces valeurs sont plus faibles d'un ordre de grandeur dans la zone de banquise saisonnière. La distribution spatiale de la concentration en chlorophylle (Fig. 15b) est à peu près similaire à celle de la production primaire avec des valeurs plus faibles en bordure de banquise qu'en zone d'eau libre et des valeurs maximales près des continents. Cette similarité entre distribution spatiale de production primaire et de chlorophylle pourrait néanmoins dériver de l'origine commune des données (Pabi et al., 2008).

La mesure par satellite présente néanmoins un certain nombre de limites. Tout d'abord, la chlorophylle n'est pas le seul élément à impacter la couleur de l'eau. Les sédiments et la matière organique en suspension peuvent aussi être responsables d'un changement dans le spectre d'irradiance reçu par le satellite. Notamment aux embouchures des rivières, où la production primaire est remarquablement élevée (Fig. 15a). Dans ces zones, l'eau est souvent turbide et de nombreuses particules colorant l'océan (CDOM) sont apportées par les rivières (Matsuoka et al., 2011). De plus, il est impossible de mesurer la couleur de l'eau sous la banquise, ainsi la zone de glace pérenne ne comporte pas de mesure par satellite de la couleur de l'eau (Fig. 15).

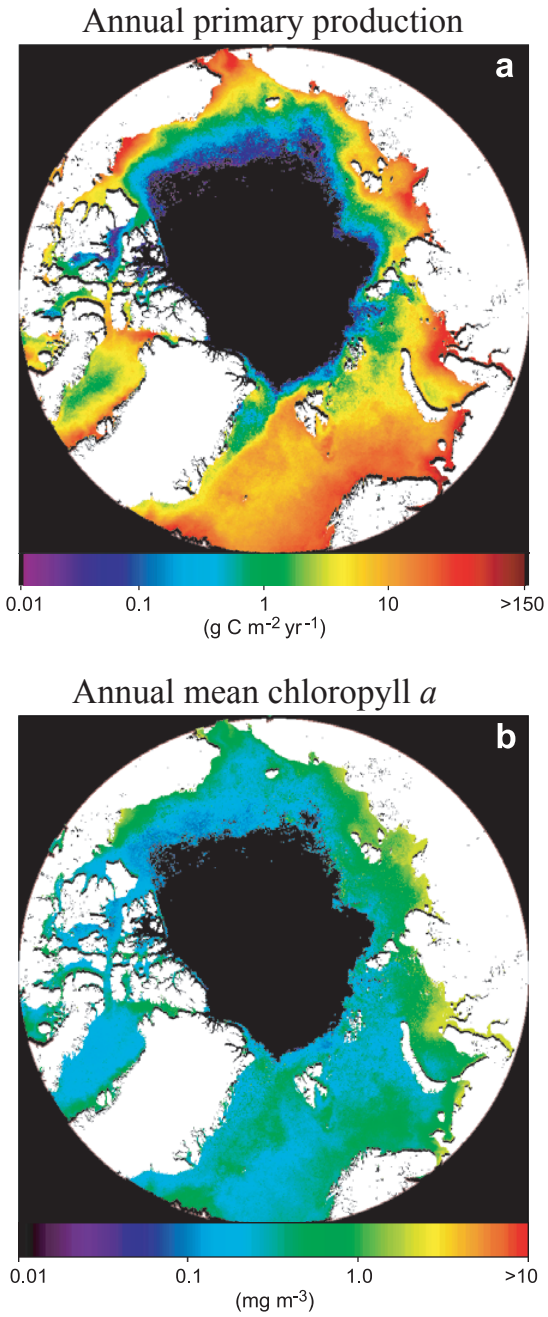

Figure 15 : Carte des moyennes annuelles des marqueurs de l'activité du plancton arctique : production primaire (a) ; concentration en chlorophylle a (b) obtenue par mesure satellite de couleur de l'eau ; et carte de la durée de la prériode d'eau libre estimée lorsque les mesures satellites de concentration en banquise dépassent 10% (c). Les cartes ont été réalisées sur la période 1998-2006 (issue de Pabi et al., 2008).

Pour les mêmes raisons, il est aussi probable que les données de production primaire ou de concentration en chlorophylle soient sous-estimées dans la zone saisonnière. De plus, la mesure de la couleur de l'eau se basant sur l'étude du rayonnement réfléchie, est impossible durant la nuit polaire. Ceci empêche d'avoir une information complète sur le cycle saisonnier du phytoplancton arctique à partir des mesures sattelites. De même, la mesure de la couleur de l'eau est impossible lorsque la nébulosité est forte, ce qui est souvent le cas en Arctique (Intrieri et al. 2002).

La mesure par satellite a tout de même permis de mettre en évidence les efflorescences de bord de glace (Fig. 16 ; Perrette et al., 2011). Ce développement intense du phytoplancton en bordure de glace quelques semaines après la fonte de la banquise a pu aussi être observé lors de nombreuses campagnes en mer en différentes régions de l'Arctique (Alexander & Niebauer, 1981 ; Hill et al., 2005 ; Randelhoff et al., 2019 ; Tremblay et al., 2006). Ces efflorescences, qui arrivent généralement une vingtaine de jours après la fonte (Perrette et al., 2011), sont attribuées à : (i) la forte stratification mise en place pendant la fonte associée à la forte quantité de nutriments stockés pendant l'hiver qui sont à l'origine d'une forte concentration en chlorophylle au niveau de la bordure de glace (Alexander & Niebauer, 1981) ; (ii) à l'augmentation de la disponibilité en lumière au moment du retrait de la banquise (Hill et al., 2005) ; (iii) et à la libération des algues de glace et du matériel associé lors de la fonte de la banquise qui permet d'ensemencer l'efflorescence de phytoplancton (Vancoppenolle et al., 2013). La courte durée de vie de cette efflorescence est attribuée à la consommation rapide des nutriments par le phytoplancton et à l'absence d'apport vertical (Perrette et al., 2011).

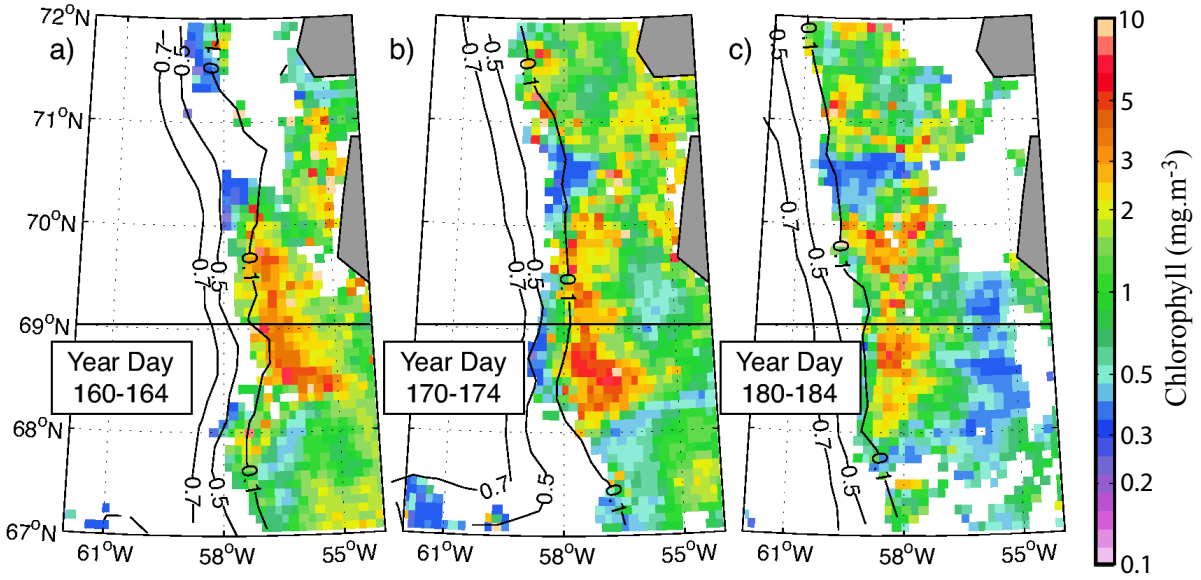

Figure 16 : Carte de concentration en chlorophylle à l'ouest du Groenland, en mer de Baffin, obtenue à partir de données satellites révélant une efflorescence de bord de glace. Les trois cartes ont été prises à 5 jours d'intervalle chacune. Les contours noirs représentent la concentration de glace à 10% ; 50% et 70% obtenues par satellite. Les zones blanches sont des zones ou les données de concentration en chlorophylle étaient manquantes (Perrette et al., 2011).

Vu le faible éclairement sous la glace, et en l'absence d'observations indiquant une activité planctonique sous la glace, on a longtemps considéré une telle activité comme quantité négligeable dans les calculs de production primaire de grande échelle (voir par exemple Pabi et al., 2008). Pourtant, les mesures effectuées lors d'un certain nombre de campagnes (Mundy et al., 2009 ; Fortier et al., 2002 ; Arrigo et al., 2012) ont mis en lumière la présence d'efflorescence de plancton sous la banquise. C'est le cas notamment de la campagne ICESCAPE (Impacts of Climate on EcoSystems and Chemistry of the Arctic Pacific Environment) en 2011 réalisée au niveau de la plateforme continentale de la mer des Tchouktches qui a révélé une efflorescence de phytoplancton dans une zone quasiment couverte à 100% de banquise de première année en partie couverte de mares de fonte (Fig. 17 ; Arrigo et al., 2012 ; Arrigo et al., 2014).

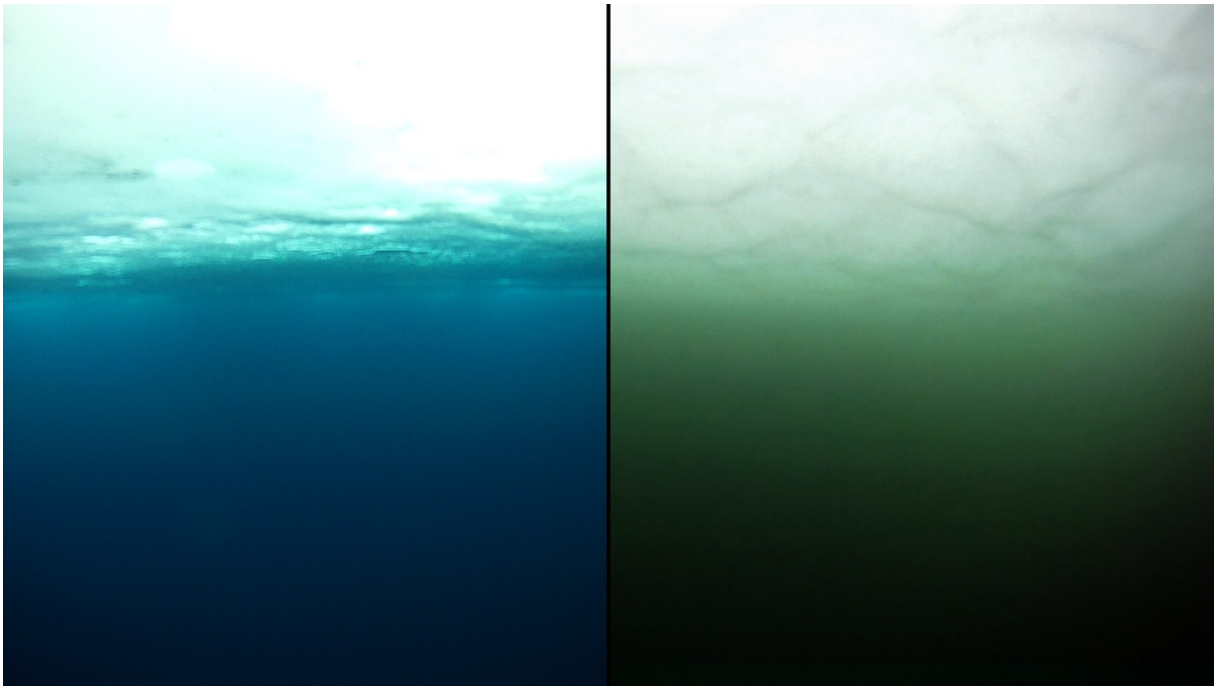

Figure 17 : Photographie mettant en évidence une efflorescence sous glace réalisée en 2011 lors de la campagne ICESCAPE en mer des Tchouktches. La photo de gauche montre un environnement sous glace typique en Arctique. La photo de droite a été prise lors de la campagne de 2011 sans retouche de couleur. La couleur verte que prend l'océan témoigne de la forte concentration de phytoplancton présent sous la banquise. (Photographie réalisée par la NASA).

La zone de plateforme continentale de la mer des Tchouktches est pourtant généralement caractérisée par une faible production primaire (Palmer et al., 2014), malgré un apport important de nutriments par les continents (Lowry et al., 2014). Ce type d'efflorescence a été attribué à l'augmentation importante de lumière disponible pour le phytoplancton au moment de la fonte, lorsque la neige fond, la banquise s'affine et se couvre de mares de fonte (Arrigo et al., 2014 ; Horvat et al., 2017 ; Mundy et al., 2014). Des mesures d'irradiance sous les mares de fonte ont d'ailleurs révélé des valeurs quatre fois supérieures aux valeurs prises sous la glace nue environnante (Arrigo et al., 2014 ; Frey et al., 2011). La nouvelle disponibilité en lumière due aux mares de fonte et la forte disponibilité en nutriments apportés par le continent permettraient au phytoplancton de se développer avant le retrait de la glace. Lorsque la banquise se retire, les nutriments ont déjà été en partie consommés et l'efflorescence est quasiment finie, révélant des valeurs faibles de production primaire lors des mesures par satellites. Il a été estimé que ce

genre d'efflorescence avait lieu tous les ans dans cette région au moins depuis 1998 (Lowry et al., 2014). Comprendre l'étendue spatiale et temporelle de ces efflorescences est fondamentale car ceux-ci ont un large impact sur la production primaire totale annuelle de l'Arctique (Palmer et al., 2014).

D'autres organismes photosynthétiques non détectés par les satellites qui contribuent pourtant en partie à la production primaire arctique (entre 2 et 15% de la PP arctique ; Legendre et al, 1992) sont les algues de glace, dites algues sympagiques. (Fig. 18) Les algues sympagiques se développent à l'interface des cristaux de glace, dans la saumure, généralement proche de la base où les conditions environnementales sont stables et où les échanges de nutriments avec l'océan sous-jacent sont possibles (Arrigo, 2016). Les efflorescences d'algues de glace se produisent généralement au printemps avant les efflorescences de phytoplancton (Ji et al., 2013 ; Leu et al., 2011, 2015).

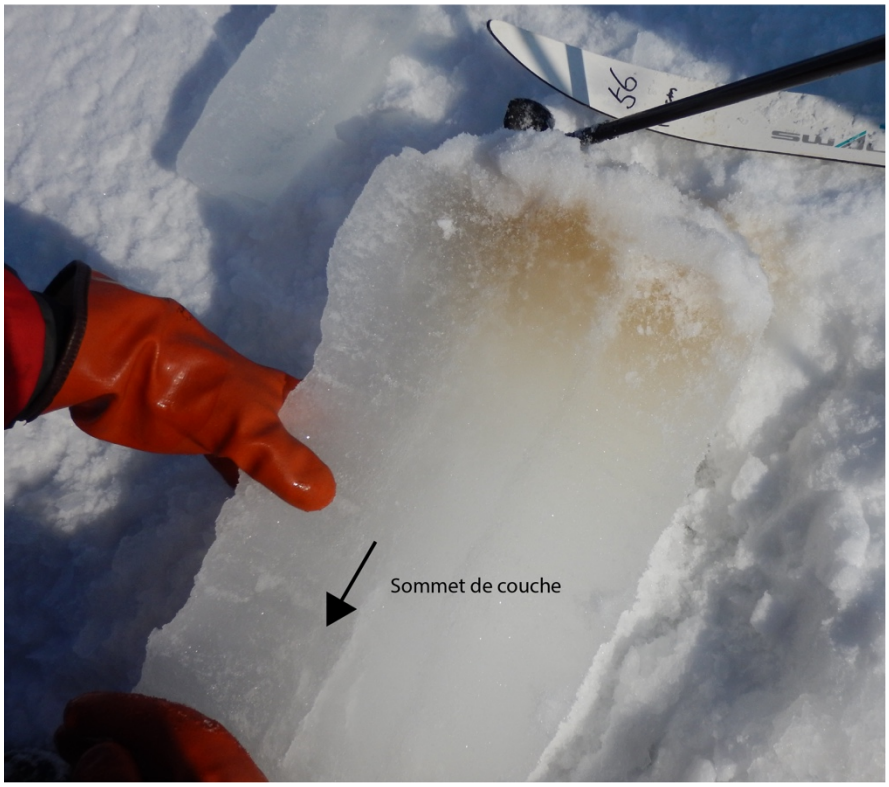

Figure 18 : Photographie d'un morceau de banquise dont la base est composée d'algues de glace (couleur marron) réalisée lors de la campagne à Hokkaido (SLOPE) en février 2019 (cf. Nomura et al, 2019 ou annexe pour plus de détail.).

Le phytoplancton arctique est influencé par la présence de banquise qui atténue une partie du rayonnement solaire incident et qui influence le mélange vertical, propice à l'apport en nutriments. La banquise arctique subit depuis ces dernières décennies de profonds changements, influencés par le changement climatique. Il est naturel de s'interroger sur la réponse du phytoplancton à ces changements et sur l'évolution future du phytoplancton dans un contexte de réchauffement global.

4.3 Réponse du phytoplancton au changement climatique

En raison du lien étroit entre phytoplancton et banquise, la réduction de la banquise arctique ces dernières décennies ainsi que l'augmentation globale de la période d'eau libre devrait avoir majoritairement influencé l'évolution du phytoplancton. Les mesures satellites de la couleur de l'eau, effectuées depuis 1997, montrent une augmentation globale de la production primaire arctique (Arrigo & van Dijken, 2011, 2015 ; Bélanger et al., 2013 ; Pabi et al., 2008) fortement corrélée à l'augmentation de la période d'eau libre (Fig. 19 ; Arrigo & van Dijken, 2011, 2015).

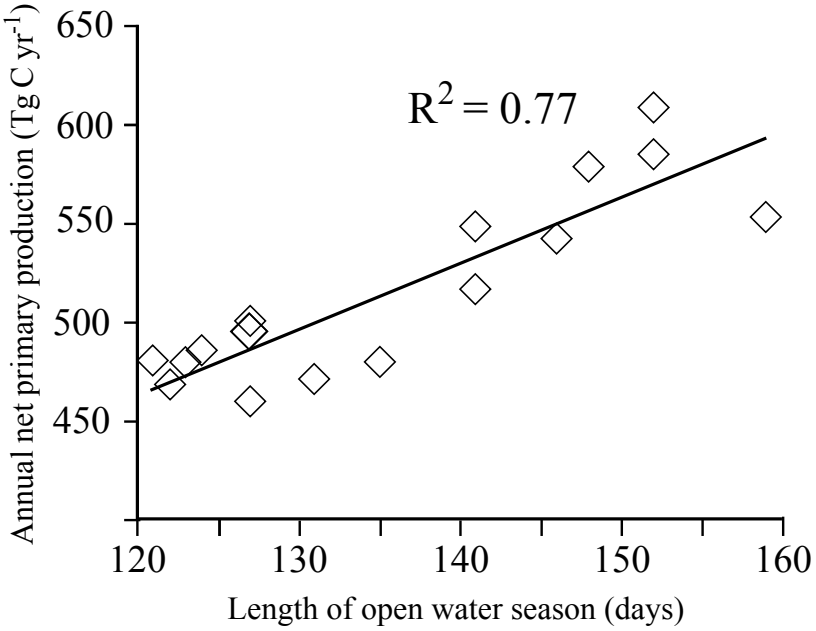

Figure 19 : Évolution de la production primaire annuelle mesure par satellite entre en fonction de la longueur de la période d'eau libre (Arrigo et al., 2015).

Cette augmentation est attribuée à l'augmentation en lumière disponible pour la croissance du phytoplancton en réponse au retrait de la banquise (Arrigo & van Dijken, 2011) ; ainsi qu'au nouvel apport de nutriments dans certaines régions (Arrigo & van Dijken, 2015). Ces résultats sont tout de même à prendre avec précaution. En effet, la mesure satellite peut grandement sous-estimer la production primaire en raison de l'absence de mesure sous et dans la banquise. De plus, l'augmentation de production primaire en Arctique peut être fortement induite par l'augmentation des apports de sédiments colorés par les rivières (Arrigo et al., 2015).

Face au futur retrait de la banquise arctique projetée par les modèles du système Terre et la disparition systématique de la banquise d'été au milieu de ce siècle, les efflorescences de phytoplancton et d'algues de glace sont vouées à changer. Une augmentation de la production primaire arctique pourrait être attendue dans les prochaines décennies en réponse à l'augmentation en lumière induite par la disparition progressive de la banquise (Tedesco et al., 2019). Néanmoins l'évolution du phytoplancton arctique n'est pas seulement contrôlée par la disponibilité en lumière, mais aussi par la disponibilité en nutriment et par la stratification (Tremblay et Gagnon 2009). De plus, la lumière n'est pas forcément amenée à augmenter partout en Arctique. Deux types de paramètres contrôlant la réponse du phytoplancton au réchauffement climatique peuvent être distingués (Wassmann & Reigstad, 2011):

(i) Les paramètres favorisant une augmentation de la production primaire arctique, tels que : l'augmentation en lumière disponible à la surface de l'océan en raison du retrait de la banquise ; l'apport épisodique de nutriment par upwelling lors des tempêtes d'automne favorisées par l'augmentation des zones d'eau libre (Ardyna et al., 2014) ; l'augmentation de l'apport des nutriments par les rivières.

(ii) Les paramètres favorisant une diminution de la production primaire arctique, tels que : l'augmentation de la stratification par l'apport d'eau douce induit par la fonte de la banquise et des glaces continentales. La diminution en lumière dans les régions

côtières en raison de l'augmentation de l'apport de sédiment par les rivières rendant les eaux turbides. La diminution en lumière induite par l'augmentation du couvert nuageux (Bélanger et al., 2013).

Le retrait plus précoce de la banquise devrait influencer la temporalité des efflorescences algales arctique. (Ji et al., 2013 ; Leu et al., 2015). Néanmoins, le signe et l'intensité de ce changement sont sujet à de fortes incertitudes (Popova et al, 2012). Yool (2015) montre par exemple que si la production primaire dans l'océan Arctique devrait augmenter en raison de l'augmentation de la disponibilité en lumière, celle de l'Atlantique Nord devrait diminuer en raison de l'augmentation de la stratification selon les projections des modèles du climat. De même, l'intercomparaison des modèles du système Terre CMIP5 montre des projections concernant l'évolution de la production primaire arctique très variable selon les modèles (Fig. 20,Vancoppenolle et al., 2013). Si tous les modèles s'accordent sur une augmentation de la production primaire dans la première partie de ce siècle, certains modèles prévoient, ensuite, une diminution plus ou moins importante de la production primaire à partir de 2050 une fois que les nutriments ont été consommés. D'autres modèles, non limités en nutriments, prévoient que l'augmentation du début du siècle est vouée à continuer.

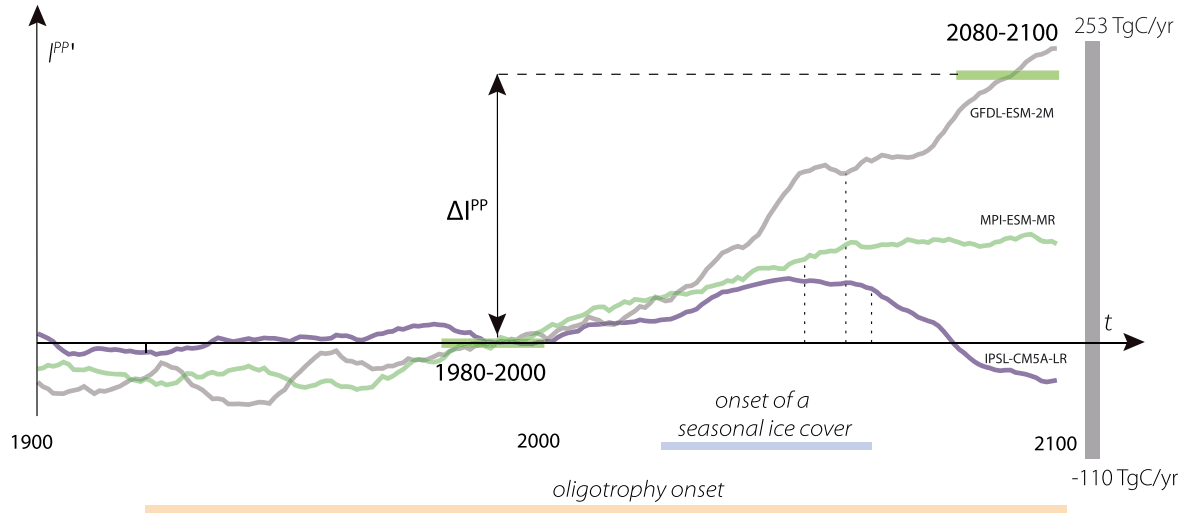

Figure 20 : Évolution typique des anomalies en production primaire intégrée arctiques (TgC/yr) durant la période 1900-2100 simulée par trois modèles de l'ensemble CMIP5.

Objectifs de cette thèse

Cette thèse vise à mieux comprendre la dynamique du phytoplancton dans la zone de banquise arctique en se focalisant sur l'interaction entre banquise, lumière et phytoplancton. Les lacunes concernant nos connaissances sur ces interactions m'ont amenée aux trois grandes problématiques discutées dans la suite de cette thèse.

Concernant la saisonnalité de la banquise, les grandes tendances de son évolution dans les données d'observations et les projections climatiques semblent converger vers un allongement de la période d'eau libre, renforcé par la rétroaction d'albédo. De plus, les évolutions récentes des diagnostics de saisonnalité, tels que la période d'eau libre, le jour d'avancée et de retrait de la glace de mer, sont, aujourd'hui bien documentés. Néanmoins, les mécanismes d'évolution n'ont pas été étudiés de façon systématique, en particulier quant à la dynamique du retrait et de l'avancée de la glace.

Quels sont les mécanismes des changements à venir pour la saisonnalité de la banquise arctique ?

La compréhension du transfert radiatif dans la zone de glace est fondamentale pour prévoir l'évolution du plancton. Le transfert radiatif dans la zone de glace est influencé à la fois par des paramètres de très fine échelle (densité de neige, poches de saumure …) et de plus grande échelle (épaisseur de glace, présence de mare de fonte…). Les observations du rayonnement transmis au travers de la banquise ont, longtemps, été rares. Pour cette raison, de nombreux modèles sont aujourd'hui mal contraints et ont une représentation biaisée du rayonnement transmis à la surface de l'océan en zone de banquise, influençant la thermodynamique de l'océan ainsi que la croissance du phytoplancton.

Les nouvelles observations de rayonnement transmis au travers de la banquise peuvent-elle permettre d'améliorer le transfert radiatif des zones de glace dans le modèle du système Terre tant en intensité du rayonnement transmis qu'en qualité du spectre ?

La croissance du phytoplancton est étroitement liée à la croissance et la fonte de la banquise. Les observations par satellite du phytoplancton arctique montrent une augmentation récente du phytoplancton fortement corrélée à la période d'eau libre, largement attribué à l'augmentation en lumière causée par la fonte. Néanmoins, l'observation récente d'efflorescences de phytoplancton sous la banquise remet en question ce lien très fort entre période d'eau libre et lumière disponible pour la croissance du phytoplancton.

Est-il possible de mieux définir la saisonnalité de la lumière disponible pour le phytoplancton dans les régions arctiques couverte de glace et de comprendre comment cette saisonnalité affecte le phytoplancton ?

Dans les prochains chapitres de cette thèse, je discute de ces trois problématiques et tente d'apporter de nouvelles connaissances quant aux interactions entre banquise, lumière, phytoplancton en Arctique. Pour cela, je m'intéresse d'abord à la saisonnalité de la banquise, en grande partie induite par l'évolution saisonnière du rayonnement solaire. Puis, j'étudie comment la banquise influence le rayonnement transmis à la surface de l'océan. Enfin, je cherche à mieux caractériser les impacts du couple banquise-lumière sur le phytoplancton Arctique.

Dans un premier chapitre, je discute de l'évolution globale présente et future des diagnostics de saisonnalité de la banquise est des mécanismes thermodynamiques associés à cette évolution. Pour cela, je m'appuie à la fois sur des données satellites et des projections climatiques d'un ensemble de modèles de CMIP5. Dans un second chapitre, je discute des valeurs des paramètres

de la loi de Beer Lambert, ainsi que du fractionnement en longueur d'onde du rayonnement transmis sous la banquise. Je m'appuie sur une étude de donnée in situ à partir de nouvelle observation de l'optique de la banquise pour mieux contraindre le modèle de l'IPSL. Enfin dans un dernier chapitre je cherche à mieux diagnostiquer la saisonnalité de la lumière disponible dans les régions englacées arctiques. Je cherche aussi à comprendre comment cette saisonnalité impacte le phytoplancton dans les modèles biogéochimiques. Les progrès dans nos connaissances suite à ces trois études sont significatifs, mais les limitations restent nombreuses, ce que je détaillerai dans mes conclusions.

Références

Aagaard, K., & Carmack, E. C. (1989). The role of sea ice and other fresh water in the Arctic circulation. *Journal of Geophysical Research: Oceans*, *94*(C10), 14485–14498. https://doi.org/10.1029/JC094iC10p14485

Alexander, V., & Niebauer, H. J. (1981). Oceanography of the eastern Bering Sea ice-edge zone in spring1. *Limnology and Oceanography*, *26*(6), 1111–1125. https://doi.org/10.4319/lo.1981.26.6.1111

Ardyna, M., Babin, M., Gosselin, M., Devred, E., Rainville, L., & Tremblay, J.-É. (2014). Recent Arctic Ocean sea ice loss triggers novel fall phytoplankton blooms. *Geophysical Research Letters*, *41*(17), 2014GL061047. https://doi.org/10.1002/2014GL061047

Arrigo, K. R. (2016). Sea ice as a habitat for primary producers. In *Sea Ice* (pp. 352–369). John Wiley & Sons, Ltd. https://doi.org/10.1002/9781118778371.ch14

Arrigo, K. R., & van Dijken, G. L. (2011). Secular trends in Arctic Ocean net primary production. *Journal of Geophysical Research: Oceans*, *116*(C9). https://doi.org/10.1029/2011JC007151

Arrigo, K. R., & van Dijken, G. L. (2015). Continued increases in Arctic Ocean primary production. *Progress in Oceanography*, *136*, 60–70. https://doi.org/10.1016/j.pocean.2015.05.002

Arrigo, K. R., Sullivan, C. W., & Kremer, J. N. (1991). A bio-optical model of Antarctic sea ice. *Journal of Geophysical Research: Oceans*, *96*(C6), 10581–10592. https://doi.org/10.1029/91JC00455

Arrigo, K. R., Perovich, D. K., Pickart, R. S., Brown, Z. W., Dijken, G. L. van, Lowry, K. E., et al. (2012). Massive Phytoplankton Blooms Under Arctic Sea Ice. *Science*, *336*(6087), 1408–1408. https://doi.org/10.1126/science.1215065

Arrigo, K. R., Perovich, D. K., Pickart, R. S., Brown, Z. W., van Dijken, G. L., Lowry, K. E., et al. (2014). Phytoplankton blooms beneath the sea ice in the Chukchi sea. *Deep Sea Research Part II: Topical Studies in Oceanography*, *105*, 1–16. https://doi.org/10.1016/j.dsr2.2014.03.018

Assmy, P., Fernández-Méndez, M., Duarte, P., Meyer, A., Randelhoff, A., Mundy, C. J., et al. (2017). Leads in Arctic pack ice enable early phytoplankton blooms below snow-covered sea ice. *Scientific Reports*, *7*, srep40850. https://doi.org/10.1038/srep40850

Babin, M., Bélanger, S., Ellingsen, I., Forest, A., Le Fouest, V., Lacour, T., et al. (2015). Estimation of primary production in the Arctic Ocean using ocean colour remote sensing and coupled physical–biological models: Strengths, limitations and how they compare. *Progress in Oceanography*, *139*, 197–220. https://doi.org/10.1016/j.pocean.2015.08.008

Barnhart, K. R., Miller, C. R., Overeem, I., & Kay, J. E. (2016). Mapping the future expansion of Arctic open water. *Nature Climate Change*, *6*(3), 280–285. https://doi.org/10.1038/nclimate2848

Behrenfeld, M. J., Randerson, J. T., McClain, C. R., Feldman, G. C., Los, S. O., Tucker, C. J., et al. (2001). Biospheric Primary Production During an ENSO Transition. *Science*, *291*(5513), 2594–2597. https://doi.org/10.1126/science.1055071

Bélanger, S., Babin, M., & Tremblay, J.-É. (2013). Increasing cloudiness in Arctic damps the increase in phytoplankton primary production due to sea ice receding. *Biogeosciences*, *10*(6), 4087–4101. https://doi.org/10.5194/bg-10-4087-2013

Bitz, C. M., & Roe, G. H. (2004). A Mechanism for the High Rate of Sea Ice Thinning in the Arctic Ocean. *Journal of Climate*, *17*(18), 3623–3632. https://doi.org/10.1175/1520-0442(2004)017<3623:AMFTHR>2.0.CO;2

Briegleb, P., & Light, B. (2007). A Delta-Eddington Mutiple Scattering Parameterization for

Solar Radiation in the Sea Ice Component of the Community Climate System Model. https://doi.org/10.5065/D6B27S71

Cavalieri, D. J., & Parkinson, C. L. (2012). Arctic sea ice variability and trends, 1979–2010. *The Cryosphere*, *6*(4), 881–889. https://doi.org/10.5194/tc-6-881-2012

Fortier, M., Fortier, L., Michel, C., & Legendre, L. (2002). Climatic and biological forcing of vertical flux and biogenic particles under seasonal Arctic sea ice. *Marine Ecology-Progress Series*, *225*, 1–16. https://doi.org/10.3354/meps225001

Fouest, V. L., Babin, M., & Tremblay, J.-É. (2013). The fate of riverine nutrients on Arctic shelves. *Biogeosciences*, *10*(6), 3661–3677. https://doi.org/10.5194/bg-10-3661-2013

France, J. L., Reay, H. J., King, M. D., Voisin, D., Jacobi, H. W., Domine, F., et al. (2012). Hydroxyl radical and NOx production rates, black carbon concentrations and light-absorbing impurities in snow from field measurements of light penetration and nadir reflectivity of onshore and offshore coastal Alaskan snow. *Journal of Geophysical Research: Atmospheres*, *117*(D14), D00R12. https://doi.org/10.1029/2011JD016639

Frey, K. E., Perovich, D. K., & Light, B. (2011). The spatial distribution of solar radiation under a melting Arctic sea ice cover. *Geophysical Research Letters*, *38*(22). https://doi.org/10.1029/2011GL049421

Gregg, W. W., Conkright, M. E., Ginoux, P., O'Reilly, J. E., & Casey, N. W. (2003). Ocean primary production and climate: Global decadal changes. *Geophysical Research Letters*, *30*(15). https://doi.org/10.1029/2003GL016889

Grenfell, T. C., & Maykut, G. A. (1977). The Optical Properties of Ice and Snow in the Arctic Basin *. *Journal of Glaciology*, *18*(80), 445–463. https://doi.org/10.3189/S0022143000021122

Haas, C. (2016). Sea ice thickness distribution. In *Sea Ice* (pp. 42–64). John Wiley & Sons, Ltd. https://doi.org/10.1002/9781118778371.ch2

Hibler, W. D. (1979). A Dynamic Thermodynamic Sea Ice Model. *Journal of Physical Oceanography*, *9*(4), 815–846. https://doi.org/10.1175/1520-0485(1979)009<0815:ADTSIM>2.0.CO;2

Hill, V., Cota, G., & Stockwell, D. (2005). Spring and summer phytoplankton communities in the Chukchi and Eastern Beaufort Seas. *Deep Sea Research Part II: Topical Studies in Oceanography*, *52*(24), 3369–3385. https://doi.org/10.1016/j.dsr2.2005.10.010

Hill, V. J., Matrai, P. A., Olson, E., Suttles, S., Steele, M., Codispoti, L. A., & Zimmerman, R. C. (2013). Synthesis of integrated primary production in the Arctic Ocean: II. In situ and remotely sensed estimates. *Progress in Oceanography*, *110*, 107–125. https://doi.org/10.1016/j.pocean.2012.11.005

Horvat, C., Jones, D. R., Iams, S., Schroeder, D., Flocco, D., & Feltham, D. (2017). The frequency and extent of sub-ice phytoplankton blooms in the Arctic Ocean. *Science Advances*, *3*(3), e1601191. https://doi.org/10.1126/sciadv.1601191

Intrieri, J. M., Fairall, C. W., Shupe, M. D., Persson, P. O. G., Andreas, E. L., Guest, P. S., & Moritz, R. E. (2002). An annual cycle of Arctic surface cloud forcing at SHEBA. *Journal of Geophysical Research: Oceans*, *107*(C10), SHE 13-1-SHE 13-14. https://doi.org/10.1029/2000JC000439

Järvinen, O., & Leppäranta, M. (2011). Transmission of solar radiation through the snow cover on floating ice. *Journal of Glaciology*, *57*(205), 861–870. https://doi.org/10.3189/002214311798043843

Ji, R., Jin, M., & Varpe, Ø. (2013). Sea ice phenology and timing of primary production pulses in the Arctic Ocean. *Global Change Biology*, *19*(3), 734–741. https://doi.org/10.1111/gcb.12074

Johnson, M., & Eicken, H. (2016). Estimating Arctic sea-ice freeze-up and break-up from the satellite record: A comparison of different approaches in the Chukchi and Beaufort Seas.

Elem Sci Anth, *4*(0). https://doi.org/10.12952/journal.elementa.000124
Katlein, C., Arndt, S., Nicolaus, M., Perovich, D. K., Jakuba, M. V., Suman, S., et al. (2015). Influence of ice thickness and surface properties on light transmission through Arctic sea ice. *Journal of Geophysical Research: Oceans*, *120*(9), 5932–5944. https://doi.org/10.1002/2015JC010914
Katlein, C., Schiller, M., Belter, H. J., Coppolaro, V., Wenslandt, D., & Nicolaus, M. (2017). A New Remotely Operated Sensor Platform for Interdisciplinary Observations under Sea Ice. *Frontiers in Marine Science*, *4*. https://doi.org/10.3389/fmars.2017.00281
Kwok, R., & Rothrock, D. A. (2009). Decline in Arctic sea ice thickness from submarine and ICESat records: 1958–2008. *Geophysical Research Letters*, *36*(15), L15501. https://doi.org/10.1029/2009GL039035
Kwok, R., Spreen, G., & Pang, S. (2013). Arctic sea ice circulation and drift speed: Decadal trends and ocean currents. *Journal of Geophysical Research: Oceans*, *118*(5), 2408–2425. https://doi.org/10.1002/jgrc.20191
Lebrun, M., Vancoppenolle, M., Madec, G., & Massonnet, F. (2019). Arctic sea-ice-free season projected to extend into autumn. *The Cryosphere*, *13*(1), 79–96. https://doi.org/10.5194/tc-13-79-2019
Lee, Y. J., Matrai, P. A., Friedrichs, M. A. M., Saba, V. S., Antoine, D., Ardyna, M., et al. (2015). An assessment of phytoplankton primary productivity in the Arctic Ocean from satellite ocean color/in situ chlorophyll-a based models. *Journal of Geophysical Research: Oceans*, *120*(9), 6508–6541. https://doi.org/10.1002/2015JC011018
Legendre, L., Martineau, M.-J., Therriault, J.-C., & Demers, S. (1992). Chlorophyll a biomass and growth of sea-ice microalgae along a salinity gradient (southeastern Hudson Bay, Canadian Arctic). *Polar Biology*, *12*(3), 445–453. https://doi.org/10.1007/BF00243115
Leu, E., Søreide, J. E., Hessen, D. O., Falk-Petersen, S., & Berge, J. (2011). Consequences of changing sea-ice cover for primary and secondary producers in the European Arctic shelf seas: Timing, quantity, and quality. *Progress in Oceanography*, *90*(1), 18–32. https://doi.org/10.1016/j.pocean.2011.02.004
Leu, E., Mundy, C. J., Assmy, P., Campbell, K., Gabrielsen, T. M., Gosselin, M., et al. (2015). Arctic spring awakening – Steering principles behind the phenology of vernal ice algal blooms. *Progress in Oceanography*, *139*, 151–170. https://doi.org/10.1016/j.pocean.2015.07.012
Light, B., Grenfell, T. C., & Perovich, D. K. (2008). Transmission and absorption of solar radiation by Arctic sea ice during the melt season. *Journal of Geophysical Research: Oceans*, *113*(C3), C03023. https://doi.org/10.1029/2006JC003977
Lowry, K. E., van Dijken, G. L., & Arrigo, K. R. (2014). Evidence of under-ice phytoplankton blooms in the Chukchi Sea from 1998 to 2012. *Deep Sea Research Part II: Topical Studies in Oceanography*, *105*, 105–117. https://doi.org/10.1016/j.dsr2.2014.03.013
Madec Gurvan, Romain Bourdallé-Badie, Pierre-Antoine Bouttier, Clément Bricaud, Diego Bruciaferri, Daley Calvert, et al. (2017). NEMO ocean engine. https://doi.org/10.5281/zenodo.3248739
Marks, A. A., & King, M. D. (2014). The effect of snow/sea ice type on the response of albedo and light penetration depth (e-folding depth) to increasing black carbon. *The Cryosphere*, *8*(5), 1625–1638. https://doi.org/10.5194/tc-8-1625-2014
Markus, T., Stroeve, J. C., & Miller, J. (2009). Recent changes in Arctic sea ice melt onset, freezeup, and melt season length. *Journal of Geophysical Research: Oceans*, *114*(C12), C12024. https://doi.org/10.1029/2009JC005436
Massicotte, P., Bécu, G., Lambert-Girard, S., Leymarie, E., & Babin, M. (2018). Estimating Underwater Light Regime under Spatially Heterogeneous Sea Ice in the Arctic. Retrieved from https://hal.sorbonne-universite.fr/hal-01996826

Massonnet, F., Fichefet, T., Goosse, H., Bitz, C. M., Philippon-Berthier, G., Holland, M. M., & Barriat, P.-Y. (2012). Constraining projections of summer Arctic sea ice. *The Cryosphere*, *6*(6), 1383–1394. https://doi.org/10.5194/tc-6-1383-2012

Massonnet, François, Vancoppenolle, M., Goosse, H., Docquier, D., Fichefet, T., & Blanchard-Wrigglesworth, E. (2018). Arctic sea-ice change tied to its mean state through thermodynamic processes. *Nature Climate Change*, *8*(7), 599–603. https://doi.org/10.1038/s41558-018-0204-z

Matrai, P., Olson, E., Suttles, S., Hill, V., A. Codispoti, L., Light, B., & Steele, M. (2013). Synthesis of primary production in the Arctic Ocean: I. Surface waters, 1954-2007. *Progress in Oceanography*, *110*, 93–106. https://doi.org/10.1016/j.pocean.2012.11.004

Matsuoka, A., Hill, V., Huot, Y., Babin, M., & Bricaud, A. (2011). Seasonal variability in the light absorption properties of western Arctic waters: Parameterization of the individual components of absorption for ocean color applications. *Journal of Geophysical Research: Oceans*, *116*(C2). https://doi.org/10.1029/2009JC005594

Maykut, G. A., & Untersteiner, N. (1971). Some results from a time-dependent thermodynamic model of sea ice. *Journal of Geophysical Research*, *76*(6), 1550–1575. https://doi.org/10.1029/JC076i006p01550

Moreau, S., Vancoppenolle, M., Bopp, L., Aumont, O., Madec, G., Delille, B., et al. (2016). Assessment of the sea-ice carbon pump: Insights from a three-dimensional ocean-sea-ice biogeochemical model (NEMO-LIM-PISCES). *Elem Sci Anth*, *4*(0), 000122. https://doi.org/10.12952/journal.elementa.000122

Morel, A. (1988). Optical modeling of the upper ocean in relation to its biogenous matter content (case I waters). *Journal of Geophysical Research: Oceans*, *93*(C9), 10749–10768. https://doi.org/10.1029/JC093iC09p10749

Mundy, C. J., Gosselin, M., Ehn, J., Gratton, Y., Rossnagel, A., Barber, D. G., et al. (2009). Contribution of under-ice primary production to an ice-edge upwelling phytoplankton bloom in the Canadian Beaufort Sea. *Geophysical Research Letters*, *36*(17). https://doi.org/10.1029/2009GL038837

Mundy, C. J., Gosselin, M., Gratton, Y., Brown, K., Galindo, V., Campbell, K., et al. (2014). Role of environmental factors on phytoplankton bloom initiation under landfast sea ice in Resolute Passage, Canada. *Marine Ecology Progress Series*, *497*, 39–49. https://doi.org/10.3354/meps10587

Nicolaus, M., & Katlein, C. (2013). Mapping radiation transfer through sea ice using a remotely operated vehicle (ROV). *The Cryosphere*, *7*(3), 763–777. https://doi.org/10.5194/tc-7-763-2013

Nicolaus, M., Katlein, C., Maslanik, J., & Hendricks, S. (2012). Changes in Arctic sea ice result in increasing light transmittance and absorption. *Geophysical Research Letters*, *39*(24), L24501. https://doi.org/10.1029/2012GL053738

Nicolaus, Marcel, Hudson, S. R., Gerland, S., & Munderloh, K. (2010). A modern concept for autonomous and continuous measurements of spectral albedo and transmittance of sea ice. *Cold Regions Science and Technology*, *62*(1), 14–28. https://doi.org/10.1016/j.coldregions.2010.03.001

Nomura, D., Wongpan, P., Toyota, T., Tanikawa, T., Kawaguchi, Y.,Ono, T.,Ishino T.,Tozawa, M., TAMURA,T, P., Yabe I, S,. Son, E, Y., Vivier, F., Louranco, A., Lebrun, M,. Nosaka, Y., Hirawake, T., Ooki, A., Aoki, S., Else, B., Fripiat, F., Inoue, J., Vancoppenolle, M. (2019) Saroma-ko Lagoon Observations for sea ice Physico-chemistry and Ecosystems 2019 (SLOPE2019). In prep

Notz, D., & Bitz, C. M. (2016). Sea ice in Earth system models. In *Sea Ice* (pp. 304–325). John Wiley & Sons, Ltd. https://doi.org/10.1002/9781118778371.ch12

Pabi, S., van Dijken, G. L., & Arrigo, K. R. (2008). Primary production in the Arctic Ocean,

1998–2006. *Journal of Geophysical Research: Oceans*, *113*(C8). https://doi.org/10.1029/2007JC004578

Palmer, M. A., Saenz, B. T., & Arrigo, K. R. (2014). Impacts of sea ice retreat, thinning, and melt-pond proliferation on the summer phytoplankton bloom in the Chukchi Sea, Arctic Ocean. *Deep Sea Research Part II: Topical Studies in Oceanography*, *105*, 85–104. https://doi.org/10.1016/j.dsr2.2014.03.016

Parkinson, C. L. (2014). Spatially mapped reductions in the length of the Arctic sea ice season. *Geophysical Research Letters*, *41*(12), 4316–4322. https://doi.org/10.1002/2014GL060434

Parmentier, F.-J. W., Christensen, T. R., Sørensen, L. L., Rysgaard, S., McGuire, A. D., Miller, P. A., & Walker, D. A. (2013). The impact of lower sea-ice extent on Arctic greenhouse-gas exchange. *Nature Climate Change*, *3*(3), 195–202. https://doi.org/10.1038/nclimate1784

Payne, R. E. (1972). Albedo of the Sea Surface. *Journal of the Atmospheric Sciences*, *29*(5), 959–970. https://doi.org/10.1175/1520-0469(1972)029<0959:AOTSS>2.0.CO;2

Peixoto, J. P., & Oort, A. H. (1992). *Physics of Climate* (1992 ed.). New York: American Institute of Physics.

Perovich, D. K., Grenfell, T. C., Light, B., & Hobbs, P. V. (2002). Seasonal evolution of the albedo of multiyear Arctic sea ice. *Journal of Geophysical Research: Oceans*, *107*(C10), 8044. https://doi.org/10.1029/2000JC000438

Perovich, Donald K. (1996). *The Optical Properties of Sea Ice.* (No. MONO-96-1). COLD REGIONS RESEARCH AND ENGINEERING LAB HANOVER NH. Retrieved from https://apps.dtic.mil/docs/citations/ADA310586

Perovich, Donald K. (2016). Sea ice and sunlight. In *Sea Ice* (pp. 110–137). John Wiley & Sons, Ltd. https://doi.org/10.1002/9781118778371.ch4

Perovich, Donald K., Light, B., Eicken, H., Jones, K. F., Runciman, K., & Nghiem, S. V. (2007). Increasing solar heating of the Arctic Ocean and adjacent seas, 1979–2005: Attribution and role in the ice-albedo feedback. *Geophysical Research Letters*, *34*(19), L19505. https://doi.org/10.1029/2007GL031480

Perrette, M., Yool, A., Quartly, G. D., & Popova, E. E. (2011). Near-ubiquity of ice-edge blooms in the Arctic. *Biogeosciences*, *8*(2), 515–524. https://doi.org/10.5194/bg-8-515-2011

Popova, E. E., Yool, A., Coward, A. C., Dupont, F., Deal, C., Elliott, S., et al. (2012). What controls primary production in the Arctic Ocean? Results from an intercomparison of five general circulation models with biogeochemistry. *Journal of Geophysical Research: Oceans*, *117*(C8), C00D12. https://doi.org/10.1029/2011JC007112

Post, E., Bhatt, U. S., Bitz, C. M., Brodie, J. F., Fulton, T. L., Hebblewhite, M., et al. (2013). Ecological consequences of sea-ice decline. *Science (New York, N.Y.)*, *341*(6145), 519–524. https://doi.org/10.1126/science.1235225

Rampal, P., Weiss, J., Marsan, D., & Bourgoin, M. (2009). Arctic sea ice velocity field: General circulation and turbulent-like fluctuations. *Journal of Geophysical Research: Oceans*, *114*(C10). https://doi.org/10.1029/2008JC005227

Randelhoff, A., Oziel, L., Massicotte, P., Bécu, G., Galí, M., Lacour, L., et al. (2019). The evolution of light and vertical mixing across a phytoplankton ice-edge bloom. *Elem Sci Anth*, *7*(1), 20. https://doi.org/10.1525/elementa.357

Saenz, B. T., & Arrigo, K. R. (2012). Simulation of a sea ice ecosystem using a hybrid model for slush layer desalination. *Journal of Geophysical Research: Oceans*, *117*(C5). https://doi.org/10.1029/2011JC007544

Sarmiento, J. L., & Gruber, N. (2006). *Ocean Biogeochemical Dynamics*. Princeton University Press. Retrieved from https://www.jstor.org/stable/j.ctt3fgxqx

Semtner, A. J. (1976). A Model for the Thermodynamic Growth of Sea Ice in Numerical Investigations of Climate. *Journal of Physical Oceanography*, *6*(3), 379–389. https://doi.org/10.1175/1520-0485(1976)006<0379:AMFTTG>2.0.CO;2

Stammerjohn, S., Massom, R., Rind, D., & Martinson, D. (2012). Regions of rapid sea ice change: An inter-hemispheric seasonal comparison. *Geophysical Research Letters*, *39*(6), L06501. https://doi.org/10.1029/2012GL050874

Stefan, J. (1891). Ueber die Theorie der Eisbildung, insbesondere über die Eisbildung im Polarmeere. *Annalen Der Physik*, *278*(2), 269–286. https://doi.org/10.1002/andp.18912780206

Stroeve, J. C., Markus, T., Boisvert, L., Miller, J., & Barrett, A. (2014). Changes in Arctic melt season and implications for sea ice loss. *Geophysical Research Letters*, *41*(4), 2013GL058951. https://doi.org/10.1002/2013GL058951

Stroeve, Julienne C., Kattsov, V., Barrett, A., Serreze, M., Pavlova, T., Holland, M., & Meier, W. N. (2012). Trends in Arctic sea ice extent from CMIP5, CMIP3 and observations. *Geophysical Research Letters*, *39*(16), L16502. https://doi.org/10.1029/2012GL052676

Stroeve, Julienne C., Crawford, A. D., & Stammerjohn, S. (2016). Using timing of ice retreat to predict timing of fall freeze-up in the Arctic. *Geophysical Research Letters*, *43*(12), 2016GL069314. https://doi.org/10.1002/2016GL069314

Sverdrup, H. U. (1953). On Conditions for the Vernal Blooming of Phytoplankton. *ICES Journal of Marine Science*, *18*(3), 287–295. https://doi.org/10.1093/icesjms/18.3.287

Taylor, P. D., & Feltham, D. L. (2004). A model of melt pond evolution on sea ice. *Journal of Geophysical Research: Oceans*, *109*(C12). https://doi.org/10.1029/2004JC002361

Tedesco, L., Vichi, M., & Scoccimarro, E. (2019). Sea-ice algal phenology in a warmer Arctic. *Science Advances*, *5*(5), eaav4830. https://doi.org/10.1126/sciadv.aav4830

Tremblay, J.-É., & Gagnon, J. (2009). The effects of irradiance and nutrient supply on the productivity of Arctic waters: a perspective on climate change. In *Influence of Climate Change on the Changing Arctic and Sub-Arctic Conditions* (pp. 73–93). Springer, Dordrecht. https://doi.org/10.1007/978-1-4020-9460-6_7

Tremblay, J.-É., Michel, C., Hobson, K. A., Gosselin, M., & Price, N. M. (2006). Bloom dynamics in early opening waters of the Arctic Ocean. *Limnology and Oceanography*, *51*(2), 900–912. https://doi.org/10.4319/lo.2006.51.2.0900

Tremblay, J.-É., Anderson, L. G., Matrai, P., Coupel, P., Bélanger, S., Michel, C., & Reigstad, M. (2015). Global and regional drivers of nutrient supply, primary production and CO2 drawdown in the changing Arctic Ocean. *Progress in Oceanography*, *139*, 171–196. https://doi.org/10.1016/j.pocean.2015.08.009

Tremblay, L.-B., & Hakakian, M. (2006). Estimating the Sea Ice Compressive Strength from Satellite-Derived Sea Ice Drift and NCEP Reanalysis Data. *Journal of Physical Oceanography*, *36*(11), 2165–2172. https://doi.org/10.1175/JPO2954.1

Vancoppenolle, M., Bouillon, S., Fichefet, T., Goosse, H., Lecomte, O., Morales Maqueda, M. Á., & Madec, G. (2012). *The Louvain-la-Neuve sea Ice Model*.

Vancoppenolle, M., Bopp, L., Madec, G., Dunne, J., Ilyina, T., Halloran, P. R., & Steiner, N. (2013). Future Arctic Ocean primary productivity from CMIP5 simulations: Uncertain outcome, but consistent mechanisms. *Global Biogeochemical Cycles*, *27*(3), 605–619. https://doi.org/10.1002/gbc.20055

Vancoppenolle, M., Meiners, K. M., Michel, C., Bopp, L., Brabant, F., Carnat, G., et al. (2013). Role of sea ice in global biogeochemical cycles: emerging views and challenges. *Quaternary Science Reviews*, *79*, 207–230. https://doi.org/10.1016/j.quascirev.2013.04.011

Wang, M., & Overland, J. E. (2015). Projected future duration of the sea-ice-free season in the Alaskan Arctic. *Progress in Oceanography*, *136*, 50–59.

https://doi.org/10.1016/j.pocean.2015.01.001
Warren, S. G. (1982). Optical properties of snow. *Reviews of Geophysics*, *20*(1), 67–89. https://doi.org/10.1029/RG020i001p00067
Wassmann, P., & Reigstad, M. (2011). Future Arctic Ocean Seasonal Ice Zones and Implications for Pelagic-Benthic Coupling. *Oceanography*, *24*(3), 220–231. https://doi.org/10.5670/oceanog.2011.74
Weeks, W. F., Ackley, S. F., Research, C. R., & Laboratory (U.S.), E. (1982). *The growth, structure, and properties of sea ice*. [Hanover, N.H.] : US Army Corps of Engineers, Cold Regions Research & Engineering Laboratory. Retrieved from https://trove.nla.gov.au/version/26182528
Yool, A., Popova, E. E., & Coward, A. C. (2015). Future change in ocean productivity: Is the Arctic the new Atlantic? *Journal of Geophysical Research: Oceans*, *120*(12), 7771–7790. https://doi.org/10.1002/2015JC011167

Chapitre 1

Décalage futur de la saison d'eau libre arctique vers l'automne.

La croissance du phytoplancton arctique est gouvernée par la saisonnalité de la banquise au premier ordre. Comprendre l'évolution présente et future de cette saisonnalité et les mécanismes qui la contrôlent est fondamental dans l'étude des interactions entre banquise et phytoplancton.

La réduction récente de la banquise arctique s'accompagne d'un allongement de la période d'eau libre, avec des contributions comparables du retrait plus précoce et d'avancée plus tardive de la banquise. Suivant les projections de l'ensemble des modèles de CMIP5, je montre que la tendance absolue dans la date d'avancée de la banquise devrait progressivement dépasser et même doubler la tendance dans la date de retrait de la banquise. Ceci aurait pour conséquence un décalage vers l'automne de la saison d'eau libre. Je montre aussi dans ce chapitre qu'un tel décalage est contrôlé par la réponse thermodynamique de la banquise au réchauffement global. L'analyse de simulation d'un modèle de thermodynamique glace-océan idéalisé révèle le rôle de deux rétroactions saisonnières positives dans le décalage de la saison d'eau libre. La rétroaction d'été est responsable d'une avancée de banquise plus tardive d'environ 1,6 jour en réponse à un retrait plus précoce d'un jour. Ceci dû à la faculté qu'a l'océan d'absorber le rayonnement solaire plus efficacement qu'il n'est capable de relâcher la chaleur juste avant l'avancée de la banquise. La rétroaction d'hiver est faible en comparaison. Elle est responsable d'un retrait plus précoce d'environ 0,3 jour en réponse à un jour de décalage dans l'avancée de la banquise. Ceci dû à une saison de croissance plus courte qui implique une glace plus fine, qui par conséquent fond plus vite. Néanmoins, la rétroaction d'hiver est tempérée par la saison de croissance qui reste tout de même relativement longue et par la relation inverse entre taux de croissance et épaisseur de la banquise. A une échelle de temps interannuelle, la réponse thermodynamique de la saisonnalité de la banquise au réchauffement global est obscurcie par la variabilité interannuelle. Toutefois, à long terme, il existe peu d'incertitude entre les modèles quant au décalage vers l'automne de la saison d'eau libre. Ceci s'explique par le fait que tous

les mécanismes de rétroaction se rapportent à des éléments fondamentaux et stables du système climatique arctique.

The Cryosphere, 13, 79–96, 2019
https://doi.org/10.5194/tc-13-79-2019

The Cryosphere Open Access EGU

Arctic sea-ice-free season projected to extend into autumn

Marion Lebrun[1], **Martin Vancoppenolle**[1], **Gurvan Madec**[1], **and François Massonnet**[2,3]

[1]Sorbonne Université, LOCEAN-IPSL, CNRS/IRD/MNHN, Paris, France
[2]Earth and Life Institute, Université catholique de Louvain, Louvain-la-Neuve, Belgium
[3]Earth Sciences Department, Barcelona Supercomputing Center, Barcelona, Spain

Correspondence: Marion Lebrun (marion.lebrun@locean-ipsl.upmc.fr)

Received: 4 April 2018 – Discussion started: 2 May 2018
Revised: 12 December 2018 – Accepted: 14 December 2018 – Published: 10 January 2019

Abstract. The recent Arctic sea ice reduction comes with an increase in the ice-free season duration, with comparable contributions of earlier ice retreat and later advance. CMIP5 models all project that the trend towards later advance should progressively exceed and ultimately double the trend towards earlier retreat, causing the ice-free season to shift into autumn. We show that such a shift is a basic feature of the thermodynamic response of seasonal ice to warming. The detailed analysis of an idealised thermodynamic ice–ocean model stresses the role of two seasonal amplifying feedbacks. The summer feedback generates a 1.6-day-later advance in response to a 1-day-earlier retreat. The underlying physics are the property of the upper ocean to absorb solar radiation more efficiently than it can release heat right before ice advance. The winter feedback is comparatively weak, prompting a 0.3-day-earlier retreat in response to a 1-day shift towards later advance. This is because a shorter growth season implies thinner ice, which subsequently melts away faster. However, the winter feedback is dampened by the relatively long ice growth period and by the inverse relationship between ice growth rate and thickness. At interannual timescales, the thermodynamic response of ice seasonality to warming is obscured by inter-annual variability. Nevertheless, in the long term, because all feedback mechanisms relate to basic and stable elements of the Arctic climate system, there is little inter-model uncertainty on the projected long-term shift into autumn of the ice-free season.

1 Introduction

Arctic sea ice has strikingly declined in coverage (Cavalieri and Parkinson, 2012), thickness (Kwok and Rothrock, 2009; Renner et al., 2014; Lindsay and Schweiger, 2015) and age (Maslanik et al., 2011) over the last 4 decades. CMIP5 global climate and Earth system models simulate and project this decline to continue over the 21st century (Massonnet et al., 2012; Stroeve et al., 2012) due to anthropogenic CO_2 emissions (Notz and Stroeve, 2016), with a loss of multi-year ice estimated for 2040–2060 (Massonnet et al., 2012), in the case of a business-as-usual emission scenario.

Less Arctic sea ice also implies changes in ice seasonality, which are important to investigate because of socio-economic (e.g. on shipping; Smith and Stephenson, 2013) and ecosystem implications. Indeed, the length of the Arctic sea ice season exerts a first-order control on the light reaching phytoplankton (Arrigo and van Dijken, 2011; Wassmann and Reigstad, 2011; Assmy et al., 2017) and is crucial to some marine mammals, such as walruses (Laidre et al., 2015) and polar bears (Stern and Laidre, 2016), who use sea ice as a living platform.

Various seasonality diagnostics are discussed in the sea ice literature and definitions as well as approaches vary among authors. The open-water season duration can be diagnosed from satellite ice concentration fields, either as the number of ice-free days (Parkinson, 2014) or as the time elapsed between ice retreat and advance dates, corresponding to the day of the year when ice concentration exceeds or falls under a given threshold (Stammerjohn et al., 2012; Stroeve et al., 2016). The different definitions of the length of the open-water season can differ in subtleties of the computations (notably filtering) and may not always entirely be consistent and comparable. In addition, the melt season duration, distinct from the open-water season duration, has also been analysed from changes in passive microwave emission signals due to

Published by Copernicus Publications on behalf of the European Geosciences Union.

the transition from a dry to a wet surface during melting (Markus et al., 2009; Stroeve et al., 2014).

As for changes in the Arctic open-water season duration, satellite-based studies indicate an increase by > 5 days per decade over 1979–2013 (Parkinson, 2014) due to earlier ice retreat and later advance (Stammerjohn et al., 2012; Stroeve et al., 2016). There are regional deviations in the contributions to a longer open-water season duration, most remarkably in the Chukchi and Beaufort seas where later ice advance takes over (Johnson and Eicken, 2016; Serreze et al., 2016), which has been attributed to increased oceanic heat advection from the Bering Strait (Serreze et al., 2016). Such changes in the seasonality of Arctic ice-covered waters reflect the response of the surface energy budget to warming. Indeed, warming and ice thinning imply earlier surface melt onset and ice retreat (Markus et al., 2009; Stammerjohn et al., 2012; Blanchard-Wrigglesworth et al., 2010). In addition, a shift towards later ice advance, tightly co-located with earlier retreat, is observed, especially where negative sea ice trends are large (Stammerjohn et al., 2012; Stroeve et al., 2016). This has been attributed to the ice–albedo feedback, namely to the combined action of (i) earlier ice retreat, implying lower surface albedo, and (ii) higher annual solar radiation uptake by the ocean. Such a mechanism (Stammerjohn et al., 2012) explains the ongoing delay in ice advance of a few days per decade from the estimated increase in solar absorption (Perovich et al., 2007), in accord with the observed in situ increase in the annual sea surface temperature (SST) maximum (Steele et al., 2008; Steele and Dickinson, 2016).

The observed increase in the ice-free season duration should continue over the next century, as projected by the CESM Large Ensemble (Barnhart et al., 2016), but this signal is obscured by important levels of internal variability. Other CMIP5 ESMs likely project a longer ice-free season as well, and this is true in the Alaskan Arctic where they have been analysed (Wang and Overland, 2015). In both these studies, the simulated future increases in the ice-free season duration are dominated by the later ice advance. Such behaviour remains unexplained and should be investigated with a larger set of models and regions.

In the present study, we aim at better quantifying the potential changes in Arctic sea ice seasonality and understanding the associated mechanisms. We first revisit the ongoing changes in Arctic sea ice retreat and advance dates using satellite passive microwave records, at both inter-annual and multi-decadal timescales. We also analyse, for the first time over the entire Arctic, all CMIP5 historical and RCP8.5 simulations covering 1900–2300 and study mechanisms at play using a one-dimensional ice–ocean model.

2 Methods

We analyse the recent past and future of sea ice seasonality by computing a series of diagnostics based on satellite observations, Earth system models and a simple ice–ocean model.

2.1 Data sources

Passive microwave sea ice concentration (SIC) retrievals, namely the GSFC Bootstrap SMMR-SSM/I quasi-daily time series product, over 1980–2015 (Comiso, 2000, updated 2015), are used as an observational basis. We also use the CMIP5 Earth system model historical simulations and future projections of SIC. Because of high inter-annual variability in ice advance and retreat dates and because some models lose multi-year ice only late into the 21st century, we retain the nine ESM simulations that pursue RCP8.5 until 2300 (first ensemble member, Table 1). Analysis focuses on 1900–2200, combining historical (1900–2005) and RCP8.5 (2005–2200) simulations. The year 2200 corresponds to the typical date of year-round Arctic sea ice disappearance (Hezel et al., 2014). We also extracted the daily SST output from IPSL-CM5A-LR. All model outputs were interpolated on a 1° geographic grid.

To investigate how mean state biases may affect ESM simulations, we also included in our analysis a 1958–2015 forced-atmosphere ISPL-CM simulation, i.e. an ice–ocean simulation that was performed with the NEMO-LIM 3.6 model (Rousset et al., 2015), driven by the DFS5 atmospheric forcing (Dussin et al., 2016). NEMO-LIM 3.6 is similar to the ice–ocean component of IPSL-CM5A-LR, except that (i) horizontal resolution is twice as high (1° with refinement near the poles and the equator), (ii) the sea ice model has been upgraded to multiple categories, among other differences, and (iii) a weak sea surface salinity restoration is applied. Such a simulation not only performs generally better than a free-atmosphere ESM run in terms of seasonal ice extent (Fig. S1 in the Supplement; Uotila et al., 2017), but also has year-to-year variations in phase with observations, a feature that is intrinsically not captured in a coupled ESM. However, a caveat of forced-atmosphere simulations is the absence of feedback from the sea ice–ocean surface state onto atmospheric conditions, which can affect the processes that drive changes in ice advance and retreat timing.

2.2 Ice seasonality diagnostics

We use slightly updated computation methods for ice retreat (d_r) and advance (d_a) dates, compared with previous contributions (Parkinson, 1994; Stammerjohn et al., 2012; Stroeve et al., 2016). Ice retreat date (d_r) is defined as the first day of the year when SIC drops below 15 %, whereas ice advance date (d_a) is the first day of the year when SIC exceeds this threshold (Stroeve et al., 2016). The choice of the SIC threshold has no significant impact on the results. All previ-

Table 1. Linear trends in ice retreat and advance dates over 2000–2200 (200 years), and long-term ice advance amplification ratios for the individual and mean CMIP5 models and for the 1-D model. Trends and ratios are given as median ± interquartile range over the seasonal ice zone in which trends are significant at a 95 % confidence level ($p = 0.05$). n/a: not applicable.

	r_r(days per decade)	r_a(days per decade)	$R_{a/r}^{long}$	Reference
CCSM4	-6.6 ± 2.1	13.4 ± 7.3	2.0 ± 0.6	Gent et al. (2011)
CNRM-CM5	-8.0 ± 2.8	13.5 ± 5.9	1.7 ± 0.3	Voldoire et al. (2013)
CSIRO-Mk3-6-0	-6.1 ± 3.3	10.4 ± 4.0	1.7 ± 0.6	Rotstayn et al. (2012)
GISS-E2-H	-2.8 ± 0.6	5.1 ± 1.6	1.8 ± 0.4	Schmidt et al. (2014)
MPI-ESM-LR	-8.6 ± 2.8	15.2 ± 8.1	1.8 ± 0.4	Giorgetta et al. (2013)
bcc-csm1-1	-5.2 ± 1.3	9.7 ± 2.6	1.9 ± 0.4	Wu et al. (2014)
GISS-E2-R	-2.0 ± 0.4	3.4 ± 0.8	1.8 ± 0.3	Schmidt et al. (2014)
HadGEM2-ES	-9.1 ± 3.0	18.6 ± 7.6	1.9 ± 0.5	Collins et al. (2011)
IPSL-CM5A-LR	-5.7 ± 1.2	11.1 ± 3.8	1.9 ± 0.5	Dufresne et al. (2013)
MEAN CMIP5	-6.0 ± 2.0	11.1 ± 4.6	1.8 ± 0.4	
1-D model	$-4.7 \pm$ n/a	$8.2 \pm$ n/a	$1.9 \pm$ n/a	

ous studies recognise that a typical 5-day temporal filtering on the input ice concentration is required to get rid of short-term dynamical events (Stammerjohn et al., 2012; Stroeve et al., 2016). By contrast, we use 15 days, in order to get rid of most short-term dynamical ice events, which barely affects trends in d_r and d_a (see Table S1). Another important issue is the reference time axis, which varies among authors. To circumvent the effect of the d_a discontinuity between 31 December and 1 January, we define the origin of time on 1 January and count d_a negatively if it falls between 1 July and 31 December. A safe limit is 1 July because there is no instance of ice advance date between early June and late July in the satellite record or in CMIP5 simulations. The length of the ice-free season is defined as the period during which SIC is lower than 15 %.

The same seasonality diagnostics are computed from model outputs. Yet, since the long-term ESM simulations used here only have monthly SIC outputs, we compute the ice seasonality diagnostics based on monthly SIC fields linearly interpolated daily. Such operation drastically reduces error dispersion but introduces a small systematic bias on d_r (early bias) and d_a (late bias), on the order of 5 ± 5 (6) days. These biases were determined from an analogous processing of satellite records. Dates of ice retreat and advance were derived from a daily interpolation of monthly averaged concentration fields and subsequently compared to direct retrievals based on daily resolved concentration fields (see Fig. S2). The identified biases apply to CMIP5 records because errors stem from the processing of data and do not depend on the type of data used (satellite or CMIP5). These small systematic biases in model ice retreat and advance dates likely contribute to the mean model bias compared to satellite data (Table 1, Fig. 1) but remain small compared to the long-term signals analysed throughout this paper.

The ice seasonality diagnostics and their spatial distribution are reasonably well captured by the mean of selected CMIP5 models over the recent past (Fig. 2). The spatial distribution of ice seasonality diagnostics varies among models, reflecting a possible dependence on the mean state or differences in the treatment of ice dynamics. Larger errors in some individual models (Fig. S3) are associated with an inaccurate position of the ice edge. Overall, ESMs tend to have a shorter open-water season than observed (Figs. 2a–c and S3), which is visible in the North Atlantic and North Pacific

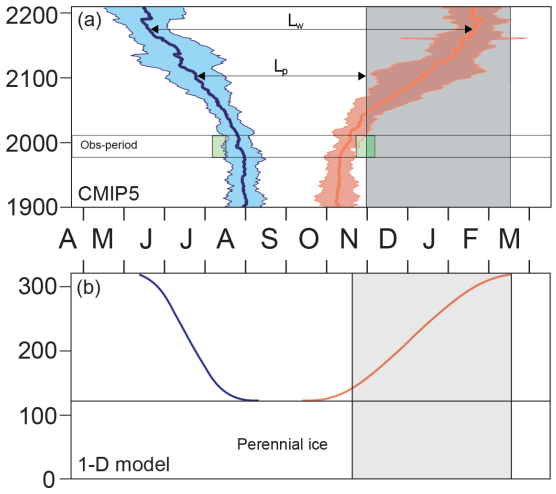

Figure 1. Evolution of the ice seasonality diagnostics (ice retreat date, blue; ice advance date, orange): **(a)** CMIP5 median and interquartile range, with corresponding range of satellite-derived values (green rectangles 1980–2015) over the 70–80° N latitude band; **(b)** one-dimensional ice–ocean model results. The ice-free period (L_w), the photoperiod (L_p) and the average polar night (grey rectangle) are also depicted. Note that the systematic difference between observations and CMIP5 models is reduced when accounting for the systematic bias due to the daily interpolation of monthly means in CMIP5 models (see Sect. 2 and Table S2).

regions and can be related to the systematic bias due to the use of interpolated monthly data, but also to the tendency of our model subset to overestimate sea ice. Such an interpretation is supported by (i) the visibly better consistency of the simulated ice seasonality diagnostics with observations in the forced-atmosphere ISPL-CM simulation than in IPSL-CM5A-LR and (ii) by the fact that models with simulated ice extent rather close to observations over the recent past (CESM, CNRM or MPI; Massonnet et al., 2012) are more in line with observed seasonality diagnostics than the other models (Figs. 2 and S3).

2.3 Trends in ice advance and retreat dates and related diagnostics

Trends in ice retreat and advance dates were calculated for each satellite or model pixel, from the slope of a least-square fit over a given period, using years when both d_r and d_a are defined. If the number of years used for calculation of the trend is less than one-third of the considered period, a missing value is assigned. One-third compromises between spatial and temporal coverage of the considered time series (see Table S1).

To describe the relative contribution of ice advance and retreat dates to changes in open-water season duration, we introduce a first diagnostic, termed the long-term ice advance vs. retreat amplification coefficient ($R^{\mathrm{long}}_{\mathrm{a/r}}$). $R^{\mathrm{long}}_{\mathrm{a/r}}$ is defined as minus the ratio of trends in ice advance to trends in ice retreat dates. The sign choice for $R^{\mathrm{long}}_{\mathrm{a/r}}$ is such that positive values arise for concomitant long-term trends toward later ice advance and earlier retreat. $R^{\mathrm{long}}_{\mathrm{a/r}}$ gives synthetic information about trends in ice advance and retreat dates within a single diagnostic. For example, $R^{\mathrm{long}}_{\mathrm{a/r}} > 0$ means that a trend towards earlier retreat ($d_\mathrm{r} < 0$) occurs concurrently with a trend towards later advance ($d_\mathrm{a} > 0$). Strictly speaking $R^{\mathrm{long}}_{\mathrm{a/r}} > 0$ could also indicate later retreat and earlier advance (i.e. a reduction of open-water season duration), which does not happen in a warming climate. Moreover, by definition, $R^{\mathrm{long}}_{\mathrm{a/r}} > 1$ if the long-term trend in ice advance date exceeds the long-term trend in retreat date in a particular pixel, otherwise $R^{\mathrm{long}}_{\mathrm{a/r}} < 1$. Note that for $R^{\mathrm{long}}_{\mathrm{a/r}}$ to be meaningful, we restrict computations to pixels in which trends in both d_r and d_a are significant at a specified confidence level. $p = 0.05$; i.e. a 95 % confidence interval gives the most robust value but heavily restricts the spatial coverage, especially for CMIP5 outputs. By contrast, $p = 0.25$; i.e. a 75 % confidence interval slightly expands coverage but loses some robustness.

In order to study the shorter-term association between retreat and ice advance, we introduce a second diagnostic, termed the short-term ice advance vs. retreat amplification coefficient ($R^{\mathrm{short}}_{\mathrm{a/r}}$). $R^{\mathrm{short}}_{\mathrm{a/r}}$ is defined by applying the same reasoning to inter-annual timescales, i.e. minus the linear regression coefficient between detrended ice advance and retreat dates. $R^{\mathrm{short}}_{\mathrm{a/r}}$ gives information on how anomalies in ice advance date scale with respect to anomalies in retreat dates over the same year, regardless of the long-term trend. Such a definition warrants comparable interpretation for $R^{\mathrm{short}}_{\mathrm{a/r}}$ and $R^{\mathrm{long}}_{\mathrm{a/r}}$. In a warming climate, $R^{\mathrm{short}}_{\mathrm{a/r}} > 0$ indicates concomitant anomalies towards earlier retreat and later advance, and $R^{\mathrm{short}}_{\mathrm{a/r}} > 1$ indicates that anomalies in advance date are larger than in retreat date.

For computations of $R^{\mathrm{long}}_{\mathrm{a/r}}$ and $R^{\mathrm{short}}_{\mathrm{a/r}}$ we use a reference period of 36 years. The length of the available observation period is 36 years and is close to the standard 30 years used in climate sciences. On one occasion (Table 1), we use 200 years as a reference period. The total number of years we can use to qualify changes is 200 years and is the most representative of a long climate change simulation.

All trends and ice advance vs. retreat amplification coefficients given in the rest of the text are the median ($\pm$ interquartile range), taken over the seasonal ice zone. We use non-parametric statistics because the distributions are not Gaussian.

2.4 1-D model

We use the Semtner (1976) zero-layer approach for ice growth and melt above an upper oceanic layer taking up heat, whereas snow is neglected. The model simplifies reality by assuming constant mixed-layer depth, no horizontal advection in ice and ocean, no heat exchange with the interior ocean, and no sensible heat storage in the snow–ice system. The ice–ocean seasonal energetic cycle is computed over 300 years, using climatological solar, latent, and sensible heat fluxes and increasing downwelling long-wave radiation, to represent the greenhouse effect. Ice retreat and advance dates are diagnosed from model outputs (see Appendix A for details). We argue that the Semtner (1976) zero-layer approach is appropriate to study the response of CMIP5 models to warming, as the CMIP5 models with more complicated thermodynamics cannot be distinguished from those using the Semtner zero-layer approach (Massonnet et al., 2018). The zero-layer approach is known to alter the sea ice seasonal cycle (Semtner, 1984), but should not fundamentally affect the processes discussed here.

3 Link between earlier ice retreat and later ice advance in observations and models

3.1 Trends in ice advance and retreat date in observations and models

Over 1980–2015, the ice-free season duration has increased by 9.8 ± 12.1 days decade^{-1}, with nearly equal contributions of earlier ice retreat (-4.8 ± 7.7 days decade^{-1}) and later ice advance (4.9 ± 5.8 days decade^{-1}, median based on satellite observation, updated figures; see Table S1). Variability is high however. Significant trends in both d_r and d_a at the 95 %

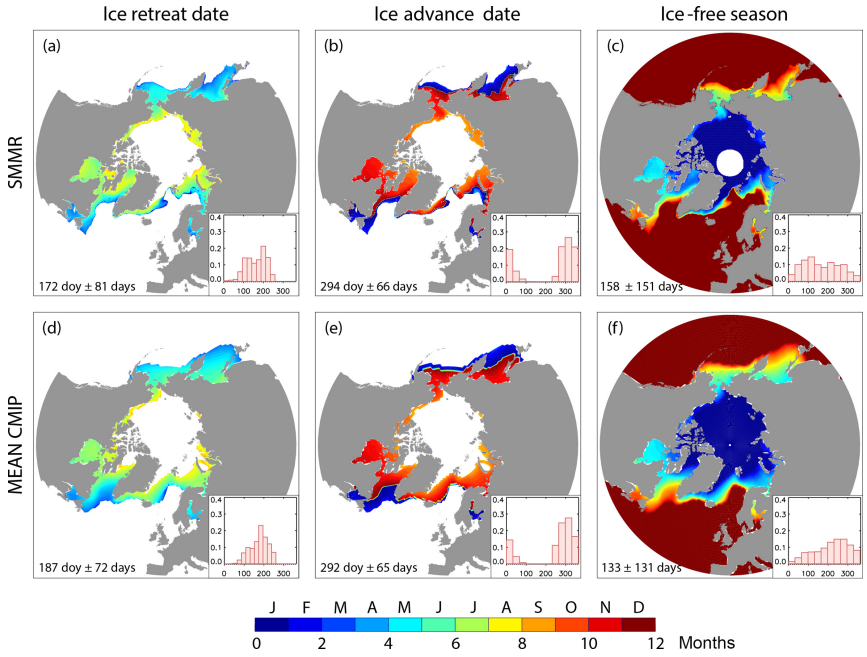

Figure 2. Maps and frequency histograms of **(a, d)** ice retreat date, **(b, e)** ice advance date and **(c, f)** ice-free season length over 1980–2015 (36 years), based on **(a, b, c)** passive microwave satellite concentration retrievals (Comiso, 2000; updated 2015) and **(d, e, f)** daily concentration fields averaged over CMIP5 models. Median ± IQR (interquartile range) refers to all points in the seasonal ice zone. See Fig. S3 for individual models.

confidence level are found over a relatively small fraction (22 %) of the seasonal ice zone (Fig. 3), independently of the details of the computation (Table S1). The patterns of changes are regionally contrasted, and Chukchi Sea is the most notable exception to the rule, where later ice advance clearly dominates changes in the ice-free season (Serreze et al., 2016, Fig. 3).

Trends simulated by the mean of selected CMIP5 models are comparable with observations, in terms of ice retreat date (-4.4 ± 3.5 days decade^{-1}), ice advance date (5.9 ± 3.3 days decade^{-1}) and ice-free season duration (10.3 ± 6.3 days decade^{-1}, Fig. 3). Individual models show larger errors (Fig. S4 to compare with Fig. 3), to be related notably with mean state issues or the spread in the strength of strong oceanic currents, in the North Atlantic and the North Pacific. One common location where trends are underestimated is the North Atlantic region, in particular the Barents Sea, which arguably reflects a weak meridional oceanic heat supply (Serreze et al., 2016). One should be reminded that as reality is a single realisation of internal climate variability (Notz, 2015), a model–observation comparison of this kind is intrinsically limited. This could be of particular relevance in the Barents Sea, which is subject to internally generated decadal-scale variations driven by ocean heat transport anomalies (Yeager et al., 2015).

3.2 Earlier sea ice retreat implies later ice advance

In terms of mean state and contemporary trends, models seem realistic enough for an analysis of changes at pan-Arctic scales but might be less meaningful at regional scales. We first study the contemporary link between earlier retreat and ice advance by looking at the sign of $R_{\mathrm{a/r}}$ values in contemporary observations and models. Because $R_{\mathrm{a/r}}^{\mathrm{long}}$ is a ratio of significant trends, and because all models have regional differences as to where trends are significant, we base our analysis on individual models.

Based on observations (Fig. 4), we find positive values of $R_{\mathrm{a/r}}^{\mathrm{long}}$ in more than 99 % of grid points in the studied zone, provided that computations are restricted where trends on ice retreat and advance dates are significant at a 95 % level ($N = 5257$). In a warming climate, positive $R_{\mathrm{a/r}}^{\mathrm{long}}$ values mean concomitant and significant trends towards earlier retreat and later advance, whereas missing values reflect either that the trends are not significant or that the point is out of the seasonal ice zone. $R_{\mathrm{a/r}}^{\mathrm{short}}$ (Fig. 6) is generally smaller (0.21 ± 0.27) than $R_{\mathrm{a/r}}^{\mathrm{long}}$ (0.71 ± 0.42, 95 % confidence level), and also positive in most pixels (87 % of 23 475 pixels).

CMIP5 models are consistent with the robust link between earlier ice retreat and later advance dates found in ob-

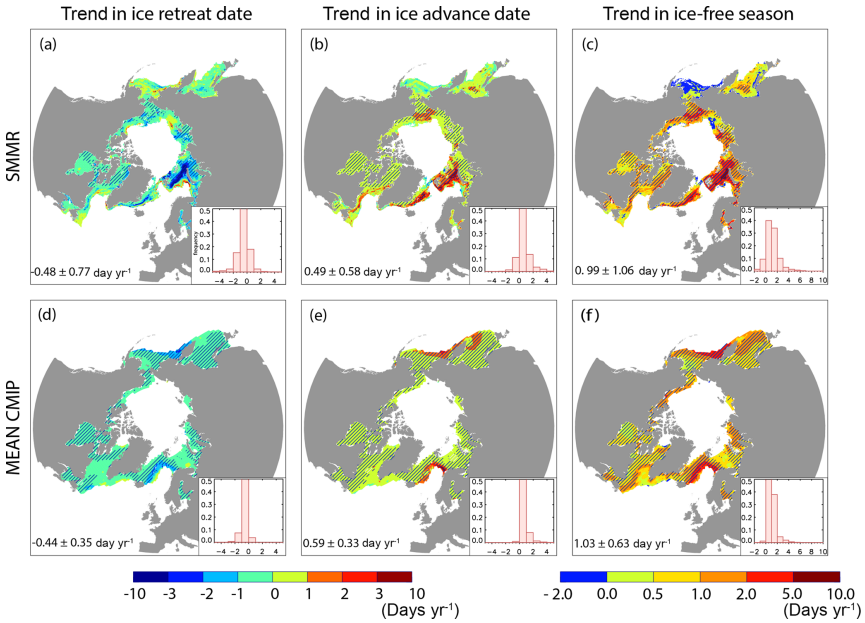

Figure 3. Maps and frequency histograms of linear trends (for hatched zones only) in **(a, d)** ice retreat date **(b, e)**, ice advance date and **(c, f)** ice-free season length over 1980–2015 (36 years), based on **(a, b, c)** passive microwave satellite concentration retrievals (Comiso, 2000; updated 2015); **(d, e, f)** the mean CMIP5 models. Hatching refers to the 95 % confidence interval ($p = 0.05$). Median ± IQR refers to significant pixels with at least one-third of the years with defined retreat and ice advance dates. See Fig. S4 for individual models.

servations (Stammerjohn et al., 2012; Stroeve et al., 2016). More generally, we find a robust link between earlier retreat and later advance in all cases: both $R_{a/r}$ values are virtually always positive for short- and long-term computations, from observations and models (Figs. 4, 5) over the three analysed periods (1980–2015 for observations and models, 2015–2050 and 2050–2085 for models only) and regardless of internal variability (Figs. S5 and S6). This finding expands previous findings from satellite observations using detrended time series (Stammerjohn et al., 2012; Serreze et al., 2016; Stern and Laidre, 2016), in particular the clear linear correlation found between detrended ice retreat and ice advance dates (Stroeve et al., 2016). Following these authors, we attribute the strong earlier retreat and later ice advance relationship as a manifestation of the ice–albedo feedback: earlier ice retreat leads to an extra absorption of heat by the upper ocean. This heat must be released back to the atmosphere before the ice can start freezing again, leading to later ice advance. Such a mechanism, also supported by satellite SST analysis in the ice-free season (Steele et al., 2008; Steele and Dickinson, 2016), explains the sign of the changes in ice advance date. However, it does not explain the relatively larger magnitude of the trends in ice advance date compared with trends in ice retreat date, studied in the next section.

3.3 Increasingly late ice advance dominates future changes in open-water season

We now focus on the respective contribution of changes in retreat and ice advance dates to the increasingly long open-water season by analysing the magnitude of $R_{a/r}^{long}$. Contemporary values of $R_{a/r}^{long}$ match between model and observations but not spatially (Fig. 4). Over 1980–2015 the simulated $R_{a/r}^{long}$ (CMIP5 mean) is slightly higher (1.1 ± 0.7) than the observational value (0.7 ± 0.4). Since none of the models position the sea ice edge correctly everywhere, it is not surprising that the spatial distribution and the modal $R_{a/r}^{long}$ differ among models and between models and observations. The fact that, by definition, satellite data only sample one realisation of internal variability could contribute to the discrepancy as well. In support of these two arguments, the forced-atmosphere ISPL-CM simulation better simulates the spatial distribution of $R_{a/r}^{long}$ (see Fig. S7), which underlines the role of mean state errors.

As far as future changes are concerned, all models show a qualitatively similar evolution (Figs. 1 and S5). Projected changes in ice retreat and ice advance dates start by approximately 2000 and continue at a nearly constant pace from 2040 until 2200. By 2040, the trend in ice advance date typically becomes larger than the trend in ice retreat date, as

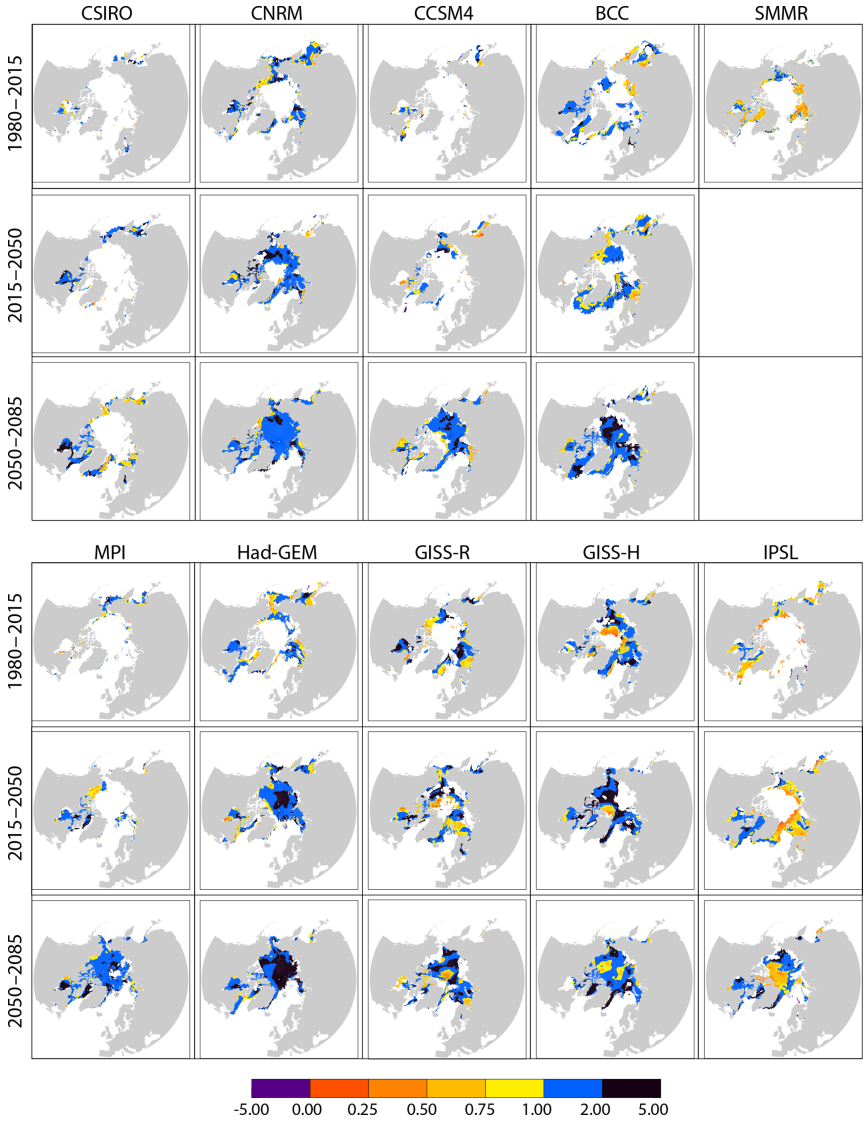

Figure 4. Long-term ice advance vs. retreat amplification coefficient from passive microwave ice concentration retrievals (SMMR; over 1980–2015), and for all individual models over 1980–2015, 2015–2050 and 2050–2085. We use a 75 % ($p = 0.25$) confidence interval for this specific computation. Similar figures (for SMMR and IPSL_CM5A_LR only) for $p = 0.05$ are available in the Supplement (Fig. S9).

indicated by the corresponding mean $R^{\text{long}}_{\text{a/r}} = 1.8 \pm 0.4$ over 2000–2200 (Table 1).

To further understand these contrasting trends between ice retreat and ice advance dates, we mapped $R^{\text{long}}_{\text{a/r}}$, over 2015–2050 and 2050–2085. We find that, in the course of the 21st century, trends in retreat and ice advance date become significant over increasingly wide regions. The overall $R^{\text{long}}_{\text{a/r}}$ value increases, as illustrated in Fig. 4. This behaviour is found independent of the considered model and of the internal variability (Figs. S5 and S6).

This finding expands the recent analyses of the CESM Large Ensemble project (Barnhart et al., 2016) and of Alaskan Arctic sea ice in CMIP5 models, finding faster ice coverage decrease in autumn than in spring (Wang and Overland, 2015). Both studies propose that the extra heat uptake in the surface ocean due to an increased open-water season as a potential explanation. As suggested earlier, this indeed

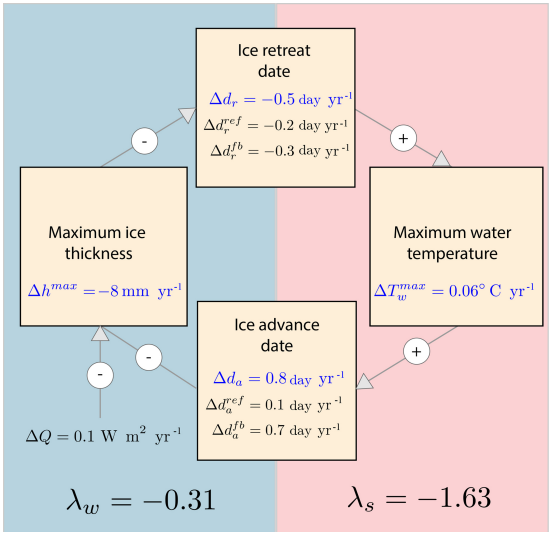

Figure 5. Schematics of the mechanisms shaping the thermodynamic response of sea ice seasonality to a radiative forcing perturbation. The numbers give annual averages simulated by the 1-D model. Changes in ice retreat and advance dates are split between reference (ref) and feedback (fb) responses. See Appendix A for details of the computations.

explains why $R_{a/r}^{long}$ would be positive but does not explain the amplified delay in ice advance date, that is, why $R_{a/r}^{long}$ would be > 1. We are now addressing this question.

3.4 A thermodynamic mechanism for an amplified delay in ice advance date

The reason why $R_{a/r}^{long}$ becomes > 1 by 2040 is related to the asymmetric response of ice–ocean thermodynamics to warming: the upper ocean absorbs solar radiation about twice as efficiently as it can release heat right before ice advance. That summer feedback processes dominate is enabled by a relatively weak winter feedback (between later ice advance and earlier retreat the next year).

To come to this statement, we would need diagnostics unavailable in CMIP5, in particular a daily description of the surface energy budget. This is why we used a 1-D thermodynamic model of sea ice growth and melt in relation with the upper-ocean energy budget (Semtner, 1976) to study the idealised thermodynamic response of seasonal ice to a radiative forcing perturbation. Without any particular tuning, the 1-D model simulations feature an evolution that is similar to the long-term behaviour of CMIP5 models (Fig. 1b), with trends in ice advance date (8.2 days decade^{-1}) of larger absolute magnitude than trends in retreat date (-4.7 days decade^{-1}), giving a corresponding value of $R_{a/r}^{long} = 1.9$. All figures fall within the CMIP5 envelope (Table 1).

As explained above, the seasonal relationships between ice advance and retreat dates are underpinned by atmosphere–ice–ocean feedbacks. The non-radiative feedback framework of Goosse et al. (2018; see Appendix A for details) clarifies the study of these relationships. Changes in dates of ice retreat (Δd_r) and advance (Δd_a) in response to a radiative forcing perturbation are split into reference and feedback response terms:

$$\begin{cases} \Delta d_r = \Delta d_r^{ref} - \lambda_w \Delta d_a, \\ \Delta d_a = \Delta d_a^{ref} - \lambda_s \Delta d_r. \end{cases} \quad (1)$$

The sign convention for the feedback terms is such that the link between earlier retreat ($\Delta d_r < 0$) and later advance ($\Delta d_a > 0$) gives positive feedback factors. The feedback response refers to the change in d_r (resp. d_a) that can solely be attributed to the change in d_a (resp. d_r). It is expressed using a feedback factor λ_w (resp. λ_s) related to winter (resp. summer) feedback processes. The reference response Δd_r^{ref} (resp. Δd_a^{ref}) is that of a virtual system in which the feedback would be absent. Expressions for the reference and feedback response terms, as well as for feedback factors, stem from physical analysis, detailed in Appendix A.

According to this analysis, feedbacks between the dates of retreat and advance dominate the thermodynamic response of ice seasonality (Fig. 5): the reference response to the applied perturbation of 0.1 W m^{-2} yr^{-1} is -0.2 day yr^{-1} of earlier retreat and 0.1 d yr^{-1} of later advance.

Ice growth and melt processes generate a relatively weak winter amplifying feedback of ice advance date onto ice retreat date: a shorter growth season implies thinner ice, which subsequently melts away faster. The winter feedback factor is (see Appendix A for derivation)

$$\lambda_w = \frac{1}{2} \cdot \left(\frac{d_r - d_h}{d_h - d_a} \right), \quad (2)$$

where d_h is the date of maximum ice thickness, and is solely a function of the ice growth and melt seasonal parameters. λ_w has a rather stable value of 0.31 ± 0.04 over the 127 years of simulated seasonal ice. This value of λ_w indicates a feedback response in ice retreat date of about one-third of the change towards later ice advance the previous autumn. λ_w is < 1 for two reasons. First the melt season is shorter than the growth season (Perovich et al., 2003); hence changes in ice advance date translate into weaker changes in ice retreat date. Second, the ice growth rate is larger for thin than for thick ice (Maykut, 1986); hence the maximum winter ice thickness does not decrease due to later advance as much as if the growth rate was constant.

Energetics of the summer ice-free ocean generate a summer amplifying feedback of ice retreat date onto ice advance date, much stronger than the winter feedback. The summer feedback factor is (see Appendix A for derivation)

$$\lambda_s = -\frac{Q_+}{Q_-}, \quad (3)$$

where $\langle Q_+ \rangle$ and $\langle Q_- \rangle$ are the average net positive (negative) atmosphere-to-ocean heat fluxes during the ice-free period. The 1-D model diagnostics give an average value of 1.63 ± 0.18 for λ_s, meaning that earlier retreat implies a feedback delay in ice advance of ~ 1.6 times the initial change in ice retreat date. Physically, the strength of the summer feedback is in direct relation with the ice-free upper-ocean energy budget and the evolution of SST. $\langle Q_+ \rangle$ mostly corresponds to net solar flux, typically $150\,\mathrm{W\,m^{-2}}$, and is typically larger than $\langle Q_- \rangle$, which corresponds to the net non-solar, mostly long-wave heat flux, at freezing temperatures, typically 75–$150\,\mathrm{W\,m^{-2}}$ (see Appendix B). Hence, after ice retreat, the SST rapidly increases due to solar absorption into the mixed layer and then decreases much slower until freezing, due to non-solar ocean-to-atmosphere fluxes (Fig. 7a), an evolution that is similar to a recent satellite-based analysis (Steele and Dickinson, 2016). In other words, the energy excess associated with later retreat, stored into the surface ocean, takes extra time to be released before ice advance.

In practise, keeping only the dominant term, $R^{\mathrm{long}}_{\mathrm{a/r}}$ (the seasonality of the system) reduces to the summer feedback factor:

$$R^{\mathrm{long}}_{\mathrm{a/r}} \approx \lambda_s. \quad (4)$$

$R^{\mathrm{long}}_{\mathrm{a/r}}$ appears to vary little among CMIP5 models and even with the 1-D model. Why this could be the case is because the winter and summer feedback factors are controlled by very basic physical processes of the Arctic ice–ocean–climate system and therefore feature relatively low uncertainty levels. Celestial mechanics, ubiquitous clouds and near-freezing temperatures provide strong constraints on the surface radiation balance and hence on the summer feedback factor, that all models likely capture. All models also include the growth and melt season asymmetry and the growth–thickness relationship (see Massonnet et al., 2018) at the source of the relatively weak winter feedback. In IPSL-CM5A-LR, the sole model for which we could retrieve daily SST (Fig. 7b), the evolution of the summer SST in seasonally ice-free regions features a rapid initial increase followed by slow decrease, an indication that the mechanism we propose is sensible.

3.5 Inter-annual variability and extra processes add to the purely thermodynamic response

The CMIP5 response of ice seasonality differs from the idealised thermodynamic response in two notable ways. First, $R^{\mathrm{long}}_{\mathrm{a/r}} > 1$ only clearly emerges by 2040 in CMIP5 models. Second, $R^{\mathrm{long}}_{\mathrm{a/r}}$ is typically < 1 over the recent past (1980–2015) from the satellite record (Fig. 4). This must be due to the contribution of processes absent from the 1-D model.

As to why the 1-D response would emerge in the course of this century, there are a series of potential reasons that we cannot disentangle with the limited available CMIP5 outputs. (i) The contribution of the subsurface ocean to the surface energy budget, neglected in the 1-D approach, is likely larger today than in the future Arctic. Over the 21st century, the Arctic stratification increases in CMIP5 models (Vancoppenolle et al., 2013; Steiner et al., 2014), whereas the oceanic heat flux convergence should decrease (Bitz et al., 2005). (ii) The solar contribution to the upper-ocean energy budget is smaller today than in the future, as the date of retreat falls closer to the summer solstice. (iii) The surface energy budget is less spatially coherent today than in the future, when the seasonal ice zone moves northwards. The solar radiation maximum drastically changes over 45 to 65° N but has small spatial variations above the Arctic circle (Peixoto and Oort, 1992). Note that in some specific regions, $R^{\mathrm{long}}_{\mathrm{a/r}}$ is already > 1, in particular in the Chukchi Sea, but this has been associated with the summer oceanic heat transport through the Bering Strait (Serreze et al., 2016), which is a localised event, that does not explain why $R^{\mathrm{long}}_{\mathrm{a/r}}$ would globally become > 1 in the future.

The aforementioned processes, ignored in the 1-D model may explain why $R^{\mathrm{long}}_{\mathrm{a/r}} > 1$ would emerge by mid-century, but internal variability, also absent in the 1-D model, should also be considered (Barnhart et al., 2016). It is remarkable that $R^{\mathrm{short}}_{\mathrm{a/r}}$ is < 1 from both satellite records and CMIP5 model simulations, for all periods and models considered (Fig. 6). This suggests that the ice advance amplification mechanism is not dominant at inter-annual timescales. Indeed, based on inter-annual satellite time series, the standard deviation of ice retreat (SD = 21.6 days) and advance dates (SD = 14.3 days) is high (Stroeve et al., 2016) and the corresponding trends over 1980–2015 are not significant. Conceivably, atmosphere, ocean and ice horizontal transport, operating at synoptic to inter-annual timescales, obscure the simple thermodynamic relation between the ice retreat and advance dates found in the 1-D model. For instance, the advection of sea ice on waters with a temperature higher than the freezing point would imply earlier ice advance. Altogether, this highlights that the ice advance amplification mechanism is a long-term process and stresses the importance of the considered timescales and period as previous studies have already shown (Parkinson et al., 2014; Barnhart et al., 2016).

4 Summary and discussion

The analysis presented in this paper, focused on changes in sea ice seasonality and the associated driving mechanisms, raised the following new findings.

1. All CMIP5 models consistently project that the trend towards later advance progressively exceeds and ultimately doubles the trend towards earlier retreat over this century, causing the ice-free season to shift into autumn.

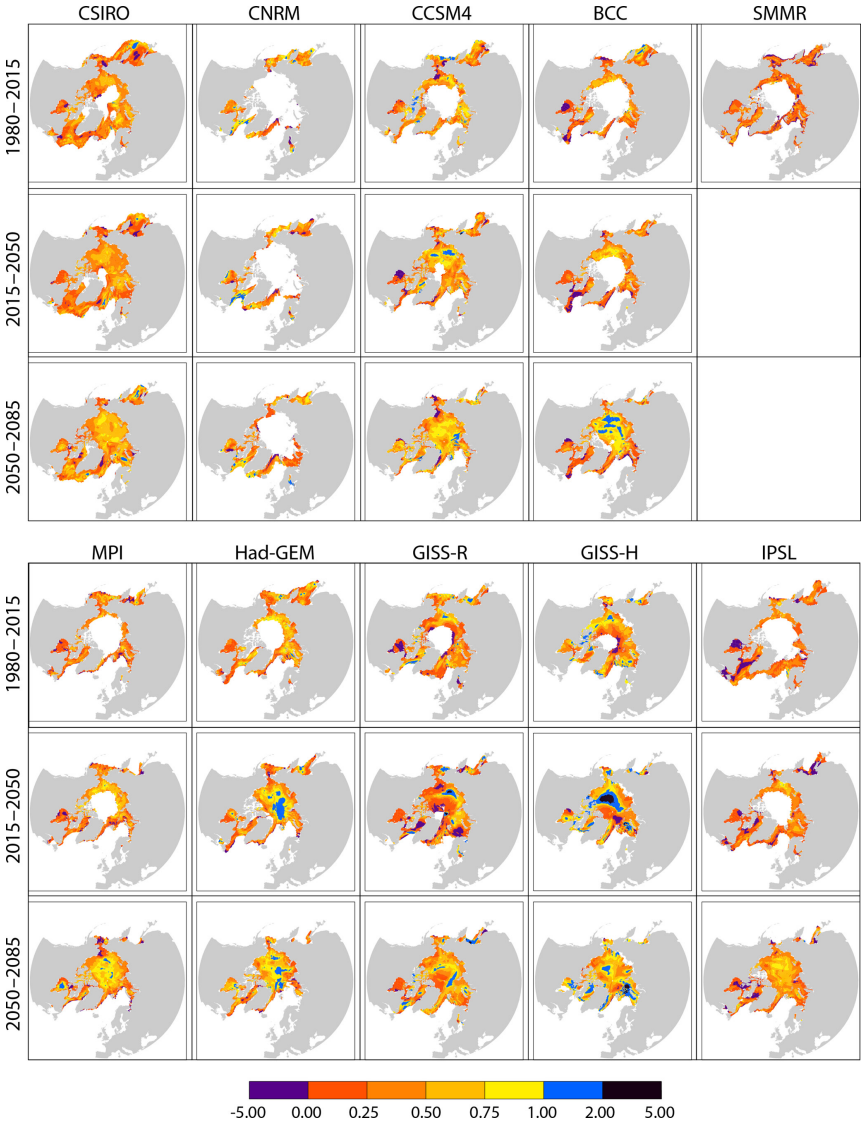

Figure 6. Short-term ice advance vs. retreat amplification coefficient from passive microwave ice concentration retrievals (SMMR; over 1980–2015), and for all individual models over 1980–2015, 2015–2050 and 2050–2085.

2. The long-term shift into autumn of the ice-free season is a basic feature of the thermodynamic response of seasonal ice to warming.

3. The thermodynamic shift into autumn of the ice-free season is caused by the combination of relatively strong summer and relatively weak winter feedback processes.

4. Thermodynamic processes only explain the long-term response of ice seasonality, not the inter-annual variations, nor the delayed emergence of the long-term response, which are both consistently simulated features among CMIP5 models.

A central contribution of this paper is the detailed study of the mechanisms shaping the thermodynamic response of sea ice seasonality to radiative forcing in the Semtner (1976) ice–ocean thermodynamic model, using the non-radiative feedback framework of Goosse et al. (2018). The low seawater albedo as compared with ice and the enhanced solar radiation uptake by the ocean had previously been put forward

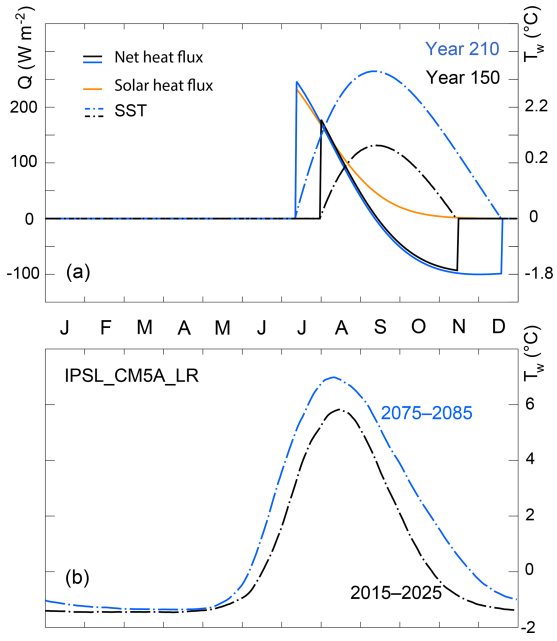

Figure 7. **(a)** Energetics of ice retreat and advance in the simple model: net atmospheric (solid) and solar (yellow) heat fluxes to the ocean; SST (dash), depicted for years 150 and 210. **(b)** Annual evolution of the simulated sea surface temperature, averaged over the seasonal ice zone, for 2 decades of reference (2015–2025, 2075–2085) as simulated by the IPSL_CM5A_LR model and showing the same temporal asymmetry as in the simple model.

to explain the increase in the length of the open-water season (Stammerjohn et al., 2012). Our analysis completes this view. Extra solar heat reaching the ocean due to earlier ice retreat is absorbed at a higher rate than it can be released until ice advance. This provides a powerful feedback at the source of the shift into autumn of the open-water season. In addition, the link between later advance and earlier retreat the next spring is weak because of the damping effects of the long ice growth period and of the inverse relationship between growth rate and ice thickness. All of these processes are simple enough to be captured by most of the climate models, which likely explains why the different models are so consistent in terms of future ice seasonality.

The link between earlier ice retreat and later advance is found in both satellite retrievals and climate projections, regardless of the considered period and timescale, expanding findings from previous works (Stammerjohn et al., 2012; Serreze et al., 2016; Stern and Laidre, 2016; Stroeve et al., 2016) and further stressing the important control of thermodynamic processes on sea ice seasonality. Yet, two notable features are in contradiction with the thermodynamic response of seasonal ice to warming. First, the long-term response of ice seasonality to warming only appears by mid-century in CMIP5 simulations, when changes in the ice-free season emerge out of variability (Barnhart et al., 2016). Second, changes in ice retreat date are larger than changes in ice advance date at inter-annual timescales. Transport or coupling processes (involving the atmosphere, sea ice, ocean) are the most likely drivers but their effect could not be formally identified because of the lack of appropriate diagnostics in CMIP5. Such a set-up, with a long-term control by thermodynamic processes, has other analogues in climate change studies (Bony et al., 2004; Kröner et al., 2017; Shepherd, 2014).

As the Arctic sea ice seasonality is a basic trait of the Arctic Ocean, a shift of the Arctic sea-ice free season would also have direct ecosystem and socio-economic impacts. The shift in the sea ice seasonal cycle will progressively break the close association between the ice-free season and the seasonal photoperiod in Arctic waters, a relation that is fundamental to photosynthetic marine organisms existing in the present climate (Arrigo and van Dijken, 2011). Indeed, because the ice advance date is projected to overtake the onset of polar night (Fig. 1), typically by 2050, changes in the photoperiod are at this point solely determined by the ice retreat date, and no more by the advance date. The duration of the sea ice season also restricts the shipping season (Smith and Stephenson, 2013; Melia et al., 2017). The second clear implication of the foreseen shift of the Arctic open-water season is that the Arctic navigability would expand to autumn, well beyond the onset of polar night, supporting the lengthening of the shipping season mostly by later closing dates (Melia et al., 2017).

Better projecting future changes in sea ice and its seasonality is fundamental to our understanding of the future Arctic Ocean. Detailed studies of the drivers of sea ice seasonality, in particular the upper-ocean energy budget, the role of winter and summer feedbacks, and the respective contribution of thermodynamic and dynamic processes, are possible tracks towards reduced uncertainties. Further knowledge can be acquired from observations (e.g. Steele and Dickinson, 2016) and Earth system model analyses, for which the expanded set of ice–ocean diagnostics expected in CMIP6, including daily ice concentration fields (Notz et al., 2016), will prove instrumental.

Code and data availability. Scripts available from Marion Lebrun (marion.lebrun@locean-ipsl.upmc.fr) upon request.

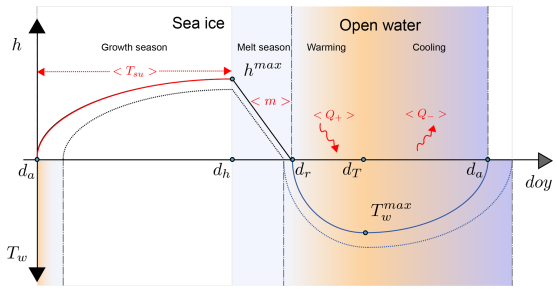

Figure A1. Schematic representation of the analysis framework applied to the 1-D model outputs, illustrating the mechanisms of change in ice seasonality between a reference year (solid line) and a subsequent year (dashed line). Ice appears at the ice advance date (d_a). The ice thickness (h) increases until the date of maximum thickness (d_h), then decreases at an average melt rate $\langle m \rangle$. Once the ice thickness vanishes at the ice retreat date d_r, the sea water temperature T_w increases due to incoming heat flux Q_+, until the date of maximum temperature (d_T), and finally decreases due to the heat loss Q_-.

Appendix A: Upper-ocean energetics and ice seasonality in the 1-D ice–ocean model

To characterise the purely thermodynamic response of seasonal ice to a radiative forcing perturbation, we use the Semtner (1976) zero-layer approach for ice growth and melt above an upper oceanic layer taking up heat. Snow is neglected. The ice model equations for surface temperature (T_su) and ice thickness (h) read

$$Q_\mathrm{atm}(T_\mathrm{su}) = Q_\mathrm{c}(T_\mathrm{su}), \tag{A1}$$

$$\rho L \frac{\mathrm{d}h}{\mathrm{d}t} = Q_\mathrm{atm}(T_\mathrm{su}) + Q_\mathrm{w}, \tag{A2}$$

where $Q_\mathrm{atm} = Q_0 + Q_\mathrm{sol}(1-\alpha_i) - \epsilon\sigma T_\mathrm{su}^4$, with Q_0 the sum of downwelling long-wave, latent and sensible heat fluxes, Q_sol the incoming solar flux, $\alpha_i = 0.64$ the ice albedo, $\epsilon = 0.98$ the emissivity, and $\sigma = 5.67 \times 10^{-8}\,\mathrm{W\,m^{-2}\,K^{-4}}$ the Stefan–Boltzmann constant. Q_c is the heat conduction flux in the ice (> 0 downwards), Q_w is the ocean-to-ice sensible heat flux at the ice base, $\rho = 900\,\mathrm{kg\,m^{-3}}$ is ice density and $L = 334\,\mathrm{kJ\,kg^{-1}}$ is the latent heat of fusion. Once the ice thickness vanishes, the water temperature T_w in a $h_\mathrm{w} = 30\,\mathrm{m}$ thick upper-ocean layer follows

$$\rho_\mathrm{w} c_\mathrm{w} \frac{\partial T_\mathrm{w}}{\partial t} h_\mathrm{w} = Q_0 + Q_\mathrm{sol}(1-\alpha_\mathrm{w})[1-\exp(-\kappa h_\mathrm{w})] - \epsilon\sigma T_\mathrm{w}^4. \tag{A3}$$

$\rho_\mathrm{w} = 1025\,\mathrm{kg\,m^{-3}}$ is water density, $c_\mathrm{w} = 4000\,\mathrm{J\,kg^{-1}\,K^{-1}}$ is water specific heat and $\kappa_\mathrm{w} = 1/30\,\mathrm{m^{-1}}$ is the solar radiation attenuation coefficient in water. Ice starts forming back once T_w returns to the freezing point $T_\mathrm{f} = -1.8\,^\circ\mathrm{C}$.

The atmospheric solar (Q_sol) and non-solar (Q_0) heat fluxes are forced using the classical standard monthly mean climatologies, typical of central Arctic conditions (Fletcher, 1965). We impose $Q_\mathrm{w} = 2\,\mathrm{W\,m^{-2}}$ following Maykut and Untersteiner (1971). We add a radiative forcing perturbation $\Delta Q = 0.1\,\mathrm{W\,m^{-2}}$ to the non-solar flux each year to simulate the greenhouse effect. Ice becomes seasonal after 127 years. The model is run until there is no ice left, which takes 324 years.

The following diagnostics of the ice–ocean seasonality (see Fig. A1) are derived from 1-D model outputs:

- d_r (ice retreat date): the first day with $T_\mathrm{w} > T_\mathrm{f} = -1.8\,^\circ\mathrm{C}$;
- d_a (ice advance date): the last day with $T_\mathrm{w} > T_\mathrm{f} = -1.8\,^\circ\mathrm{C}$.

Two other markers of the ice–ocean seasonality prove useful and were also diagnosed:

- d_T (maximum water temperature date): the last day with $Q > 0$.
- d_h (maximum thickness date): the date of maximum ice thickness.

The simulated trend towards later ice advance is on average 1.9 times the trend towards earlier retreat, a value consistent with the CMIP5 value. An advantage of the 1-D model is that the required diagnostics to investigate the ice seasonality drivers are easily available.

Nevertheless, the response of ice seasonality is not straightforward because there are feedbacks between ice retreat and advance dates. First, later advance delays ice growth, reduces the winter maximum thickness and, in turn, implies earlier retreat. Second, earlier retreat adds extra solar heat to the upper ocean, delaying ice advance. To understand the changes in ice seasonality and attributing their causes, we apply the non-radiative feedback framework introduced by Goosse et al. (2018).

A1 Analysis framework

We split the changes in ice retreat (Δd_r) and advance (Δd_a) dates in response to a radiative forcing perturbation into reference and feedback contributions (Goosse et al., 2018):

$$\begin{cases} \Delta d_\mathrm{r} = \Delta d_\mathrm{r}^\mathrm{ref} - \lambda_\mathrm{w} \Delta d_\mathrm{a}, \\ \Delta d_\mathrm{a} = \Delta d_\mathrm{a}^\mathrm{ref} - \lambda_\mathrm{s} \Delta d_\mathrm{r}. \end{cases} \tag{A4}$$

The reference response in ice retreat date to the perturbation ($\Delta d_\mathrm{r}^\mathrm{ref}$) is defined using a virtual reference system in which winter feedbacks (from d_a onto d_r) would not operate. The feedback response ($\Delta d_\mathrm{r}^\mathrm{fb}$) is the total minus the reference response and is assumed proportional to the change in ice advance date (Δd_a). Equivalently it is the part of the total change in d_r that can solely be linked to changes in

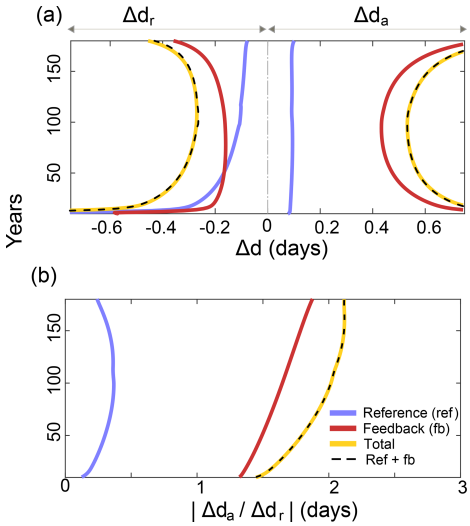

Figure A2. Thermodynamic response of sea ice seasonality to warming in the 1-D model. **(a)** Evolution over the years of the annual contributors to changes in ice retreat and advance date, as simulated by the 1-D model. The yellow line gives the total response Δd_r (resp. Δd_a) as diagnosed from model output. The blue curve gives the reference response $\Delta d_\mathrm{r}^\mathrm{ref}$ (resp. $\Delta d_\mathrm{a}^\mathrm{ref}$) to the radiative forcing perturbation as calculated with Eq. (A11) (resp. A16). The red curve gives the feedback response $\Delta d_\mathrm{r}^\mathrm{fb}$ (resp. $\Delta d_\mathrm{a}^\mathrm{fb}$), attributed to the feedback from d_a (resp. d_r), calculated with Eqs. (A9) and (A10) (resp. A13 and A15). The black dashed line testifies that the sum of reference and feedback responses matches the total. **(b)** Evolution over the years of the simulated freeze-up amplification ratio in the 1-D model. The yellow curve gives the freeze-up amplification R, calculated as the ratio of the total response in d_a (Δd_a) divided by the total response in d_r (Δd_r), as diagnosed from the 1-D model. The blue curve gives the contribution of the reference response to the freeze-up amplification ratio ($\Delta d_\mathrm{a}^\mathrm{ref}/\Delta d_\mathrm{r}$). The red curve gives the contribution of the summer feedbacks ($\Delta d_\mathrm{a}^\mathrm{ref}/\Delta d_\mathrm{r} = \lambda_\mathrm{s}$). The black dashed line testifies that the sum of reference and feedback contributions matches the total.

d_a in the previous autumn. The feedback factor λ_w quantifies the strength of this link. The sign convention is such that concomitant later advance ($\Delta d_\mathrm{a} > 0$) and earlier retreat ($\Delta d_\mathrm{r} > 0$) give a positive feedback factor. The definitions for the feedback and reference response terms in ice advance date are similar. The only difference is that the summer feedback factor λ_s quantifies the link between earlier retreat and later advance in the same year.

A2 Winter response

To formulate what determines the changes in ice retreat date, we focus on the ice season (Fig. A1) and use the maximum ice thickness to connect d_a to d_r. The ice thickness increases from zero on $d = d_\mathrm{a}$ until a maximum h^max reached when $d = d_\mathrm{h}$. Stefan's law of ice growth (Stefan, 1981) gives

$$h^\mathrm{max} \approx \sqrt{-\frac{2k\langle T_\mathrm{su}\rangle}{\rho L}\cdot(d_\mathrm{h}-d_\mathrm{a})}, \tag{A5}$$

where $\langle T_\mathrm{su}\rangle$ is the surface temperature averaged over $[d_\mathrm{a}, d_\mathrm{h}]$, i.e. over the ice growth period. Stefan's law is not exact but precise enough, reproducing the simulated annual values of h^max within $2\pm2\,\%$ of the 1-D model simulation over the 197 years of seasonal ice. The other advantage of Stefan's ice thickness is to be differentiable. Defining $v = k/\left(\rho \mathrm{L} h^\mathrm{max}\right)$, the change in ice thickness due to the radiative forcing perturbation is, after linearisation,

$$\Delta h^\mathrm{max} = v\cdot\langle T_\mathrm{su}\rangle\cdot\left[\Delta d_\mathrm{a} - \Delta d_\mathrm{h} + (d_\mathrm{a}-d_\mathrm{h})\frac{\Delta\langle T_\mathrm{su}\rangle}{\langle T_\mathrm{su}\rangle}\right]. \tag{A6}$$

Now, to connect the maximum ice thickness to the ice retreat date, we consider the melt season. The ice melts from h^max on $d = d_\mathrm{h}$ until ice thickness vanishes on $d = d_\mathrm{r}$. Hence

$$h^\mathrm{max} = \langle m\rangle\cdot(d_\mathrm{r}-d_\mathrm{h}), \tag{A7}$$

where $\langle m\rangle$ is the average melt rate, assumed to be negative.

We now combine growth and melt seasons and eliminate h^max. Differentiating (Eq. A7), then injecting Δh^max from (Eq. A6) and dividing by $\langle m\rangle$, we get

$$\frac{\Delta\langle m\rangle}{\langle m\rangle}\cdot(d_\mathrm{r}-d_\mathrm{h}) + \Delta d_\mathrm{r} - \Delta d_\mathrm{h} = \frac{v\cdot\langle T_\mathrm{su}\rangle}{\langle m\rangle}\cdot \left[\Delta d_\mathrm{a} - \Delta d_\mathrm{h} + (d_\mathrm{a}-d_\mathrm{h})\frac{\Delta\langle T_\mathrm{su}\rangle}{\langle T_\mathrm{su}\rangle}\right]. \tag{A8}$$

Using Stefan's law (Eq. A5) to replace h^max in the definition of v, the first factor on the right-hand side of Eq. (A8) can be rewritten as

$$\frac{v\cdot\langle T_\mathrm{su}\rangle}{\langle m\rangle} = -\frac{1}{2}\cdot\left(\frac{d_\mathrm{r}-d_\mathrm{h}}{d_\mathrm{h}-d_\mathrm{a}}\right) \equiv -\lambda_\mathrm{w}. \tag{A9}$$

Substituting Eq. (A9) into (A8) and rearranging terms gives the desired decomposition between reference and feedback responses:

$$\Delta d_\mathrm{r} = \Delta d_\mathrm{r}^\mathrm{ref} - \lambda_\mathrm{w}\Delta d_\mathrm{a}, \tag{A10}$$

where the reference response gathers all terms independent of Δd_a:

$$\Delta d_\mathrm{r}^\mathrm{ref} = (1-\lambda_\mathrm{w})\,\Delta d_\mathrm{h} + (d_\mathrm{r}-d_\mathrm{h})\cdot\left(\frac{\Delta\langle T_\mathrm{su}\rangle}{2\langle T_\mathrm{su}\rangle} - \frac{\Delta\langle m\rangle}{\langle m\rangle}\right). \tag{A11}$$

The terms on the right-hand side reflect the contributions of (i) changes in the date of maximum thickness, (ii) changes in surface temperature and (iii) changes in surface melt rate. The feedback term in (Eq. A10) isolates the contribution of changes in ice advance date and λ_w now clearly appears as a feedback factor. To compute the forced and feedback terms

from model output, the annual time series of $\langle T_{su} \rangle$, $\langle m \rangle$ and d_h were extracted from model outputs.

The proposed decomposition (Eq. A10) is supported by analysis: the sum of calculated reference and feedback responses (black dashed line in Fig. A2a) matches the total change in ice retreat date as diagnosed from model output (yellow line in Fig. A2a).

A3 Summer forced and feedback responses

The link between ice advance date and the previous ice retreat date stems from the conservation of energy in the ice-free upper ocean. Once ice disappears on $d = d_r$, the upper ocean takes up energy (see Fig. A1). The surface ocean temperature T_w increases from the freezing point until a maximum, reached on $d = d_T$. Then the upper ocean starts losing energy and T_w decreases, reaching the freezing point at the date of ice advance d_a. Over this temperature path, the energy gain from d_a to d_T must equal the energy loss from d_T to d_a:

$$\langle Q_+ \rangle (d_T - d_r) = -\langle Q_- \rangle (d_a - d_T), \tag{A12}$$

where $\langle Q_+ \rangle$ is the average net heat flux from the atmosphere to the upper ocean over $[d_r, d_T]$ and $\langle Q_- \rangle$ is the average net heat flux over $[d_{max}, d_a]$. Defining

$$\lambda_s = -\frac{\langle Q_+ \rangle}{\langle Q_- \rangle} \tag{A13}$$

and rearranging terms in (Eq. A12), we relate d_a to d_r via surface energy fluxes:

$$d_a = -\lambda_s d_r + d_T (1 + \lambda_s). \tag{A14}$$

By differentiating this expression, we get the sought decomposition between reference and feedback responses:

$$\Delta d_a = \Delta d_a^{ref} - \lambda_s \Delta d_r. \tag{A15}$$

The reference response groups all terms independent of Δd_r:

$$\Delta d_r^{ref} = -d_r \Delta \lambda_s + \Delta d_T + \Delta (\lambda_s d_T). \tag{A16}$$

The terms on the right-hand side reflect the contributions of (i) changes in energy fluxes, (ii) change in the date of maximum water temperature and (iii) non-linearities between both. The feedback term in Eq. (A15) isolates the contribution of changes in ice retreat date and λ_s clearly now appears as a feedback factor. To compute the reference and feedback terms from the 1-D model output, the annual time series of $\langle Q_+ \rangle$, $\langle Q_- \rangle$ and d_T were extracted.

Analysis supports the proposed decomposition: the sum of calculated feedback and reference responses (black dashed curve in Fig. A2a) is equal to the total response diagnosed from model outputs (yellow curve in Fig. A2a).

A4 Analysis

Forced and feedback responses clarify the drivers of the shift into autumn that characterises the thermodynamic response of ice seasonality to the perturbation of the radiative forcing. The response of the system is dominated by changes in ice advance date, which are by far dominated by the feedback response ($0.8\,\mathrm{d\,yr^{-1}}$), much larger than the reference response ($0.1\,\mathrm{d\,yr^{-1}}$; see Fig. A2a). The summer feedback factor λ_s, equal on average to 1.63, largely amplifies changes in retreat date. The positive sign of λ_s indicates that earlier retreat implies later advance. Why $\lambda_s > 1$ is because positive heat fluxes into the ocean $\langle Q_+ \rangle$ are typically larger than the heat losses $\langle Q_- \rangle$ that follow the ocean temperature maximum. Hence it takes more time for the surface ocean to release the extra energy than it takes to absorb it.

The response of ice retreat date, following winter processes, is characterised by roughly equal contributions of reference ($-0.2\,\mathrm{d\,yr^{-1}}$) and feedback ($-0.3\,\mathrm{d\,yr^{-1}}$) responses. The feedback factor λ_w is equal to 0.31 on average; hence changes in d_a imply changes in d_r of smaller magnitude. The positive sign means that later advance implies earlier retreat. Why $\lambda_w < 1$ is because of two robust features of the ice seasonal cycle that dampen the impact of changes in d_a on d_r. First the melt season is shorter than the growth season; hence changes in ice advance date translate into weaker changes in ice retreat date. Second, the ice growth rate is larger for thin than for thick ice; hence the maximum winter ice thickness does not decrease due to later advance as much as if the growth rate were constant. (The $1/h$ dependence in growth rate explains the extra 0.5 factor in λ_w.)

Now considering the ice advance vs. retreat amplification coefficient, it can be expressed as a function of feedback and reference responses:

$$R \equiv -\frac{\Delta d_a}{\Delta d_r} = \lambda_s + \frac{\Delta d_a^{ref}}{\Delta d_r}. \tag{A17}$$

R and its two contributors are depicted in Fig. A2b. Summer feedbacks largely dominate R, such that $R \approx \lambda_s$ is a reasonable approximation.

Let us finally note that both feedback factors are determined by fundamental physical features of ice–ocean interactions, likely going beyond climate uncertainties. The winter feedback is determined by the shape of the seasonal cycle and the non-linear dependence of ice growth rate, which are likely invariant across models. As for the summer feedback, the scaling detailed in Appendix B indicates that the related feedback factor is constrained by celestial mechanics, ubiquitous clouds and near-freezing temperatures. This likely contributes to the low level of uncertainty in R among the different climate models.

Appendix B: Scaling of the ice-free ocean energy budget

The 1-D model results show a direct link between, on the one hand, the ratio of long-term trends in ice advance and retreat date ($R_{\mathrm{a/r}}^{\mathrm{long}}$) and the energetics of the ice-free ocean on the other hand:

$$R_{\mathrm{a/r}}^{\mathrm{long}} \approx \lambda_{\mathrm{s}} = -\langle Q_{+}\rangle / \langle Q_{-}\rangle, \tag{B1}$$

where $\langle Q_{+}\rangle$ and $\langle Q_{-}\rangle$ are the average net positive (negative) atmosphere-to-ocean heat fluxes during the ice free-period. CMIP5 and 1-D model results suggest that over long timescales, this ratio is stable and does not vary much among models, with values ranging from 1.5 to 2. Why this ratio would have so little variability is because celestial mechanics, ubiquitous clouds and near-freezing temperatures provide strong constraints on the radiation balance, which dominates the surface energy budget.

Assuming that non-solar components cancel each other, the mean heat gain is mostly solar:

$$\langle Q_{+}\rangle = \langle Q_{\mathrm{sol}}\,(1-\alpha_{\mathrm{w}})\left[1-\exp\left(-\kappa h_{\mathrm{w}}\right)\right]\rangle_{\text{early ice-free season}}, \tag{B2}$$

where the mean is taken over the first part of the ice-free period, typically covering July or June. Of remarkable importance is that the magnitude of clear-sky solar flux above the Arctic Circle deviates by less than $20\,\mathrm{W\,m^{-2}}$, both in space and time, around the summer solstice (see, e.g. Peixoto and Oort, 1992). Assuming summer cloud skies would remain the norm, we take $150\,\mathrm{W\,m^{-2}}$ as representative for $\langle Q_{+}\rangle$.

The mean heat loss is mostly non-solar:

$$\langle Q_{-}\rangle = \langle Q_{\mathrm{lw}} - \epsilon\sigma T_{\mathrm{w}}^{4} + Q_{\mathrm{sh}} + Q_{\mathrm{lh}}\rangle_{\text{late ice-free season}}, \tag{B3}$$

and corresponds to the second part of the ice-free period, typically covering August to October. Downwelling longwave radiation flux Q_{lw} corresponds to cloud skies at near-freezing temperatures, for which $250\,\mathrm{W\,m^{-2}}$ seems reasonable (Persson et al., 2002). The thermal emission would be that of the ocean, a nearly ideal black body, at near-freezing temperatures, and should not depart much from $300\,\mathrm{W\,m^{-2}}$. The sensible (Q_{sh}) and latent (Q_{lh}) heat fluxes are relatively more uncertain. In current ice-covered conditions, turbulent fluxes imply a net average heat loss, typically smaller than $10\,\mathrm{W\,m^{-2}}$ (Persson et al., 2002). Over an ice-free ocean, however, turbulent heat losses would obviously increase, in particular through the latent heat flux, but also become more variable at synoptic timescales. Assuming that turbulent heat fluxes would in the future Arctic compare to what they are today in ice-free ocean regions of the North Pacific, we argue that they would correspond to a $25\,\mathrm{W\,m^{-2}}$ heat loss, definitely not exceeding $100\,\mathrm{W\,m^{-2}}$ (Yu et al., 2008).

Taken together, these elements give an estimated R value ranging from 1 to 2, for which uncertainties on the dominant radiation terms of the energy budget are small and inter-model differences in turbulent heat fluxes would be decisive in determining the actual value of the ratio.

Supplement. The supplement related to this article is available online at: https://doi.org/10.5194/tc-13-79-2019-supplement.

Author contributions. All authors conceived the study and co-wrote the paper. ML and MV performed analyses.

Competing interests. The authors declare that they have no conflict of interest.

Acknowledgements. We thank Sebastien Denvil for technical support and Roland Seferian, Jean-Baptiste Sallée, Olivier Aumont and Laurent Bopp for scientific discussions. We also thank the anonymous reviewers for their constructive comments that helped to improve the paper.

Edited by: Dirk Notz
Reviewed by: two anonymous referees

References

Arrigo, K. R. and van Dijken, G. L.: Secular trends in Arctic Ocean net primary production, J. Geophys. Res., 116, C09011, https://doi.org/10.1029/2011JC007151, 2011.

Assmy, P., Fernández-Méndez, M., Duarte, P., Meyer, A., Randelhoff, A., Mundy, C. J., Olsen, L. M., Kauko, H. M., Bailey, A., Chierici, M., Cohen, L., Doulgeris, A. P., Ehn, J. K., Fransson, A., Gerland, S., Hop, H., Hudson, S. R., Hughes, N., Itkin, P., Johnsen, G., King, J. A., Koch, B. P., Koenig, Z., Kwasniewski, S., Laney, S. R., Nicolaus, M., Pavlov, A. K., Polashenski, C. M., Provost, C., Rösel, A., Sandbu, M., Spreen, G., Smedsrud, L. H., Sundfjord, A., Taskjelle, T., Tatarek, A., Wiktor, J., Wagner, P. M., Wold, A., Steen, H., and Granskog, M. A.: Leads in Arctic pack ice enable early phytoplankton blooms below snow-covered sea ice, Sci. Rep., 7, srep40850, https://doi.org/10.1038/srep40850, 2017.

Barnhart, K. R., Miller, C. R., Overeem, I., and Kay, J. E.: Mapping the future expansion of Arctic open water, Nat. Clim. Change, 6, 280–285, https://doi.org/10.1038/nclimate2848, 2016.

Bitz, C. M., Holland, M. M., Hunke, E. C., and Moritz, R. E.: Maintenance of the Sea-Ice Edge, J. Climate, 18, 2903–2921, https://doi.org/10.1175/JCLI3428.1, 2005.

Blanchard-Wrigglesworth, E., Armour, K. C., Bitz, C. M., and DeWeaver, E.: Persistence and Inherent Predictability of Arctic Sea Ice in a GCM Ensemble and Observations, J. Climate, 24, 231–250, https://doi.org/10.1175/2010JCLI3775.1, 2010.

Bony, S., Dufresne, J.-L., Treut, H. L., Morcrette, J.-J., and Senior, C.: On dynamic and thermodynamic components of cloud changes, Clim. Dynam., 22, 71–86, https://doi.org/10.1007/s00382-003-0369-6, 2004.

Cavalieri, D. J. and Parkinson, C. L.: Arctic sea ice variability and trends, 1979–2010, The Cryosphere, 6, 881–889, https://doi.org/10.5194/tc-6-881-2012, 2012.

Collins, W. J., Bellouin, N., Doutriaux-Boucher, M., Gedney, N., Halloran, P., Hinton, T., Hughes, J., Jones, C. D., Joshi, M., Liddicoat, S., Martin, G., O'Connor, F., Rae, J., Senior, C., Sitch, S., Totterdell, I., Wiltshire, A., and Woodward, S.: Development and evaluation of an Earth-System model – HadGEM2, Geosci. Model Dev., 4, 1051–1075, https://doi.org/10.5194/gmd-4-1051-2011, 2011.

Comiso, J. "Joey": Bootstrap Sea Ice Concentrations from Nimbus-7 SMMR and DMSP SSM/I-SSMIS, Version 2, https://doi.org/10.5067/J6JQLS9EJ5HU, 2000.

Dufresne, J.-L., Foujols, M.-A., Denvil, S., Caubel, A., Marti, O., Aumont, O., Balkanski, Y., Bekki, S., Bellenger, H., Benshila, R., Bony, S., Bopp, L., Braconnot, P., Brockmann, P., Cadule, P., Cheruy, F., Codron, F., Cozic, A., Cugnet, D., Noblet, N. de, Duvel, J.-P., Ethé, C., Fairhead, L., Fichefet, T., Flavoni, S., Friedlingstein, P., Grandpeix, J.-Y., Guez, L., Guilyardi, E., Hauglustaine, D., Hourdin, F., Idelkadi, A., Ghattas, J., Joussaume, S., Kageyama, M., Krinner, G., Labetoulle, S., Lahellec, A., Lefebvre, M.-P., Lefevre, F., Levy, C., Li, Z. X., Lloyd, J., Lott, F., Madec, G., Mancip, M., Marchand, M., Masson, S., Meurdesoif, Y., Mignot, J., Musat, I., Parouty, S., Polcher, J., Rio, C., Schulz, M., Swingedouw, D., Szopa, S., Talandier, C., Terray, P., Viovy, N., and Vuichard, N.: Climate change projections using the IPSL-CM5 Earth System Model: from CMIP3 to CMIP5, Clim. Dynam., 40, 2123–2165, https://doi.org/10.1007/s00382-012-1636-1, 2013.

Dussin, R., Barnier, B., and Brodeau, L.: The making of Drakkar forcing set DFS5. Tech. report DRAKKAR/MyOcean Report 01-04-16, LGGE, Grenoble, France, 2016.

Fletcher, J. O.: The heat budget of the Arctic Basin and its relation to climate, Rep. R-444-PR, RAND Corp., Santa Monica, Calif., 1965.

Gent, P. R., Danabasoglu, G., Donner, L. J., Holland, M. M., Hunke, E. C., Jayne, S. R., Lawrence, D. M., Neale, R. B., Rasch, P. J., Vertenstein, M., Worley, P. H., Yang, Z.-L., and Zhang, M.: The Community Climate System Model Version 4, J. Climate, 24, 4973–4991, https://doi.org/10.1175/2011JCLI4083.1, 2011.

Giorgetta, M. A., Jungclaus, J., Reick, C. H., Legutke, S., Bader, J., Böttinger, M., Brovkin, V., Crueger, T., Esch, M., Fieg, K., Glushak, K., Gayler, V., Haak, H., Hollweg, H.-D., Ilyina, T., Kinne, S., Kornblueh, L., Matei, D., Mauritsen, T., Mikolajewicz, U., Mueller, W., Notz, D., Pithan, F., Raddatz, T., Rast, S., Redler, R., Roeckner, E., Schmidt, H., Schnur, R., Segschneider, J., Six, K. D., Stockhause, M., Timmreck, C., Wegner, J., Widmann, H., Wieners, K.-H., Claussen, M., Marotzke, J., and Stevens, B.: Climate and carbon cycle changes from 1850 to 2100 in MPI-ESM simulations for the Coupled Model Intercomparison Project phase 5, J. Adv. Model. Earth Syst., 5, 572–597, https://doi.org/10.1002/jame.20038, 2013.

Goosse, H., Kay, J. E., Armour, K. C., Bodas-Salcedo, A., Chepfer, H., Docquier, D., Jonko, A., Kushner, P. J., Lecomte, O., Massonnet, F., Park, H.-S., Pithan, F., Svensson, G., and Vancoppenolle, M.: Quantifying climate feedbacks in polar regions, Nat. Commun., 9, 1919, https://doi.org/10.1038/s41467-018-04173-0, 2018.

Hezel, P. J., Fichefet, T., and Massonnet, F.: Modeled Arctic sea ice evolution through 2300 in CMIP5 extended RCPs, The Cryosphere, 8, 1195–1204, https://doi.org/10.5194/tc-8-1195-2014, 2014.

Johnson, M. and Eicken, H.: Estimating Arctic sea-ice freeze-up and break-up from the satellite record: A comparison of different approaches in the Chukchi and Beaufort Seas, Elem. Sci. Anth.,

4, 000124, https://doi.org/10.12952/journal.elementa.000124, 2016.

Kröner, N., Kotlarski, S., Fischer, E., Lüthi, D., Zubler, E., and Schär, C.: Separating climate change signals into thermodynamic, lapse-rate and circulation effects: theory and application to the European summer climate, Clim. Dynam., 48, 3425–3440, https://doi.org/10.1007/s00382-016-3276-3, 2017.

Kwok, R. and Rothrock, D. A.: Decline in Arctic sea ice thickness from submarine and ICESat records: 1958–2008, Geophys. Res. Lett., 36, L15501, https://doi.org/10.1029/2009GL039035, 2009.

Laidre, K. L., Stern, H., Kovacs, K. M., Lowry, L., Moore, S. E., Regehr, E. V., Ferguson, S. H., Wiig, Ø., Boveng, P., Angliss, R. P., Born, E. W., Litovka, D., Quakenbush, L., Lydersen, C., Vongraven, D., and Ugarte, F.: Arctic marine mammal population status, sea ice habitat loss, and conservation recommendations for the 21st century, Conserv. Biol., 29, 724–737, https://doi.org/10.1111/cobi.12474, 2015.

Lindsay, R. and Schweiger, A.: Arctic sea ice thickness loss determined using subsurface, aircraft, and satellite observations, The Cryosphere, 9, 269–283, https://doi.org/10.5194/tc-9-269-2015, 2015.

Markus, T., Stroeve, J. C., and Miller, J.: Recent changes in Arctic sea ice melt onset, freeze-up, and melt season length, J. Geophys. Res., 114, C12024, https://doi.org/10.1029/2009JC005436, 2009.

Maslanik, J., Stroeve, J., Fowler, C., and Emery, W.: Distribution and trends in Arctic sea ice age through spring 2011, Geophys. Res. Lett., 38, L13502, https://doi.org/10.1029/2011GL047735, 2011.

Massonnet, F., Fichefet, T., Goosse, H., Bitz, C. M., Philippon-Berthier, G., Holland, M. M., and Barriat, P.-Y.: Constraining projections of summer Arctic sea ice, The Cryosphere, 6, 1383–1394, https://doi.org/10.5194/tc-6-1383-2012, 2012.

Massonnet, F., Vancoppenolle, M., Goosse, H., Docquier, D., Fichefet, T., and Blanchard-Wrigglesworth, E.: Arctic sea ice change tied to its mean state through thermodynamic processes, Nat. Clim. Change, 8, 599–603, 2018.

Maykut, G. A.: The surface heat and mass balance, in: The Geophysics of Sea Ice, edited by: Untersteiner, N., Plenum Press, New York, 146, 395–463, 1986.

Maykut, G. A. and Untersteiner, N.: Some results from a time-dependent thermodynamic model of sea ice, J. Geophys. Res., 76, 1550–1575, https://doi.org/10.1029/JC076i006p01550, 1971.

Melia, N., Haines, K., Hawkins, E., and Day, J. J.: Towards seasonal Arctic shipping route predictions, Environ. Res. Lett., 12, 084005, https://doi.org/10.1088/1748-9326/aa7a60, 2017.

Notz, D.: How well climate models must agree with observations, Philos. Trans. R. Soc. A, 373, 20140164, https://doi.org/10.1098/rsta.2014.0164, 2015.

Notz, D. and Stroeve, J.: Observed Arctic sea-ice loss directly follows anthropogenic CO_2 emission, Science, 354, aag2345, https://doi.org/10.1126/science.aag2345, 2016.

Notz, D., Jahn, A., Holland, M., Hunke, E., Massonnet, F., Stroeve, J., Tremblay, B., and Vancoppenolle, M.: The CMIP6 Sea-Ice Model Intercomparison Project (SIMIP): understanding sea ice through climate-model simulations, Geosci. Model Dev., 9, 3427–3446, https://doi.org/10.5194/gmd-9-3427-2016, 2016.

Parkinson, C. L.: Spatial patterns in the length of the sea ice season in the Southern Ocean, 1979–1986, J. Geophys. Res., 99, 16327–16339, https://doi.org/10.1029/94JC01146, 1994.

Parkinson, C. L.: Global Sea Ice Coverage from Satellite Data: Annual Cycle and 35-Yr Trends, J. Climate, 27, 9377–9382, https://doi.org/10.1175/JCLI-D-14-00605.1, 2014.

Peixoto, J. P. and Oort, A. H.: Physics of Climate, 1992 ed., American Institute of Physics, New York, 1992.

Perovich, D. K., Grenfell, T. C., Richter-Menge, J. A., Light, B., Tucker, W. B., and Eicken, H.: Thin and thinner: Sea ice mass balance measurements during SHEBA, J. Geophys. Res.-Oceans, 108, 8050, https://doi.org/10.1029/2001JC001079, 2003.

Perovich, D. K., Light, B., Eicken, H., Jones, K. F., Runciman, K., and Nghiem, S. V.: Increasing solar heating of the Arctic Ocean and adjacent seas, 1979–2005: Attribution and role in the ice-albedo feedback, Geophys. Res. Lett., 34, L19505, https://doi.org/10.1029/2007GL031480, 2007.

Persson, P. O. G., Fairall, C. W., Andreas, E. L., Guest, P. S., and Perovich, D. K.: Measurements near the Atmospheric Surface Flux Group tower at SHEBA: Near-surface conditions and surface energy budget, J. Geophys. Res.-Oceans, 107, 8045, https://doi.org/10.1029/2000JC000705, 2002.

Renner, A. H. H., Gerland, S., Haas, C., Spreen, G., Beckers, J. F., Hansen, E., Nicolaus, M., and Goodwin, H.: Evidence of Arctic sea ice thinning from direct observations, Geophys. Res. Lett., 41, 5029–5036, https://doi.org/10.1002/2014GL060369, 2014.

Rotstayn, L. D., Jeffrey, S. J., Collier, M. A., Dravitzki, S. M., Hirst, A. C., Syktus, J. I., and Wong, K. K.: Aerosol- and greenhouse gas-induced changes in summer rainfall and circulation in the Australasian region: a study using single-forcing climate simulations, Atmos. Chem. Phys., 12, 6377–6404, https://doi.org/10.5194/acp-12-6377-2012, 2012.

Rousset, C., Vancoppenolle, M., Madec, G., Fichefet, T., Flavoni, S., Barthélemy, A., Benshila, R., Chanut, J., Levy, C., Masson, S., and Vivier, F.: The Louvain-La-Neuve sea ice model LIM3.6: global and regional capabilities, Geosci. Model Dev., 8, 2991–3005, https://doi.org/10.5194/gmd-8-2991-2015, 2015.

Schmidt, G. A., Kelley, M., Nazarenko, L., Ruedy, R., Russell, G. L., Aleinov, I., Bauer, M., Bauer, S. E., Bhat, M. K., Bleck, R., Canuto, V., Chen, Y.-H., Cheng, Y., Clune, T. L., Del Genio, A., de Fainchtein, R., Faluvegi, G., Hansen, J. E., Healy, R. J., Kiang, N. Y., Koch, D., Lacis, A. A., LeGrande, A. N., Lerner, J., Lo, K. K., Matthews, E. E., Menon, S., Miller, R. L., Oinas, V., Oloso, A. O., Perlwitz, J. P., Puma, M. J., Putman, W. M., Rind, D., Romanou, A., Sato, M., Shindell, D. T., Sun, S., Syed, R. A., Tausnev, N., Tsigaridis, K., Unger, N., Voulgarakis, A., Yao, M.-S., and Zhang, J.: Configuration and assessment of the GISS ModelE2 contributions to the CMIP5 archive, J. Adv. Model. Earth Syst., 6, 141–184, https://doi.org/10.1002/2013MS000265, 2014.

Semtner, A. J.: A Model for the Thermodynamic Growth of Sea Ice in Numerical Investigations of Climate, J. Phys. Oceanogr., 6, 379–389, https://doi.org/10.1175/1520-0485(1976)006<0379:AMFTTG>2.0.CO;2, 1976.

Semtner, A. J.: On modelling the seasonal thermodynamic cycle of sea ice in studies of climatic change, Clim. Change, 1, 27–37, 1984.

Serreze, M. C., Crawford, A. D., Stroeve, J. C., Barrett, A. P., and Woodgate, R. A.: Variability, trends, and pre-

dictability of seasonal sea ice retreat and advance in the Chukchi Sea, J. Geophys. Res.-Oceans, 121, 7308–7325, https://doi.org/10.1002/2016JC011977, 2016.

Shepherd, T. G.: Atmospheric circulation as a source of uncertainty in climate change projections, Nat. Geosci., 7, 703–708, https://doi.org/10.1038/ngeo2253, 2014.

Smith, L. C. and Stephenson, S. R.: New Trans-Arctic shipping routes navigable by midcentury, P. Natl. Acad. Sci. USA, 110, E1191–E1195, https://doi.org/10.1073/pnas.1214212110, 2013.

Stammerjohn, S., Massom, R., Rind, D., and Martinson, D.: Regions of rapid sea ice change: An inter-hemispheric seasonal comparison, Geophys. Res. Lett., 39, L06501, https://doi.org/10.1029/2012GL050874, 2012.

Steele, M. and Dickinson, S.: The phenology of Arctic Ocean surface warming, J. Geophys. Res.-Oceans, 121, 6847–6861, https://doi.org/10.1002/2016JC012089, 2016.

Steele, M., Ermold, W., and Zhang, J.: Arctic Ocean surface warming trends over the past 100 years, Geophys. Res. Lett., 35, L02614, https://doi.org/10.1029/2007GL031651, 2008.

Stefan, J.: Uber die Theorie der Eisbildung, insbesondere uber Eisbildung im Polarmeer, Ann. Phys. 3rd. Ser., 42, 269–286, 1891.

Steiner, N. S., Christian, J. R., Six, K. D., Yamamoto, A., and Yamamoto-Kawai, M.: Future ocean acidification in the Canada Basin and surrounding Arctic Ocean from CMIP5 earth system models, J. Geophys. Res.-Oceans, 119, 332–347, https://doi.org/10.1002/2013JC009069, 2014.

Stern, H. L. and Laidre, K. L.: Sea-ice indicators of polar bear habitat, The Cryosphere, 10, 2027–2041, https://doi.org/10.5194/tc-10-2027-2016, 2016.

Stroeve, J. C., Kattsov, V., Barrett, A., Serreze, M., Pavlova, T., Holland, M., and Meier, W. N.: Trends in Arctic sea ice extent from CMIP5, CMIP3 and observations, Geophys. Res. Lett., 39, L16502, https://doi.org/10.1029/2012GL052676, 2012.

Stroeve, J. C., Markus, T., Boisvert, L., Miller, J., and Barrett, A.: Changes in Arctic melt season and implications for sea ice loss, Geophys. Res. Lett., 41, 1216–1225, https://doi.org/10.1002/2013GL058951, 2014.

Stroeve, J. C., Crawford, A. D., and Stammerjohn, S.: Using timing of ice retreat to predict timing of fall freeze-up in the Arctic, Geophys. Res. Lett., 43, GL069314, https://doi.org/10.1002/2016GL069314, 2016.

Uotila, P., Iovino, D., Vancoppenolle, M., Lensu, M., and Rousset, C.: Comparing sea ice, hydrography and circulation between NEMO3.6 LIM3 and LIM2, Geosci. Model Dev., 10, 1009–1031, https://doi.org/10.5194/gmd-10-1009-2017, 2017.

Vancoppenolle, M., Bopp, L., Madec, G., Dunne, J., Ilyina, T., Halloran, P. R., and Steiner, N.: Future Arctic Ocean primary productivity from CMIP5 simulations: Uncertain outcome, but consistent mechanisms, Global Biogeochem. Cy., 27, 605–619, https://doi.org/10.1002/gbc.20055, 2013.

Voldoire, A., Sanchez-Gomez, E., Mélia, D. S. Y., Decharme, B., Cassou, C., Sénési, S., Valcke, S., Beau, I., Alias, A., Chevallier, M., Déqué, M., Deshayes, J., Douville, H., Fernandez, E., Madec, G., Maisonnave, E., Moine, M.-P., Planton, S., Saint-Martin, D., Szopa, S., Tyteca, S., Alkama, R., Belamari, S., Braun, A., Coquart, L., and Chauvin, F.: The CNRM-CM5.1 global climate model: description and basic evaluation, Clim. Dynam., 40, 2091–2121, https://doi.org/10.1007/s00382-011-1259-y, 2013.

Wang, M. and Overland, J. E.: Projected future duration of the sea-ice-free season in the Alaskan Arctic, Progr. Oceanogr., 136, 50–59, https://doi.org/10.1016/j.pocean.2015.01.001, 2015.

Wassmann, P. and Reigstad, M.: Future Arctic Ocean Seasonal Ice Zones and Implications for Pelagic-Benthic Coupling, Oceanography, 24, 220–231, https://doi.org/10.5670/oceanog.2011.74, 2011.

Wu, T., Song, L., Li, W., Wang, Z., Zhang, H., Xin, X., Zhang, Y., Zhang, L., Li, J., Wu, F., Liu, Y., Zhang, F., Shi, X., Chu, M., Zhang, J., Fang, Y., Wang, F., Lu, Y., Liu, X., Wei, M., Liu, Q., Zhou, W., Dong, M., Zhao, Q., Ji, J., Li, L., and Zhou, M.: An overview of BCC climate system model development and application for climate change studies, Acta Meteorol. Sin., 28, 34–56, https://doi.org/10.1007/s13351-014-3041-7, 2014.

Yeager, S. G., Karspeck, A. R., and Danabasoglu, G.: Predicted slowdown in the rate of Atlantic sea ice loss, Geophys. Res. Lett., 42, 10704–10713, https://doi.org/10.1002/2015GL065364, 2015.

Yu, L., Jin, X., and Weller, R. A.: Multidecade Global Flux Datasets from the Objectively Analyzed Air-sea Fluxes (OAFlux) Project: Latent and sensible heat fluxes, ocean evaporation, and related surface meteorological variables, Tech. Report Woods Hole Oceanographic Institution, OAFlux Project Technical Report, OA-2008-01, 64 pp., Woods Hole, Massachusetts, 2008.

Chapitre 2

Contraindre le transfert radiatif dans NEMO à partir d'observations dans la banquise saisonnière arctique

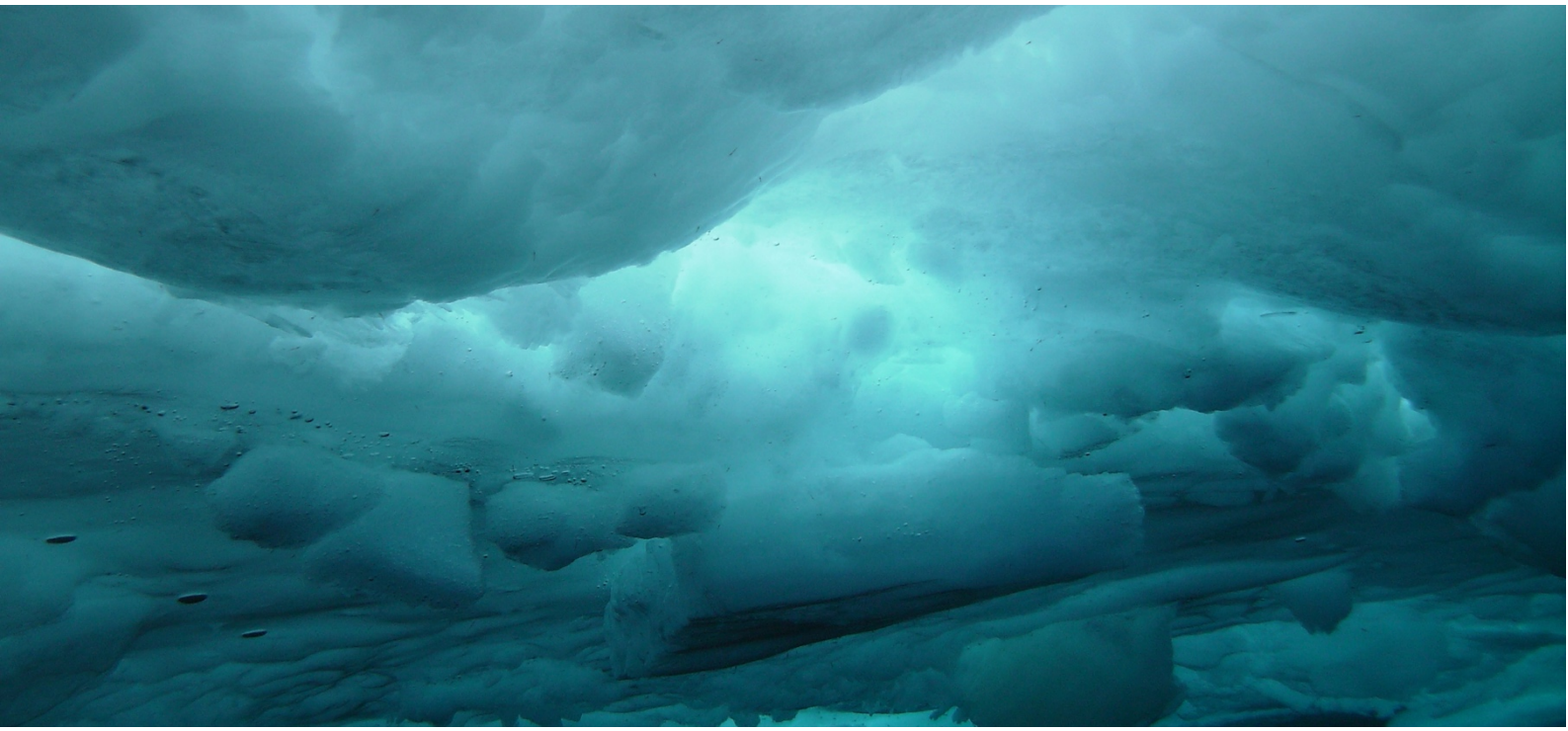

© K. Meiner

Les projections des modèles du système Terre sur le futur de la production primaire en Arctique comportent de larges incertitudes. Une des principales sources d'incertitude est la transmission du rayonnement solaire à l'océan au travers des zones de glace de mer. Celle-ci n'est pas bien contrainte en raison d'un manque d'observation et d'analyses.

Dans ce chapitre, j'évalue la version originale ainsi qu'une version modifiée du schéma de transfert radiatif dans le modèle de glace-océan NEMO. Pour cela j'utilise les récentes mesures de lumière au-dessus et sous la banquise saisonnière arctique, réalisées en baie de Baffin, au Svalbard et sur l'ile d'Hokkaido, dans le cadre des programmes *Green Edge, Optimism* et *SLOPE* (auquel j'ai participé dans le cadre de cette thèse).

Le schéma de transfert radiatif NEMO est basé sur une loi de Beer-Lambert en deux couches dans la neige et dans la glace de mer. Il est aussi basé sur un fractionnement de la lumière en différentes bandes de longueurs d'onde (3 bandes pour le spectre visible + 1 pour le spectre non visible).

Deux diagnostics sont évalués dans ce chapitre : la transmittance dans le système neige-banquise et le fractionnement du rayonnement transmis en 3+1 bande spectrale.

Concernant l'étude des transmittances, je montre que la version originale du schéma de transfert radiatif de NEMO, qui exclut la transmission de la lumière au travers de la neige, doit être rejetée. Je suggère aussi que considérer l'effet des mares de fonte dans le calcul de transmittance serait grandement bénéfique à la simulation du rayonnement transmis dans les zones de banquise. Cependant, des erreurs dans le calcul de la transmittance restent non résolues, je suggère l'effet non résolu de la microstructure de la neige comme potentielle source à ces erreurs.

Enfin, je montre dans ce chapitre que la distribution spectrale de la lumière est influencée par la neige, la banquise et les algues de glace, je suggère ainsi des changements dans les valeurs décrivant le fractionnement spectral du rayonnement dans les régions englacées dans NEMO.

Constraining the representation of radiative transfer in NEMO using observations from the Arctic seasonal ice zone

Marion Lebrun[1], Martin Vancoppenolle[1], Gurvan Madec[1], Antonio Lourenço[1], Frederic Vivier[1]

[1] Sorbonne Université, LOCEAN-IPSL, CNRS/IRD/MNHN, Paris, France

Manuscript in prep

July 2019

Marion Lebrun, Laboratoire d'Océanographie et du Climat, IPSL Boite 100, 4 Place Jussieu, 75252 Paris CEDEX 05, France.

Abstract

Future Arctic Ocean primary production, as projected from Earth System Models, is largely uncertain. One of the main uncertainty sources relates to light transmission in ice-covered waters, not well constrained due to a lack of observations and understanding.

Here we use observations from the Arctic seasonal ice zone to evaluate the radiative transfer scheme of NEMO, the ice-ocean component of several state-of-the-art Earth System Models. An observational database was assembled, with concomitant measurements of the light field above and under sea ice, and snow and ice characteristics. Observations were collected from Baffin Bay, Svalbard coastal fjords and an Okhotsk Sea inlet, in the framework of the *GreenEdge, OPTIMISM* and *SLOPE* programs.

The NEMO radiative transfer scheme is based on (i) a well-tested system of empirical expressions for the dependence of the surface albedo on environmental characteristics ; (ii) Beer-Lambert law for attenuation within snow and ice and (iii) prescribed energy fractionation at the uppermost ocean surface, into 3 visible and 1 non-visible spectral bands. The original version of the scheme precludes light transmission in presence of snow, hindering the onset of planktonic activity in spring. The scheme was therefore expanded to enable light transmission through snow.

We then compare observations and the modified NEMO radiative transfer scheme on two diagnostics : the transmittance of the snow-ice system, and the 3+1 under-ice spectral energy fractions. We first show that attenuation and surface transmission coefficients can be adjusted to obtain broad consistency between model and observational transmittance calculations. We also suggest that considering the effect of melt ponds is beneficial to transmittance calculations. However, large-point-to-point transmittance inconsistencies remain. Unresolved effects of snow microstructure appear as the most likely explanation.

Second, we analyse how the observed light energy within the model spectral fractions evolves with snow depth, ice thickness and *Chl-a* content in sea ice. We suggest significant deviations from the reference values. Our results point to easy improvements to the representation of light transmission in ice-covered waters. This may prove applicable to the many large-scale ice-ocean models based on similar principles. And this may ultimately reduce uncertainties on the drivers of planktonic activity in ice-covered waters as simulated by Earth System Models.

Introduction

Sea ice plays an important role in phytoplankton activity in ice-covered waters. The reason why is that available light for photosynthesis is largely affected by sea ice (Arrigo & van Dijken, 2011; Assmy et al., 2017; Nicolaus et al., 2010; Wassmann & Reigstad, 2011). Arctic sea ice cover has decreased over the last four decades (Cavalieri & Parkinson, 2012; Kwok & Rothrock, 2009; Lindsay & Schweiger, 2015; Maslanik et al., 2011; Renner et al., 2014), and this retreat is projected to continue into this century, according to Earth System (Massonnet et al., 2012; Stroeve et al., 2012).

Less sea ice increases light availability and photosynthesis, provided sufficient nutrient supply (Horvat et al., 2017; Pistone et al., 2014; Popova et al., 2012; Vancoppenolle et al., 2013). This has possibly large implications on the carbon cycle and upper trophic levels (Parmentier et al., 2013; Post et al., 2013). Yet, large uncertainties remain in the projections of Arctic phytoplankton activity, attributed to inconsistent simulations of light and nutrients (Popova et al., 2012; Vancoppenolle et al., 2013). Both aspects are characterised by specific issues. Here, we focus on how models represent the under-ice light climate, which has not thoroughly been evaluated.

The under-ice light climate depends on how much the incoming light attenuates due to absorption and scattering within snow, meltwater, and ice (Perovich, 1996). Light absorption and scattering ultimately depend on microstructure, in particular grain shape, size and orientation within snow, as well as brine inclusions and gas bubbles in sea ice. Because of changes in sea ice scape at low scales (<1 m), under-ice light intensity can vary over up to two orders of magnitude (Katlein et al., 2019). Under ice radiative transfer is also wavelength-dependent (Perovich, 1996).

In Earth System Models, the under-ice light climate depends on the model radiative transfer formulations, within sea ice and ocean. For sea ice, two approaches are currently used. The first is based on a direct specification of apparent optical properties, namely empirical albedo fits (e.g., Pedersen et al., 2009; Shine & Henderson-Sellers, 1985) and attenuation coefficients within snow and ice, used in the context of the Beer-Lambert law (Grenfell & Maykut, 1977; Maykut & Untersteiner, 1971). This approach is used for instance in the LIM3 sea ice model (Vancoppenolle et al., 2009) and within MPI-ESM (Notz et al., 2013).The second approach is based on inherent optical properties (scattering, absorption and asymmetry coefficients), used in the framework of the Delta-Eddington approximation, and dependent on a prescribed microstructure (Briegleb & Light, 2007; Saenz & Arrigo, 2012). This approach is used in the CICE sea ice model (Hunke et al., 2019). Both schemes suffer from limited observations to constrain model coefficients and from the fact that neither the full 3D distribution of snow, ice and meltwater nor microstructure changes (brine excepted) are represented.

The simulated under-ice light climate also depends on assumptions made in the ocean component, which are rarely detailed in models' documentation. Light is typically spectrally distributed because of largely different penetration lengths over the optical spectrum. For instance, in NEMO, the available light at the ocean surface is split into 2 to 4 wavebands following the approach of Morel (1988) simplified by Lengaigne et al. (2007). Yet this totally ampirical formulation has been developed for ice-free waters at low latitude and never been evaluated in ice-covered regions.

Under-ice light and ancillary observations from recent field programs in the Arctic seasonal ice zone, such as *GreenEdge* (Baffin Bay 2015-2016; Randelhoff et al., 2019; Oziel et al., 2019), OPTIMISM (Svalbard Archipelago, 2015-2018) and SLOPE (Saroma-ko Lagoon, Hokkaido, Japan, February 2019, Nomura et al., 2019; See Annexes) provide tests for the representation of radiative transfer in ice-covered seas. In this study, we use these observations to evaluate and

adjust the radiative transfer scheme of NEMO, the ice-ocean component of several state-of-the-art Earth System Models.

We first evaluated different ice-snow transmittances considering various approaches :(i) the reference NEMO parameterisation providing transmitted light under snow-covered ice; (ii) an improved parameterisation considering transmission of light in both bare ice and snow-covered ice following the Beer-Lambert law; (iii) and three approaches based on the improved parameterisation, which evaluated the influence of melt ponds, ice algae or the small-scale variation of snow depth on the transmittance.

We then analyse how ice, snow and ice algae influence the spectral wavebands define in NEMO. From this analysis, we suggest a spectral distribution of under-ice/snow light which is closer to the observations.

1. Data and methods

We evaluate the radiative transfer scheme from the NEMO ice-ocean model using in situ light measurements above and under Arctic seasonal ice, from Baffin Bay, Svalbard and the Hokkaido regions, in the framework of the Green Edge, Optimism and SLOPE programs.

1.1 Representation of radiative transfer in NEMO

1.1.1 Reference radiative transfer scheme

The reference (**REF**) parameterisation of radiative transfer in ice-covered waters in NEMO (Madec et al., 2017; Rousset et al., 2015; Vancoppenolle et al. 2009) is based on three basic elements : surface albedo, vertical attenuation by snow and ice both integrated in all wavelength, and the spectral fractionation of light at the ice-ocean interface.

The **surface albedo** α is specified empirically from environmental factors :

$$\alpha = \alpha(h_i, h_s, T_{su}, c) \ , \quad (1)$$

based on ideas developed by Shine and Henderson-Sellers (1985) and Fichefet and Morales Maqueda (1997). The retained influential factors are h_i, the ice thickness ; h_s, the snow depth ; T_{su}, the surface temperature and c, the cloud fraction. T_{su} intervenes as a switch from melting to freezing conditions ; whereas cloud fraction is included to mimic the spectral change of incident light from direct to diffuse conditions. Four parameters must be specified. These correspond to asymptotic reference albedo values for thick ice and snow, for wet and dry conditions. The parameterisation used is a small revision introduced in NEMOv4. It is designed to suppress rare spurious discontinuities in the original parameterisation, and to better match cloud fraction dependence with observations. Note that a prescribed correction to the albedo of melting bare ice is applied by default to account for the presence of melt ponds — we ignore the latter, here.

Attenuation within the snow-ice system assumes two layers. The uppermost layer is a thin, highly scattering surface layer (SSL, depth h_o=10 cm), and the lower one, much thicker has a much weaker impact. Formally, the irradiance I at depth z within the snow-ice system is :

$$I(z) = i_o \mathrm{I}(0) exp[-\kappa(z - h_o)], \quad (2)$$

Where $I(0) = F_{sw}^0 \ (1 - \alpha)$; with F_{sw}^0, the incident downwelling irradiance at the ice surface (W.m^{-2}). Two parameters are to be specified : i_o, the surface transmission parameter, describing the transmission of light through the SSL (of thickness h_o) and κ, the attenuation coefficient (m^{-1}) in the ice interior. Light absorbed in the SSL is converted into sensible heat and directly contributes to the surface energy budget, whereas light absorbed in the deeper layer contributes to warm sea ice internally. In the **REF** parameterisation snow is assumed fully opaque (i_o= 0 when $h_s > 0$), for simplicity. This assumption is unrealistic to some degree, depending on the context. It could, in particular, be problematic to capture the onset of phytoplankton activity in early spring. It will be, consequently revised in the context of this paper (see below).

A last aspect to mention is the **spectral partitioning** of downwelling irradiance at the ice-ocean interface. In the ocean component of NEMO, irradiance is spectrally resolved. This is because of the wavelength dependence of the attenuation in water (Morel, 1988) .Red and green light attenuate more rapidly than blue light in seawater, which affects the vertical distribution of heating rate and of photosynthesis. At the ocean surface, the energetic fraction of near-surface irradiance within each waveband is specified. The choice of wavelength bands is application-dependent. The most common decomposition, retained here, uses 3 visible + 1 non-visible bands (Lengaigne et al., 2007), designed to emulate the spectral distribution of light penetration following the 61 wavebands formulation of Morel (1988). A prescribed 58% of the net radiation is assumed to lie in the non-visible (mostly infrared) band and is assumed to rapidly attenuate in the upper few tens of centimetres of seawater. The remainder of the energy (42%) is equally distributed into the three visible wavebands (blue, 400-500 nm; green, 500-600 nm; red, 600-700 nm). This partitioning is deemed reasonable for ice-free ocean conditions. In the absence of information, such partitioning is currently also applied in ice-covered waters. However, common sense suggests this to be somehow wrong, in particular to assume a large fraction of non-visible light below sea ice. We will explore which adjustments in the fractions should be applied for ice-covered waters based on the analysis developed in this paper (see below).

Model grid cells also include **open-water** and **multiple ice thickness categories**. These aspects are not considered here and treated more extensively in the next chapter. In the present chapter, we assume that observations are purely 1D, i.e., that they represent an infinitely wide region covered by sea ice of uniform snow depth and ice thickness. In the model world, this would correspond to a grid cell with a single ice thickness category with 100% ice concentration.

1.1.2 Applied modifications to the reference radiative transfer scheme

The **REF** scheme quickly showed obvious limits, questioning its validity. Hence, a series of modifications were applied, which we now describe.

The first series of modifications (**IMP)** aims to improve the simple referenced parameterisation and to enabling light transmission through snow. To do so, we assume that a 2-level Beer-Lambert formulation holds in the snow as it does in the sea ice, with specific parameter values. Whereas Beer-Lambert law is considered invalid within snow because of high scattering, using it has the advantage of simplicity. We retain 3 cm for the surface scattering layer thickness (h_o), 0.3 for the surface transmission parameter (i_o) and 10 (7) m^{-1} for the attenuation coefficient in snow for dry (and wet) conditions (see Table 1). These values were chosen based on the few available observations of light transmission through snow (Järvinen & Leppäranta, 2011; Light et al., 2008; Perovich, 1996). To simplify calculation, we also change the reference i_o in the ice and set it also to 0.3. Analysis suggests possibly large variations in these parameters. Hence the values that we use are to be considered with caution and seen as rough observation-based guesses.

	REF		IMP		
	$h_s > 0$	$h_s = 0$	$h_s > 0$		$h_s = 0$
			dry snow	wet snow	
i_0	n.a	0.38[a]	0.3	0.3	0.3[c]
h_0	n.a	10[b]	3[b]	3[b]	10[b]
κ_s	n.a	n.a	10[d]	7[d]	n.a
κ_i	n.a	1[b]	1[b]	1[b]	1[b]

Table 1: Values of each Beer Lambert law diagnostics for both parametrization (REF and IMP). n.a means "not applicable". [a] calculated from the Grenfell and Maykut (1977) formula: $i_0 = 0.18\,(1-c) + 0.35$ (using c = 0.8 for nebulosity); [b] Light et al. (2008); [c] Bitz-Liscomb (1999); [d] adjustment from LIM1D parametrization (mean of coefficients from Järvinen et Leppäranta (2011)).

Based on the **IMP** parameterisation, we also integrate other modifications to evaluate the effect of (i) melt ponds ($\mathbf{M_{pnd}}$); (ii) ice algae ($\mathbf{M_{alg}}$) and (iii) the small-scale variation in snow depth ($\mathbf{M_{sn\text{-}dis}}$) on the transmitted light field.

Considering the M_{pnd} modifications, we assume that transmitted irradiance in sea ice is an average of bare ice (I_{ice}) and ponded ice (I_{mp}) contributions, weighted by the ponds fraction. The datasets we utilised (see Section 1.2) have no quantitative melt ponds observations, yet daily pictures of the ice surface were taken, from which the presence of melt ponds can be detected (Oziel et al., 2019). Hence, to specify the pond fraction, we assume a linear increase from 5%, at the melt ponds onset date, to 25%, at the end of the observational period, in line of what is classically seen in the Arctic (Perovich et al., 2002). To estimate the irradiance through ponded ice (I_{mp}), we use the same formula as for bare ice, but with an albedo of 0.27, representative of ponded ice (Lecomte et al., 2015), and the same surface transmission parameter as in surface seawater (0.58 ; Morel,1988).

The $\mathbf{M_{alg}}$ modifications aims at considering ice algae, virtually always present near the ice base in various amounts. To incorporate their effect on transmitted irradiance, we assume a constant ice algal chlorophyll-a in the lowermost 10 cm (coming from observations), and that this changes the attenuation coefficient in the lowermost 10 cm following Arrigo et al. (1993) and Vancoppenolle and Tedesco (2017) :

$$\kappa = \kappa_i + a^*.Chla.(1 + f_{det}), \quad (3)$$

where a^* is the spectral absorption of chlorophyll in m^{-1} per mg *Chl-a* per litre, f_{det} = 0.2 is the specified fraction of optically active detrital matter. We consider two observation-based a^* values at the extreme ends of the uncertainty range. The first value (0.008) comes from Antarctic sea ice algae (Arrigo et al., 1991), the other (0.035) comes from Arctic ice algae (Smith et al., 1988).

Considering the $\mathbf{M_{sn\text{-}dis}}$ modifications, we express light transmission in snow-covered ice as the integral contribution of the different snow depths, expressed using a snow depth distribution g(hs) (Abraham et al., 2015) :

$$I(z) = F_{sw} exp(-\kappa_i h_i).\int_0^{\infty} g(h_s).i_o[1-\alpha(h_s)].exp(-\kappa_s h_s).dh_s. \quad (4)$$

We assume a uniform snow distribution, between 0 and twice the mean snow depth, which does not greatly affect calculations as compared with more sophisticated functional forms.

1.2 Observations

1.2.1 Sampling sites

To evaluate how the under-ice light field is represented in the model, we use concomitant observations of the sea ice environment (snow and ice thickness), *Chl-a* in sea ice, and above and under-ice light fields, from three regions of the Northern Hemisphere seasonal sea ice zone (Fig. 1a.).

The **Baffin Bay** (Fig. 1b) activities took place in 2015 & 2016 under the auspices of the Green Edge project. Two land-fast sea ice camps were set from April to July 2015/2016 near Qikiqtarjuaq Island. A cruise onboard the CCGS Amundsen across the pack ice edge occurred in June-July 2016 in Baffin Sea. Many other physical and biogeochemical sampling activities took place in the framework of Green Edge (Oziel et al., 2019; Randelhoff et al., 2019).

Two other locations were sampled in the framework of the OPTIMISM-BIO and SLOPE projects (Fig. 1c, d). The **Svalbard** activities took place on land-fast sea ice from two fjords (Van Mijen Fjorden and Storfjorden), in April, over 2015-2018. 12 stations were visited, 3 per year of sampling.

Land-fast sea ice from the saltwater **Saroma Lake** on the Okhotsk Sea coast of Hokkaido (Japan) was studied for five days in February 2019 with the same instrument set up as in Svalbard.

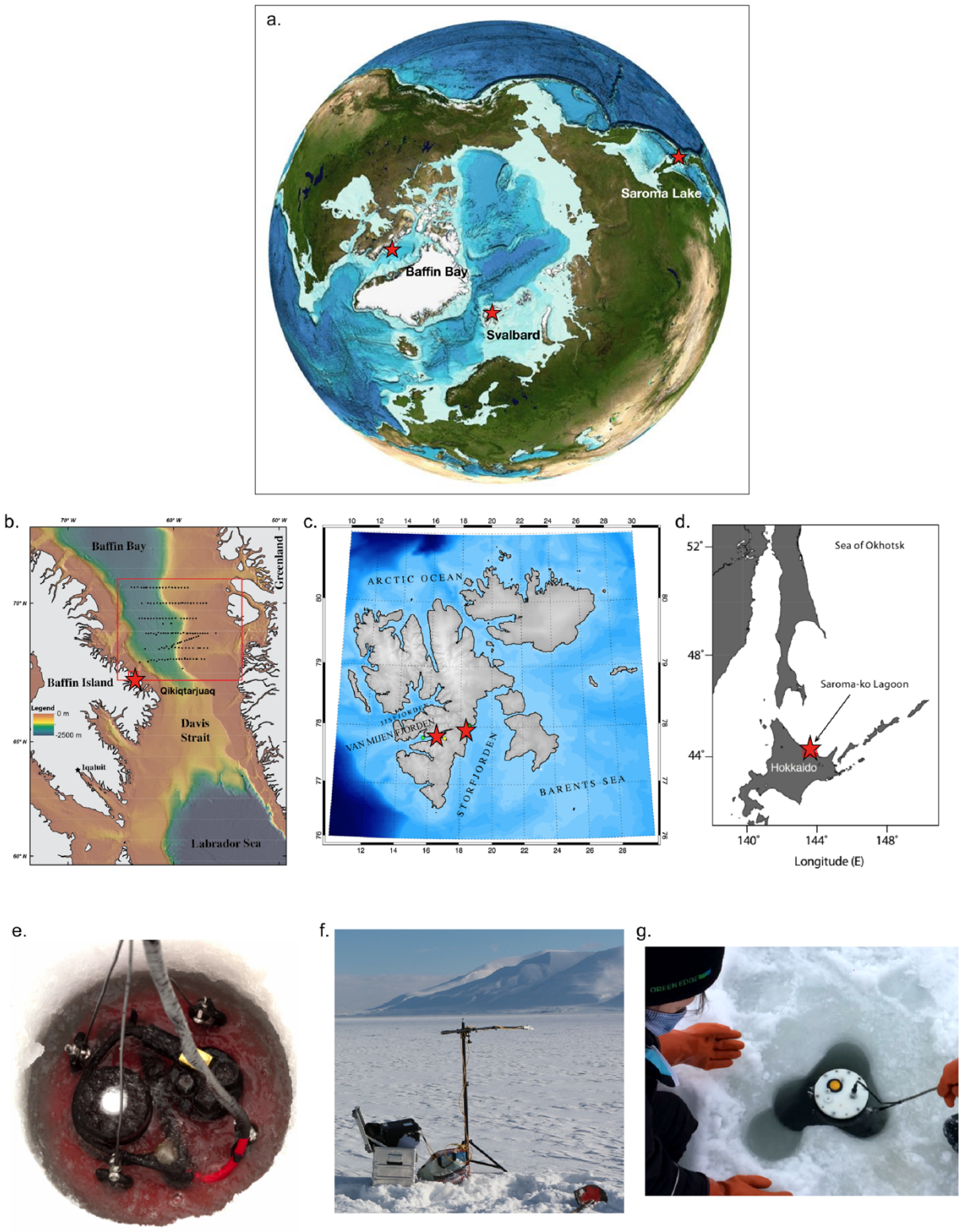

Figure 1: Location of (a) all sampling sites (red stars) on a global map (Baffin Bay ~ 67°N64°W; Svalbard 77°N15°E and Saroma Lake 43°N143°E); (b) Baffin Bay featuring the Qikiqtarjuaq land fast sea ice (red stars) and the track of the CCGS Amundsen during summer cruise in 2016 (black points); (c) Svalbard site (Van Mijen Fjorden and Storfjorden; red stars); (d) Saroma Lake site in Hokkaido. Instrument deployed: (e) C-OPS instrument (used during Baffin Bay campaigns); (f) CNR4 radiometer and (g) STS-VIS micro spectrometer on the Ice-T fish (used during Svalbard and Saroma campaigns).

1.2.2 Snow depth and ice thickness observations

Snow depth was typically measured using a measuring stick. At the Svalbard and Saroma sites, snow depth and ice thickness were measured right at the light measurement site. For Baffin Bay, the available snow depth value is an average over several measurements over the ice camp or floe. Hence, the snow depth values may not precisely correspond to their actual values at the light measurement site. This is particularly likely in 2015 which featured large levels of horizontal variability.

At Svalbard and Saroma stations, the ice cores were extracted close to the light measurement site, and as a reference ice thickness value, we take the average core length. In Baffin Bay, ice cores were also extracted, but not directly in the vicinity of the light measurement site. This can be a small source of error in the model transmittance calculation.

1.2.3 *Chl-a* from melted ice core sections

Chl-a content in sea ice was measured by fluorometry using standard protocols (Holm-Hansen et al., 1965; Lorenzen, 1967; Yentsch & Menzel, 1963) from melted and filtered ice core sections. In Baffin Bay, only the bottom 10 cm were sampled, whereas in Svalbard and Saroma, entire cores were sampled. Volumic concentrations (in µg/L) were converted into vertically integrated values (in mg/m^2) following Meiners et al. (2012).

1.2.4 Optical measurements

The GreenEdge program based light measurements on C-OPS (Compact Optical Profiling System, Biospherical Instruments Inc; Morrow et al., 2010; Fig. 1e) radiometers, composed of 19 micro-radiometers, each corresponding to a 10-nm-wide band, centred on wavelengths ranging from 380 nm to 875 nm. Here we use downwelling spectral irradiance (W/m^2/nm)

measured above the ice surface (F_{sw}^{0}) and right under the ice base (F_{sw}^{tr}). A spline interpolation was applied, giving spectral irradiance at 1 nm resolution. To retrieve the actual incoming radiation, instead of only short wave radiation, we multiplied the above-surface value by 2.1 as suggested by Frouin & Pinker (1995).

The OPTIMISM-BIO program included light measurements based on a Kipp and Zonen CNR4 pyranometer covering the 300-2800 nm spectrum (Fig .1f), placed about 1.5 m above the ice surface, measuring the incoming and reflected solar irradiance (W/m^2) and on an Ocean Optics STS-VIS micro-spectrometer (Fig. 1g) placed under the ice, onboard the Ice-T fish system hanging below the ice at depth up to 5 m, measuring radiance ($W/m^2/nm$). The wavelength range covers 350-800 nm, with 1024 channels. As the effective spectrometer resolution is 1 nm, a three-channel smoothing filter was applied. Radiances are converted to irradiance assuming an elliptical angular distribution of radiance in the water column, following Mobley (2004). We retained data for depths above 3 m.

Both C-OPS radiometer and STS_VIS micro-spectrometers instruments were deployed on the same day at slightly different locations and times, but for very similar ice conditions, during the 2015 Green Edge ice camp (Fig. 2). Both instruments provide consistent results in terms of normalised spectra but not in terms of irradiance intensity (more than one order of magnitude between both) likely due to STS-processing issues during measurement. However, STS micro-spectrometers and a hyperspectral radiometer (Trios Ramses ACC UV/VIS) were inter-compared during Saroma lake campaign and gave consistent downwelling spectral irradiance both in terms of shape and intensity (Nomura et al., 2019, see Annexe). For this reason, we are confident with both instrument and set of data.

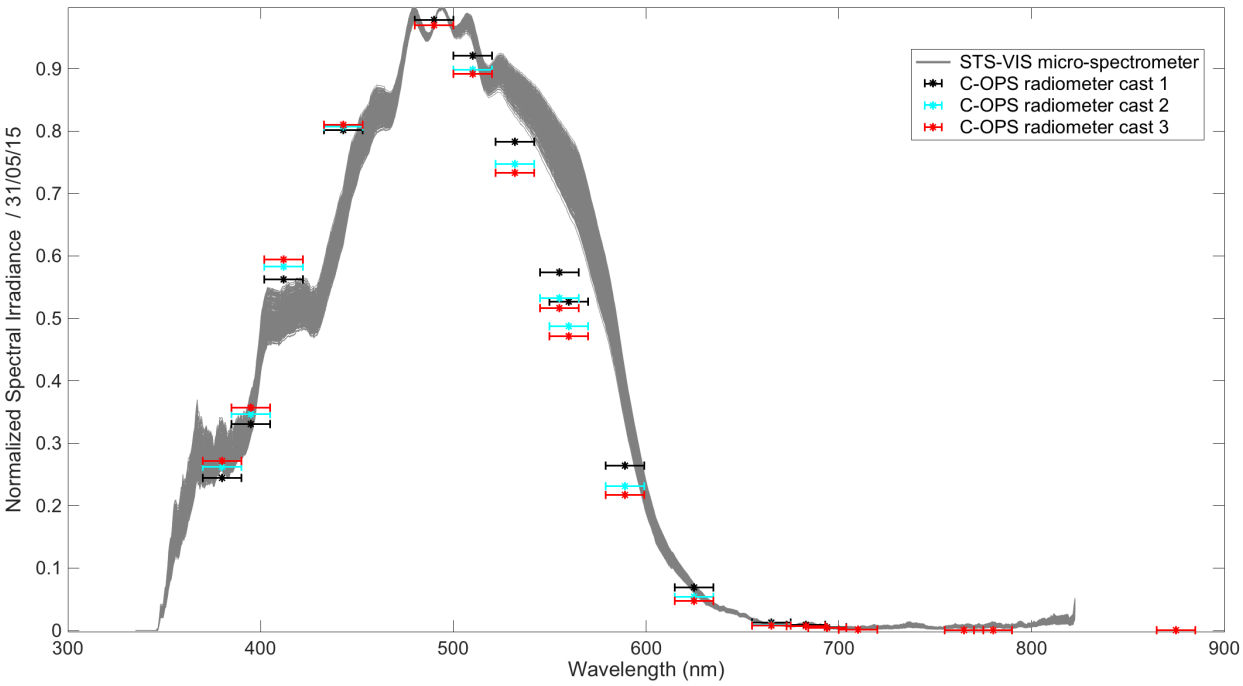

Figure 2: Irradiance spectrum from STS-VIS data (grey envelope) and three casts of C-OPS cast (black; cyan and red stars) recorded at nearby sites, in Baffin Bay land fast sea ice during the Green Edge ice camp 2015 (May 31, 2015). The STS-VIS records were done from 15:00 to 17:30 at 5m depth with an ice thickness of 1.22 m and a snow thickness of 0.32 m whereas C-OPS recorded from 17:10 to 18:00 at few centimetres under the ice with a snow thickness of about 0.27 m and an ice thickness of 1.41 m.

1.3 Observation-model comparison protocol

To evaluate the model radiative transfer scheme, a first diagnostic we use is transmittance (T), the ratio of under-ice to surface irradiance. T has the advantage to integrate the optical effects of the whole snow-ice system, including surface albedo and vertical attenuation, independently of surface irradiance. Observation-based estimates of T are obtained from the ratio of surface to under-ice irradiance, which can be associated with local observations of snow depth (h_s) and ice thickness (h_i). To get corresponding model transmittance values, we must place ourselves in the idealised model world, assuming that such observations correspond to what the model would see as coming through a single model ice thickness category with 100% ice concentration. This is equivalent to assume an infinitely wide region covered by sea ice of uniform snow depth and ice thickness. Using the observational values of h_s and h_i, we can

retrieve a model estimate of transmittance by dividing F_{sw}^{tr} evaluated at the ice base (corresponding to $I(z = h_i)$) by incoming shortwave radiation F_{sw}^{0}.

The second series of diagnostics we use to evaluate the model representation of radiative transfer are the under-ice spectral irradiance fractions. Observational retrievals of the spectral distribution of irradiance were calculated from spectral transmitted shortwave irradiance integrated over the four wavebands used in NEMO (RGB and non-visible, i.e., below 400 nm and above 700 nm).

To get the appropriate spectral fractions, individual waveband were divided by visible irradiance (for RGB fractions), and by shortwave irradiance (for non-visible fractions). Using a incomplete spectrum for the transmitted shortwave radiation in the transmittance calculation of the Non-Visible fraction calculation is not an issue because most of the non-visible wavelengths are attenuated through the ice (see section 2.3).

2. Results

2.1- Description of environmental conditions sites

The data set is mostly representative of northern hemisphere first-year landfast sea ice (see Table 2). A small part (<15%) of the data is from first-year pack ice, sampled in the ice edge region. Despite a seasonal bias towards spring and early summer, a reasonable range of ice thicknesses (0.3 to 1.5 m), snow depths (0 to 0.5 m) and *Chl-a* content in sea ice (0 to 35 mg/m^2) is covered.

Regionally, Baffin Bay dominates the data set, with >95%. Hence, we focus our analysis on Baffin Bay. Svalbard and Saroma lake put the former in a larger context.

location	Years	Nb of stations	hi (m)	hs (m)	*Chl-a* (mg/m2) [Q25-Q75]	**Blue (%)**	**Green (%)**	**Red (%)**	**NRGB (%)**
Qikiqtarjuaq	2015	153	1.21 ± 0.07	0.20 ± 0.11	[9.04 - 22.21]	**45** ± 10	**46** ± 6	**8** ± 6	**4** ± 2
	2016	71	1.28 ± 0.11	0.19 ± 0.14	[1.12 - 5.38]	**43** ± 4	**45** ± 3	**12** ± 4	**4** ± 1
Baffin Sea	2017	34	0.72 ± 0.18	0.02 ± 0.04	0	**41** ± 4	**40** ± 4	**18** ± 4	**16** ± 2
Storfjorden	2015 - 2018	5	0.53 ± 0.15	0.19 ± 0.11	[0.27-0.79]	**37** ± 8	**43**± 5	**20** ± 3	**5** ± 1
Van Mijen Fjorden		7	0.57 ± 0.15	0.14 ± 0.10	[0.63 - 6.25]	**43**± 4	**40** ± 2	**17** ± 2	**6** ± 1
Saroma Lake	2019	5	0.49 ± 0.03	0.07 ± 0.01	[21.30-25.61]	**16** ± 1	**55** ± 1	**29** ± 1	**2** ± 0.3

Table 2: Mean ± standard deviation of ice thickness, snow thickness (mean ± standard deviation) and ice chlorophyll a concentration (Quartile [25% -75%]) and blue, green, red and non-visible (NRGB) fraction for all sampling sites: Qikiqtarjuaq 2015, 2016, Baffin Sea stations (ice stations only), Svalbard sites (Storfjorden and Van Mijen Fjorden) and during Saroma campaign.

Figure 3 (a-c) presents time series of ice thickness, snow depth and *Chl-a* content in sea ice from the entire Green Edge program, including the Qiqitarjuak landfast ice site and the Amundsen cruise data from Baffin Bay. These are put in the context of melt onset and appearance of melt ponds, which were diagnosed from near-surface air temperature data and pictures of the site (Oziel et al., 2019). Melt onset was assumed to occur when surface temperature becomes positive for more than five hours in a day, giving May 26 in 2015 ; and May 20 in 2016). The appearance of melt ponds was on June 22 in 2015 and June 15 in 2016. In both 2015 and 2016, snow depth starts decreasing right after melt onset, whereas ice thickness starts effectively decreasing after the melt ponding onset. Finally, ice *Chl-a* content seems to also depend on melt onset. In 2015, it rapidly increases before the melt onset, then decreases to value less than 0.5 mg/m^2. In 2016, the ice *Chl-a* content is very weak and we cannot see any variation during the season.

Evolution of each diagnostic stays rather similar between both sites and both years but values of each diagnostic largely differs from a site to another (table 2). Ice thickness is similar between both ice camp years (~ 120 ± 10 cm) while summer cruise 2016 ice layer is more than half as thin (~70 ± 20 cm). The ice thickness decrease is also larger in cruise 2016 data than in Qikiqtarjuaq data. This can be attributed to less snow during Amundsen cruise (2 ± 4 cm) than in ice camp data (~20 ± 10 cm for both sites) which allowed more efficient ice melting. It can also be due to an open-water fraction larger during cruise 2016 than during ice camp, or because of different effects of stratification between both sites.

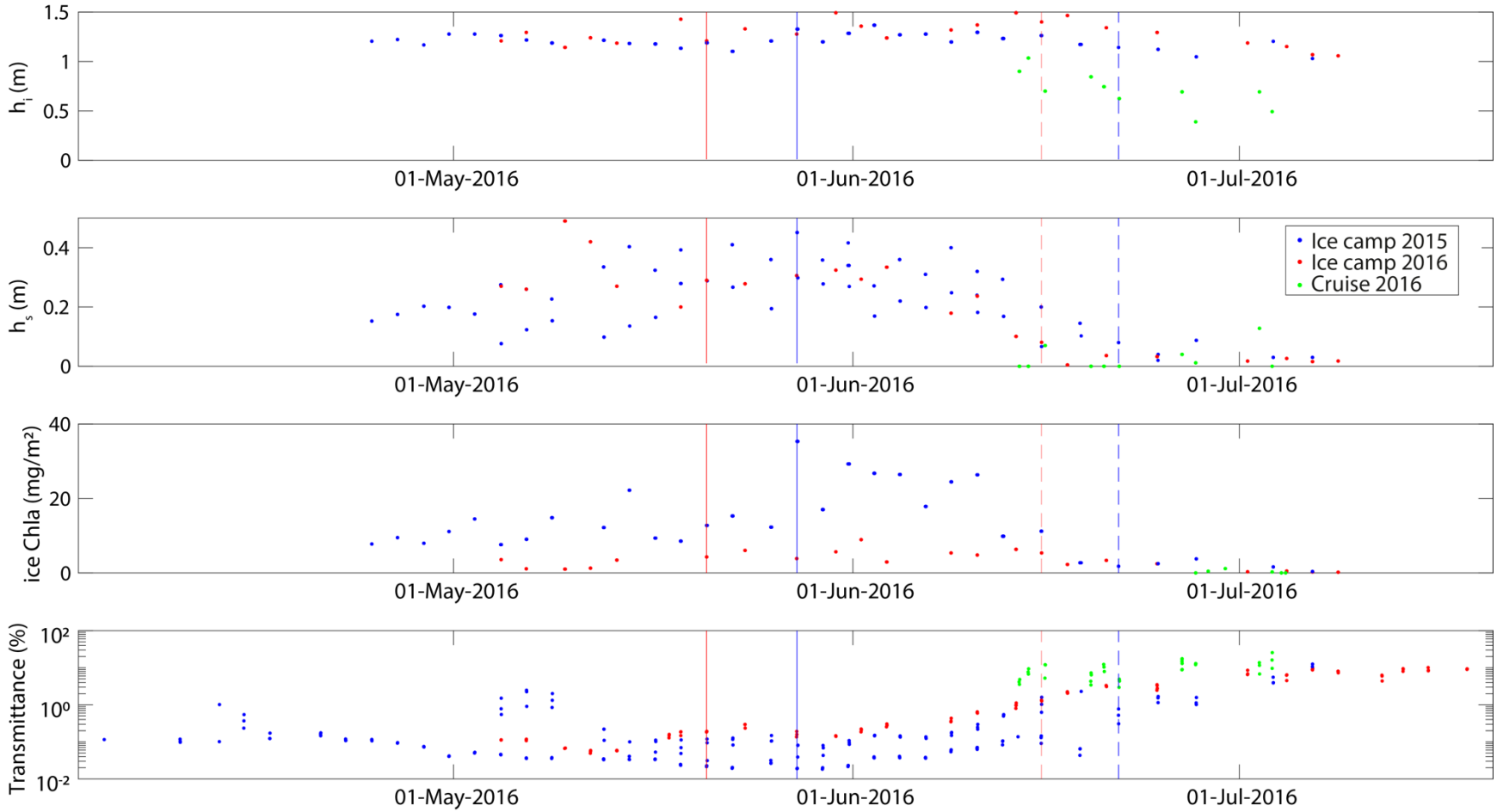

Fig 3: Time series of a) ice thickness; b) snow thickness; c) ice *Chl-a* content; and d) transmittance for all Baffin Bay sampling sites: ice camp 2015 (blue); ice camp 2016 (red) and for cruise 2016 (green). Vertical line refers to melt onset (solid) and appearance of melt pond (dash).

Finally, *Chl-a* content in sea ice is also different between each data set. While the average ice *Chl-a* content in sea ice is low in ice camp 2016 (3.2 ± 2.4 mg/m^2) and even almost null in cruise data (0.03 ± 0.1 mg/m^2), it is five times larger in ice camp 2015 (14.9 ± 8.8 mg/m^2) than in land fast ice camp 2016.

Svalbard and Saroma lake data conditions (Table. 2) differ from Baffin Bay. Average ice thickness is nearly similar between Saroma and both Svalbard sites (~50-60 ± 3-10cm) and it is half as high in Qikiqtarjuaq ice camp data. Svalbard average snow depth (~15-20 ± 10 cm) is close to Qikiqtarjuaq ice camp, while Saroma snow layer is very thin (~ 10 ± 2 cm). Average *Chl-a* content in sea ice is low during Svalbard campaign with rather less *Chl-a* in Storfjorden (~0.6 ± 0.5 mg/m^2) than in Van Mijen Fjorden ice (3.2 ± 3.6 mg/m^2). Finally, Saroma average ice *Chl-a* is high (23.2 ± 3.2 mg/m^2) with value close to Qikiqtarjuaq ice camp 2015 maximum (~25 mg/m^2).

2.2- Under-ice transmittance

Figure 3d shows evolution of observed transmittances at Baffin Bay sites. Observed transmittance increases during the sampling period from ~0.02% initially, to ~26% at the end of the sampling period. This increase is mostly influenced by both snow depth and *Chl-a* content in sea ice evolution (significant correlation : R~ -0.6 between transmittance and snow depth and R~ -0.4 between transmittance *Chl-a* content). The transmittance begins to increase after melt onset when both snow depth and *Chl-a* content in sea ice begin to decrease as it is shown by Perovich et al. (1993). The evolution of the transmittance is then influenced by ice thickness (significant correlation: R~ -0.5 for bare ice only) and by melt ponds (Frey et al., 2011; Nicolaus et al., 2012). The transmittance continues to increase after the appearance of melt ponds, when there is no more *Chl-a* in the ice and when snow is very thin or entirely melted.

The Qikiqtarjuaq 2015 average transmittance (0.5 ± 1.5%) is four times lower than for Qikiqtarjuaq 2016 (2 ± 3%) while the Amundsen cruise average transmittance (10 ± 5%) is five times larger than for Qikiqtarjuaq 2016. Since both Qikiqtarjuaq ice camp years have similar ice and snow depth, their differences may be attributed to larger *Chl*-a content in sea ice in 2015. Snow distribution could also explain these differences as 2015 snow featured larger levels of horizontal variability than in 2016. Differences between Amundsen cruise and Qikiqtarjuaq site could be easily explained by the thinner snow during the Baffin sea pack-ice cruise. Transmittances in 2016 (Qikiqtarjuaq and Amundsen cruise) are also more variable than in 2015. The Qikiqtarjuaq 2015 campaign ended two weeks earlier than in 2016. We attribute the difference in transmittance variability to thinner snow, and thus to a larger transmittance during the summer 2016 cruise and at the end of the Qikiqtarjuaq ice camp 2016 season than at the end of the Qikiqtarjuaq ice camp 2015.

To sum up, the transmittance seasonal increase seems to depend on snow depth, ice thickness for bare ice, ice *Chl-a* content, melt ponds and snow horizontal distribution. We need to consider all these parameters to have the best representation of the transmitted shortwave radiation under the ice in sea ice models.

REF parameterisation assumes 0 for transmittance under snow-covered ice yet observed transmittance is never null even under snow (Fig. 3). REF parameterisation also overestimates Amundsen cruise transmittance under bare ice with a bias of about 4 ± 5% for an average observed transmittance, $\bar{T}_{obs}$, of about 8% (Fig. 4a). The IMP parameterisation better captures the seasonal increase in transmittance (Fig. 4b) by considering non-null transmittance under snow-covered ice and by changing i_0 from ~0.4 to 0.3 (Table. 1). This is true for Baffin Bay data but also for Svalbard and Saroma lake data. The bias on all points is four times smaller and the dispersion around the bias is twice as small (-0.3 ± 2%) than for IMP parameterisation (-1.2 ± 4%). The IMP parameterisation also considers the influence of snow type by considering an

extinction coefficient larger for dry snow (κ_s =10m^{-1}) than for wet snow (κ_s = 7 m^{-1}). This leads to a transmittance close to the observation in both cases (dry snow bias = 0.1 ± 0.4% wet snow bias = -0.9 ± 3%).

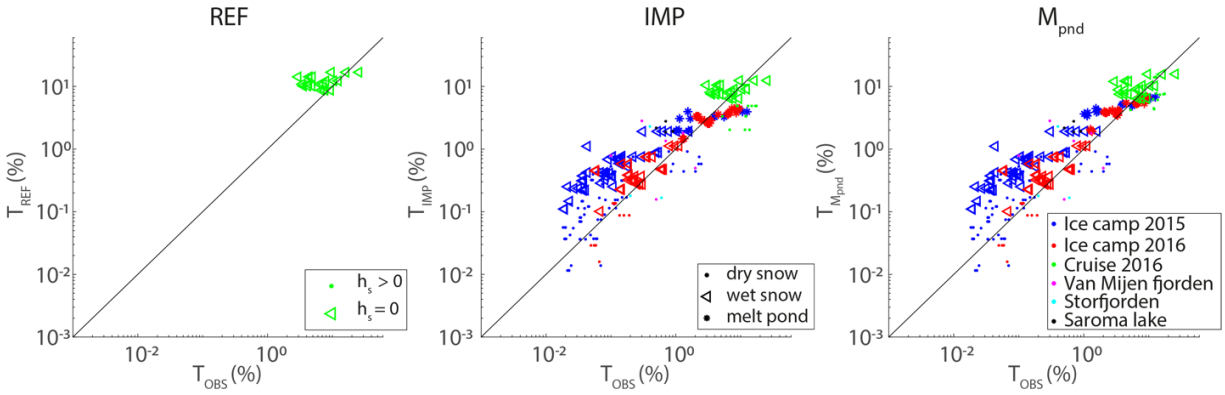

Figure 4: Model vs observational transmittance for (a) REF; (b) IMP; (c) M_{pnd} parametrisations. Colours refer to the different sites; symbols refer to the different surface types encountered.

Nevertheless, the IMP parameterisation does not consider the other diagnostics which seemingly influence the seasonal increase of observed transmittance as melt ponds, ice algae or snow distribution.

The IMP transmittance for points without melt ponds seems better represented (bias~ 0.2 ± 0.7%) than points with melt ponds (bias ~ -2 ± 4%). This highlights the importance to consider melt ponds in the model parameterisation. Figure 5a represents M_{pnd} parameterisation which now considers melt ponds (Eq. 4) in the calculation in comparison with the observed transmittance. The transmittance is better represented when melt ponds are considered (bias = -0.06 ± 2%) but fraction of melt ponds needs to be well defined in the model to prevent large error (if f_{mp} = 100%, bias~ 2.6 ± 5%).

In contrast, considering *Chl-a* content in sea ice in the improved parameterisation (M_{alg}) does not influence the retrieval transmittances for both a* (Fig. 5b). This is because ice *Chl-a* content is too small for a significant ice algal influence on transmitted radiation (Vancoppenolle &

Tedesco, 2017). Differences between observed transmittance during Qikiqtarjuaq ice camps 2015 and 2016 cannot therefore be explained by differences in ice-*Chl-a* content.

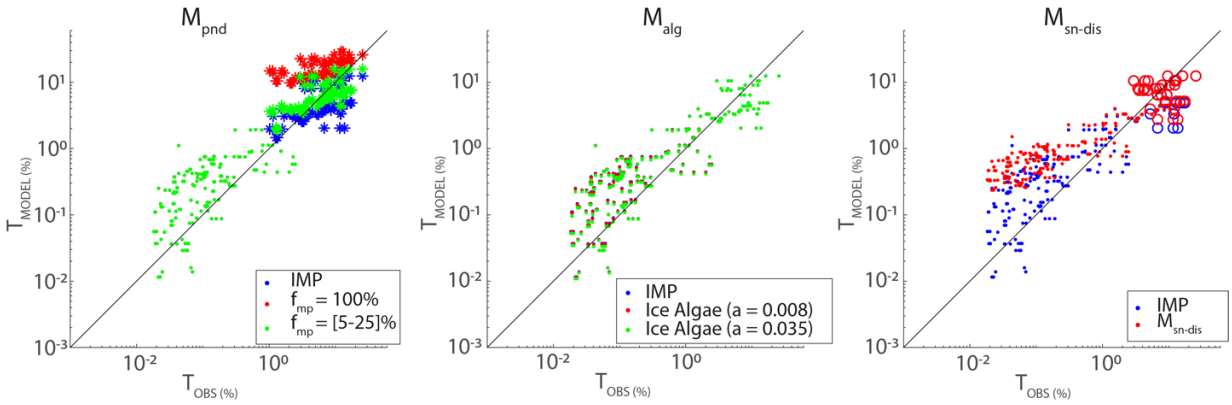

Figure 5: Model vs observed transmittance for (left) M_{pnd} parametrization with different pond fractions (ponded ice records are identified from star symbols); (middle) M_{alg} parametrization with two specific *Chl-a* absorption coefficient; and (right) $M_{sn\text{-}dis}$ parametrization where the effect of a small-scale snow distribution is included (drift ice records are identified with circle symbols).

The other suggested explanation (i.e., the impact of horizontal snow distribution on the Qikiqtarjuaq transmittance) also seemingly needs to be rejected. The transmittance considering nonconstant snow distribution ($M_{sn\text{-}dis}$) visually improve pack-ice points only. But the number of pack-ice stations is too weak to conclude on the impact of snow distribution on transmittance. Although transmittances obtained from M_{pnd} (Fig. 4c) are close to the observation, especially at low transmittances, the dispersion of the error remains large and cannot be explained by the ice *Chl-a* content in sea ice or the snow distribution.

In table 3, we evaluate the impact of à 10% error on each input parameters. Most errors in transmittance calculation come from albedo (40% of error when albedo is increased by 10%). Snow parameters (extinction coefficient and depth) and surface scattering layer coefficient (i_0) for bare ice are also large sources of error in the calculation (between 15 and 20% each). Finally, ice parameters and i_0 in snow-covered ice have less impacts on transmittance (less than 15% each).

In this study we assume that albedo of sea ice have been largely documented (Eicken et al., 2004; Perovich et al., 2002; Perovich et Polashenski, 2012; Curry et al., 2001) and that the albedo parameterisation in LIM is reasonably precise. Therefore, we choose to focus on the other input parameters. However, it is important to keep in mind that albedo definition can be the major source of error in this parameterisation. Values for snow-covered ice highlight the importance to well define the snow extinction coefficient in the parameterisation, and to well represent the snow depth in simulations. Because of the major impact of snow in the transmittance calculation, we attribute the great dispersion of the error to unresolved effects of snow density and microstructure rather than to the effects of ice microstructure which is low compared to the effect of ice thickness (Maykut & Grenfell, 1975).

	dry snow	melt snow	melt pond	no snow
h_i (m)	1.2	1.2	1.1	0.8
h_s (m)	0.3	0.2	0.05	0
h0	3	2	2	8
i_0	10	10	10	18
α	-40	-40	-40	-18
κ_s	-20	-12	-1	-
h_s	-23	-14	-3	-
κ_i	-11	-12	-10	-0.2
h_i	-11	-12	-10	-1

Table 3: Impact of each parameter on retrieved transmittance for different ice/snow conditions (ice and snow thickness for each case are given in the table (lines 2 and 3). From line 4 The number represents the relative error between the perturbed transmittance (in %) and the reference transmittance (in %). Perturbed transmittances are obtained by increasing each selected parameter by 10% individually.

To conclude with transmittance analysis, we suggest a new parameterisation that considers a non-null transmittance under snow-covered ice with a distinction between dry and wet snow. We also suggest that melt ponds should be considered in the transmittance calculation since it improves the representation of the under-ice transmittance in the calculation. More

observations, especially in the ice-edge regions, would allow us to refine this parameterisation. Finally, although this improved transmittance remains close to the observation, more studies about the impacts of snow density and microstructure or organic matter in sea ice is needed to reduce errors in simulated under-ice transmittance.

2.3- Spectral repartition of under-ice light

Once light is transmitted through the snow-ice layer, it is divided into four wavebands in the model. This spectral repartition of light impacts both ocean thermodynamics and phytoplankton growth. It is consequently crucial to define it properly. Model currently considers that more than half of the light transmitted to the ocean is composed of non-visible wavelengths and rapidly attenuates in the upper few centimetres of the ocean (see section 1.1.1). The remaining half, composed of visible wavelengths, is then equally split into three wavebands (red, green and blue). Whereas this assumption is correct in open-water, it is wrongly applied to ice-covered water. Indeed, sea ice impacts the spectral repartition of light, for example by strongly absorbing the infrared wavelengths.

Figure 6 represents the normalised spectrum of under-ice transmitted irradiance for each data set. Firstly, all spectra present lower irradiance at non-visible wavelengths. This is in contradiction with the 58% of non-visible fraction in the model. Secondly, we can distinguish two types of spectrum. Baffin Bay and Svalbard spectra have nearly similar shape with a maximum between 450 nm 550 nm (blue) and some differences link to site and year environmental characteristics. Saroma spectra differ from other sites spectra. It presents two peaks near 600 nm and 700 nm (red) and a minimum at 675 nm.

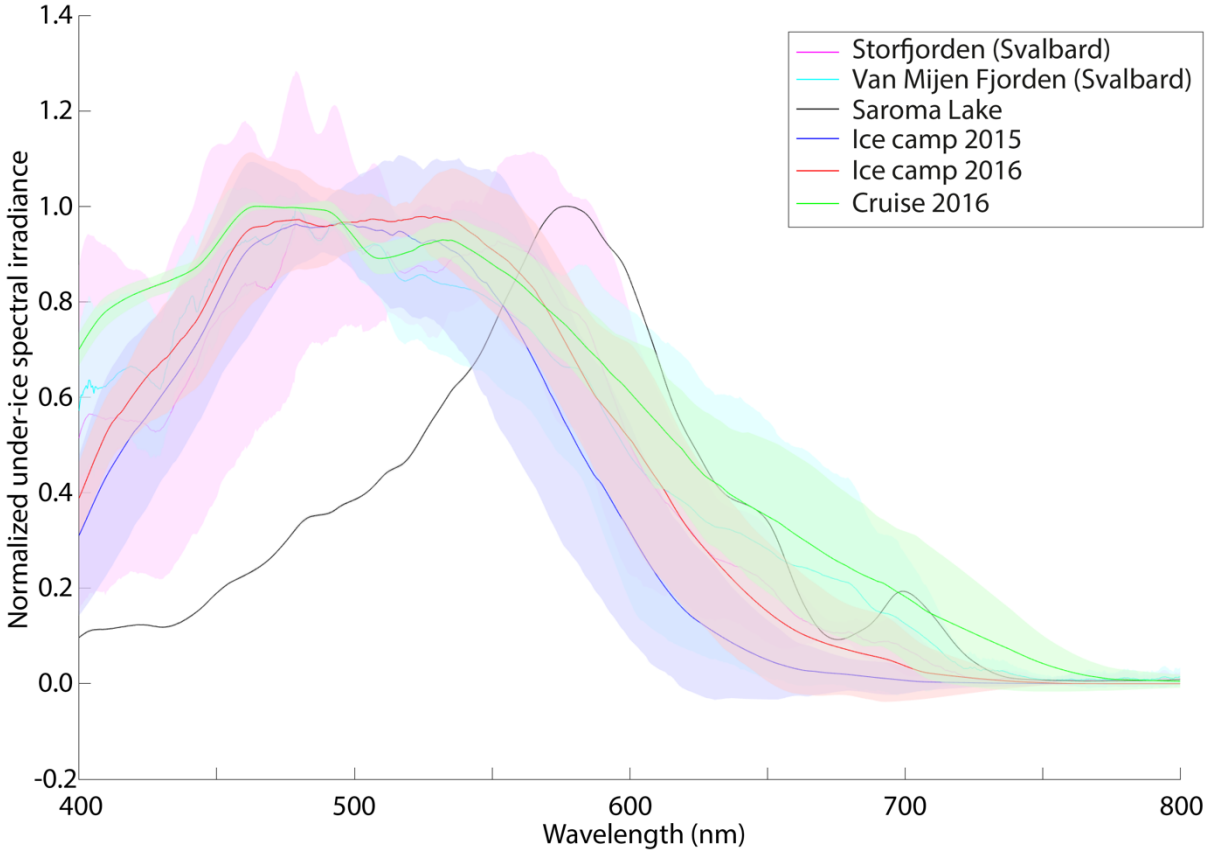

Figure 6: Median (solid lines) ± IQR (envelopes) of normalised under ice transmitted irradiance spectra average over all records, for each site.

In table 2, the four under ice spectral irradiance fractions is given for each site. Baffin Bay and Svalbard fractions are close together with about 40 to 45% of green and blue and between 10 and 20% of red. NRGB fraction is around 5% for both sites except for the pack ice during Amundsen Cruise. Although Saroma NRGB fraction is close to other land-fast sea ice sites (~2%), fractions of blue (16%) green (55%) and red (29%) largely differ from other sites.

For all sites, change in fractions stay rather low (standard deviation of each fraction <= 10%; table 2) and seemingly mostly depend on both snow depth and ice *Chl-a* content considering the Qikiqtarjuaq ice-camp sites (Fig. 7; other sites are not considered here because they do not have enough stations). Wavelength fractions are not significantly impacted by the ice thickness, except for the green and NRGB fractions, but with a very low trend (0.1 %/cm for green and -0.04 %/cm for NRGB). In contrast blue fractions are significantly impacted by snow depth

(0.4%/cm) while green is less impacted (-0.06%/cm). This is consistent with Perovich et al. (1993; see Appendix). Considering red fraction, it decreases with snow decrease (- 0.4%/cm) which is not consistent with Perovich et al. (1993)

Since snow depth and *Chl-a* content in sea ice are linked, all these variations are similar considering ice *Chl-a* variation. Thus, red fraction, which decreases with deeper snow, also decreases with *Chl-a* content in sea ice increase (-0.35%/(mg/m$^{2)}$). This can be attributed to the absorption peak of *Chl-a* which is in red wavelengths (~ 675 nm; Gates et al., 1965). However, the strong link between snow and *Chl-a* content in sea ice prevents us to conclude on the contribution of this change due to snow depth and due to ice *Chl-a* content.

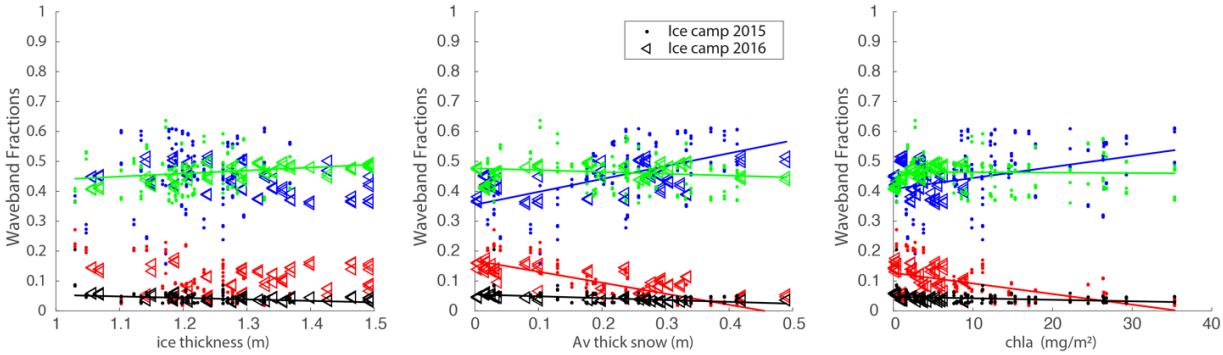

Figure 7: Blue, green, red and non-visible (black) waveband fractions (colours) vs a) ice thickness b) snow thickness and c) *Chl-a* content in sea ice from both Baffin Bay landfast sea ice sites (symbols) Lines represent significant trends.

To conclude with spectral analysis, the suggested parameterisation considers a fraction of non-visible wavelengths significantly lower (~5%) compared with the 58% of the current parameterisation due to the strong infrared absorption by sea ice. In the REF parameterisation, visible fraction is equally split between red, blue and green wavelengths. We suggest that the red fraction (10-15%) should be reduced, as red wavelengths are less transmitted by sea ice and that green and blue fractions should be consequently increased (40-45%). According to fraction standard deviation and figure 7, we assume that all fractions can remain constant whatever the ice and snow depth or the *Chl-a* content in sea ice. Nevertheless, some exceptions in this

parameterisation remain since (i) the NRGB fraction of the Amundsen cruise stations is much larger (~ 15%) than other sites and (ii)Saroma spectrum shape and thus visible fractions largely differ from other sites. These exceptions cannot be explained by variation in snow depth, ice thickness or ice *Chl-a* content. Other parameters should influence the value of each fraction.

The large values of NRGB wavelengths during the Amundsen cruise may be explained by a different snow structure than in land fast sea ice. But the number of pack-ice stations in this our dataset is too weak to make any clear conclusion.

Saroma spectra should be considered with caution since the number of stations during the Saroma campaign is also weak (only five stations). Despite the fact that such shape in the Saroma spectra is very close to spectra influenced by *Chl-a* absorption (Mundy et al., 2007), the ice *Chl-a* content is too weak to explain this shape (Table 3). We speculate this to be due to a high concentration of coloured dissolved inorganic matter (CDOM). Saroma lake is a special site compared to Baffin Bay and Svalbard since it is a lagoon close to the sea with only two artificial inlets connected to the Okhotsk Sea. The lagoon is connected at two rivers. Due to these rivers discharge and the narrow output, the CDOM concentration in the lagoon water may be high during winter (Nomura et al., 2009) and could explain the spectrum shape during the Saroma campaign.

3-Discussion/Conclusion

The analysis presented in this paper focused on the evaluation of the radiative transfer scheme from the NEMO ice-ocean model using recent light measurements above and under Arctic sea ice. The NEMO radiative transfer scheme is based on (i) a well-tested system of empirical expressions for the dependence of the surface albedo on environmental characteristics; (ii) Beer-Lambert law for attenuation within snow and ice and (iii) prescribed energy fractionation at the uppermost ocean surface, into 3 visible and 1 non-visible spectral bands.

Summary of main results

In this study we have first focused on the evaluation of the input parameters from the Beer-Lambert law (extinction and surface scattering layer coefficients for snow and ice). The current parameterisation assumes that transmitted light to the upper ocean is null under snow-covered ice. However, according to the in-situ observation, transmitted light in seaice-covered water is never null even under snow. We have consequently show that the current parameterisation of NEMO ice-ocean model should be revised.

We have then focused on the current fractionation of transmitted light into 4 wavebands. The NEMO radiative transfer scheme is based on open-water study considering spectral repartition of light in the ocean (Morel, 1988). It considers that more than half (58%) of the light transmitted to the upper ocean is composed of non-visible wavelengths (mostly infrared) and absorbed in the first few centimetres of the ocean. The remainder of the energy (42%) is then equally distributed into three visible wavebands (blue, green, red) and penetrated at different depths according to the wavelength. The current parameterisation considers the same spectral repartition of light for both open ocean and ice-covered water assuming that sea ice does not have any impact on the spectral repartition of light. We show in this study that such assumption should be revised since sea ice-snow system largely influence the spectral repartition of light transmitted to the ocean.

Suggestions to improve the NEMO radiative transfer scheme

By analysing several modified parameterisations based on the reference parameterisation of the NEMO radiative transfer scheme, we suggest a set of improvement which should be applied in the model to better represent the light transmission in sea ice zone.

- We first suggest that **a non-null transmitted light should be applied under snow covered pixels**. In this improved parameterisation, we consider a Beer-Lambert law into

snow with a distinction between dry and wet snow extinction coefficient. We also adjust the surface scattering layer coefficient in bare ice to better conciliate model and observations.

- We also show that melt ponds have a significant impact on transmitted light to the upper ocean. For this reason, we also suggest that **melt ponds should be considered** in the parameterisation.
- Considering spectral repartition of light underice-covered pixels, sea ice strongly absorbs the infrared wavelengths. We, consequently suggest that **the non-visible waveband fraction should be reduced in the improved parameterisation from 58% to less than 5%.**
- Finally, as sea ice system attenuates more red wavelengths than blue and green, we suggest that visible fractions should be revised as follows : **Red fraction should be reduced from 33% to 10-15% while the green and blue fractions should be increased from 33% to 40-45%.**

Discussion

The suggested improved parameterisation should lead to largely increase the light in seaice-covered waters impacting phytoplankton by reducing light limitation. Because the response of phytoplankton growth to available light is not linear (Long et al., 2015), it is complex to quantify how simulated phytoplankton should be impacted by improved parameterisation. The induced increase in the light in seaice-covered waters should also influence the ocean heating rate. This could be easily evaluated.

The modifications applied to the Beer-Lambert Law parameters should significantly increase the transmitted light to the upper ocean of about 6 ± 10 W/m^2 to be compared with the average

observed shortwave irradiance under ice ($\bar{F}_{sw}^{tr}$ = 7 ± 14 W/m^2). We can estimate that this should increase the ocean heating rate of about +0.3 ± 0.4 °C/day.

The current parameterisation largely underestimates the deep under-ice light by absorbing 58% of the transmitted light in the first few centimetres of the ocean. By reducing the non-visible fraction in the improved parameterisation, we contribute to increase the light which penetrates deeper of 53%. At the same time, it should also contribute to reduce the ocean heating rate in the first metres (of about -0.1°/day).

Finally, compared to change in transmitted light due to improvement in Beer-Lambert Law parameters or in non-visible fraction, changes in visible fractions may appear trivial. But, as red, blue and green wavebands do not penetrate at the same depth in the ocean, the improved parameterisation should largely influence the under-ice light profile. Figure 8 represents the impact of not considering change in visible fraction in the improved parameterisation in terms of energy and heating rate. In the model, red wavelengths are firstly attenuated to the ocean in the first metres (~5 m) while blue and green penetrate deeper into the ocean (~10 m for green and ~50 m for blue) following Lengaigne et al. (2007). Considering this attenuation law, we assume that change in visible fraction should decrease the heat rate in the first five metres of the ocean (of about -0.03 °C/day; Fig. 8) and slightly increase in the deeper ocean (less than +0.005 °C/day in the ten-following metre).

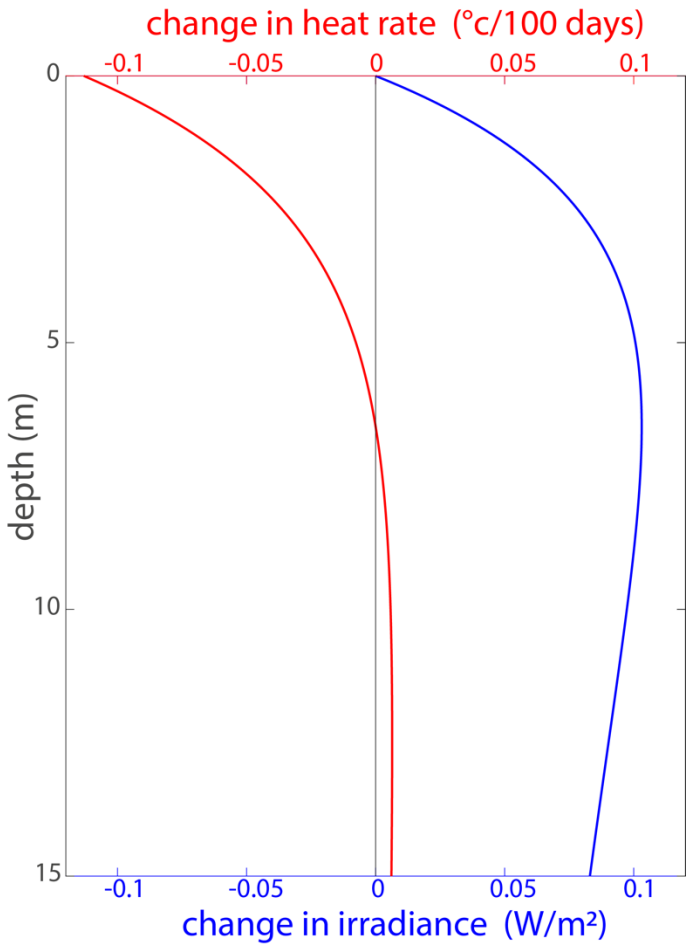

Figure 8: Vertical profile of anomaly in transmitted irradiance (W/m^2; blue) and in ocean heating rate due to solar radiation penetration (°C/100days; red) between two parameterisations (Param1 - Param2). This figure illustrates the impact of changing the R, G and B fractions in the improved parameterisation under ice. The same transmitted shortwave irradiance under ice is set for both parameterisations. The non-visible fraction is assumed to be equal to 5%. Param1 assumed equal visible waveband fractions (R = G = B) while Param2 assumed: R = 12% and B = G = 42.5%. Each waveband penetrates the ocean following Lengaigne et al. (2007) formulation considering a vertically constant *Chl-a* content in the ocean ([*Chl-a*] = 0.02 mg/m^3).

Perspectives

To conclude, the improved parameterisation should have a large impact on simulated fields of phytoplankton and sea ice and ocean heat flux in the model. The real impact of improved parameterisation in these simulated fields should be explored further based on forced and coupled simulation analysis.

We show that improved parameterisation should be closer to the observation than the current parameterisation. However, some uncertainties remain in this parameterisation. And some

aspects of the radiative transfer in sea ice should be further explored to reduce uncertainties, as: (i) the impact of snow metamorphism on under-ice transmittance; (ii) the influence of pack ice in the transmitted light compared with the land-fast ice (iii) and the possible influence of organic matter in sea ice.

In this study we only explore the Beer-Lambert parameterisation for transmitted light calculation. This is not the only parameterisation used in sea ice models. Delta Eddington approximation approach (Briegleb & Light, 2007; Saenz & Arrigo, 2012) is based on inherent optical properties such as ice and snow absorption and scattering instead of transmittance and albedo. This approach may be more precise than the Beer-Lambert law since inherent optical properties are not dependent on the ambient light field. Comparing approach with the Beer-Lambert law should reduce the uncertainties.

Given that this study is mostly based on first-year land fast ice data, continue the analysis with more pack ice data should also reduce uncertainties.

Finally, in this study we focus on the extinction and the surface scattering layer coefficient to adjust the radiative transfer scheme. Yet, we show that albedo is the main source of error in the model parameterisation. More studies based on the albedo in our data set is needed to further reduce the uncertainties and maybe adjust the empirical expressions for the surface albedo.

References

Abraham, C., Steiner, N., Monahan, A., & Michel, C. (2015). Effects of subgrid-scale snow thickness variability on radiative transfer in sea ice. *Journal of Geophysical Research: Oceans*, 5597–5614. https://doi.org/10.1002/2015JC010741@10.1002/(ISSN)2169-9291.FAMOS1

Arrigo, K. R., Sullivan, C. W., & Kremer, J. N. (1991). A bio-optical model of Antarctic sea ice. *Journal of Geophysical Research: Oceans*, *96*(C6), 10581–10592. https://doi.org/10.1029/91JC00455

Arrigo, K. R., & van Dijken, G. L. (2011). Secular trends in Arctic Ocean net primary production. *Journal of Geophysical Research: Oceans*, *116*(C9), C09011. https://doi.org/10.1029/2011JC007151

Assmy, P., Fernández-Méndez, M., Duarte, P., Meyer, A., Randelhoff, A., Mundy, C. J., et al. (2017). Leads in Arctic pack ice enable early phytoplankton blooms below snow-covered sea ice. *Scientific Reports*, *7*, srep40850. https://doi.org/10.1038/srep40850

Bitz, C. M., & Lipscomb, W. H. (1999). An energy-conserving thermodynamic model of sea ice. *Journal of Geophysical Research: Oceans*, *104*(C7), 15669–15677. https://doi.org/10.1029/1999JC900100

Briegleb, P., & Light, B. (2007). A Delta-Eddington Mutiple Scattering Parameterization for Solar Radiation in the Sea Ice Component of the Community Climate System Model. https://doi.org/10.5065/D6B27S71

Cavalieri, D. J., & Parkinson, C. L. (2012). Arctic sea ice variability and trends, 1979–2010. *The Cryosphere*, *6*(4), 881–889. https://doi.org/10.5194/tc-6-881-2012

Curry, J. A., Schramm, J. L., Perovich, D. K., & Pinto, J. O. (2001). Applications of SHEBA/FIRE data to evaluation of snow/ice albedo parameterizations. *Journal of Geophysical Research: Atmospheres*, *106*(D14), 15345–15355. https://doi.org/10.1029/2000JD900311

Eicken, H., Grenfell, T. C., Perovich, D. K., Richter-Menge, J. A., & Frey, K. (2004). Hydraulic controls of summer Arctic pack ice albedo. *Journal of Geophysical Research: Oceans*, *109*(C8). https://doi.org/10.1029/2003JC001989

Fichefet, T., & Morales Maqueda, M. A. (1997). Sensitivity of a global sea ice model to the treatment of ice thermodynamics and dynamics. *Journal of Geophysical Research: Oceans*, *102*(C6), 12609–12646. https://doi.org/10.1029/97JC00480

Frey, K. E., Perovich, D. K., & Light, B. (2011). The spatial distribution of solar radiation under a melting Arctic sea ice cover. *Geophysical Research Letters*, *38*(22). https://doi.org/10.1029/2011GL049421

Frouin, R., & Pinker, R. T. (1995). Estimating Photosynthetically Active Radiation (PAR) at the earth's surface from satellite observations. *Remote Sensing of Environment*, *51*(1), 98–107. https://doi.org/10.1016/0034-4257(94)00068-X

Gates, D. M., Keegan, H. J., Schleter, J. C., & Weidner, V. R. (1965). Spectral Properties of Plants. *Applied Optics*, *4*(1), 11–20. https://doi.org/10.1364/AO.4.000011

Grenfell, T. C., & Maykut, G. A. (1977). The Optical Properties of Ice and Snow in the Arctic Basin *. *Journal of Glaciology*, *18*(80), 445–463. https://doi.org/10.3189/S0022143000021122

Holm-Hansen, O., Lorenzen, C. J., Holmes, R. W., & Strickland, J. D. H. (1965). Fluorometric Determination of Chlorophyll. *ICES Journal of Marine Science*, *30*(1), 3–15. https://doi.org/10.1093/icesjms/30.1.3

Horvat, C., Jones, D. R., Iams, S., Schroeder, D., Flocco, D., & Feltham, D. (2017). The frequency and extent of sub-ice phytoplankton blooms in the Arctic Ocean. *Science Advances*, *3*(3), e1601191. https://doi.org/10.1126/sciadv.1601191

Hunke, E., Richard Allard, David A. Bailey, Philippe Blain, Amelie Bouchat, Tony Craig, … Michael Winton. (2019, July 25). CICE-Consortium/CICE: CICE Version 6.0.1 (Version CICE6.0.1). Zenodo. http://doi.org/10.5281/zenodo.3351684

Järvinen, O., & Leppäranta, M. (2011). Transmission of solar radiation through the snow cover on floating ice. *Journal of Glaciology*, *57*(205), 861–870. https://doi.org/10.3189/002214311798043843

Katlein, C., Arndt, S., Belter, H. J., Castellani, G., & Nicolaus, M. (2019). Seasonal Evolution of Light Transmission Distributions Through Arctic Sea Ice. *Journal of Geophysical Research: Oceans*, *0*(0). https://doi.org/10.1029/2018JC014833

Kwok, R., & Rothrock, D. A. (2009). Decline in Arctic sea ice thickness from submarine and ICESat records: 1958–2008. *Geophysical Research Letters*, *36*(15), L15501. https://doi.org/10.1029/2009GL039035

Lecomte, O., Fichefet, T., Flocco, D., Schroeder, D., & Vancoppenolle, M. (2015). Interactions between wind-blown snow redistribution and melt ponds in a coupled ocean–sea ice model. *Ocean Modelling*, *87*, 67–80. https://doi.org/10.1016/j.ocemod.2014.12.003

Lengaigne, M., Menkes, C., Aumont, O., Gorgues, T., Bopp, L., André, J.-M., & Madec, G. (2007). Influence of the oceanic biology on the tropical Pacific climate in a coupled general circulation model. *Climate Dynamics*, *28*(5), 503–516. https://doi.org/10.1007/s00382-006-0200-2

Light, B., Grenfell, T. C., & Perovich, D. K. (2008). Transmission and absorption of solar radiation by Arctic sea ice during the melt season. *Journal of Geophysical Research: Oceans*, *113*(C3), C03023. https://doi.org/10.1029/2006JC003977

Lindsay, R., & Schweiger, A. (2015). Arctic sea ice thickness loss determined using subsurface, aircraft, and satellite observations. *The Cryosphere*, *9*(1), 269–283. https://doi.org/10.5194/tc-9-269-2015

Long, M. C., Lindsay, K., & Holland, M. M. (2015). Modeling photosynthesis in sea ice-covered waters. *Journal of Advances in Modeling Earth Systems*, *7*(3), 1189–1206. https://doi.org/10.1002/2015MS000436

Lorenzen, C. J. (1967). Determination of Chlorophyll and Pheo-Pigments: Spectrophotometric Equations1. *Limnology and Oceanography*, *12*(2), 343–346. https://doi.org/10.4319/lo.1967.12.2.0343

Madec Gurvan, Romain Bourdallé-Badie, Pierre-Antoine Bouttier, Clément Bricaud, Diego Bruciaferri, Daley Calvert, et al. (2017). NEMO ocean engine. https://doi.org/10.5281/zenodo.3248739

Maslanik, J., Stroeve, J., Fowler, C., & Emery, W. (2011). Distribution and trends in Arctic sea ice age through spring 2011. *Geophysical Research Letters*, *38*(13), L13502. https://doi.org/10.1029/2011GL047735

Massonnet, F., Fichefet, T., Goosse, H., Bitz, C. M., Philippon-Berthier, G., Holland, M. M., & Barriat, P.-Y. (2012). Constraining projections of summer Arctic sea ice. *The Cryosphere*, *6*(6), 1383–1394. https://doi.org/10.5194/tc-6-1383-2012

Maykut, G. A., & Grenfell, T. C. (1975). The spectral distribution of light beneath first-year sea ice in the Arctic Ocean1. *Limnology and Oceanography*, *20*, 554–563. https://doi.org/10.4319/lo.1975.20.4.0554

Maykut, G. A., & Untersteiner, N. (1971). Some results from a time-dependent thermodynamic model of sea ice. *Journal of Geophysical Research*, *76*(6), 1550–1575. https://doi.org/10.1029/JC076i006p01550

Meiners, K. M., Vancoppenolle, M., Thanassekos, S., Dieckmann, G. S., Thomas, D. N., Tison, J.-L., et al. (2012). Chlorophyll a in Antarctic sea ice from historical ice core data. *Geophysical Research Letters*, *39*(21). https://doi.org/10.1029/2012GL053478

Mobley. (2004). Optical Modeling of Ocean Waters: Is the Case 1 - Case 2 Classification Still

Useful? *Oceanography*, *17*, 60–67. https://doi.org/10.5670/oceanog.2004.48#sthash.3v8sNZac.dpuf

Morel, A. (1988). Optical modeling of the upper ocean in relation to its biogenous matter content (case I waters). *Journal of Geophysical Research: Oceans*, *93*(C9), 10749–10768. https://doi.org/10.1029/JC093iC09p10749

Morrow, J. H., Booth, C., Lind, R. N., & Hooker, S. B. (2010). The Compact-Optical Profiling System (C-OPS). *NASA Tech. Memo.*, 42–50.

Mundy, C. J., Ehn, J. K., Barber, D. G., & Michel, C. (2007). Influence of snow cover and algae on the spectral dependence of transmitted irradiance through Arctic landfast first-year sea ice. *Journal of Geophysical Research: Oceans*, *112*(C3), C03007. https://doi.org/10.1029/2006JC003683

Nicolaus, M., Katlein, C., Maslanik, J., & Hendricks, S. (2012). Changes in Arctic sea ice result in increasing light transmittance and absorption. *Geophysical Research Letters*, *39*(24), L24501. https://doi.org/10.1029/2012GL053738

Nicolaus, Marcel, Hudson, S. R., Gerland, S., & Munderloh, K. (2010). A modern concept for autonomous and continuous measurements of spectral albedo and transmittance of sea ice. *Cold Regions Science and Technology*, *62*(1), 14–28. https://doi.org/10.1016/j.coldregions.2010.03.001

Nomura, D., Takatsuka, T., Ishikawa, M., Kawamura, T., Shirasawa, K., & Yoshikawa-Inoue, H. (2009). Transport of chemical components in sea ice and under-ice water during melting in the seasonally ice-covered Saroma-ko Lagoon, Hokkaido, Japan. *Estuarine, Coastal and Shelf Science*, *81*(2), 201–209. https://doi.org/10.1016/j.ecss.2008.10.012

Nomura, D., Wongpan, P., Toyota, T., Tanikawa, T., Kawaguchi, Y.,Ono, T.,Ishino T.,Tozawa, M., TAMURA,T, P., Yabe I, S,. Son, E, Y., Vivier, F., Louranco, A., Lebrun, M,. Nosaka, Y., Hirawake, T., Ooki, A., Aoki, S., Else, B., Fripiat, F., Inoue, J., Vancoppenolle, M. (2019) Saroma-ko Lagoon Observations for sea ice Physico-chemistry and Ecosystems 2019 (SLOPE2019). In prep

Notz, D., Haumann, F. A., Haak, H., Jungclaus, J. H., & Marotzke, J. (2013). Arctic sea-ice evolution as modeled by Max Planck Institute for Meteorology's Earth system model. *Journal of Advances in Modeling Earth Systems*, *5*(2), 173–194. https://doi.org/10.1002/jame.20016

Oziel, L., Massicotte, P., Randelhoff, A., Ferland, J., Vladoiu, A., Lacour, L., Galindo, V., Lambert-Girard, S., Dumont, D., Cuypers, Y., Bouruet-Aubertot, P., Mundy, C. J., Ehn, J., Bécu, G., Marec, C., Forget, M. H., Garcia, N., Coupel, P., Raimbault, P., Houssais, M. N. and Babin, M. (2019). Environmental Factors Influencing the Seasonal Dynamics of Under-Ice Spring Blooms in Baffin Bay. Submitted to *Elem Sci Anth*

Parmentier, F.-J. W., Christensen, T. R., Sørensen, L. L., Rysgaard, S., McGuire, A. D., Miller, P. A., & Walker, D. A. (2013). The impact of lower sea-ice extent on Arctic greenhouse-gas exchange. *Nature Climate Change*, *3*(3), 195–202. https://doi.org/10.1038/nclimate1784

Pedersen, C. A., Roeckner, E., Lüthje, M., & Winther, J.-G. (2009). A new sea ice albedo scheme including melt ponds for ECHAM5 general circulation model. *Journal of Geophysical Research: Atmospheres*, *114*(D8). https://doi.org/10.1029/2008JD010440

Perovich, D. K., Cota, G. F., Maykut, G. A., & Grenfell, T. C. (1993). Bio-optical observations of first-year Arctic sea ice. *Geophysical Research Letters*, *20*(11), 1059–1062. https://doi.org/10.1029/93GL01316

Perovich, Donald K. (1996). *The Optical Properties of Sea Ice.* (No. MONO-96-1). COLD REGIONS RESEARCH AND ENGINEERING LAB HANOVER NH. Retrieved from https://apps.dtic.mil/docs/citations/ADA310586

Perovich, D. K., Grenfell, T. C., Light, B., & Hobbs, P. V. (2002). Seasonal evolution of the

albedo of multiyear Arctic sea ice. *Journal of Geophysical Research: Oceans*, *107*(C10), 8044. https://doi.org/10.1029/2000JC000438

Perovich, Donald K., & Polashenski, C. (2012). Albedo evolution of seasonal Arctic sea ice. *Geophysical Research Letters*, *39*(8), L08501. https://doi.org/10.1029/2012GL051432

Pistone, K., Eisenman, I., & Ramanathan, V. (2014). Observational determination of albedo decrease caused by vanishing Arctic sea ice. *Proceedings of the National Academy of Sciences of the United States of America*, *111*(9), 3322–3326. https://doi.org/10.1073/pnas.1318201111

Popova, E. E., Yool, A., Coward, A. C., Dupont, F., Deal, C., Elliott, S., et al. (2012). What controls primary production in the Arctic Ocean? Results from an intercomparison of five general circulation models with biogeochemistry. *Journal of Geophysical Research: Oceans*, *117*(C8), C00D12. https://doi.org/10.1029/2011JC007112

Post, E., Bhatt, U. S., Bitz, C. M., Brodie, J. F., Fulton, T. L., Hebblewhite, M., et al. (2013). Ecological consequences of sea-ice decline. *Science (New York, N.Y.)*, *341*(6145), 519–524. https://doi.org/10.1126/science.1235225

Randelhoff, A., Oziel, L., Massicotte, P., Bécu, G., Galí, M., Lacour, L., et al. (2019). The evolution of light and vertical mixing across a phytoplankton ice-edge bloom. *Elem Sci Anth*, *7*(1), 20. https://doi.org/10.1525/elementa.357

Renner, A. H. H., Gerland, S., Haas, C., Spreen, G., Beckers, J. F., Hansen, E., et al. (2014). Evidence of Arctic sea ice thinning from direct observations. *Geophysical Research Letters*, *41*(14), 5029–5036. https://doi.org/10.1002/2014GL060369

Rousset, C., Vancoppenolle, M., Madec, G., Fichefet, T., Flavoni, S., Barthélemy, A., et al. (2015). The Louvain-La-Neuve sea ice model LIM3.6: global and regional capabilities. *Geosci. Model Dev.*, *8*(10), 2991–3005. https://doi.org/10.5194/gmd-8-2991-2015

Saenz, B. T., & Arrigo, K. R. (2012). Simulation of a sea ice ecosystem using a hybrid model for slush layer desalination. *Journal of Geophysical Research: Oceans*, *117*(C5). https://doi.org/10.1029/2011JC007544

Shine, K. P., & Henderson-Sellers, A. (1985). The sensitivity of a thermodynamic sea ice model to changes in surface albedo parameterization. *Journal of Geophysical Research: Atmospheres*, *90*(D1), 2243–2250. https://doi.org/10.1029/JD090iD01p02243

Smith, R., Anning, J., Clément, P., & Cota, G. F. (1988). Abundance and production of ice algae n Resolute Passage, Canadian Arctic. https://doi.org/10.3354/meps048251

Stroeve, J. C., Kattsov, V., Barrett, A., Serreze, M., Pavlova, T., Holland, M., & Meier, W. N. (2012). Trends in Arctic sea ice extent from CMIP5, CMIP3 and observations. *Geophysical Research Letters*, *39*(16), L16502. https://doi.org/10.1029/2012GL052676

Vancoppenolle, M., Fichefet, T., Goosse, H., Bouillon, S., Madec, G., & Maqueda, M. A. M. (2009). Simulating the mass balance and salinity of Arctic and Antarctic sea ice. 1. Model description and validation. *Ocean Modelling*, *27*(1), 33–53. https://doi.org/10.1016/j.ocemod.2008.10.005

Vancoppenolle, M., Bopp, L., Madec, G., Dunne, J., Ilyina, T., Halloran, P. R., & Steiner, N. (2013). Future Arctic Ocean primary productivity from CMIP5 simulations: Uncertain outcome, but consistent mechanisms. *Global Biogeochemical Cycles*, *27*(3), 605–619. https://doi.org/10.1002/gbc.20055

Vancoppenolle, M., & Tedesco, L. (2017). Numerical models of sea ice biogeochemistry. In D. N. Thomas (Ed.), *Sea Ice* (pp. 492–515). John Wiley & Sons, Ltd. https://doi.org/10.1002/9781118778371.ch20

Wassmann, P., & Reigstad, M. (2011). Future Arctic Ocean Seasonal Ice Zones and Implications for Pelagic-Benthic Coupling. *Oceanography*, *24*(3), 220–231. https://doi.org/10.5670/oceanog.2011.74

Yentsch, C. S., & Menzel, D. W. (1963). A method for the determination of phytoplankton

chlorophyll and phaeophytin by fluorescence. *Deep Sea Research and Oceanographic Abstracts*, *10*(3), 221–231. https://doi.org/10.1016/0011-7471(63)90358-9

Appendix

Evolution of wavelength fraction depending on snow depth from Perovich et al. 1993.

We recover the spectral transmittance for two types of snow (high snow h_s = 19 cm and low snow h_s = 0 cm) by digitalising figure 2 of Perovich et al. (1993) paper. After applying this transmittance on the surface irradiance measured during Baffin Field trip 2016 for nearly similar snow depth, we have calculated the wavelength fractions. Since figure 2 of Perovich et al., 1993 paper gives only visible transmittances we could not calculate the NRGB fraction. This study shows that blue fraction increase (from 40% to 43%) when snow depth increases while the green and red fractions do not change clearly (~49% for green and ~9% for red for both snow type). But variation in fractions remain low for all wavebands.

Chapitre 3

Saisonnalité de la lumière dans la zone de banquise arctique dans un contexte d'étude du phytoplancton

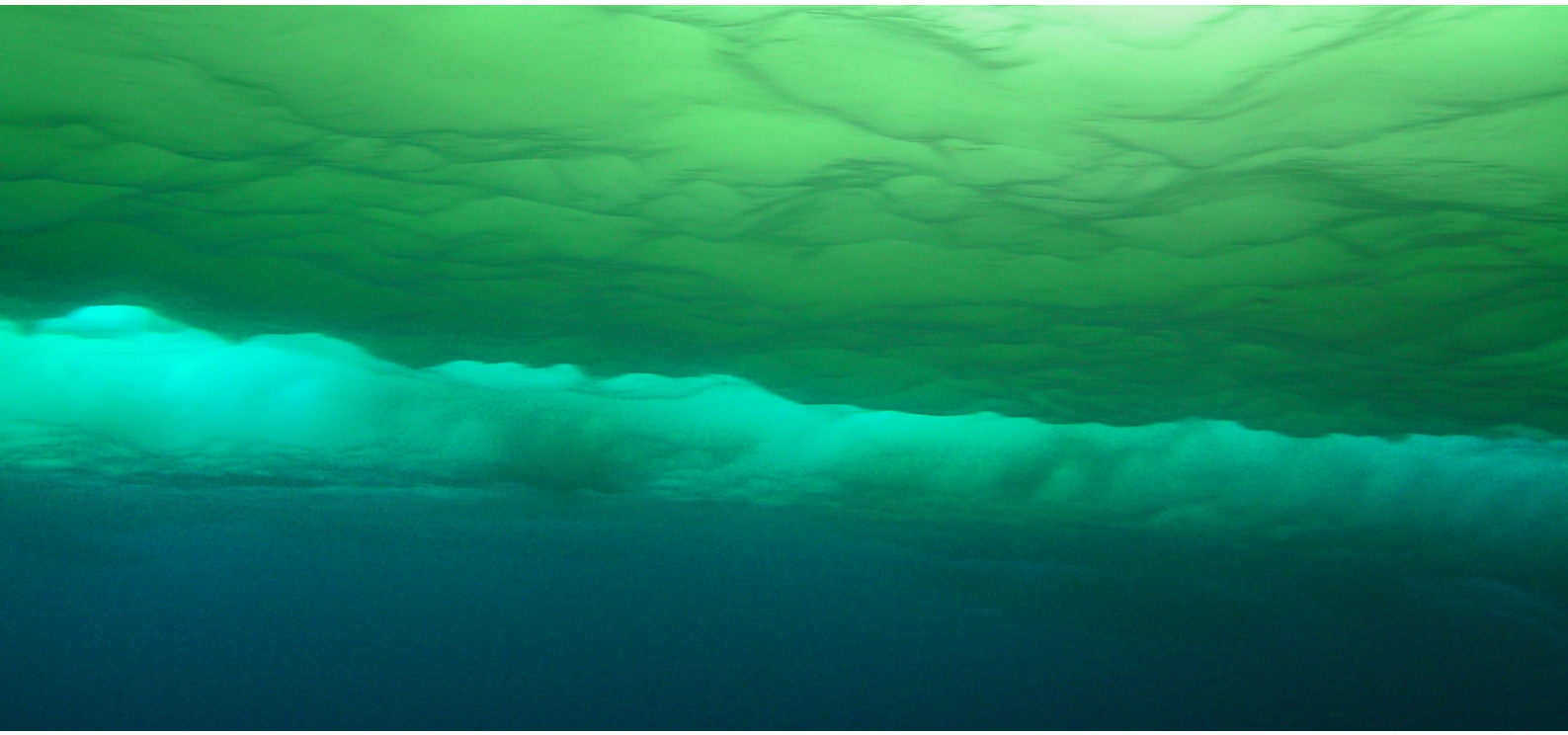

© C. Fritsen

Dans un contexte de réchauffement global et de retrait de la banquise arctique, mieux comprendre les interactions entre banquise et phytoplancton est fondamental pour prévoir les impacts du retrait de la banquise sur les écosystèmes et les activités humaines en Arctique, en particulier l'impact sur les populations autochtones et sur la pêche. L'une des sources majeures d'incertitudes dans ces interactions est le rôle de la limitation en lumière et en nutriments dans la zone de banquise arctique. Dans l'étude du phytoplancton arctique à grande échelle, il est courant d'utiliser la saison d'eau libre pour décrire la saisonnalité de la lumière disponible dans les régions englacées. Cependant, de récentes observations ont révélé que le phytoplancton pouvait ne plus être limité par la lumière bien avant le retrait de la banquise en raison de l'effet de l'ouverture de chenaux d'eau libre dans la banquise, de la fonte de la neige ou encore de la formation de mare de fonte sur la banquise.

Dans cette étude, je montre que l'utilisation de la saison d'eau libre pour décrire la saisonnalité en lumière en zones englacées n'est pas toujours appropriée. J'introduis la photopériode comme le nombre de jours durant lesquels la quantité de lumière est suffisante pour la croissance du phytoplancton. Je montre que la photopériode peut être très différente de la période d'eau libre, dans certaines conditions. Elle semble aussi meilleure pour décrire la saisonnalité de la lumière dans les eaux englacées arctiques, comme le suggèrent les observations (satellite et in situ) et les simulations des modèles du système Terre.

Bien que les simulations pour les prochains siècles prévoient une augmentation de la photopériode indépendamment de la période d'eau libre, il reste un certain nombre d'incertitudes à résoudre avant de pouvoir utiliser la photopériode pour décrire la limitation en lumière pour le phytoplancton. Deux principales catégories de processus devraient être mieux caractérisées pour réduire ces incertitudes : l'optique dans la zone de glace et la physiologie du

phytoplancton. De plus, les hypothèses formulées dans les modèles, quant à l'évaluation de la croissance du phytoplancton dans les zones de banquise, devraient être davantage explorées.

Light seasonality in the Arctic sea ice zone in the context of phytoplankton studies

Marion Lebrun[1], Martin Vancoppenolle[1], Gurvan Madec[1]

[1] Sorbonne Université, LOCEAN-IPSL, CNRS/IRD/MNHN, Paris, France

Manuscript in prep

August, 2019

Marion Lebrun, Laboratoire d'Océanographie et du Climat, IPSL Boite 100, 4 Place Jussieu, 75252 Paris CEDEX 05, France.

Abstract

In the context of global warming and Arctic sea ice retreat, better understanding the link between sea ice and phytoplankton is critical to project impacts of sea ice retreat on ecosystem and human activities in the Arctic, with particular relevance to indigenous people and fisheries. One of the major sources of uncertainty is the respective role of light and nutrient limitations in sea ice zones. A standard approach in large-scale phytoplankton studies is to use the open-water season as proxy for light seasonality in sea ice zone. However, recent observational studies have pointed out that light limitation could be relieved well before ice retreat, because of fractures in the ice (leads), melting snow and melt ponds. Besides, satellite observations suggest that ice advance sometimes occur beyond polar night, a situation that should become more prevalent in the future. Both aspects complicate the link between plankton activity and open-water season. In this study we try to address these two issues. We show that open-water season duration is not always appropriate to describe light seasonality. We introduce photoperiod as the number of days with assumed sufficient light for phytoplankton growth. Photoperiod may significantly differ from the open-water season and seems a priori better to describe light seasonality than the open-water season, as suggested by observations (satellite and in situ) and Earth System Model simulations. Photoperiod is projected to increase independently of ice-free period in the next centuries. However, large uncertainties remain before photoperiod can be reliably used as a proxy for light limitation for phytoplankton. Two broad categories of processes should be better characterised: optics in the sea ice zone and phytoplankton physiology. Model assumptions to compute phytoplankton growth in sea ice zone should also be further explored.

Introduction

Phytoplankton studies in Arctic sea ice zone are facing new issues since Arctic sea ice is changing by decreasing in coverage (Cavalieri & Parkinson, 2012), thickness (Kwok & Rothrock, 2009; Lindsay & Schweiger, 2015; Renner et al., 2014) and age (Maslanik et al., 2011) these recent years. Earth System Models project that these changes are expected to continue in the future (Massonnet et al., 2012; Stroeve et al., 2012), questioning the future evolution of phytoplankton in Arctic sea ice zone.

Photosynthesis is primarily governed by light availability and nutrient supply. However, the respective importance of light and nutrients on phytoplankton growth is largely uncertain (Popova et al.,2012; Lewis et al., 2019; Mundy et al., 2014; Tremblay & Gagnon, 2009). Present understanding stresses the important role of light for phytoplankton bloom initiation whereas nutrient availability mostly impacts the intensity and the end of the bloom. Observational studies suggest an important role for the distribution of ice and open-water for light availability (Arrigo & van Dijken, 2011; Assmy et al., 2017; Wassmann & Reigstad, 2011). In addition, changes towards thinner ice with more melt ponds seem favourable to plankton (Arrigo et al., 2012;Arrigo et al., 2014; Horvat et al., 2017; Mundy et al., 2007; Palmer et al., 2014) challenging the classical view of no plankton activity under sea ice (English, 1961).

Actually, ice and snow drastically reduce light supply for phytoplankton in sea ice regions, because of their high albedo and low transmittance (Grenfell & Maykut, 1977; Perovich, 1996). Because of this, it is common to use the open-water season as a proxy for light seasonality (Arrigo & van Dijken, 2011; Hill et al., 2013; Mundy et al., 2009; Rysgaard et al., 1999). Open-water season (L_w) has been used in the context of several recent large-scale studies. It is defined as the number of ice-free days (Parkinson, 2014), practically the period during which sea ice concentration drop below a given threshold (Stammerjohn et al., 2012; Stroeve et al., 2016).

Using L_w to understand the light seasonality in the sea ice zone is based on the assumption that (i) the sea ice zone is fully opaque and (ii) the open-water season never occur during the polar night. Recent field observations and Earth System Model simulations contradict both assumptions. They first show that light is transmitted under sea ice (Frey et al., 2011; Hill et al., 2018; Horvat et al., 2017). Second, future open-water season may overlap with polar night, especially in the future (Lebrun et al., 2019).

In this chapter we try to better describe the light seasonality in the sea ice zone in the context of phytoplankton studies. We first explain why open-water season is not always appropriate to describe light seasonality in Arctic sea ice zone. We then define the photoperiod as a better proxy for light seasonality in sea ice zone. The third part is focused on uncertainties about the link between photoperiod and the light limitation for phytoplankton in the Arctic sea ice zone.

1. Data and methods

1.1) Data:

We base our analysis on passive microwave sea ice concentration retrievals, namely the GSFC Bootstrap SMMR-SSM/I quasi-daily time series product, over 1980–2015 (Comiso, 2000, updated 2015), to calculate both light and sea ice seasonality.

Similarly, we use monthly interpolated daily sea ice concentration from CMIP5 Earth System Model historical simulations and projections (RCP8.5). Some models lose their multi-year ice only late into the 21st century. To compare sea ice and light seasonality in Arctic sea ice zone, we only retain the nine ESM simulations that pursue projections until 2300. We focus CMIP5 analysis on 1900-2200, combining historical (1900–2005) and RCP8.5 (2005–2200) simulations. The year 2200 corresponds to the typical date of year-round Arctic sea ice disappearance (Hezel et al., 2014).

SMMR/SSM-I data and CMIP5 simulation do not provide daily fields of ice and snow thickness, light transmitted to the ocean surface or primary production. To circumvent this problem and, to investigate interactions between light and phytoplankton in sea ice zone, we also use daily field of sea ice concentration, ice and snow thickness, SST, primary production vertically integrated, or shortwave irradiance at the ocean surface based on a 1948-1957 forced atmosphere ice ocean IPSL-CM simulation. This simulation was performed with NEMO-LIM3.6 (Rousset et al., 2015) coupled with the biogeochemical model PISCES (Aumont et al., 2015). The physical component of our experiment follows the protocol of the Coordinated Ocean-ice Reference Experiments (CORE) (Danabasoglu et al., 2014; Griffies et al., 2009) interannually varying experiment (CORE-II). The CORE-II experiment forces physical ocean fields through use of the interannually varying atmospheric state of Large and Yeager (2009), along with river runoff data based on modifications of Dai and Trenberth (2002) and Dai et al. (2009). The full forcing data set covers the 62-year period from 1948 to 2009.

1.2) Ice seasonality diagnostics

To describe ice seasonality, the length of open-water season (L_w) is defined as the number of days during which sea ice concentration is lower than 15% following Parkinson (1994); Stammerjohn et al. (2012) and Stroeve et al. (2016). Day of ice retreat (d_r) and day of ice advance (d_a) are respectively defined as the first day of the year when sea ice concentration drops below, or exceeds, 15%. Time axis must be well defined to circumvent the effect of the d_a discontinuity between December 31 and January 1st (Lebrun et al., 2019).

Here, because we represent differences between d_a and polar night onset, we can not just use negative value for d_a as Lebrun et al. (2019). We consequently add 365 to values of d_a falling before the 20th of June.

1.3) Daily shortwave irradiance at the ocean surface

Since daily shortwave irradiance at the ocean surface ($\overline{F_{sw}^{tr}}$) from SMMR/SSM-I satellite data and CMIP5 simulations are not available, we recovered this field using a very simple formulation. It is based on satellite or simulated daily sea ice concentration (A) and daily incoming solar irradiance (F_{sw}^{0}) obtained following Shine clear sky formula (Shine, 1984):

$$\overline{F_{sw}^{tr}} = F_{sw}^{0}.[\mathrm{A}.T_{ice} + (1 - A).(1 - \alpha_{oce})] \quad (1).$$

Where α_{oce} = 0.06 is the open-water albedo and T_{ice} is the ice transmittance. We perform two calculations. The first one considers opaque ice (T_{ice}= 0%) and the second consider non-opaque ice. Considering non-opaque ice parameterisation, we assume a constant ice transmittance, T_{ice}= 5%, as a good compromise between the average ice transmittance for land-fast sea ice (0.9 ± 2%) and for pack ice (9 ± 5%) based on data set used in chapter 2.

Regarding NEMO-LIM3.6 simulations, we could retrieve daily shortwave irradiance at the ocean surface. The output shortwave irradiance is based on a parameterisation which assumes opaque snow and the attenuation of light by ice following a two-level Beer-Lambert law (Maykut & Untersteiner, 1971) in bare ice (**REF** parameterisation; eq.2).

$$\overline{F_{sw}^{tr}} = \begin{cases} 0, if \;\; h_s > 0 \\ F_{sw}^{0}.(1 - \alpha_{ice}).i_0 e^{-\kappa_i (h_i - h_0)}, \;\; if \; h_s = 0 \end{cases} \quad (2).$$

Where h_i and h_s are the simulated ice and snow thickness; α_{ice} is the ice albedo calculated depending on sea ice thickness and properties (dry or wet) which are defined by air temperature (negative or positive) following Shine & Henderson-Sellers (1985) formulation, as updated by C. Rousset, to regularise a few numerical issues with little physical impact; $i_0 = 0.18\,(1 - c) + 0.35$ with c is the cloud fraction; and h_0 = 0.10 m are respectively the surface scattering layer coefficient and thickness; κ_i = 1 m^{-1} is the attenuation coefficient for bare ice and F_{sw}^{0} is the incoming shortwave irradiance given by atmospheric forcing.

From the simulated sea ice field, we also calculate another shortwave irradiance at the ocean surface, following improved parameterisation (**IMP**) presented in Chapter 2 (eq. 3).

$$\overline{F_{sw}^{tr}} = \begin{cases} F_{sw}^{0}.(1-\alpha_{snw}).i_0 e^{-\kappa_s(h_s-h_0)} e^{-\kappa_i h_i}, if\ \ h_s > 0 \\ F_{sw}^{0}.(1-\alpha_{ice}).i_0 e^{-\kappa_i(h_i-h_0)}\ ,\ if\ h_s = 0 \end{cases} \quad (3).$$

In this equation, h_i and h_s are simulated ice and snow thickness and κ_i = 1 m^{-1} is the attenuation coefficient for bare ice. Value of other parameters change a little bit following Chapter 2: i_0 = 0.3, h_0 = 0.10 m for bare ice and h_0 = 0.03 m for snow-covered ice; κ_s is the attenuation coefficient for snow. κ_s= 10 m^{-1} for dry snow and κ_s = 7 m^{-1} for melt snow. α_{ice} and α_{snw} are based on the same computation as for REF parameterisation. But as output of air temperature was not available in this study, we use a proxy of temperature assuming that air temperature is close to the sea surface temperature except between July 1st and August 15, when it is assumed to be positive. Finally, outputs of incoming shortwave irradiance were also not available. To circumvent this, we use the Shine clear sky formulation only for IMP parameterisation.

These assumptions due to the lack of output availability could be a large source of error in the transmitted shortwave irradiance calculation. But since REF and IMP NEMO-LIM3.6 shortwave irradiance at the ocean surface are not compared in this study, we assume that these errors remain smaller enough for our study. These sources of error should also disappear as the IMP parameterisation should ultimately be introduced in the sea ice model, LIM.

Finally, $\overline{F_{sw}^{tr}}$, for all data sets, is converted into a photosynthetically available radiation at the ocean surface (PAR_{tr} in µE/m^2/day) as follows:

$$PAR_{tr} = 2.33\ .\overline{F_{sw}^{tr}}.86400\ .10^{-6} \quad (4).$$

1.4) Daily Primary production in NEMO-LIM3.6 simulations

Sea ice zone primary production is computed in PISCES following Long et al. (2015) formulation which recommends calculating two intermediate productions before obtaining the

area-weighted grid cell average primary production. The first production should depend on light transmitted through open-water whereas the second should depend on light transmitted through the sea ice/snow system. Long et al. (2015) explain this method to be more precise, since primary production non-linearly depends on light supply, leading to largely underestimate the primary production by directly computing it from the total short-wave irradiance at the ocean surface.

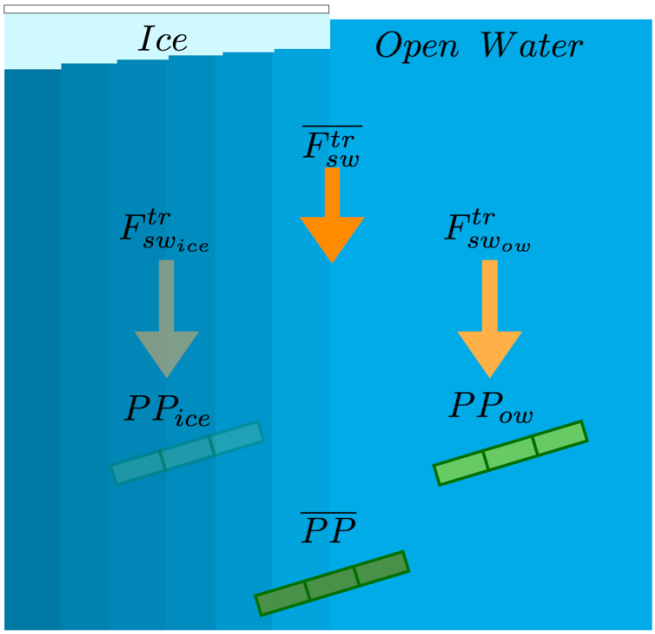

Figure 1: Scheme representing the calculation of primary production in ice-covered grid cells in the PISCES biogeochemical model.

To simplify calculations and according to former assumptions which consider no production under ice (PP_{ice} = 0), PISCES considers no-production in the ice-covered part of the grid cell and reallocate the grid cell average transmitted shortwave irradiance at the ocean surface only under open-water (eq.4; Fig. 1 left part).

$$F_{sw_{ow}}^{tr} = \overline{F_{sw}^{tr}} / (1 - A) \quad (5).$$

This shortwave irradiance under open-water is then used to calculate the growth rate for phytoplankton (eq.5; Fig. 1 right part).

$$\overline{PP} = C.PP_{max}.f_{lim} \quad (6).$$

Where C is the phytoplankton concentration, PP_{max} is the ideal growth rate and f_{lim} range between 0 and 1, is the limiting factor containing the impact of $F_{sw_{ow}}^{tr}$, nutrients, temperature and mixed layer depth. In sea ice zone, C represents the grid-cell average concentration value. This is equivalent to assume that vertical and horizontal mixing are strong enough to redistribute phytoplankton from leads to the entire grid cell faster than phytoplankton grows. The growth rate is then vertically integrated (INTPP).

1.5) Light seasonality diagnostics

We first define polar night onset (or ending) as the first day of the year when incoming shortwave radiation based on the clear sky Shine formula exceeds (or drop below) 0.1 W/m^2. We assume that 0.1 W/m^2 (0.02 µE/m^2/day) is small enough to consider that there is no more available light for phytoplankton after penetration in the ocean.

Photoperiod is defined as the number of days during which PAR^{tr} exceeds a threshold. For both satellite and CMIP5 data, we use four PAR^{tr} thresholds (i) 0.010 µE/m^2/day; (ii) 0.415 µE/m^2/day; (iii) 1.600 µE/m^2/day and (iv) 5.000 µE/m^2/day. Both intermediate thresholds (ii and iii) come from literature (Letelier et al., 2004; Tremblay et al., 2006) while the first and the last thresholds are assumed to be extreme cases.

For NEMO-LIM3.6 simulations, the PAR threshold (1 µE/m2/day) is visually defined as equal to the simulated PAR^{tr} for which integrated primary production begins to grow.

2. Results

2.1) Length of open-water season: not the ideal proxy of light seasonality in Arctic sea ice zone.

The length of open-water season is a common proxy for light seasonality in Arctic sea ice zone, in the context of phytoplankton studies. This suggests two assumptions. The first one assumes

that open-water season never happens during the polar night while the second one assumes no transmission of light in sea ice zones. In this section we explain why both assumptions should be revised using results from Chapters 2 and 3.

Overlap between ice-free season and polar night

Arctic sea ice melting and freezing processes are primarily controlled by the seasonality of solar irradiance. During fall and winter, solar irradiance decreases and may even become null in the Arctic during polar night. Once sea surface temperature reaches -1.8 °C, water can freeze. During spring and summer solar irradiance warms the sea ice surface. Once the ice surfaces reaches 0°C, surface melting starts. Solar absorption by the upper ocean is practically converted into basal melt. There are admittedly mechanisms, as ocean heat flux or sea ice dynamics, which also influence sea ice growth and melt. However, solar forcing is the main driver of the sea ice seasonal cycle.

Figures 2 and 3 represent the relation between sea ice retreat and advance date and polar night ending and onset for present (en of the 20th century) based on satellite retrievals and for future (2080-2099) based on CMIP5 Earth System Models.

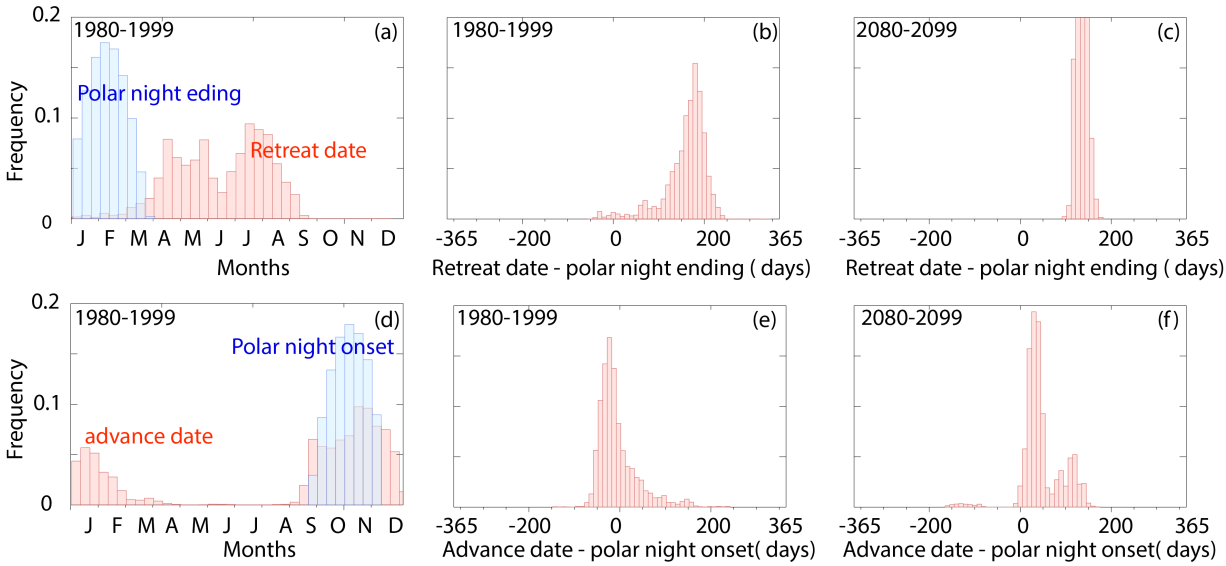

Figure 2. Frequency histograms of (a) observed ice retreat date (red) and polar night ending dates (blue) ; (b) difference between both for (b) 1980-1999 and (c) for 2080-99 for the northern hemisphere. (d-f) Same for ice advance date and polar night onset. Sources of calculations are passive microwave ice concentration retrievals for 1980-1999 and CMIP5 simulations for 2080-2099.

Fig. 2 and 3 (a, b, c) represent the relation between retreat date (d_r) and polar night ending. While d_r falls from March to August (Fig. 2a, 3a) in present Arctic, polar night ends during late winter (between January and March; Fig. 2a; Fig. 3a). d_r falls after polar night ending everywhere in present Arctic seasonal ice zone (Fig. 3b). Differences between both are around four to six months (Fig. 2b) and could even reach eight months in North West Passage (Fig. 3b). This delay highlights the fact that sea ice needs sunlight to melt. The difference between d_r and polar night ending is the smallest in the Atlantic sector of the Arctic Ocean, as well as in Barents Sea (Fig. 3b) due to early melting (in February) led by the inflow of warm Atlantic water in this region (Årthun et al., 2012; Ivanov et al., 2012; Polyakov et al., 2017; Sandø et al., 2010). During 2080 to 2099 period, CMIP5 Earth System Models project that d_r still falls after polar night ending. But the gap between polar night ending and ice retreat date is expected to decrease (between three and four months; Fig. 2c) due to global ocean warming and thinner ice which enables earlier sea ice melting during early spring.

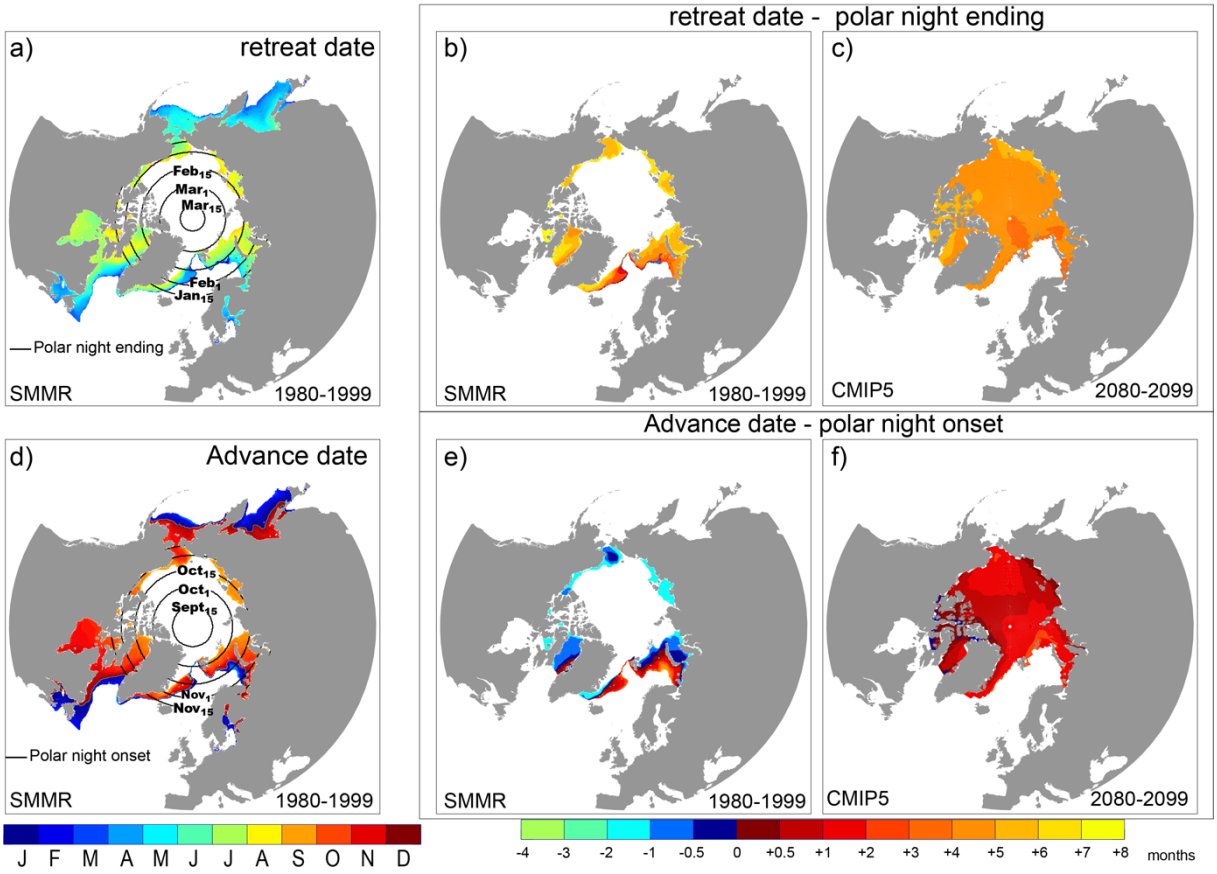

Figure 3. Distribution of (a) observed retreat date and polar night ending dates (black circles); (b) difference between both for (b) 1980-1999 and (c) for 2080-99. (d-f) Same for ice advance date and polar night onset. Sources of calculations are passive microwave ice concentration retrievals for 1980-1999 and CMIP5 simulations for 2080-2099.

Panels d), e) and f) of figures 2 and 3 represent the present and future relations between sea ice advance date (d_a) and polar night onset. d_a and polar night onset are close to each other (Fig. 2d and 3d), unlike d_r and polar night ending. They both occur around fall. d_a falls between September and February while polar night onset falls from September to November (Fig. 2d). The difference between them is consequently weak (less than two months; Fig. 2e). Advance usually occurs before polar night onset but not everywhere (Fig 2e and Fig. 3e). The warm Atlantic water also impacts ice advance in the Atlantic sector of the Arctic Ocean, as well as in Barents Sea. This leads to shift the ice advance from some weeks to several months after polar night onset (Fig. 3e). Future d_a is expected to fall from some days to two months after polar night onset everywhere in Arctic by 2050 (Fig. 2f and Fig. 3f). This is due to the freeze-up

amplification mechanisms discussed in Chapter 1 (Lebrun et al., 2019) which shifts the advance date twice as much as the offset in ice retreat.

This figure highlights the strong link between seasonality of sea ice and solar irradiance. Ice retreat always falls after polar night ending despite global warming. In contrast, ice advance could already fall after polar night onset in present in some regions and this is expected to become global by 2050. The assumption that there is no overlap between open-water season and polar night should consequently be revised for some regions in present conditions, and for all of them in the future

Light transmitted in sea ice zone

In Chapter 2 we show that ice transmittance is never null even under snow-covered ice based on an in-situ data analysis. We suggest a new parameterisation for sea ice radiative transfer which is more precise than actual NEMO-LIM3.6 parameterisation.

Figure 4 represents the distribution of shortwave irradiance in the Arctic calculated from this IMP parameterisation based on NEMO-LIM3.6 ice and snow thickness over sunlit months (April to September) during 1947 to 1958. Two contours are represented in these maps: the contour where light is assumed to be sufficient for phytoplankton growth (PAR^{tr} = 1 $\mu E/m^2/day$); and the ice edge defined as the 15% ice concentration contour. The most important information on this figure is that the PAR^{tr} contour is always within the sea ice zone. This means that there is always a fraction of the sea ice zone that is suitable of primary production. This is due to both the presence of leads in sea ice zone (which is responsible for ~83 ± 20% of the total transmitted irradiance during the sunlit month) and the light transmitted through ice-covered pixels. In April, the 1 $\mu E/m^2/day$ contour and the ice edge are rather close, with most of the sea ice zone seemingly unsuitable to primary production.

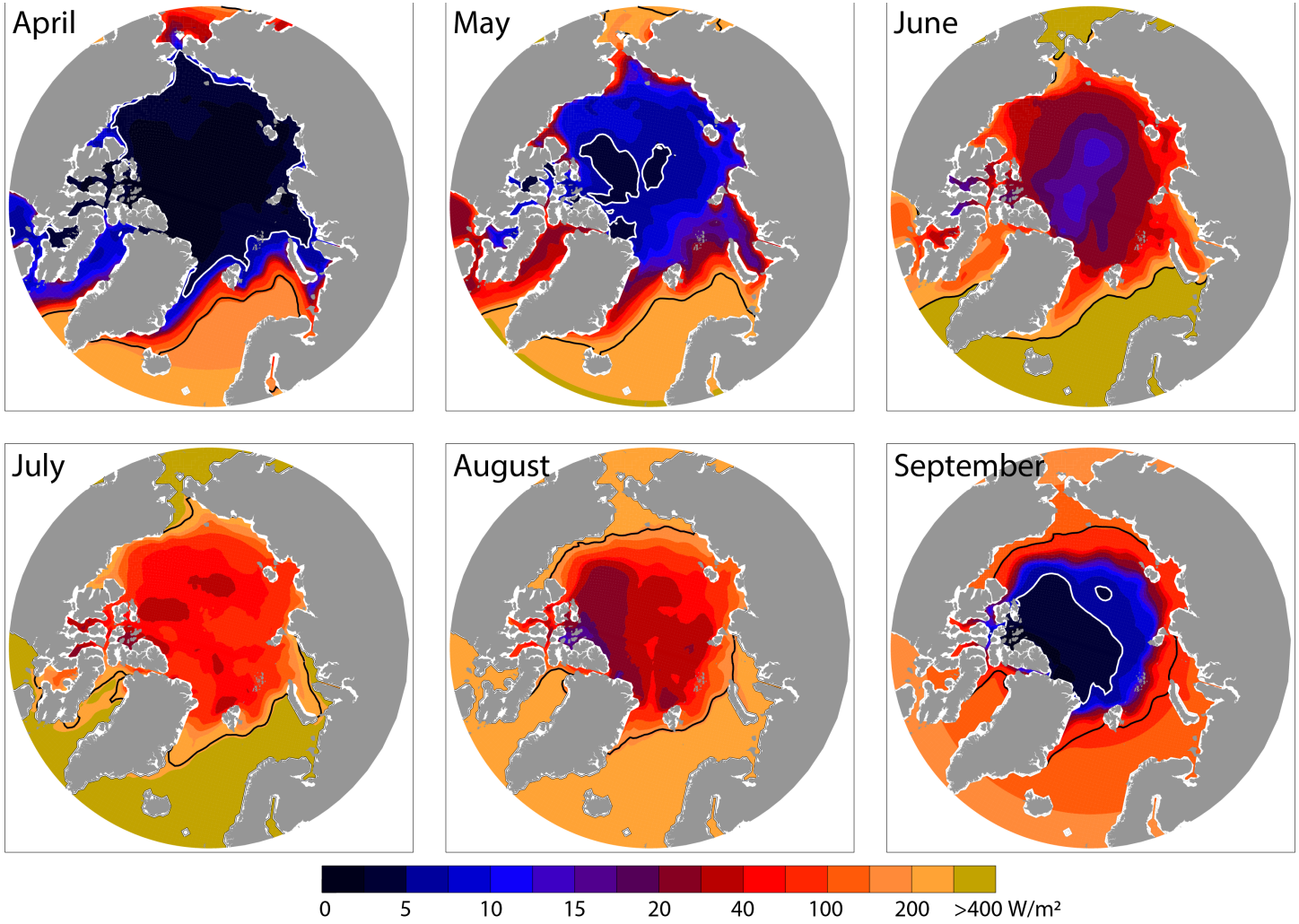

Figure 4: Distribution of transmitted short-wave irradiance average monthly between 1948 and 1957 from **IMP** parametrization based on daily outputs of sea ice and snow thickness from a NEMO simulation. The black line refers to the ice edge (A= 15%) while the white line refers to NEMO_LIM3.6 PAR^{tr} threshold (PAR^{tr} = 1 mol/m^2/day).

During May, leads are opening in sea ice zone and this with the ice thinning ans snow melt contributes to expand the photo-productive zone while the ice edge does not clearly move. From June to August, the entire Arctic is photo-productive with a maximum $\overline{F_{sw}^{tr}}$ during July (with an average of about 120 W/m^2). Finally, in September the photo-productive zone starts shrinking, with the onset of sea ice growth in the Central Arctic, and the reduction of incoming solar irradiance.

By describing the light seasonality only based on a sea ice concentration threshold, we miss a large sunlit zone in the seaice-covered Arctic.

2.2) Toward better characterization of light seasonality in Arctic sea ice zone

The aim of this section is to find a diagnostic better related to light seasonality than the length of open-water season. We call photoperiod (L_p) the period of the year during which the photosynthetically available radiation at the ocean surface (PAR_{tr}) is assumed to be sufficient for phytoplankton growth. Since L_p is directly related to transmitted light at the ocean surface, it seems a better diagnostic to describe light seasonality. However, we show in this section that there are large sources of uncertainties in the definition of this diagnostic.

Photoperiod for present conditions

The photoperiod is influenced by both incoming shortwave irradiance, and sea ice. The photoperiod depends on latitude as the incoming shortwave irradiance decrease and the sea ice concentration increases with latitude (Fig. 5).

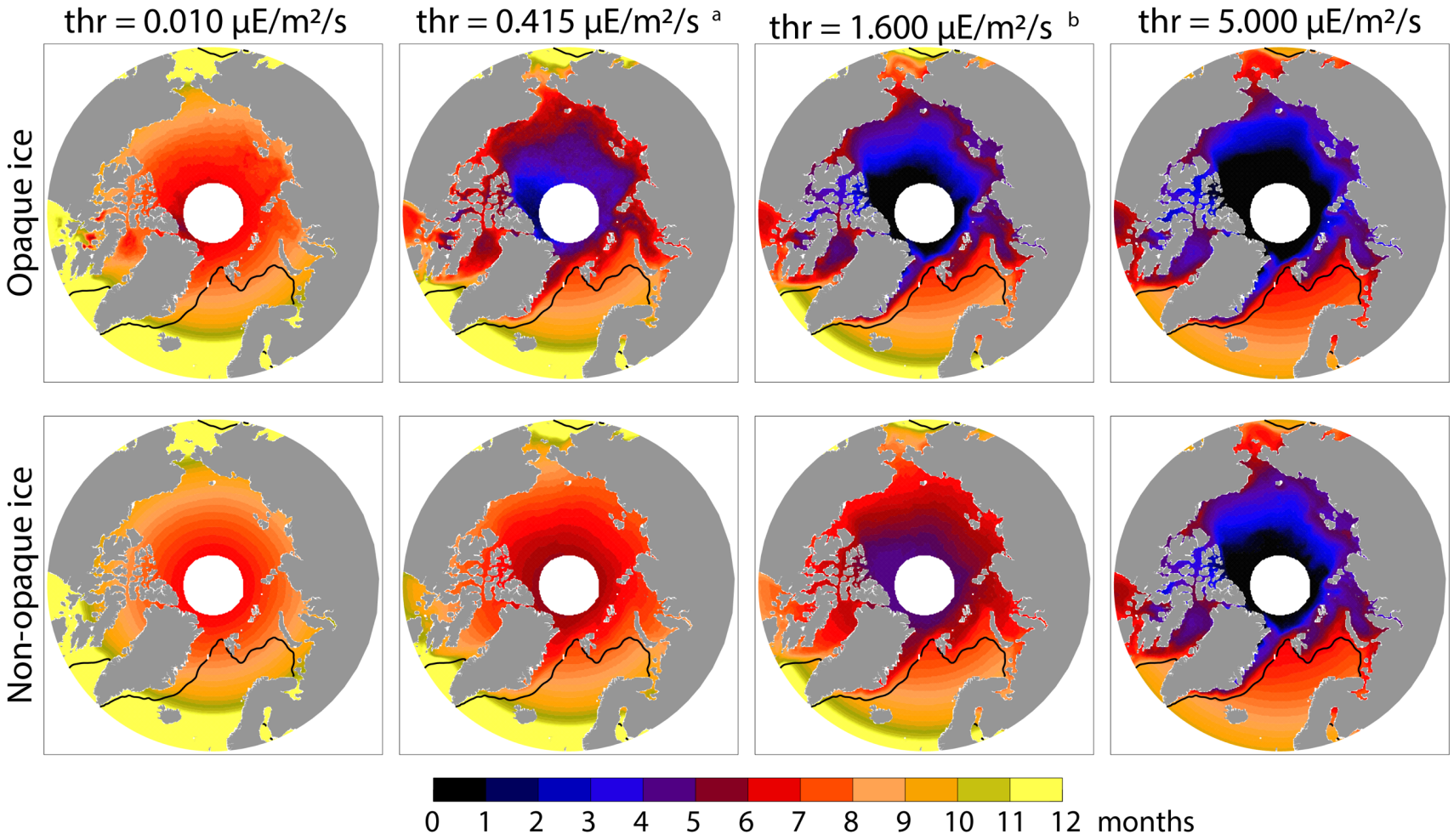

Figure 5 : Distribution of the photoperiod from satellite retrievals between 1980 and 2015 considering opaque ice (top) or non-opaque ice (T_{ice} = 5%;bottom) with an increasing PAR^{tr} threshold (thr) from left to right, ([a] Letelier et al., 2004; [b] Tremblay et al., 2006). Black contour refers to the ice edge (A = 15%). The PAR^{tr} is based on daily sea ice concentration from satellite retrievals.

However, the impact of sea ice concentration on photoperiod is determined by the chosen PAR^{tr} threshold. At very low threshold (0.010 µE/m^2/day), sea ice concentration has a weak impact on photoperiod which remains relatively large in Arctic sea ice zone (~9 ± 4 months). For a high threshold (5 µE/m^2/day), photoperiod in Arctic sea ice zone is mostly impacted by sea ice and is consequently lower (~5 ± 3 months). The source of error due to PAR^{tr} threshold remains large. Even with the observational uncertainty range (Letelier et al.,2004; Tremblay et al., 2006), the average difference is of about 2 months between both (~8 ± 3 months for PAR^{tr} threshold = 0.415 µE/m^2/day and 6 ± 3 months for PAR^{tr} threshold = 1.6 µE/ m^2/day).

The length of the photoperiod is also impacted by light transmitted through sea ice (Fig. 5 bottom panel). On average, the increase in the ice transmittance of 5% leads to increase the photoperiod from two weeks to two months for every PAR^{tr} threshold. Since the impact of sea ice depends on the PAR^{tr} threshold, the level of impact due to ice transmittance is also dependent on the PAR^{tr} threshold.

Future evolution of photoperiod

These uncertainties due to PAR^{tr} threshold and ice transmittance remain unresolved in the CMIP5 simulations. But, despite these uncertainties, the future evolution of photoperiod projected by CMIP5 Earth System Models strongly differs from the open-water season evolution, regardless of the threshold value (Fig. 6).

We can distinguish two steps in the simultaneous evolution of photoperiod length and L_w. The first step is between 1900 to about 2050-2100. During this step, L_p is larger than L_w due to the presence of leads in sea ice zone (where A<15%) and due to the non-null ice transmittance. During the second step (after 2050-2100), L_p becomes limited by the polar night when the ice advance date occurs after the polar night ending, and L_p become lower than open water season.

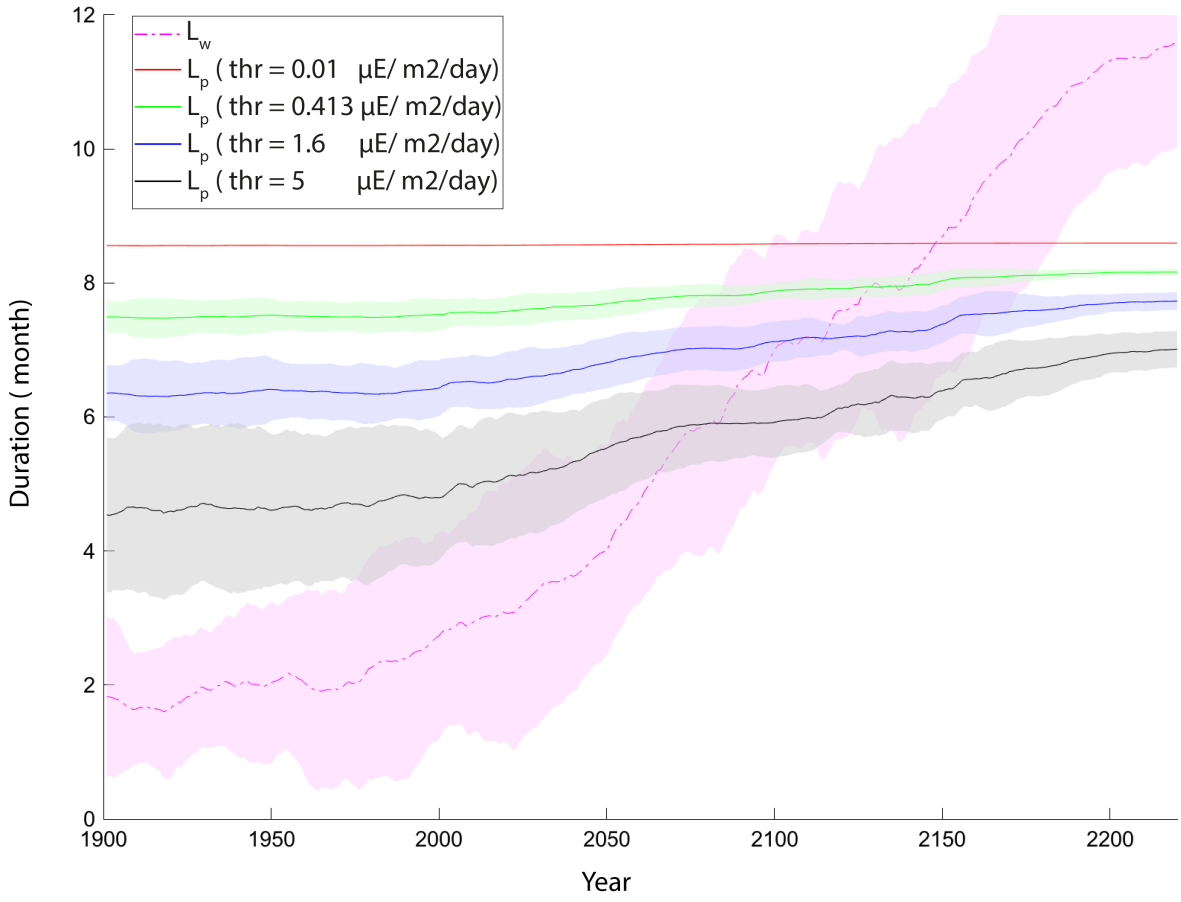

Figure 6: Time series of CMIP5 (median ± inter quartile range of the 9 models) photoperiod (solid lines) for the four PAR^{tr} thresholds and open-water season (dashed pink line) for 70-80°N latitudinal band considering non-opaque ice.

In conclusion, photoperiod should be better proxy for light seasonality in Arctic sea ice zone because it does not depend anymore on assumptions such as an opaque ice zone or no overlap between open-water season and polar night. However, large uncertainties remain in the photoperiod definition led by PAR^{tr} threshold and ice transmittance. Better understanding phytoplankton physiology to better constrain the PAR^{tr} threshold and better define the ice radiative transfer in models are key to understand the impact of sea ice melt on light seasonality in the Arctic sea ice zone in the context of phytoplankton studies.

2.3) Is Photoperiod really a better diagnostic for light limitation?

Although photoperiod better represents light seasonality in Arctic sea ice zone (section 2.2), this does not imply that L_p well represents the light limitation for phytoplankton in the Arctic sea ice zone. The link between photoperiod and primary production, in climate projections, strongly depends on the model assumptions.

Whereas light in the Arctic sea ice zone is limited by both sea ice cover and polar night, in some models, nutrients are the main limiting factor for photosynthesis (Vancoppenolle et al., 2013). This leads to reduce the link between primary production and photoperiod.

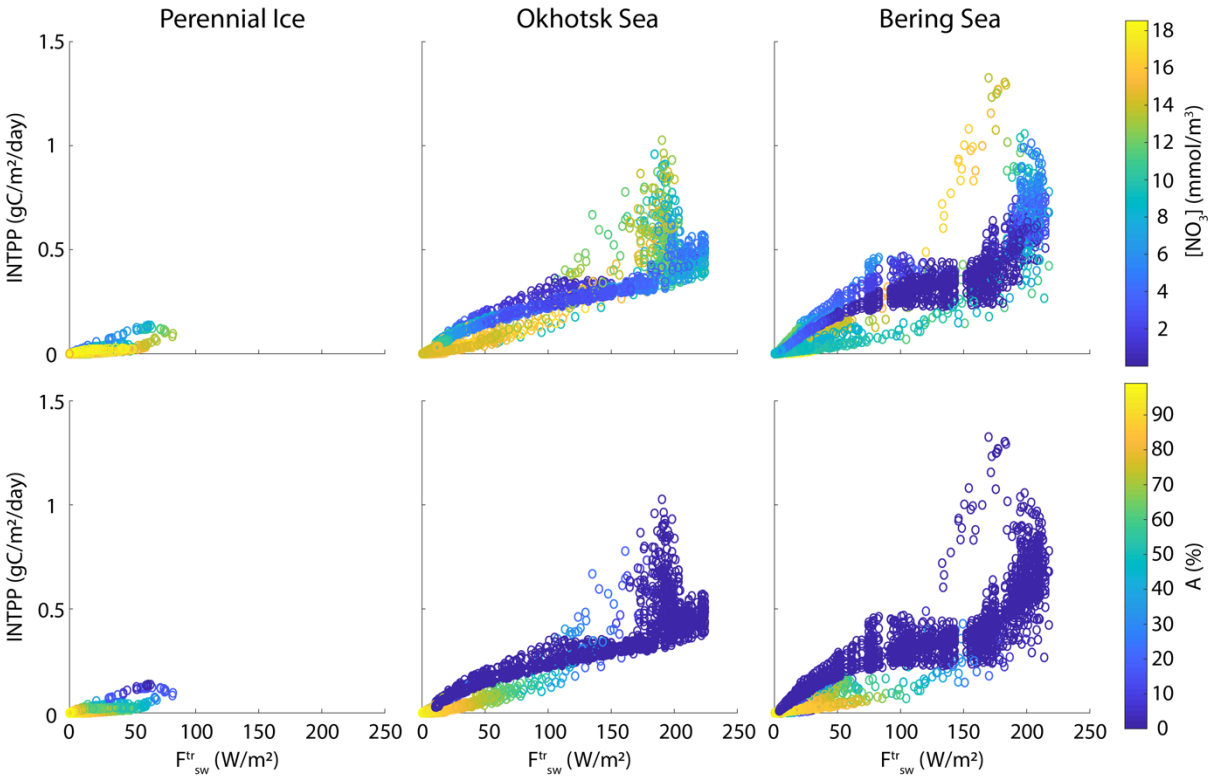

Figure 7: Daily values of irradiance available at the ocean surface (under-ice if ice present), versus vertically integrated primary production (INTPP) over 1948-1957 from NEMO-LIM3.6 REF simulation for three distinct points (PIZ: 80.9 °N-159.3 °W; Okhotsk Sea: 55.8 °N-150.5 °E and Bering Sea: 61.9 °N-175.9 °W). Colours represent the NO3 concentration (upper panel) or the sea ice concentration for each point (bottom panel).

There are also built-in assumptions in some models, for example in NEMO-PISCES, which constrains primary production to be strongly correlated to open-water season. Because of such assumptions, photoperiod may not better explain photosynthesis than the open water season. For instance, in PISCES, the correlation between yearly and vertically integrated primary

production and photoperiod (~86%) is not better than the correlation between primary production and length of open-water season (~88%). This can be explained by the assumption made in PISCES biogeochemical model (see section 1.4) which considers that there is no light and consequently no production under the ice-covered part of the grids cells. This assumption is justified by the belief that vertical and horizontal mixing occur faster than phytoplankton growth. For the same reasons, in the model, the concentration of plankton is diluted over the entire (ice+open water) grid cell over one time step.

Both assumptions contribute to reduce primary production in high sea ice concentration regions even if the light and nutrient concentrations are high (Fig. 7).

Such assumptions prevent us from using photoperiod to describe light limitation of phytoplankton in Arctic sea ice zone.

4. Conclusion

The analysis presented is this chapter focuses on the seasonality of available light in the Arctic sea ice zone in the context of phytoplankton studies.

A commonly used proxy for light available for photosynthesis in the sea ice zone is the open-water season (Arrigo & van Dijken, 2011; Hill et al., 2013; Mundy et al., 2009; Rysgaard et al., 1999). The use of this diagnostic is based on two implicit assumptions: (i) there is no overlap between open-water season and polar night; (ii) light is not transmitted to the upper ocean in the sea ice zone. We argue that both assumptions should be revised and that the length of open-water season is consequently not appropriate to describe light seasonality in Arctic sea ice zone. We show a strong link between solar irradiance cycle and sea ice seasonality. Sea ice needs sunlight to melt, and ice retreat is found to always fall after polar night ending, so that the early ice-free period is always sunlit. By contrast, the ice advance date may fall several weeks after polar night onset in some regions, so that the late ice-free period is not always sunlit. This

overlap between sea ice-free season and polar night is expected to be widespread in the future due to the larger offset in sea ice advance than in sea ice retreat (Lebrun et al., 2019). We also suggest that the region where light is sufficient for photosynthesis does not restrict to the open-water zone, due to the presence of leads and non-opaque ice.

We then discuss a new diagnostic, photoperiod, more suitable to describe the light seasonality in Arctic sea ice zone. We define photoperiod as the period during which available light at the ocean surface is assumed to be sufficient for phytoplankton growth. It seems to better embrace light seasonality than the open-water season because it considers the effects on light of both sea ice and sunlight seasonalities.

However, large uncertainties remain in the photoperiod definition, mostly due to ambiguities on radiative transfer in sea ice and on phytoplankton physiology. These uncertainties stain model projections as well. A priori, photoperiod should increase in the future, due to sea ice retreat. But the impact of sea ice retreat on photoperiod is unclear. It strongly depends on the PAR^{tr} threshold, somehow uncertain as well (Fig. 8). Whereas photoperiod would increase by about one to four months during 1900 to 2200 considering the higher threshold, it would remain unchanged for the lowest threshold, even in the Central Arctic. Light transmission through sea ice is another source of uncertainty since it reduces the impact of the ice on the photoperiod. A less opaque sea ice limits the possible future increase in photoperiod, regardless of the PAR^{tr} threshold.

Finally, we confirm the intuition that purely light-based diagnostics are insufficient to fully characterise phytoplankton dynamics in the Arctic sea ice zone. Large uncertainties remain in model assumptions about the link between phytoplankton growth and photoperiod : (i) uncertainties about the role of nutrient limitation in the Arctic sea ice zone (Vancoppenolle et al., 2013); (ii) uncertainties about the response of phytoplankton to light in ice-covered water and (iii) uncertainties about the strength of mixing of phytoplankton in the sea ice-covered

water.

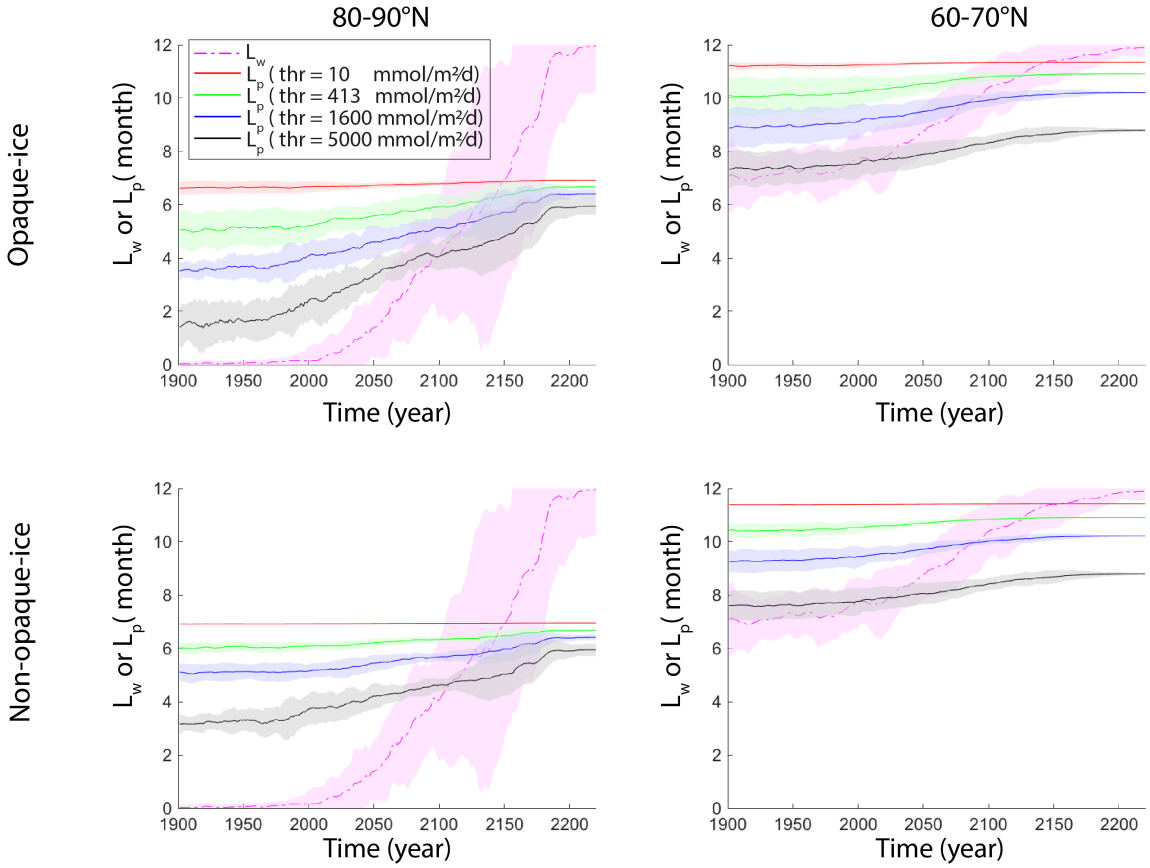

Figure 8: Time series of CMIP5 (median ± inter quartile range of the 9 models) photoperiod (solid lines) for the four PAR thresholds and open-water season (dashed pink line) for 60-70°N (right) and 80-90°N (left) latitudinal band considering opaque (top) and non-opaque ice (bottom).

It is necessary to reduce all uncertainties on photoperiod before it can be reliably used as a proxy for light limitation for phytoplankton.

Some studies already try to better understand the response of phytoplankton to light in the Arctic, based on in situ observations (Hill et al., 2018; Lewis et al., 2019) and laboratory experiments (Huot et al., 2013; Lewis et al., 2019; Ferland et al., 2017). Due to the lack of pan-Arctic observations, these studies are focused on a few regions but they highlight that the response of phytoplankton to light is very variable in space and time due to phytoplankton adaptation to environmental conditions. This leads to large uncertainties in a PAR^{tr} threshold definition in the entire Arctic region. Future studies should reduce the photoperiod uncertainties and may help us to better understand the impact of sea ice melt on phytoplankton growth.

Finally, several studies highlight the importance to analyse both light and nutrients to better understand phytoplankton growth in the Arctic. While light is expected to impact the initiation of phytoplankton bloom (Arrigo et al., 2017; Hill et al., 2005; Lowry et al., 2018; Tremblay & Gagnon, 2009), the intensity and the end of the bloom are mostly controlled by nutrient supply (Lowry et al., 2015; Tremblay & Gagnon, 2009). Focus only on light availability to study phytoplankton is not sufficient since we conceal half of the drivers of phytoplankton bloom.

References

Arrigo, K. R., & van Dijken, G. L. (2011). Secular trends in Arctic Ocean net primary production. *Journal of Geophysical Research: Oceans*, *116*(C9), C09011. https://doi.org/10.1029/2011JC007151

Arrigo, K. R., Perovich, D. K., Pickart, R. S., Brown, Z. W., Dijken, G. L. van, Lowry, K. E., et al. (2012). Massive Phytoplankton Blooms Under Arctic Sea Ice. *Science*, *336*(6087), 1408–1408. https://doi.org/10.1126/science.1215065

Arrigo, K. R., Perovich, D. K., Pickart, R. S., Brown, Z. W., van Dijken, G. L., Lowry, K. E., et al. (2014). Phytoplankton blooms beneath the sea ice in the Chukchi sea. *Deep Sea Research Part II: Topical Studies in Oceanography*, *105*, 1–16. https://doi.org/10.1016/j.dsr2.2014.03.018

Arrigo, K. R., Mills, M. M., van Dijken, G. L., Lowry, K. E., Pickart, R. S., & Schlitzer, R. (2017). Late Spring Nitrate Distributions Beneath the Ice-Covered Northeastern Chukchi Shelf. *Journal of Geophysical Research: Biogeosciences*, 2017JG003881. https://doi.org/10.1002/2017JG003881

Årthun, M., Eldevik, T., Smedsrud, L. H., Skagseth, Ø., & Ingvaldsen, R. B. (2012). Quantifying the Influence of Atlantic Heat on Barents Sea Ice Variability and Retreat. *Journal of Climate*, *25*(13), 4736–4743. https://doi.org/10.1175/JCLI-D-11-00466.1

Assmy, P., Fernández-Méndez, M., Duarte, P., Meyer, A., Randelhoff, A., Mundy, C. J., et al. (2017). Leads in Arctic pack ice enable early phytoplankton blooms below snow-covered sea ice. *Scientific Reports*, *7*, srep40850. https://doi.org/10.1038/srep40850

Aumont, O., Ethé, C., Tagliabue, A., Bopp, L., & Gehlen, M. (2015). PISCES-v2: an ocean biogeochemical model for carbon and ecosystem studies. *Geoscientific Model Development*, *8*(8), 2465–2513. https://doi.org/10.5194/gmd-8-2465-2015

Cavalieri, D. J., & Parkinson, C. L. (2012). Arctic sea ice variability and trends, 1979–2010. *The Cryosphere*, *6*(4), 881–889. https://doi.org/10.5194/tc-6-881-2012

Comiso, Josephino `Joey`. (2000). Bootstrap Sea Ice Concentrations from Nimbus-7 SMMR and DMSP SSM/I-SSMIS, Version 2. NASA National Snow and Ice Data Center Distributed Active Archive Center. https://doi.org/10.5067/J6JQLS9EJ5HU

Dai, A., & Trenberth, K. E. (2002). Estimates of Freshwater Discharge from Continents: Latitudinal and Seasonal Variations. *Journal of Hydrometeorology*, *3*(6), 660–687. https://doi.org/10.1175/1525-7541(2002)003<0660:EOFDFC>2.0.CO;2

Dai, A., Qian, T., Trenberth, K. E., & Milliman, J. D. (2009). Changes in Continental Freshwater Discharge from 1948 to 2004. *Journal of Climate*, *22*(10), 2773–2792. https://doi.org/10.1175/2008JCLI2592.1

Danabasoglu, G., Yeager, S. G., Bailey, D., Behrens, E., Bentsen, M., Bi, D., et al. (2014). North Atlantic simulations in Coordinated Ocean-ice Reference Experiments phase II (CORE-II). Part I: Mean states. *Ocean Modelling*, *73*, 76–107. https://doi.org/10.1016/j.ocemod.2013.10.005

English, T. S. (1961). *Some biological oceanographic observations in the central North Polar Sea Drift Station Alpha, 1957-1958 /*. Washington : Retrieved from http://hdl.handle.net/2027/uc1.31822026346429

Frey, K. E., Perovich, D. K., & Light, B. (2011). The spatial distribution of solar radiation under a melting Arctic sea ice cover. *Geophysical Research Letters*, *38*(22). https://doi.org/10.1029/2011GL049421

Ferland, J., Bruyant, F., Larivière, J., Forget, M.-H., Massicotte, P., & Babin, M. (2017). *Seasonal light acclimation capacity (Ek) of phytoplankton community under landfast ice*. Poster session presented at the Green Edge Meeting 2017, Quebec city, Quebec.

Grenfell, T. C., & Maykut, G. A. (1977). The Optical Properties of Ice and Snow in the Arctic Basin *. *Journal of Glaciology*, *18*(80), 445–463. https://doi.org/10.3189/S0022143000021122

Griffies, S. M., Biastoch, A., Böning, C., Bryan, F., Danabasoglu, G., Chassignet, E. P., et al. (2009). Coordinated Ocean-ice Reference Experiments (COREs). *Ocean Modelling*, *26*(1), 1–46. https://doi.org/10.1016/j.ocemod.2008.08.007

Hezel, P. J., Fichefet, T., & Massonnet, F. (2014). Modeled Arctic sea ice evolution through 2300 in CMIP5 extended RCPs. *The Cryosphere*, *8*(4), 1195–1204. https://doi.org/10.5194/tc-8-1195-2014

Hill, V., Cota, G., & Stockwell, D. (2005). Spring and summer phytoplankton communities in the Chukchi and Eastern Beaufort Seas. *Deep Sea Research Part II: Topical Studies in Oceanography*, *52*(24), 3369–3385. https://doi.org/10.1016/j.dsr2.2005.10.010

Hill, V. J., Matrai, P. A., Olson, E., Suttles, S., Steele, M., Codispoti, L. A., & Zimmerman, R. C. (2013). Synthesis of integrated primary production in the Arctic Ocean: II. In situ and remotely sensed estimates. *Progress in Oceanography*, *110*, 107–125. https://doi.org/10.1016/j.pocean.2012.11.005

Hill, V. J., Light, B., Steele, M., & Zimmerman, R. C. (2018). Light Availability and Phytoplankton Growth Beneath Arctic Sea Ice: Integrating Observations and Modeling. *Journal of Geophysical Research: Oceans*, *123*(5), 3651–3667. https://doi.org/10.1029/2017JC013617

Horvat, C., Jones, D. R., Iams, S., Schroeder, D., Flocco, D., & Feltham, D. (2017). The frequency and extent of sub-ice phytoplankton blooms in the Arctic Ocean. *Science Advances*, *3*(3), e1601191. https://doi.org/10.1126/sciadv.1601191

Huot, Y., Babin, M., & Bruyant, F. (2013). Photosynthetic parameters in the Beaufort Sea in relation to the phytoplankton community structure. *Biogeosciences*, *10*(5), 3445–3454. https://doi.org/10.5194/bg-10-3445-2013

Ivanov, V. V., Alexeev, V. A., Repina, I., Koldunov, N. V., & Smirnov, A. (2012). Tracing Atlantic Water Signature in the Arctic Sea Ice Cover East of Svalbard [Research article]. https://doi.org/10.1155/2012/201818

Kwok, R., & Rothrock, D. A. (2009). Decline in Arctic sea ice thickness from submarine and ICESat records: 1958–2008. *Geophysical Research Letters*, *36*(15), L15501. https://doi.org/10.1029/2009GL039035

Large, W. G., & Yeager, S. G. (2009). The global climatology of an interannually varying air–sea flux data set. *Climate Dynamics*, *33*(2), 341–364. https://doi.org/10.1007/s00382-008-0441-3

Lebrun, M., Vancoppenolle, M., Madec, G., & Massonnet, F. (2019). Arctic sea-ice-free season projected to extend into autumn. *The Cryosphere*, *13*(1), 79–96. https://doi.org/10.5194/tc-13-79-2019

Letelier, R. M., Karl, D. M., Abbott, M. R., & Bidigare, R. R. (2004). Light driven seasonal patterns of chlorophyll and nitrate in the lower euphotic zone of the North Pacific Subtropical Gyre. *Limnology and Oceanography*, *49*(2), 508–519. https://doi.org/10.4319/lo.2004.49.2.0508

Lewis, K. M., Arntsen, A. E., Coupel, P., Joy-Warren, H., Lowry, K. E., Matsuoka, A., et al. (2019). Photoacclimation of Arctic Ocean phytoplankton to shifting light and nutrient limitation. *Limnology and Oceanography*, *64*(1), 284–301. https://doi.org/10.1002/lno.11039

Lindsay, R., & Schweiger, A. (2015). Arctic sea ice thickness loss determined using subsurface, aircraft, and satellite observations. *The Cryosphere*, *9*(1), 269–283. https://doi.org/10.5194/tc-9-269-2015

Long, M. C., Lindsay, K., & Holland, M. M. (2015). Modeling photosynthesis in sea ice-

covered waters. *Journal of Advances in Modeling Earth Systems*, *7*(3), 1189–1206. https://doi.org/10.1002/2015MS000436

Lowry, K. E., Pickart, R. S., Mills, M. M., Brown, Z. W., van Dijken, G. L., Bates, N. R., & Arrigo, K. R. (2015). The influence of winter water on phytoplankton blooms in the Chukchi Sea. Retrieved from https://darchive.mblwhoilibrary.org/handle/1912/7572

Lowry, K. E., Pickart, R. S., Selz, V., Mills, M. M., Pacini, A., Lewis, K. M., et al. (2018). Under-Ice Phytoplankton Blooms Inhibited by Spring Convective Mixing in Refreezing Leads. *Journal of Geophysical Research: Oceans*, n/a-n/a. https://doi.org/10.1002/2016JC012575

Maslanik, J., Stroeve, J., Fowler, C., & Emery, W. (2011). Distribution and trends in Arctic sea ice age through spring 2011. *Geophysical Research Letters*, *38*(13), L13502. https://doi.org/10.1029/2011GL047735

Massonnet, F., Fichefet, T., Goosse, H., Bitz, C. M., Philippon-Berthier, G., Holland, M. M., & Barriat, P.-Y. (2012). Constraining projections of summer Arctic sea ice. *The Cryosphere*, *6*(6), 1383–1394. https://doi.org/10.5194/tc-6-1383-2012

Maykut, G. A., & Untersteiner, N. (1971). Some results from a time-dependent thermodynamic model of sea ice. *Journal of Geophysical Research*, *76*(6), 1550–1575. https://doi.org/10.1029/JC076i006p01550

Mundy, C. J., Ehn, J. K., Barber, D. G., & Michel, C. (2007). Influence of snow cover and algae on the spectral dependence of transmitted irradiance through Arctic landfast first-year sea ice. *Journal of Geophysical Research: Oceans*, *112*(C3), C03007. https://doi.org/10.1029/2006JC003683

Mundy, C. J., Gosselin, M., Ehn, J., Gratton, Y., Rossnagel, A., Barber, D. G., et al. (2009). Contribution of under-ice primary production to an ice-edge upwelling phytoplankton bloom in the Canadian Beaufort Sea. *Geophysical Research Letters*, *36*(17). https://doi.org/10.1029/2009GL038837

Mundy, C. J., Gosselin, M., Gratton, Y., Brown, K., Galindo, V., Campbell, K., et al. (2014). Role of environmental factors on phytoplankton bloom initiation under landfast sea ice in Resolute Passage, Canada. *Marine Ecology Progress Series*, *497*, 39–49. https://doi.org/10.3354/meps10587

Palmer, M. A., Saenz, B. T., & Arrigo, K. R. (2014). Impacts of sea ice retreat, thinning, and melt-pond proliferation on the summer phytoplankton bloom in the Chukchi Sea, Arctic Ocean. *Deep Sea Research Part II: Topical Studies in Oceanography*, *105*, 85–104. https://doi.org/10.1016/j.dsr2.2014.03.016

Parkinson, C. L. (1994). Spatial patterns in the length of the sea ice season in the Southern Ocean, 1979–1986. *Journal of Geophysical Research: Oceans*, *99*(C8), 16327–16339. https://doi.org/10.1029/94JC01146

Parkinson, C. L. (2014). Spatially mapped reductions in the length of the Arctic sea ice season. *Geophysical Research Letters*, *41*(12), 4316–4322. https://doi.org/10.1002/2014GL060434

Perovich, D. K. (1996). *The Optical Properties of Sea Ice.* (No. MONO-96-1). COLD REGIONS RESEARCH AND ENGINEERING LAB HANOVER NH. Retrieved from https://apps.dtic.mil/docs/citations/ADA310586

Polyakov, I. V., Pnyushkov, A. V., Alkire, M. B., Ashik, I. M., Baumann, T. M., Carmack, E. C., et al. (2017). Greater role for Atlantic inflows on sea-ice loss in the Eurasian Basin of the Arctic Ocean. *Science (New York, N.Y.)*, *356*(6335), 285–291. https://doi.org/10.1126/science.aai8204

Popova, E. E., Yool, A., Coward, A. C., Dupont, F., Deal, C., Elliott, S., et al. (2012). What controls primary production in the Arctic Ocean? Results from an intercomparison of five general circulation models with biogeochemistry. *Journal of Geophysical*

Research: Oceans, *117*(C8), C00D12. https://doi.org/10.1029/2011JC007112
Renner, A. H. H., Gerland, S., Haas, C., Spreen, G., Beckers, J. F., Hansen, E., et al. (2014). Evidence of Arctic sea ice thinning from direct observations. *Geophysical Research Letters*, *41*(14), 5029–5036. https://doi.org/10.1002/2014GL060369
Rousset, C., Vancoppenolle, M., Madec, G., Fichefet, T., Flavoni, S., Barthélemy, A., et al. (2015). The Louvain-La-Neuve sea ice model LIM3.6: global and regional capabilities. *Geosci. Model Dev.*, *8*(10), 2991–3005. https://doi.org/10.5194/gmd-8-2991-2015
Rysgaard, S., Nielsen, T. G., & Hansen, B. W. (1999). Seasonal variation in nutrients, pelagic primary production and grazing in a high-Arctic coastal marine ecosystem, Young Sound, Northeast Greenland. *Marine Ecology Progress Series*, *179*, 13–25. https://doi.org/10.3354/meps179013
Sandø, A. B., Nilsen, J. E. Ø., Gao, Y., & Lohmann, K. (2010). Importance of heat transport and local air-sea heat fluxes for Barents Sea climate variability. *Journal of Geophysical Research: Oceans*, *115*(C7). https://doi.org/10.1029/2009JC005884
Shine, K. P. (1984). Parametrization of the shortwave flux over high albedo surfaces as a function of cloud thickness and surface albedo. *Quarterly Journal of the Royal Meteorological Society*, *110*(465), 747–764. https://doi.org/10.1002/qj.49711046511
Shine, K. P., & Henderson-Sellers, A. (1985). The sensitivity of a thermodynamic sea ice model to changes in surface albedo parameterization. *Journal of Geophysical Research: Atmospheres*, *90*(D1), 2243–2250. https://doi.org/10.1029/JD090iD01p02243
Stammerjohn, S., Massom, R., Rind, D., & Martinson, D. (2012). Regions of rapid sea ice change: An inter-hemispheric seasonal comparison. *Geophysical Research Letters*, *39*(6), L06501. https://doi.org/10.1029/2012GL050874
Stroeve, J. C., Kattsov, V., Barrett, A., Serreze, M., Pavlova, T., Holland, M., & Meier, W. N. (2012). Trends in Arctic sea ice extent from CMIP5, CMIP3 and observations. *Geophysical Research Letters*, *39*(16), L16502. https://doi.org/10.1029/2012GL052676
Stroeve, J. C., Crawford, A. D., & Stammerjohn, S. (2016). Using timing of ice retreat to predict timing of fall freeze-up in the Arctic. *Geophysical Research Letters*, *43*(12), 2016GL069314. https://doi.org/10.1002/2016GL069314
Tremblay, J.-É., & Gagnon, J. (2009). The effects of irradiance and nutrient supply on the productivity of Arctic waters: a perspective on climate change. In *Influence of Climate Change on the Changing Arctic and Sub-Arctic Conditions* (pp. 73–93). Springer, Dordrecht. https://doi.org/10.1007/978-1-4020-9460-6_7
Tremblay, J.-É., Michel, C., Hobson, K. A., Gosselin, M., & Price, N. M. (2006). Bloom dynamics in early opening waters of the Arctic Ocean. *Limnology and Oceanography*, *51*(2), 900–912. https://doi.org/10.4319/lo.2006.51.2.0900
Vancoppenolle, M., Bopp, L., Madec, G., Dunne, J., Ilyina, T., Halloran, P. R., & Steiner, N. (2013). Future Arctic Ocean primary productivity from CMIP5 simulations: Uncertain outcome, but consistent mechanisms. *Global Biogeochemical Cycles*, *27*(3), 605–619. https://doi.org/10.1002/gbc.20055
Wassmann, P., & Reigstad, M. (2011). Future Arctic Ocean Seasonal Ice Zones and Implications for Pelagic-Benthic Coupling. *Oceanography*, *24*(3), 220–231. https://doi.org/10.5670/oceanog.2011.74

Conclusions et Perspectives

1. Conclusions

Les modèles du système Terre sont mal contraints concernant la réponse du phytoplancton arctique au changement climatique (Vancoppenolle et al., 2013). Ceci est dû aux nombreuses lacunes dans nos connaissances sur les mécanismes gouvernant la croissance du phytoplancton dans les régions englacées arctiques. L'une des incertitudes majeures est liée à la réponse du phytoplancton au retrait de la banquise arctique et au rôle de la lumière dans l'évolution du phytoplancton dans ces régions englacées. L'objectif de cette thèse est d'étudier certaines des interactions entre banquise, lumière et phytoplancton arctiques dans le but de mieux contraindre les modèles du système Terre. Cette étude s'appuie sur trois axes principaux posant trois problématiques majeures :

- Peut-on projeter de façon cohérente les potentiels changements dans la saisonnalité de la banquise arctique et avancer de solides mécanismes d'évolution ?
- Est-ce que le transfert radiatif dans la zone de glace est représenté de façon réaliste dans les modèles du Système Terre ? Doit-on en améliorer la représentation ?
- Suite aux conclusions obtenues aux deux précédentes problématiques, est-il possible de mieux caractériser la saisonnalité de la lumière disponible pour le phytoplancton dans les régions englacées arctiques et de comprendre comment cette saisonnalité affecte le phytoplancton ?

1.1 Évolution de la saisonnalité de la banquise arctique

Concernant la saisonnalité de la banquise, il y avait jusqu'alors peu d'études concernant l'évolution future des diagnostics de saisonnalité de la banquise et que peu d'information quant aux mécanismes associés à cette évolution. Dans le premier chapitre de cette thèse, j'étudie l'évolution présente et future de la période d'eau libre arctique ainsi que les relations entre jours de retrait et jour d'avancée de la banquise. Si l'évolution présente de la période d'eau libre est dominée par des tendances similaires entre date de retrait et date d'avancée de la banquise, cette configuration va changer dans les décennies à venir, d'après les projections climatiques. Tous les modèles de CMIP5 utilisés dans cette analyse projettent une tendance de la date d'avancée de la banquise qui devrait excéder, voir même doubler la tendance dans le jour de retrait, décalant la période d'eau libre vers l'automne. Les mécanismes à l'origine de cette asymétrie entre évolution du retrait et de l'avancée de la banquise sont purement thermodynamiques. Deux rétroactions positives sont à l'origine de cette asymétrie. La rétroaction d'été est la plus forte. Elle s'explique par le fait que le rayonnement solaire pénètre l'océan plus rapidement que le rayonnement non solaire ne le quitte. Lors d'un décalage dans la date de retrait en réponse au forçage radiatif, de l'énergie va être stockée dans l'océan et va décaler la date d'avancée (Perovich et al., 2007). Cette énergie mettant plus de temps à s'évacuer qu'à pénétrer dans l'océan, la date d'avancée va être d'autant plus décalée. La rétroaction d'hiver plus faible, quant à elle, est due à la période de croissance de la banquise relativement plus longue que la période de fonte et à la rétroaction croissance-épaisseur. Ce mécanisme d'amplification mis en place par ces deux rétroactions n'est, néanmoins pas retrouvé dans les évolutions présentes et interannuelles de la période d'eau libre. Ceci est attribué à la forte variabilité interannuelle ainsi qu'à d'autres processus qui tempèrent la réponse thermodynamique de la banquise au réchauffement climatique.

1.2 Transfert radiatif dans les zones de banquise arctique

Le second chapitre vise à évaluer le schéma de transfert radiatif dans la zone de glace arctique dans le modèle d'océan de l'IPSL, NEMO, à partir d'analyse de données in situ. En raison du manque d'observations, le schéma de transfert radiatif dans NEMO est basé sur de nombreuses hypothèses simplificatrices et présente par conséquent de larges incertitudes. Les récentes campagnes de mesures optiques dans la zone de glace arctique, réalisées ces dernières années, ont permis de proposer des améliorations dans le schéma de transfert radiatif. Deux spécificités du modèle NEMO sont évaluées dans ce chapitre : (i) les valeurs des paramètres utilisés dans le calcul de la transmittance au travers des différents types de glace (banquise nue, enneigée et couverte de mares de fonte) ; (ii) le fractionnement en bandes spectrales (trois dans le visible, une dans le non visible) du rayonnement transmis à l'océan pour décrire la quantité de rayonnement pénétrant en profondeur dans l'océan. Cette étude a montré que l'hypothèse formulée dans le modèle NEMO selon laquelle la transmittance est nulle dans la neige est fausse. En effet, une certaine quantité de rayonnement est transmise même au travers de la banquise couverte de neige dans les données in situ. Un ajustement des paramètres dans la glace nue est aussi proposé pour réduire l'écart entre les valeurs de transmittance simulées et observées. De plus, les résultats présentés dans cette étude ont mis en lumière l'importance de considérer les mares de fonte dans le calcul de rayonnement transmis au travers de la banquise. Concernant le fractionnement en bande de longueurs d'onde, l'étude a démontré que la banquise influence grandement le spectre du rayonnement incident avant de le transmettre à l'océan. Ainsi, utiliser les mêmes fractions de bandes spectrales pour la lumière transmise dans un océan couvert de glace que pour un océan libre de glace contribue à grandement sous-estimer le rayonnement dans les zones de banquise.

L'ensemble des améliorations suggérées lors de ce chapitre devrait contribuer à sensiblement augmenter le rayonnement simulé transmis en profondeur dans les zones englacées et pourrait notamment influencer la croissance du phytoplancton.

1.3 Cycle saisonnier de la lumière dans la zone de banquise arctique

L'étude présentée en troisième chapitre reprend les conclusions des chapitres précédents pour définir un meilleur diagnostic pour décrire le cycle saisonnier de la lumière disponible pour le phytoplancton à la surface de l'océan. Aujourd'hui, l'approche usuelle est de décrire le cycle saisonnier de la lumière transmise à l'océan, dans les régions englacées à partir de la période d'eau libre. J'ai néanmoins montré, dans les précédents chapitres, que cycle saisonnier de la lumière et période d'eau libre pouvaient être fortement décorrélés. Il a alors été défini dans le dernier chapitre un nouveau diagnostic, la photopériode, prenant en compte ces grandes conclusions et décrivant mieux le cycle du rayonnement transmis à l'océan dans les régions englacées. Toutefois, de larges incertitudes sur la photopériode gouvernées notamment par la réponse du phytoplancton à la lumière persistent. L'utilisation de la photopériode comme diagnostic de la limitation en lumière pour le phytoplancton n'est, par conséquent, pas encore possible tant que ces incertitudes perdurent. Une étude préliminaire de la réponse du phytoplancton à la lumière dans le modèle d'océan NEMO a notamment montré que le phytoplancton était par construction lié à la période d'eau libre du fait de nombreuses hypothèses du modèle, notamment la photosynthèse nulle sous la banquise et un mélange horizontal beaucoup plus rapide que la photosynthèse.

A partir des conclusions majeures de cette thèse, la figure 1 propose un bilan des divers acteurs gouvernant les liens entre banquise, lumière et phytoplancton arctiques ainsi que leur possible évolution future. La période d'eau libre est majoritairement contrôlée par le cycle solaire, par

les échanges thermodynamiques entre océan et atmosphère durant l'été, ainsi que par l'épaisseur de la glace, qui contrôlent sa date de retrait. L'évolution de la période d'eau libre est majoritairement gouvernée par la date d'avancée plus tardive de la banquise. La période d'eau libre est projetée à augmenter et à se décaler vers l'automne, ayant lieu en partie pendant la nuit polaire à l'avenir. Parallèlement, la photopériode est aujourd'hui supérieure à la période d'eau libre en raison notamment de la transmission du rayonnement solaire au travers de la banquise. La photopériode est projetée à augmenter en raison de (i) l'augmentation de la période d'eau libre ; (ii) l'amincissement de la banquise. Toutefois, cette augmentation va être limitée par la nuit polaire. Ces deux évolutions parallèles de la période d'eau libre et de la photopériode ont toutes deux un impact sur l'évolution du phytoplancton arctique. Mais la non-linéarité entre croissance du phytoplancton et disponibilité en lumière rend la quantification de ces impacts complexe.

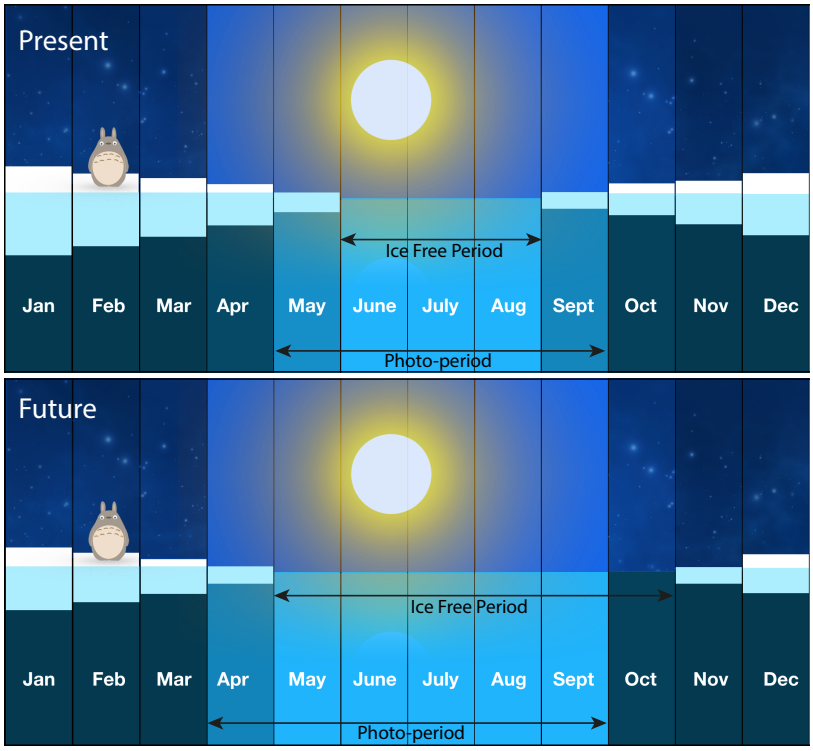

Figure 1. Schéma résumant les trois résultats majeurs de la thèse et suggérant une évolution future à la période d'eau libre et à la photopériode.

2. Perspectives

Les nombreuses limitations et questions non résolues abordées lors de cette thèse offrent de nombreuses pistes à des travaux futurs.

Dans un premier temps, j'ai pour projet de poursuivre l'amélioration du schéma de transfert radiatif dans le modèle glace-océan, NEMO-LIM. L'étude actuelle s'appuie sur l'analyse de trois récentes campagnes de mesure majoritairement focalisées sur la banquise côtière. L'analyse de certaines données issues de campagnes de mesures réalisées dans de la banquise dérivante tel que la dérive de Tara en 2007 (Nicolaus et al., 2010), ainsi que, plus récemment, la dérive du Polarstern entre 2012 et 2017 (Castellani et al., 2019; Katlein et al., 2019) permettrait de lever le voile sur un certain nombre d'incertitudes.

Toujours dans l'idée d'améliorer le schéma de transfert radiatif dans la banquise dans le modèle, j'ai aussi pour ambition d'évaluer l'approximation de delta Eddington parallèlement à la loi de Beer Lambert en m'appuyant sur le code issu des travaux réalisé par Briegleb et Light (2007) et utilisé dans le modèle américain, CICE (Hunke et al., 2019).

Une autre de mes priorités à l'issue de cette thèse sera d'étudier les impacts des changements apportés par une amélioration de la représentation du transfert radiatif dans la banquise, sur :

(i) Les simulations forcées. Ceci me permettrait d'analyser la réponse du phytoplancton simulé aux changements de rayonnement transmis dans la zone de banquise arctique.

(ii) Les simulations couplées. Je m'attends à ce que l'augmentation du rayonnement transmis au travers de la neige et la banquise impacte la thermodynamique de la banquise et de l'océan et influence les processus de fonte et de formation de la banquise. De plus, le phytoplancton, influencé par l'apport de lumière disponible dans la zone de glace pourrait modifier l'intensité de la rétroaction bio-optique

entre fonte de glace, croissance du plancton et absorption de rayonnement solaire dans l'océan superficiel (Lengaigne et al., 2007).

(iii) D'autres modifications en plus de celles apportées au schéma de transfert radiatif pourraient approfondir cette analyse. J'envisage notamment d'étudier l'impact d'une discrétisation sous maille de l'épaisseur de banquise (Long et al., 2015) ainsi que de la fraction de neige (Abraham et al., 2015) sur le phytoplancton simulé.

Enfin, à plus long terme, d'autres études retiennent mon attention. Si le mécanisme thermodynamique d'amplification dans le décalage du jour d'avancée de la banquise, discuté en chapitre 1 semble robuste par sa simplicité et par le fait qu'il fait consensus auprès des modèles de CMIP5, il n'a pas pu être clairement démontré, faute d'avoir les diagnostics appropriés. Les nouvelles simulations de CMIP6 permettent maintenant l'accès à ces diagnostics (Notz et al., 2016), notament les champs diurnes et pourrait éventuellement permettre de démontrer les hypothèses formulées dans le premier chapitre de cette thèse.

L'ensemble de cette thèse se focalise sur les régions englacées arctiques. La banquise australe (Antarctique) se différencie de la banquise boréale (Arctique) dans de nombreux aspects. Ces différences devraient jouer un rôle fondamental notamment sur les processus de fonte et de formation de la banquise et sur son cycle saisonnier, mais aussi sur la microstructure et par conséquent l'optique de la banquise antarctique et finalement sur les relations entre banquise, lumière et phytoplancton en Antarctique. Il serait donc intéressant de réaliser les mêmes analyses, mais pour l'Antarctique.

Enfin, la lumière n'est pas le seul paramètre à influencer la croissance du phytoplancton. En se focalisant essentiellement sur les interactions entre banquise, lumière et phytoplancton, une partie des processus liés à la banquise et qui influencent la croissance du phytoplancton est oubliée. Les nutriments jouent un rôle fondamental dans la limitation du phytoplancton en

Arctique (Tremblay & Gagnon, 2009) et mieux comprendre le bilan des nutriments dans les régions englacées arctiques (et antarctiques) est fondamental pour mieux contraindre les modèles du système Terre concernant la réponse du phytoplancton au changement climatique dans les régions englacées.

Références

Abraham, C., Steiner, N., Monahan, A., & Michel, C. (2015). Effects of subgrid-scale snow thickness variability on radiative transfer in sea ice. *Journal of Geophysical Research: Oceans*, 5597–5614. https://doi.org/10.1002/2015JC010741@10.1002/(ISSN)2169-9291.FAMOS1

Briegleb, P., & Light, B. (2007). A Delta-Eddington Mutiple Scattering Parameterization for Solar Radiation in the Sea Ice Component of the Community Climate System Model. https://doi.org/10.5065/D6B27S71

Castellani, G., Flores, H., Lange, B. A., Schaafsma, F. L., Ehrlich, J., David, C., et al. (2019). Sea ice draft, under-ice irradiance and radiance, and surface water temperature, salinity and chlorophyl a from Surface and Under Ice Trawl (SUIT) measurements in 2012-2017 [Data set]. *Alfred Wegener Institute, Helmholtz Centre for Polar and Marine Research, Bremerhaven*. Retrieved from https://doi.pangaea.de/10.1594/PANGAEA.902056

Hunke, E. C., Lipscomb, W. H., & Turner, A. K. (2010). Sea-ice models for climate study: retrospective and new directions. *Journal of Glaciology*, *56*, 1162–1172. https://doi.org/10.3189/002214311796406095

Katlein, C., Arndt, S., Belter, H. J., Castellani, G., & Nicolaus, M. (2019). Seasonal Evolution of Light Transmission Distributions Through Arctic Sea Ice. *Journal of Geophysical Research: Oceans*, *0*(0). https://doi.org/10.1029/2018JC014833

Lengaigne, M., Menkes, C., Aumont, O., Gorgues, T., Bopp, L., André, J.-M., & Madec, G. (2007). Influence of the oceanic biology on the tropical Pacific climate in a coupled general circulation model. *Climate Dynamics*, *28*, 503–516. https://doi.org/10.1007/s00382-006-0200-2

Long, M. C., Lindsay, K., & Holland, M. M. (2015). Modeling photosynthesis in sea ice-covered waters. *Journal of Advances in Modeling Earth Systems*, *7*(3), 1189–1206. https://doi.org/10.1002/2015MS000436

Nicolaus, M., Gerland, S., Hudson, S. R., Hanson, S., Haapala, J., & Perovich, D. K. (2010). Seasonality of spectral albedo and transmittance as observed in the Arctic Transpolar Drift in 2007. *Journal of Geophysical Research: Oceans*, *115*(C11), C11011. https://doi.org/10.1029/2009JC006074

Notz, D., Jahn, A., Holland, M., Hunke, E., Massonnet, F., Stroeve, J., et al. (2016). The CMIP6 Sea-Ice Model Intercomparison Project (SIMIP): understanding sea ice through climate-model simulations. *Geosci. Model Dev.*, *9*(9), 3427–3446. https://doi.org/10.5194/gmd-9-3427-2016

Perovich, D. K., Light, B., Eicken, H., Jones, K. F., Runciman, K., & Nghiem, S. V. (2007). Increasing solar heating of the Arctic Ocean and adjacent seas, 1979–2005: Attribution and role in the ice-albedo feedback. *Geophysical Research Letters*, *34*(19), L19505. https://doi.org/10.1029/2007GL031480

Tremblay, J.-É., & Gagnon, J. (2009). The effects of irradiance and nutrient supply on the productivity of Arctic waters: a perspective on climate change. In *Influence of Climate Change on the Changing Arctic and Sub-Arctic Conditions* (pp. 73–93). Springer, Dordrecht. https://doi.org/10.1007/978-1-4020-9460-6_7

Vancoppenolle, M., Bopp, L., Madec, G., Dunne, J., Ilyina, T., Halloran, P. R., & Steiner, N. (2013). Future Arctic Ocean primary productivity from CMIP5 simulations: Uncertain outcome, but consistent mechanisms. *Global Biogeochemical Cycles*, *27*(3), 605–619. https://doi.org/10.1002/gbc.20055

ANNEXES

Annexes I :

Supplement of The Cryosphere, 13, 79–96, 2019
https://doi.org/10.5194/tc-13-79-2019-supplement

The Cryosphere Open Access EGU

Supplement of

Arctic sea-ice-free season projected to extend into autumn

Marion Lebrun et al.

Correspondence to: Marion Lebrun (marion.lebrun@locean-ipsl.upmc.fr)

Supplementary Material

Table S1. Impact of statistical parameters on observation-based trends and seasonality diagnostics. The table gives satellite-derived sea ice seasonality statistics (1980-2015): trends in ice retreat date (r_r), ice advance date (r_a) and length of the ice-free season (r_l), as well as long-term ($R^{long}_{a/r}$) and short-term ($R^{short}_{a/r}$) ice advance offset ratios, given for varying computational parameters. Trends and ratios are given as median ± interquartile range, taken over a specified ensemble of satellite pixels, verifying two conditions: (i) N_{ij}, the number of years for which the retreat and advance dates are both defined, is larger than N_{min}; (ii) the trends in retreat and advance dates both characterised by a p-value $p_{ij} < p_{max}$. When $p_{max}=1$, there is no selection of pixels based on the significance of the trends. T_{smooth} corresponds to the smoothing period applied to raw ice concentration time series.

N_{min}	p_{max}	T_{smooth} (days)	r_r (days/decade)	r_a (days/decade)	r_l (days/decade)	$R^{long}_{a/r}$	$R^{short}_{a/r}$	N (% of SIZ)
4	**1**	**15**	-4.6 ± 8.6	4.8 ± 6.7	9.4 ± 13.3	0.65 ± 1.38	0.21 ± 0.31	23475 (100%)
12	**1**	**15**	-4.8 ± 7.7	4.9 ± 5.8	9.8 ± 12.1	0.71 ± 1.14	0.21 ± 0.27	19500 (83%)
30	**1**	**15**	-5.4 ± 6.4	4.6 ± 4.3	10.3 ± 9.9	0.77 ± 0.83	0.21 ± 0.23	10047 (43%)
12	**0.25**	**15**	-7.6 ± 6.5	6.1 ± 5.3	13.8 ± 1.1	0.78 ± 0.60	0.23 ± 0.23	9493 (40.4 %)
12	**0.05**	**15**	-8.8 ± 7.2	6.1 ± 5.3	15.3 ± 11.4	0.71 ± 0.42	0.24 ± 0.23	5243 (22.3 %)
12	**0.05**	**5**	-9.4 ± 8.8	6.7 ± 6.2	17.0 ± 13.1	0.69 ± 0.43	0.20 ± 0.22	4910 (23.8 %)

Figure S1. CMIP5 (blue; median ± IQR of the 9 models), Satellite observations (black) and forced-atmosphere IPSL-CM simulation (red) sea ice extent seasonal cycle between 1980-2015.

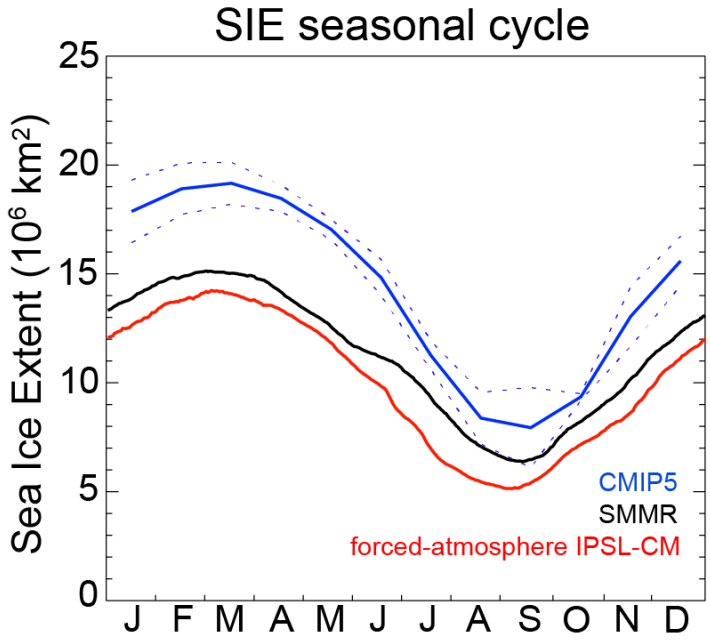

Figure S2. Evaluation of the impact of using monthly mean values as a basis for the CMIP5 computation of ice retreat and advance dates and ice-free season. To do this we have calculated ice retreat and advance date and ice-free season length from three different sources: (i) the daily ice concentration directly from satellite observations ("daily"); (ii) the monthly sea ice concentration, averaged from satellite daily concentrations ("monthly"); (iii) the satellite monthly fields, re-interpolated daily ("interpolated").

For each ice seasonality diagnostics, the maps represent the spatial distribution of the difference between the interpolated (top) or monthly (bottom) field and the daily field. Median ± IQR refers to all points in the seasonal ice zone.

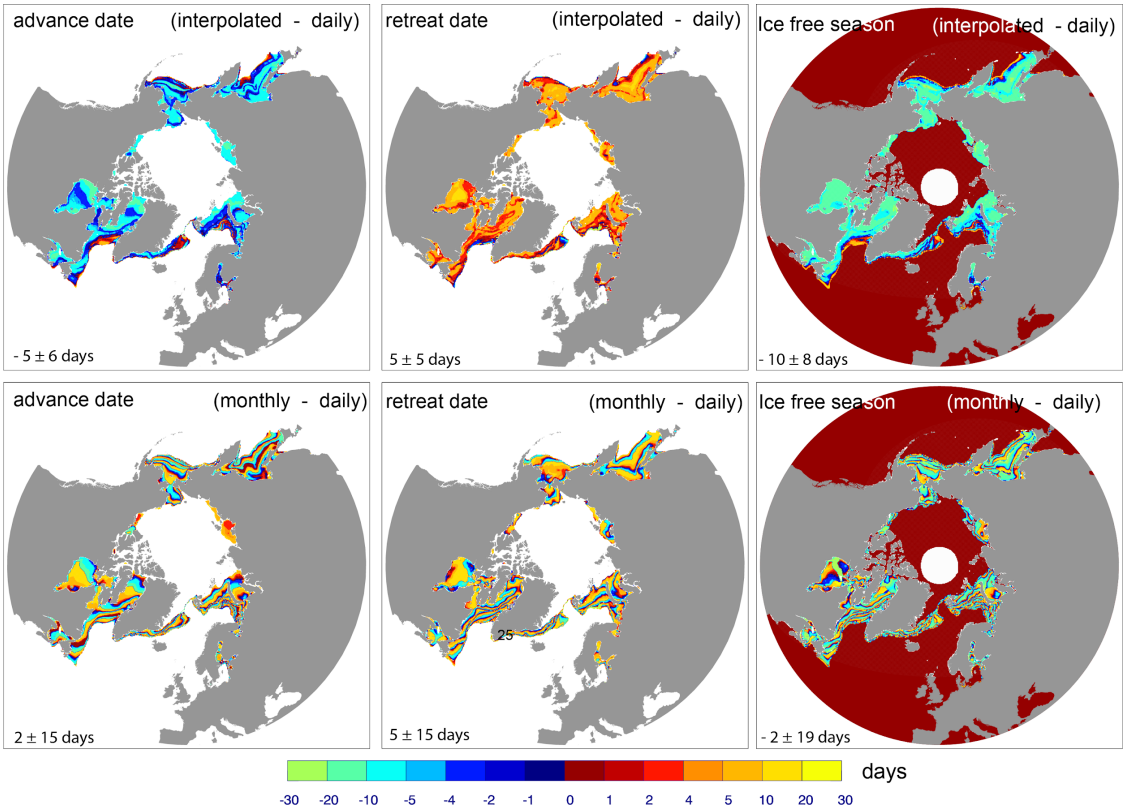

Figure S3. Maps of ice retreat date, ice advance date and ice-free season length over 1980-2015 (36 years) for the individual CMIP5 models and a forced-atmosphere IPSL-CM simulation.

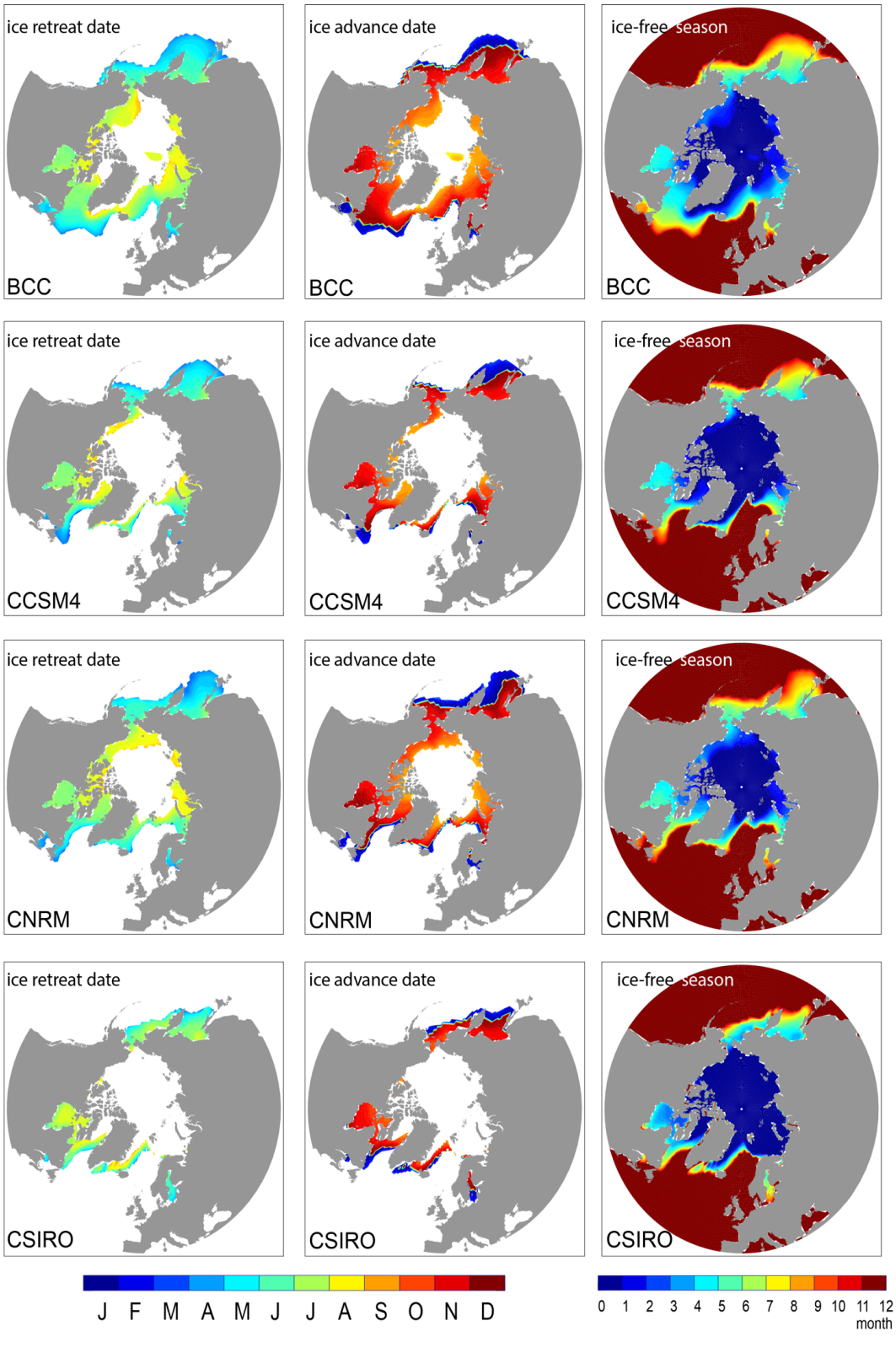

5

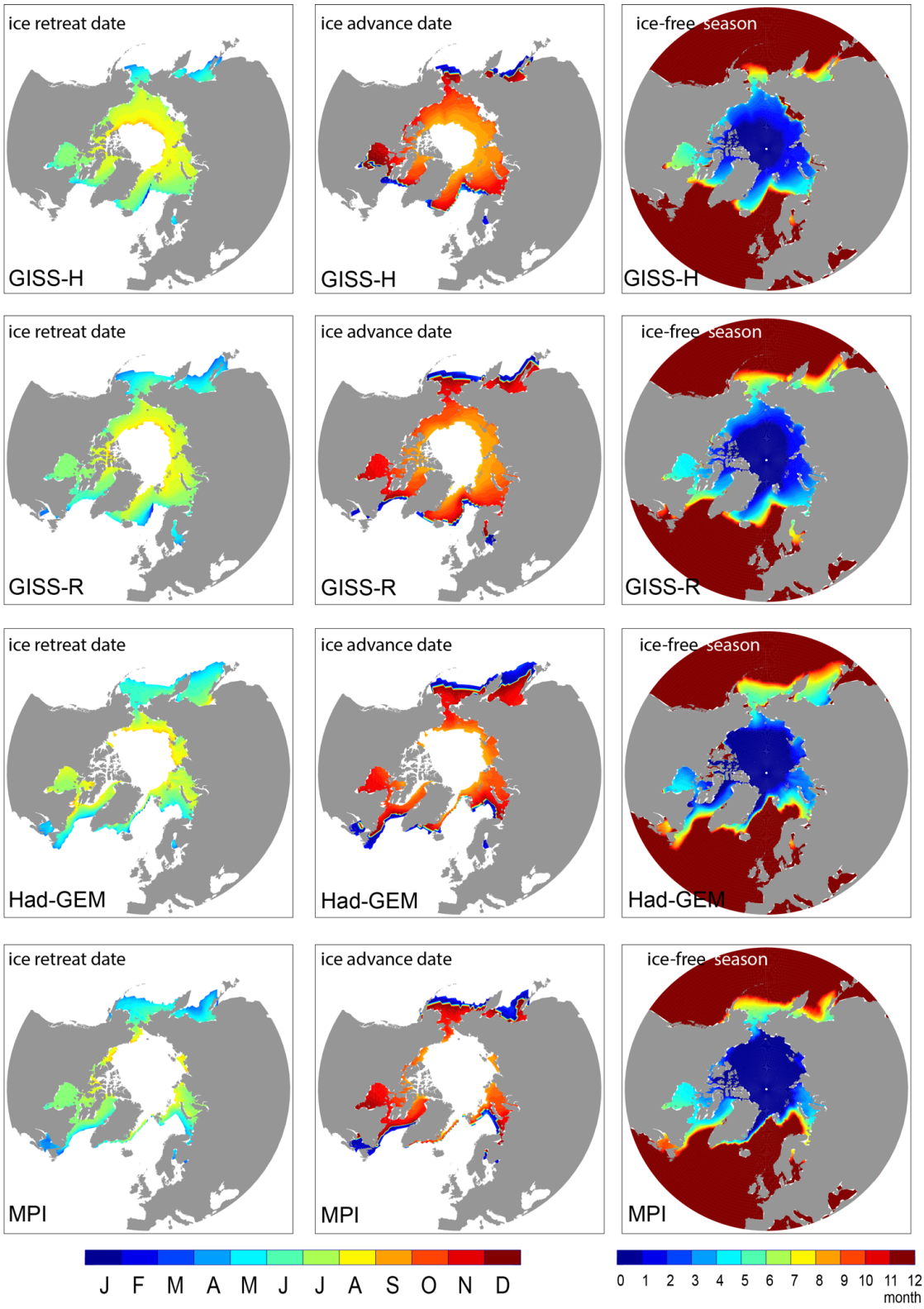
ice retreat date
ice advance date
ice-free season
GISS-H
GISS-R
Had-GEM
MPI
J F M A M J J A S O N D
0 1 2 3 4 5 6 7 8 9 10 11 12
month

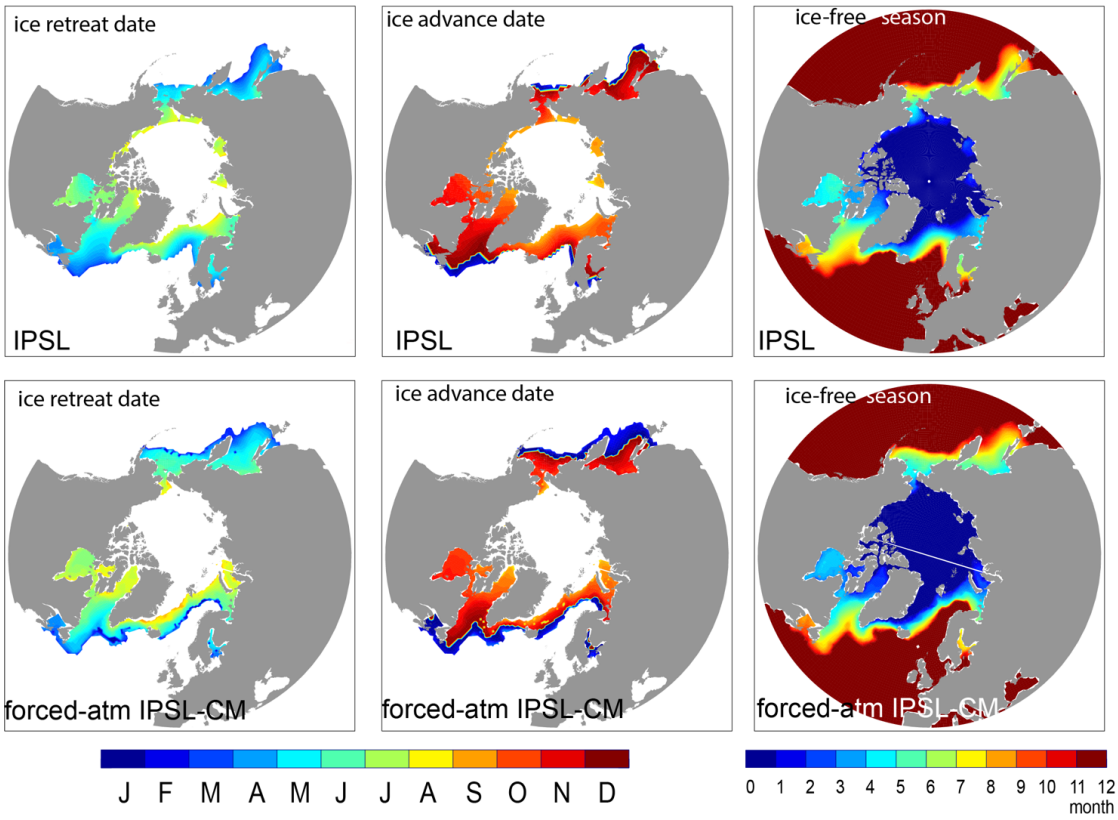
ice retreat date
IPSL
ice advance date
IPSL
ice-free season
IPSL
ice retreat date
forced-atm IPSL-CM
ice advance date
forced-atm IPSL-CM
ice-free season
forced-atm IPSL-CM
J F M A M J J A S O N D
0 1 2 3 4 5 6 7 8 9 10 11 12
month

Figure S4. Maps of trend in ice retreat date, ice advance date and ice-free season length over 1980-2015 (36 years) for the individual CMIP5 models and a forced-atmosphere IPSL-CM simulation. Hatching refers to the 95% confidence interval (p=0.05).

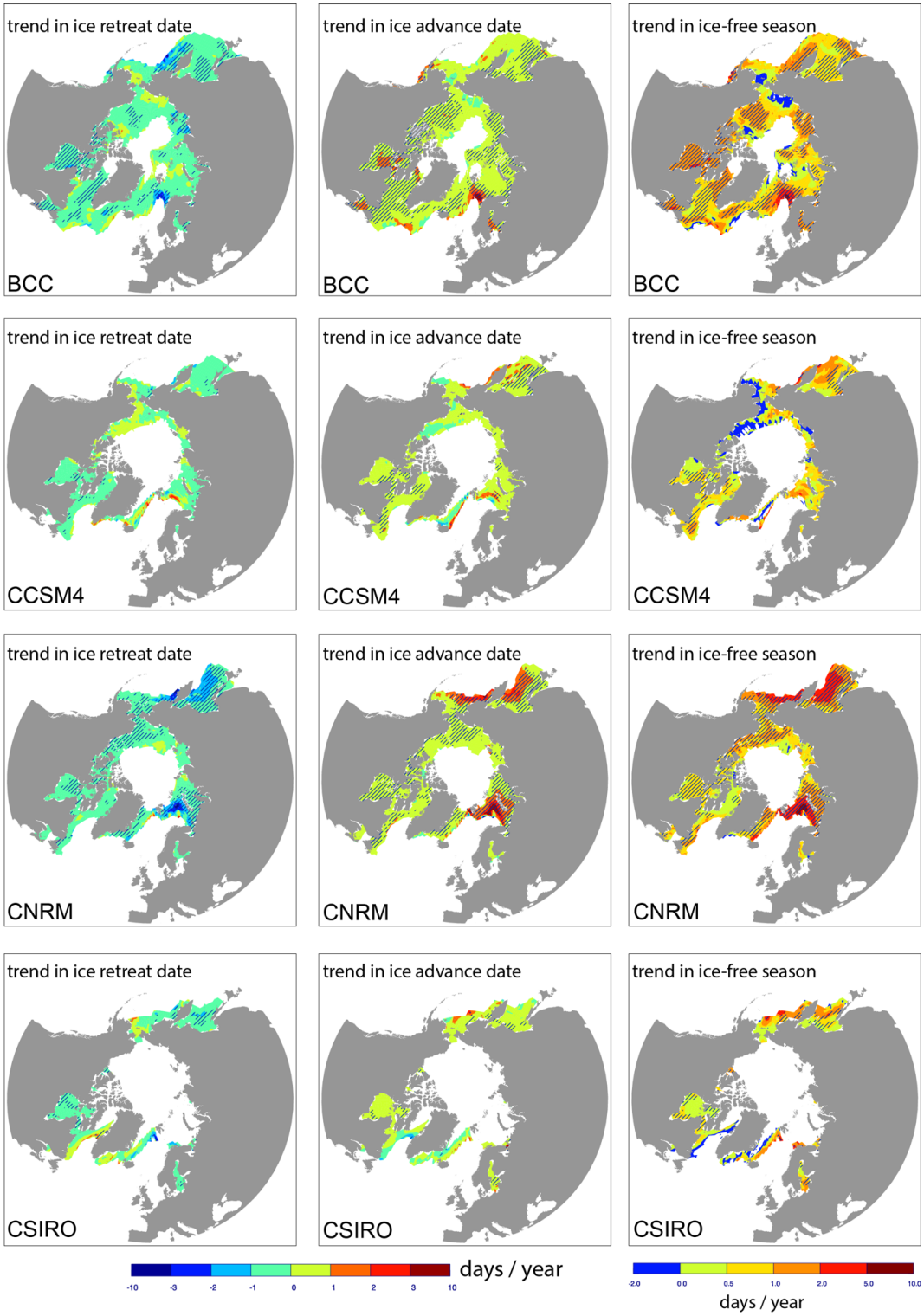

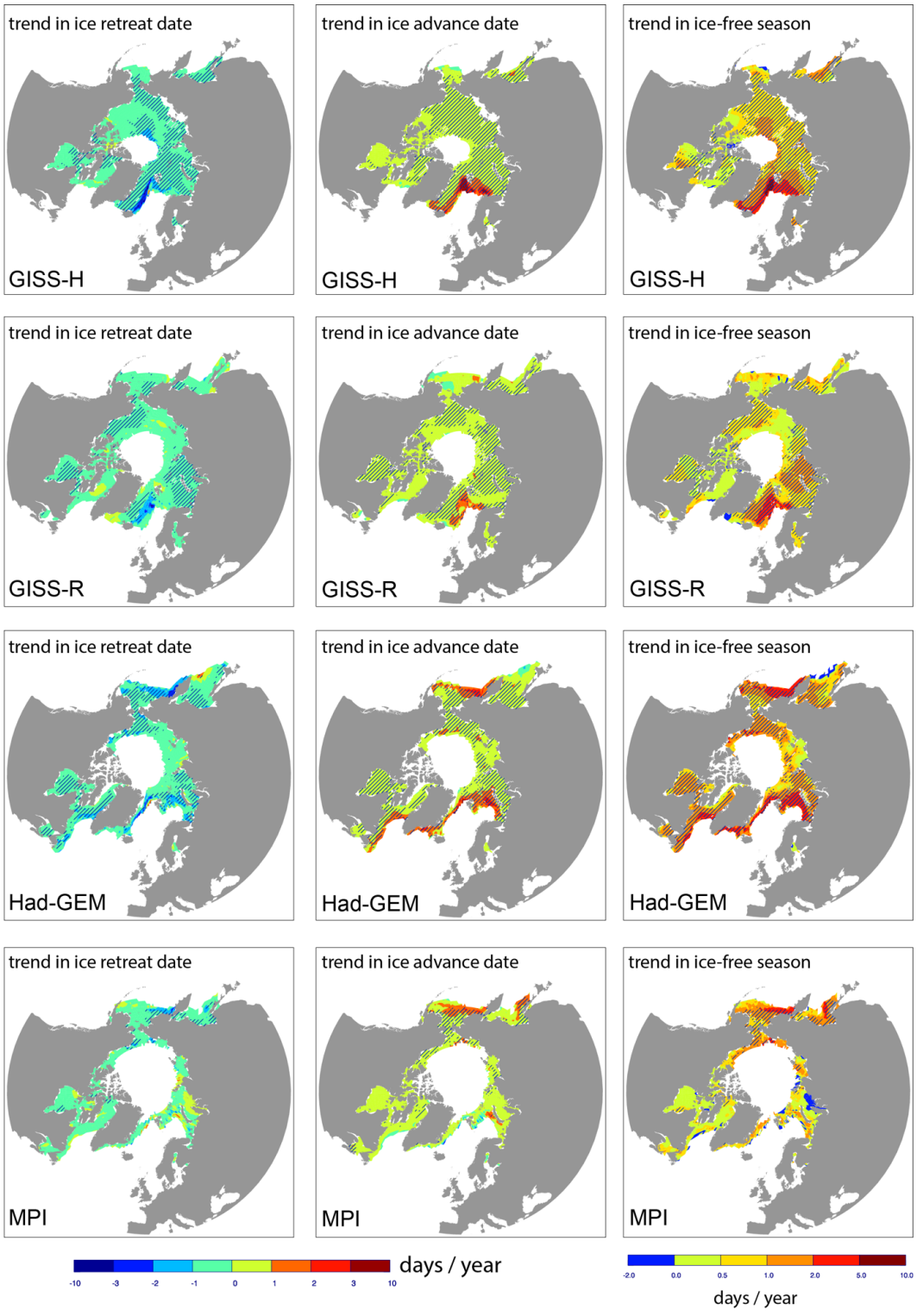
trend in ice retreat date
trend in ice advance date
trend in ice-free season
GISS-H
GISS-H
GISS-H
trend in ice retreat date
trend in ice advance date
trend in ice-free season
GISS-R
GISS-R
GISS-R
trend in ice retreat date
trend in ice advance date
trend in ice-free season
Had-GEM
Had-GEM
Had-GEM
trend in ice retreat date
trend in ice advance date
trend in ice-free season
MPI
MPI
MPI
-10 -3 -2 -1 0 1 2 3 10
days / year
-2.0 0.0 0.5 1.0 2.0 5.0 10.0
days / year

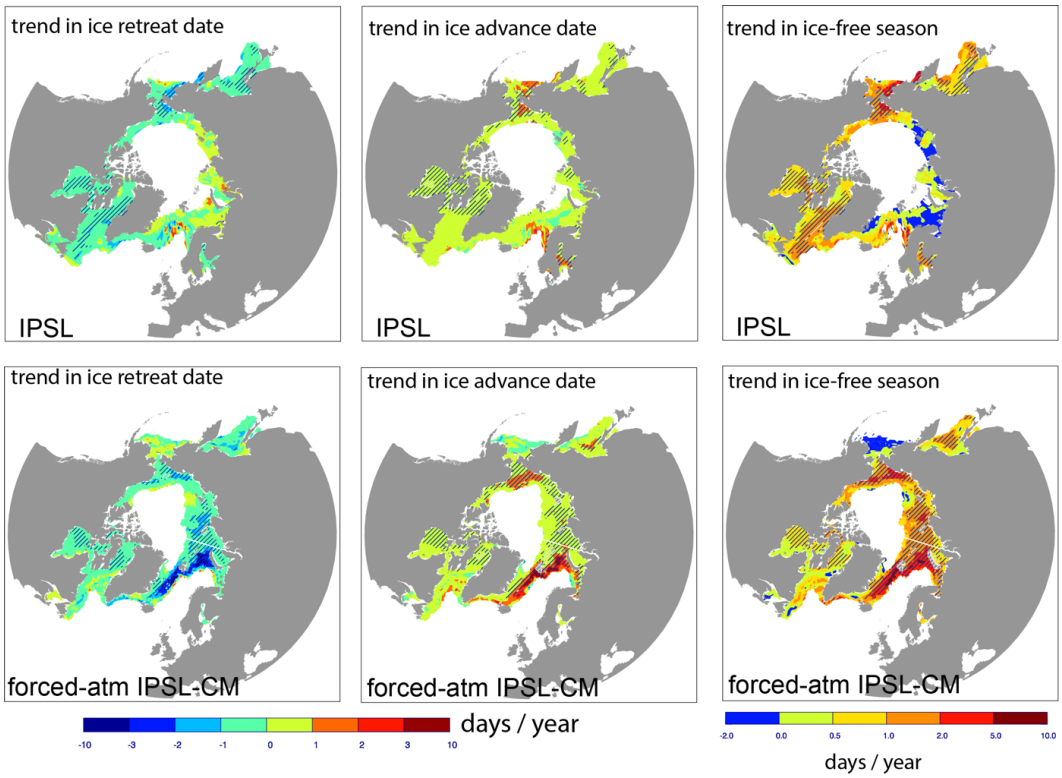
trend in ice retreat date
IPSL
trend in ice advance date
IPSL
trend in ice-free season
IPSL
trend in ice retreat date
forced-atm IPSL-CM
trend in ice advance date
forced-atm IPSL-CM
trend in ice-free season
forced-atm IPSL-CM
-10 -3 -2 -1 0 1 2 3 10
days / year
-2.0 0.0 0.5 1.0 2.0 5.0 10.0
days / year

10

Figure S5. Evaluation of the impact of internal variability. Long-term ice advance vs. retreat amplification coefficient from four realizations of IPSL-CM5A-LR over 1980-2015, 2015-2050 and 2050-2085.

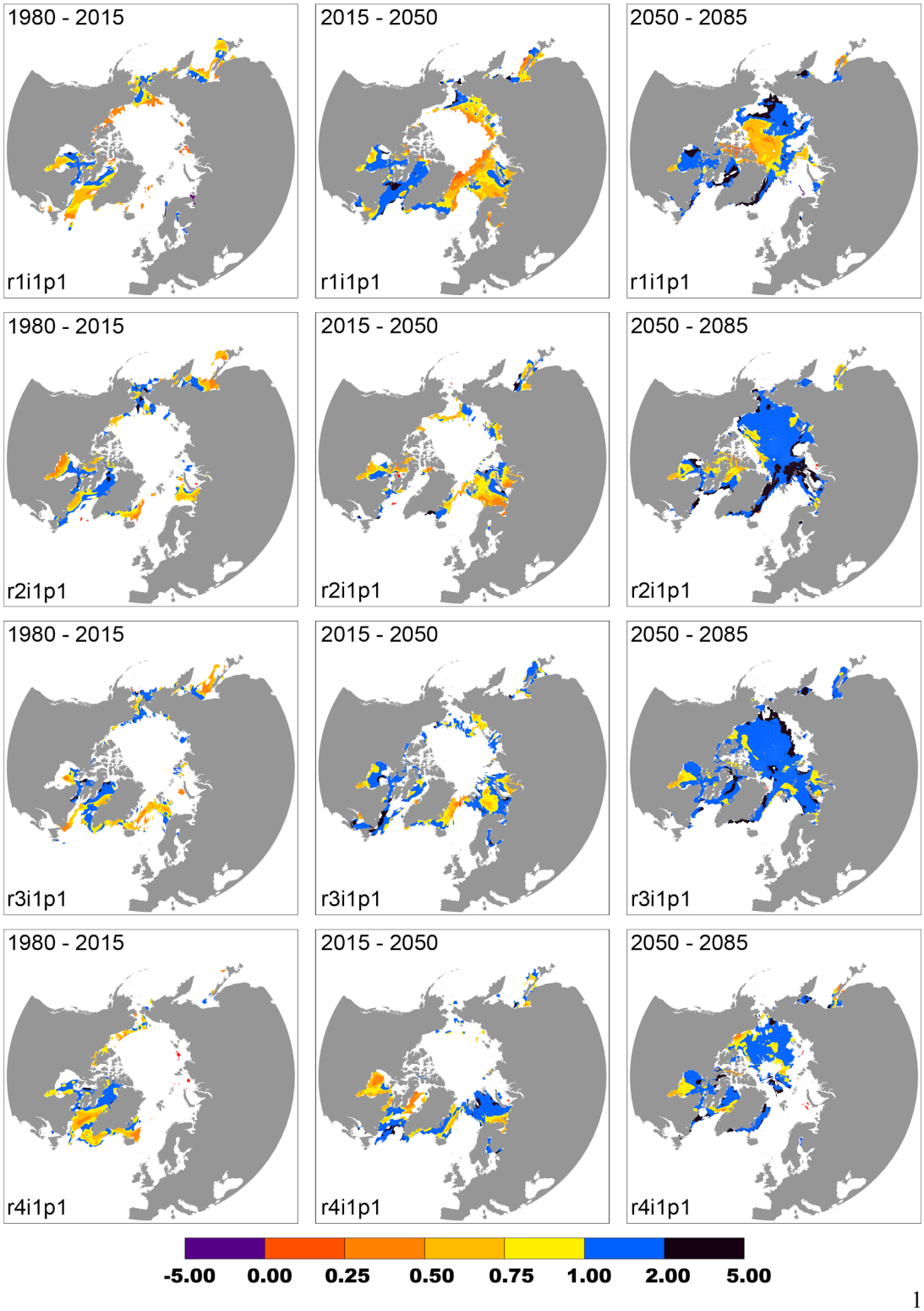

11

Figure S6. Evaluation of the impact of internal variability. Short-term ice advance vs. retreat amplification coefficient from four realizations of IPSL-CM5A-LR over 1980-2015, 2015-2050 and 2050-2085.

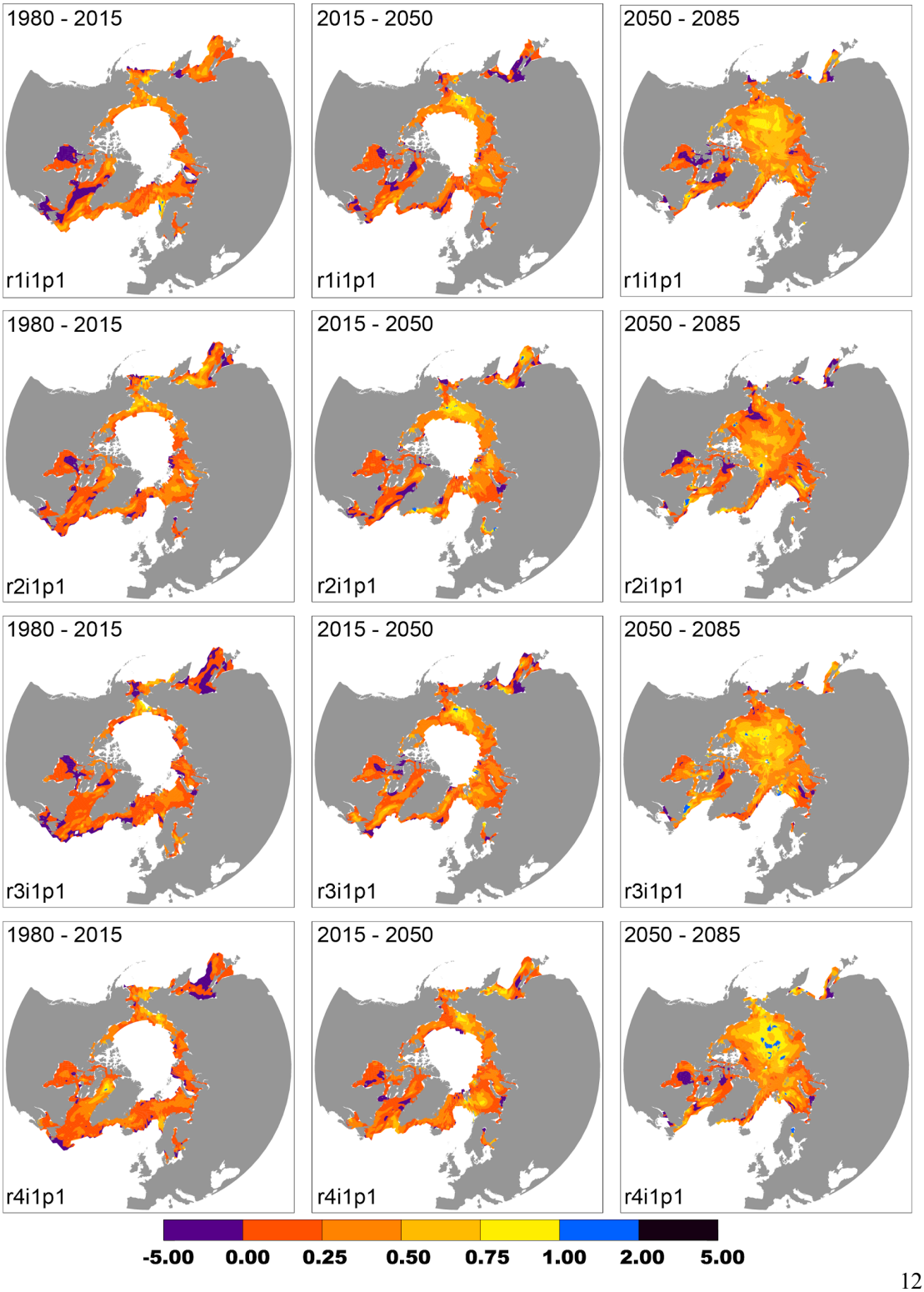

12

Figure S7. Impact of simulated mean state on the long-term ice advance vs. retreat amplification coefficient (1980-2015, 75% confidence interval). To illustrate this, we show the satellite-derived coefficient (centre), a forced-atmosphere IPSL-CM simulation (left) with better mean state than the fully-coupled IPSL-CM5A-LR simulation (right).

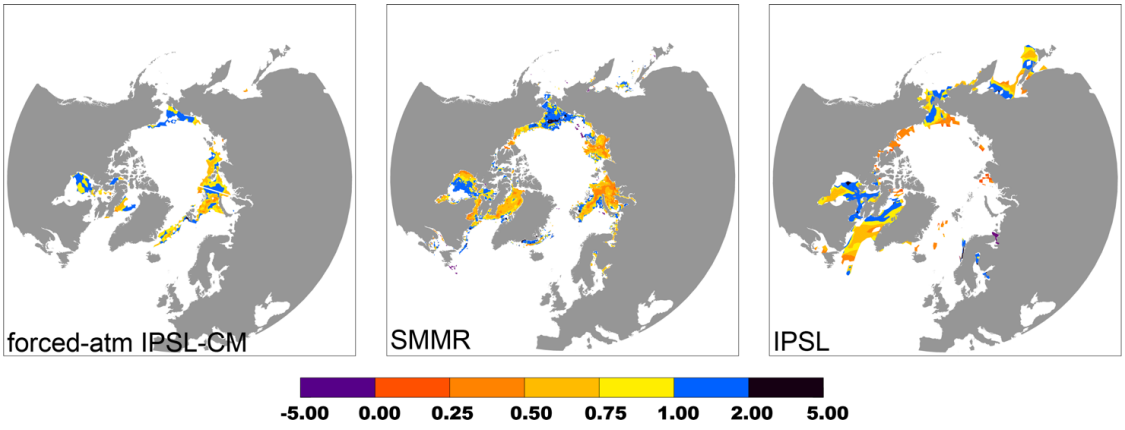

Figure S8. Evolution of the ice seasonality diagnostics (day of ice retreat, blue; and day of ice advance d_a, orange), for all individual models with corresponding range of satellite derived-values (green rectangles 1980-2015) over the 70-80°N latitude band. the average polar night is also depicted (grey rectangles).

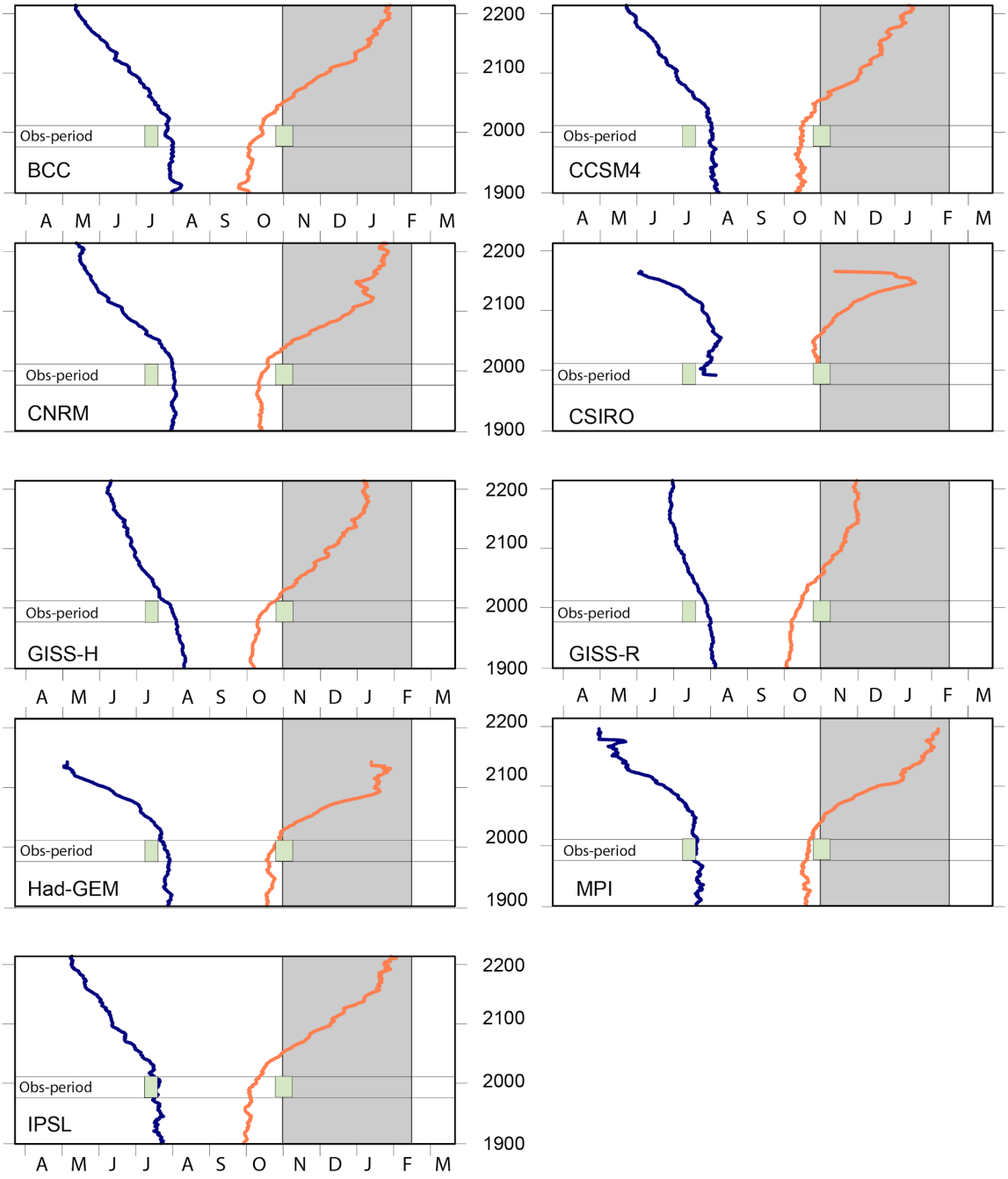

Figure S9. Impact of using a more restrictive confidence interval for the long-term ice advance vs. retreat amplification coefficient (to be compared with Fig. 2). long-term ice advance vs. retreat amplification coefficient using a more restrictive (95%) confidence interval for (a) passive microwave retrievals over 1980-2015; IPSL-CM5A-LR over (b) 1980-2015, (c) 2015-2050, (d) 2050-2085.

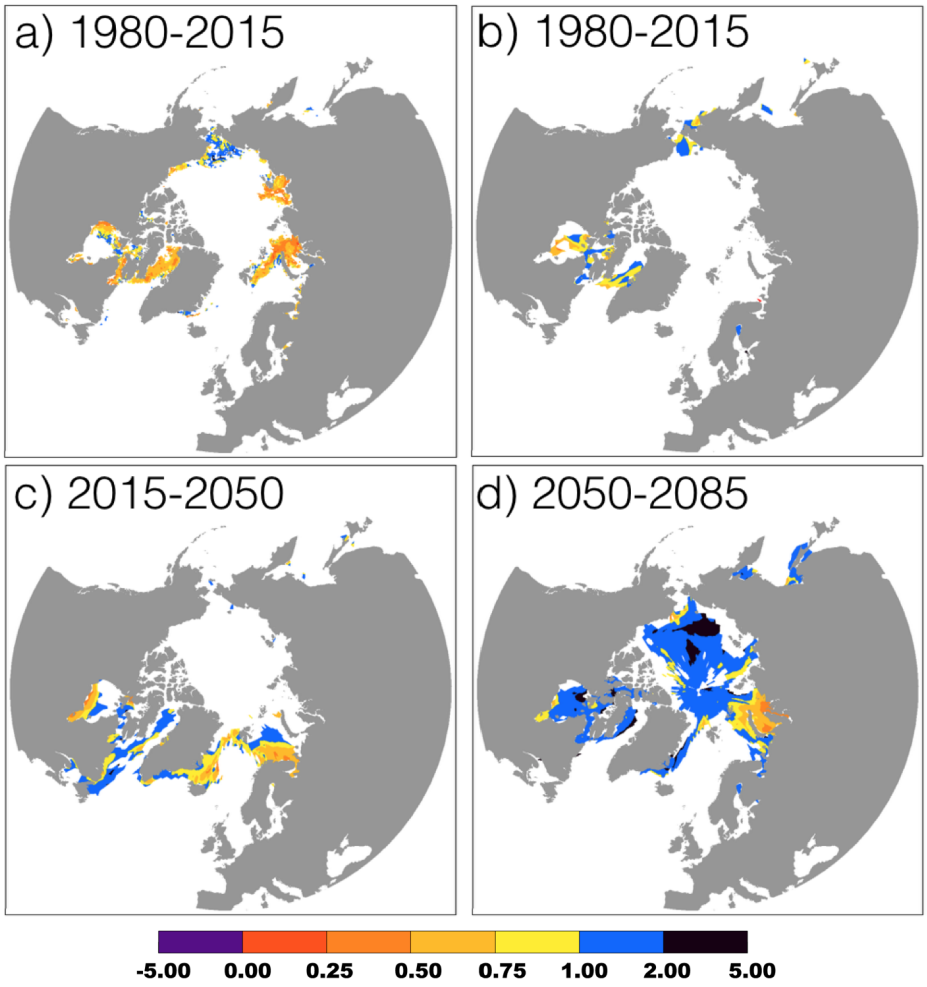

Annexes II : SLOPE 2019 Repport ; Nomura et al. (2019)

Saroma-ko Lagoon Observations for sea ice Physico-chemistry and Ecosystems 2019 (SLOPE2019)

Daiki NOMURA[1, 2, 3*], Pat WONGPAN[4, 5], Takenobu TOYOTA[4], Tomonori TANIKAWA[6], Yusuke KAWAGUCHI[7], Takashi ONO[4], Tomomi ISHINO[1], Manami TOZAWA[1], Tetsuya P. TAMURA[1], Itsuka S. YABE[7], Eun Yae SON[7], Frederic VIVIER[8], Antonio LOURENCO[8], Marion LEBRUN[8], Yuichi NOSAKA[9], Toru HIRAWAKE[1, 2], Atsushi OOKI[1, 2], Shigeru AOKI[4], Brent ELSE[10], Francois FRIPIAT[11], Jun INOUE[12], and Martin VANCOPPENOLLE[8]

1 Faculty of Fisheries Sciences, Hokkaido University, Hakodate, Japan.
*daiki.nomura@fish.hokudai.ac.jp (corresponding author)

2 Arctic Research Center, Hokkaido University, Sapporo, Japan.

3 Global Station for Arctic Research, Global Institution for Collaborative Research and Education, Hokkaido University, Sapporo, Japan.

4 Institute of Low Temperature Science, Hokkaido University, Sapporo, Japan

5 JSPS International Research Fellow, Japan Society for the Promotion of Science, Tokyo, Japan.

6 Meteorological Research Institute, Japan Meteorological Agency, Tsukuba, Japan.

7 Atmosphere and Ocean Research Institute, The University of Tokyo, Tokyo, Japan.

8 Sorbonne Université, Laboratoire d'Océanographie et du Climat/Institut Pierre-Simon Laplace, CNRS/IRD/MNHN, Paris, France.

9 School of Biological Sciences, Tokai University, Sapporo, Hokkaido, Japan.

10 University of Calgary, Calgary, Canada.

11 Max Planck Institute for Chemistry, Mains, Germany.

12 National Institute of Polar Research, Tokyo, Japan.

Abstract

Saroma-ko Lagoon, located on the Okhotsk Sea coast of Hokkaido, is seasonally covered by flat, homogeneous, easily accessible and safe sea ice. As such, it proves a very useful experimental site for the study of sea ice processes, the inter-comparison of methods, the testing of equipment and the training to polar regions. In this contribution, we describe the a physical, chemical, and ecosystem survey at Saroma-ko Lagoon, conducted over February 23–28, 2019 under the auspices of the SLOPE2019 (Saroma-ko Lagoon Observations for sea ice Physico-chemistry and Ecosystems 2019) program. Sea ice cores were collected to examine temperature, salinity, oxygen isotopic ratio, thin sections, and chemical and biological parameters such as carbonate chemistry, CH_4, nutrients, chlorophyll *a* concentrations, and ice algae community assemblage. Broadband and spectral irradiance measurements were carried out above/under the sea ice, and different sensors were inter-compared at close positions and environments. Equipment such as spectrometers, air–sea ice CO_2/CH_4 flux chamber, and under-ice turbulent heat flux systems were tested for future Arctic and Antarctic expeditions. Finally, an artificial pool was dug into the sea ice to understand the effect of snow particles on ice growth and to compare the gas exchange process over sea ice with an ice-free water surface. Our SLOPE2019 field campaign activities provided useful information for inter-comparison work and future sea ice research in the polar oceans.

Key words: sea ice, light, training and test measurement, inter-comparison, Saroma-ko Lagoon

1. Introduction

Saroma-ko Lagoon (surface area, 151.59 km^2 and maximum depth, 22 m) is located on the northeast coast of Hokkaido, Japan, and is connected to the southern part of the Sea of Okhotsk through two inlets. Saroma-ko Lagoon and the surrounding areas are located at the lowest-latitude where sea ice forms in the northern hemisphere (e.g. Liu *et al*., 2018). The water mass of the eastern part of the lagoon consists mainly of Okhotsk Sea water with freshwater input from the Saromabetsu River (Shirasawa and Leppäranta, 2003; Nomura *et al*., 2009, 2010). Almost the entire surface of the lagoon is covered with sea ice from early January through early April (Shirasawa and Leppäranta, 2003; Shirasawa *et al*., 2005). Because the sea ice forms in a semi-enclosed lagoon protected from dynamical disturbance, the sea ice conditions are kept almost stable which produces flat and homogeneous land-fast ice, and thus provide safe and comfortable conditions for sea ice research. This also provides good conditions of training for students and researchers, and for equipment testing in conditions easier and safer than in the context of Southern or Arctic Ocean field work. International sea ice field courses for interdisciplinary sea-ice research have been carried out in collaboration with USA, Finland, and Australia.

Observations over recent decades suggest that sea ice plays a significant role in the biogeochemical cycles within polar seas and oceans, providing an active biogeochemical interface at the ocean–atmosphere boundary (Vancoppenolle *et al*., 2013). However, a pressing need exists to perform methodological inter-comparison experiments in order to

obtain reliable measurements of basic biogeochemical properties (Miller *et al.*, 2015). With newly emerging techniques, and pressed by the rapid changes in sea ice, the time has come to evaluate and improve our approach to study sea-ice systems. In 2016, the Scientific Committee on Oceanic Research (SCOR) launched Working Group 152 on Measuring Essential Climate Variables in Sea Ice (ECV-Ice). This working group will synthesize past inter-comparison exercises and design and coordinate new experiments. The ultimate goal is to provide the international community with standardized protocols for processing sea-ice samples and collecting data for key variables. Saroma-ko Lagoon is especially suited for inter-comparison experiments of sea ice measurement methods. So far inter-comparison experiments conducted in Saroma-ko Lagoon focused on the effect of melting treatments on the assessment of biomass and nutrients in sea ice in 2016 (Roukaerts *et al*., 2019) and sea ice primary production in 2018.

The purpose of the 2019 campaign was to 1) examine the physical, chemical, and ecosystems of sea ice and snow for light measurement above/under the sea ice, 2) inter-compare different light measurement methods performed with different sensors, 3) test equipment for future Arctic and Antarctic expeditions, such as spectroradiometers, air–sea ice CO_2/CH_4 flux chamber, and under-ice turbulent heat flux systems, 4) document the link between meteorological conditions and ice crystal alignment in young sea ice, 5) compare gas exchange processes over sea ice and ice-free water surface by using artificial pool, and 6) train and educate students and young scientists for future polar expeditions.

2. Sampling site and environmental conditions

Field work was conducted from February 23 to 28, 2019 by several sub-groups organized around different locations near 44°07’091’’N, 143°57’238’’E, 2 km from the eastern coast of the Saroma-ko Lagoon, (Figure 1). Snow depth was 8.4 ± 1.2 cm (n=150) and sea ice thickness was 47.5 ± 3.2 cm (n=30), whereas water depth was about 6 m.

Air temperature, and wind direction and speed were monitored at one minute intervals by the automatic weather system (AWS) (Kestrel manufacturer) at site C2 with an accuracy of 0.5°C for air temperature and 3% of reading for wind speed. Air temperature ranged from –15°C to +2°C during the observation period (Figure 2a) and featured a clear day-night cycle. Southerly to westerly wind dominated with wind speed ranging from 0 to 5 m s^{-1}. Wind data were not obtained at night, presumably due to freezing of the propeller. Yet, since daytime wind speed was consistent with the nearby Tokoro weather station (Figure 1c) and run by the Japan Meteorological Agency (Figure 2b), the wind data at the latter site were used for analysis. Upward and downward radiative fluxes, including shortwave and longwave radiation, were monitored at one minute intervals by the radiometer (MR-40, EKO Instruments Co., Ltd) near the AWS (Figure 3a).

Light conditions during SLOPE2019 were typically beautiful weather, clear skies, with occasional cirrostrati and cirrocumuli, and rarely full overcast conditions. The last day (28 February 2019) was entirely free of clouds. Every day, near sunset (around 18:00 LT), the solar disk was disappearing behind the mountains and the moon was showing up, from waning gibbous to last quarter (81–51% of visible moon disk).

3. Sea ice and snow properties

Sea ice cores and overlying snow were sampled at site C2 on 23 (16:00 LT), 25 (15:45 LT), and 27 February 2019 (15:49 LT). Sea ice cores were taken using a standard sea ice corer (Mark II coring system, Kovacs Enterprises, Inc.). Snow was sampled using a plastic shovel. Vertical temperature profiles within ice core and snow were inferred from a needle temperature probe (Testo 110 NTC, Brandt Instruments, Inc.). Ice cores were then cut every 10 cm from the bottom of the ice. Snow samples and sea ice core sections were placed into the air-tight Smart bags PA (AAK 5L, GL Sciences Inc.) and melted in the dark at +4°C. After melting, meltwater was poured in the bottles for each parameter, and samples were processed/analyzed.

Figure 4 shows the vertical profile of temperature, salinity, brine volume fraction, carbonate chemical parameters such as dissolved inorganic carbon (DIC) and total alkalinity (TA), and chlorophyll *a* (chl. *a*) concentrations within sea ice and snow (other parameters such as water oxygen isotopic ratio, CH_4, and nutrients are currently being processed and analyzed). . Vertical temperature profiles in sea ice were remarkably stable through the experiment (Figure 4a). By contrast snow temperature profiles were more variable (Figure 4a). This is because the specific heat of saline ice is much higher than that of snow, buffering temperature changes in sea ice. The variability in snow temperature reflects changes in sampling time combined with a strong air temperature diurnal cycle. High salinities (S >17 psu) characterized the bottom of the snow and the sea ice surface, and the profile within the sea ice was C-shaped (Figure 4b). Brine volume fraction of sea ice calculated from the temperature and salinity ranged from 8 to 30% (Figure 4c), indicating permeable sea ice. Vertical profiles of DIC and TA were similar with that of salinity and ranged from 42 to 1159 μmol kg^{-1} for DIC and 26 to 1305 μmol kg^{-1} for TA (Figures 4d and e). Chl. *a* concentration was high at the bottom of the sea ice (>166 μg L^{-1}) (Figure 4f), and these concentrations were higher than typically observed at the site (Nomura *et al*., 2011) presumably due to the low snow depth during this campaign and higher light penetration through the snowpack and sea ice. Basically, there was no temporal variation during the ice sampling period (within 5 days) for each parameter, except for the temperature within the snowpack (the variability in snow temperature was affected by a strong air temperature diurnal cycle). The vertical thin-section photographs of the sea ice core at site C2 on 25 February 2019 (Figure 4g) indicated that most of the ice core was dominated by the granular ice (snow-ice plus frazil ice) (89% of the ice thickness in the upper parts of the ice core), and columnar ice made up to 11% of the lower parts of the core. The sea-ice algal community was overwhelmingly dominated by diatoms (98%, cell counts) (Figure 5) and the remaining were cryptophytes and dinoflagellates.

Snow analyses were conducted at sites T1 and T2, including snow classification and measurements of snow depth, grain size, density, temperature, and mass concentrations in impurities. Figure 6 shows an example of the snow conditions in the sampling layers. At site T1, the snowpack of 7 cm depth was spread over the sea ice of approximately 51 cm. The observed snow form in the upper layers consisted of rounded grains of $r_1 \sim 400$ μm and $r_2 \sim 100$ μm (median) while the lower layers mainly consisted of melt forms of $r_1 \sim 1500$ μm and $r_2 \sim 600$ μm (median) corresponding to the snow grain size where two measures of snow grain size were measured (Tanikawa *et al*., 2014). The temperatures of snow were all below freezing. Snow density was approximately 300 kg m^{-3}. The mass concentrations of snow impurity of organic carbon, elemental carbon, and dust were 0.39, 0.18, and 7.14 for a top

layer and 0.18, 0.08, and 2.71 for a bottom layer, respectively. Technical details of snow analyses were described in Tanikawa *et al*. (2014) and Kuchiki *et al*. (2015).

4. Optical measurements above/under the sea ice

Optical measurements were performed above and under the ice by three different sub-groups. This included broadband and spectral measurements, above and under sea ice, and this section gives an overview of the instruments deployed and measurements performed. These provide a detailed view of the light field above and under the sea ice. Inter-comparison of the different instruments deployed provides additional insights on uncertainties. All measurements have in common that care was taken to minimize the footprints and shadow effects.

4.1 Optical and ancillary measurements

4.1.1 Pyranometers (broadband radiation)

Broadband, near-surface, planar irradiances, in their down- and up-welling shortwave (SW) and longwave components, were collected with two different instruments: the MR-40 (EKO Instruments Co., Ltd) (Figure 3a), and the CNR4 (Kipp and Zonen, Delft) (Figure 3b). Both instruments were deployed at about 30 m from each other, near site C2 (see Figure 1). Both instruments have slightly different spectral range: 285 nm–3 μm for MR-40 and 305 nm–2.8 μm for CNR4. The MR-40 was mounted on a table-shaped stand (Figure 3a). The CNR4 was mounted on a tripod with a 2-m arm extension (Figure 3b). Broadband albedo was retrieved by dividing the upwelling by downwelling irradiance. Because of radiometer errors at low irradiance and solar angles and of concomitant drastic changes in albedo, we used a threshold of 50 W m^{-2} on incoming irradiance to calculate albedo. Both instruments were deployed during the full survey, starting on 23 February 2019, slightly after solar noon and ending on 27 February 2019, in the afternoon. CNR4 failed on the last measurement day (27 February 2019). Three full daily cycles were captured by both instruments. Both instruments sampled at 1 minute resolution.

4.1.2 Spectrometers and spectral radiometers (spectral radiation)

A second set of experiments was focused on spectral measurements above and under the sea ice. Three different instruments were used for specific purposes and deployed at distinct locations. Occasionally, they were also deployed jointly during several short inter-comparison sessions.

(i) The FieldSpec FR grating spectrometer (PANalytical) was mostly used to measure surface spectral albedo. The FieldSpec FR covers λ = 0.35–2.5 μm, with a spectral resolution of 3 nm for λ = 0.35–1.0 μm; and of 10 nm for λ = 1.0–2.5 μm. To integrate over a half-sphere and measure irradiance, a cosine collector was used. The latter consisted of a white reference standard of a Spectralon diffuser panel, SRT-90 (Labsphere). The spectral upwelling and downwelling irradiance fluxes were retrieved, from which spectral albedo was deduced. The

FieldSpec FR was deployed at sites T1 and T2 (200 m away from the eastern coast of Saroma-ko Lagoon) (Figure 3c).

(ii) Two TriOS RAMSES ACC UV/VIS hyperspectral radiometers (SAM 8182 and SAM 8033, TriOS) were used for a spatial survey of under-ice spectral light transmission (Figures 3d–f). The TriOS RAMSES covers a wavelength range of 350 to 920 nm, with spectral resolution of 3.3 nm. Protocols from Wongpan *et al*. (2018) were applied. A first sensor (SAM 8182) was deployed above the sea ice, mounted on a tripod at about 1 m height (Figure 3f). A second sensor (SAM 8033) was deployed under the ice using a retractable L-arm (Figure 3d). The L-arm was inserted through a 0.11 m (diameter) borehole drilled with the Mark II Kovacs corer. The horizontal arm was 1.3 m long, and the sensor was placed ~7.5 cm below the ice–ocean interface. The two sensors were connected to a laptop using the IPS104-4 Plus interface (Figure 3f). The MSDA software was used, enabling synchronous measurements above and under the sea ice. Specific calibration files were used for the above- (air) and under-sea ice (water) measurements. At least three joint above- and under-ice spectra were recorded at each measurement location. Finally, spectral transmittance was retrieved from the ratio of under- and above-ice downwelling planar irradiant fluxes.

Once done the optical measurements, snow and ice sampling for biogeochemical parameters were started. The location of the under-ice radiometer and snow depth were recorded. Snow samples were collected in a Ziploc bag. A sea ice core was taken and sliced into bottom 0.1 m, and equal-length middle and top sections. The melting of snow and ice samples, filtration and measurement of chl. *a* concentration (Turner Designs 10AU Field and Laboratory Fluorometer) were done following standard protocol (e.g. Roukaerts *et al*. 2018) by melting without addition of filtered seawater at low temperature (around +5°C) in the dark. Optical measurements with the TriOS RAMSES spectrometers, and sampling of snow and ice core were performed at 27 sites over a 250 m×250 m area (see Figure 1d), from 23 to 26 February 2019. The sampling sites were located on three east-west lines at 0, 2, 4, 8, 16, 32, 64, 128, and 256 m. The three lines were separated by 128 m in the south-north direction.

(iii) An STS-VIS grating micro-spectrometer (Ocean Optics), was deployed in the framework of a temporal survey of under-ice spectral light transmission (Figure 3g). The STS-VIS photodiode array covers the 350–800 nm wavelength range, with 1024 channels. As the effective spectrometer resolution is ~10 nm, a 30-channel smoothing was applied to all outputs. The STS-VIS was deployed under the ice, onboard the Ice-T *fish* system, an ice-tethered sealed cavity hanging below the ice at depth up to 5 m, and inclined with an angle of 10–20°, depending on current intensity (Figures 3h). An optical fiber placed through the upper lid of the Ice-T *fish* connects the STS-VIS to the exterior. Radiances (W m^{-2} nm^{-1}) were retrieved from counts, then converted to irradiances assuming an elliptical angular radiance distribution in the water column. Irradiance over the visible range is finally computed by wavelength-integration.

The STS-VIS was deployed at site C2 during February 23–24, 2019 and taken home at night, to ensure proper data collection. On 25 February 2019, the STS spectrometer was deployed at site C4 and left under water, during two complete days and nights.

4.2 Above-ice measurements: irradiance and albedo

4.2.1 Solar irradiance above sea ice

Time series of incoming solar irradiance from MR-40 and CNR4 show the expected solar irradiance diurnal cycle (Figure 7a). During daytime, irradiance typically was within the range of 0–600 W m^{-2}. At night, irradiance was within the range of 0.5–20 W m^{-2}. This suggests substantial light pollution, since a full moon would irradiate at 10^{-3} W m^{-2}. By all means, the amount of noise suggests that the detection limits of both MR-40 and CNR4 are reached at night.

MR-40 and CNR4 can be compared when simultaneously operational. Both instruments suggest extremely consistent irradiance variations at temporal scales as small as 1 minute. There are systematic differences between both instruments. Indeed, downwelling SW irradiance was 120.2 W m^{-2} for MR-40 and 117.8 W m^{-2} for CNR4, equivalent to a +2% difference. The systematic difference between both instruments was opposite for upwelling SW: MR-40 recorded 90.8 W m^{-2} on average, whereas CNR4 recorded 93.1 W m^{-2} (–2.5%).

Since the differences for downwelling and upwelling irradiances have opposite sign, we suggest that they are not due to actual differences between the MR-40 and CNR4. Rather, these differences most likely reflect actual signals, due for instance to different mounting of the instruments (shadow and height), or to different surface type. These differences are hard to disentangle, because MR-40 and CNR4 were not deployed under close enough mounting and environmental conditions.

4.2.2 Surface albedo

The median surface broadband albedo obtained from MR-40 and CNR4 falls within the 0.75–0.80 range (Figure 7b), typical of dry snow-covered sea ice (e.g. Perovich and Grenfell, 1981). Due to differences in recorded downwelling and upwelling irradiances, retrieved albedos are significantly different at both MR-40 and CNR4 sites: 0.76 ± 0.05 for MR-40 and 0.79 ± 0.04 for CNR4.

The FieldSpec FR provides a spectral view of the surface albedo, for snow-covered and snow-free sea ice (Figure 8). Snow-free sea ice was obtained by artificially removing snow around the measurement point. Measurements suggest that snow-covered sea ice albedo is lower than typical continental snow albedo values, yet with similar spectral shape. This is because the albedo integrates contributions from both snow and the sea ice below, which scatters light less efficiently than snow. The spectral albedo of the snow-free sea ice was 0.6–0.7 in the visible region, 0.1–0.4 in the near-infrared region typically < 0.1 in the 1.5–2.0 µm range. In the visible window, albedo would be affected by multiple scattering of air bubbles and brine within the sea ice. In the near-infrared and shortwave infrared wavelengths, the albedo would be dominated by direct surface (Fresnel) reflection at the sea ice surface, because of the relatively strong light absorption at such wavelengths.

4.3. Under-ice measurements: irradiance and transmittance

4.3.1 Inter-comparison of TriOS RAMSES and STS-VIS spectrometers

On four occasions, the TriOS RAMSES and STS-VIS were jointly deployed at close locations and environments, for inter-comparison. The transmitted spectral irradiance recorded by both instruments is depicted in Figure 9. During each session, several acquisitions were performed, indicating measurement uncertainty associated with small variations in sensor position.

For three of the four inter-comparison cases (C2, C4#1, 256M5), the depth of the Ice-T *fish* was left at its standard depth of deployment (about 5 m), whereas the TriOS RAMSES on its L-arm was held at about 0.5 m (0.075 m below the ice-ocean interface) (Figure 9). In these three instances, the STS-VIS spectrum typically shows smaller red-light intensity than the TriOS RAMSES device, consistently with attenuation of irradiance with depth, stronger in seawater for red than for blue light. For the C4#2 deployment, the Ice-T *fish* was brought to about 70 cm depth, much closer to the TriOS RAMSES. In that case, both spectrometers give very close results. All in all, this exercise suggests that within uncertainties in spectral irradiance (about 1 mW m^{-2} nm^{-1}), both instruments can be used interchangeably.

4.3.2 Broadband irradiance

The time series of under-ice irradiance, as recorded by STS-VIS, show a diurnal cycle of under-ice irradiance synchronized with surface irradiance (Figure 7a). The recorded under-ice irradiance was within the range of 10^{-4}–2 W m^{-2}. Transmittance was within the range of 0.1–0.5% at 5 m depth.

4.3.3 Spectral irradiance, transmittance and chl. *a*

Both STS-VIS and Trios RAMSES consistently show under-ice light spectra typical of high-chlorophyll conditions, with irradiance peak shifted towards 550–600 nm. Under-ice spectral shape was independent of location (Trios RAMSES) or time of the day (STS-VIS). Spectral irradiance was within the range of 0–20 mW m^{-2} nm^{-1}.

Spectral transmittance of sea ice was < 1%. As 85–90% of incoming visible light is reflected at the surface and that less than 1% is transmitted under the ice, bout 10% of the incoming light must be absorbed within snow and sea ice.

The pair measurements of hyperspectral normalized transmittance and chl. *a* are displayed in Figure 10. Integrated chl. *a* was within the range of 6.8–29.4 mg m^{-2}, with a mean of 18.8 ± 6.0 mg m^{-2}. Larger integrated chlorophyll is typically associated with more transmitted green light and less transmitted red light (Figure 10). This is consistent with the arguments proposed by Mundy *et al.* (2007), based on observations from Arctic first-year landfast sea ice of the Canadian Arctic. Snow effects have their weakest spectral dependence on transmitted light within the range of 400–570 nm. In addition, chl. *a*, one of the major pigments of sea ice algae, has a distinct absorption band center at 440 nm.

5. Physical properties of under-ice water

In this section, the programs and preliminary results from the physical oceanographic observations are described. The main purpose of the research was to evaluate the ice–ocean heat exchange associated with evolution of the fast ice in the Saroma-ko Lagoon. In addition, these measurements were experimental training and test for the Multidisciplinary drifting Observatory for the Study of Arctic Climate (MOSAiC) during the year-round expedition from 2019 to 2020 into the central Arctic.

To investigate thermodynamic features in the near-surface layer during ice formation, we created a 1 m×1 m square pool at site Y1 and then deployed an autonomous temperature-profiling buoy (IceTC2/30, Marlin-Yug) at its corner (Figure 11). The instrument is a 2 m-long thermistor chain, with a 20 cm constant interval, and transmits the data via the Iridium satellite at an hourly time interval. As one of the main observations, the turbulent heat flux in the ice-water boundary layer was directly measured with an eddy-covariance flux system, which consists of an acoustic Doppler velocimeter (Vector, Nortek) and a fast-response thermometer (Rinko-EC by JFE Advantech Inc.). The two fast sensors were linked with a cable to make synchronized data sampling. The eddy-covariance system was installed in an ice hole 15 cm in diameter at a place 1 m apart from the pool.

We also established a wind-insulating shelter, which was located 10 m aside the experimental pool. Inside the shelter, an ADCP (400 kHz AquaDopp profiler) was deployed to observe horizontal current at multi-depths (approximate 3, 5, and 7 m). We also conducted profiles with a CTD probe (RINKO profiler, JFE Advantech). The data acquisition was performed as daily routine during a period between 24 and 27 February 2019, and resulted in 17 vertical profiles.

The preliminary results are described in the following. Averaged vertical profiles from overall CTD casts suggest that the sea-ice melt water created a 1-m thick, strongly stratified layer at the top (Figure 12). In the layer, water temperature is always higher than the freezing point (Figure 12a). Meanwhile, a vertical gradient in salinity determines the shallow, strong stratification, where salinity changes by more than 10 over 1 m water depth (Figure 12b). In the experiment pool, where the water surface was exposed to the air, surface temperature was rather sensitive to the solar radiation (Figure 13). Regularly, it attained its maximum around noon, and then dropped in a few hours. Solar-heated water remained for longer hours at depths a few tens of centimeter below the ice-water boundary. It is added that the density of chl. *a* is coincidently high in the surface stratified layer, reaching 6 μg L^{-1} (Figure 12d).

The eddy-covariance system, measuring temperature and velocity at approximately 1-m depth, shows recurrent events of upward turbulent heat transfer (Figure 13a). The events were quite intermittent, and occasionally reached 5–10 W m^{-2}. The most prominent peak was one that occurred around 22:00 LT on 26 February, achieving greater than 60 W m^{-2} in magnitude. With respect to the horizontal current, we cannot say any conclusion at this point. That is, we did not find any prevailing current, neither tidal signals from the current field (Figure 13c). The only notable exception was the northward current that happened during the evening of the first sampling day. The current was seen solely at 3 m depth, with nearly 20 cm s^{-1} of magnitude. The northward flow could be related to the upward heat flux, being 5–10 W m^{-2}, which was observed by the eddy-covariance system at nearly same timing.

6. Artificial pool experiment

6.1. Effects of snow on the sea ice structure at the early growth stage

To clarify the meteorological conditions which differentiate two crystal types of granular and columnar ice, and their formation processes especially for granular ice quantitatively, we made a square pool with a dimension of 1.5 m×1.5 m at 200 m away from the eastern shore of the Saroma-ko Lagoon and conducted field experiments to grow sea ice for the period from 25 to 27 February (Figure 14). The salinity and depth of seawater at the pool were 31.2 psu and 1.2 m, respectively, and the pool was surrounded by 32 cm thick fast ice with 9 cm thick snow on it. The ice growth conditions were monitored with a camera mounted near the pool. The radiative fluxes were measured with a radiometer equipped near the AWS.

During the period, relatively cold and calm conditions prevailed, which provided a favorable condition for the bottom freezing rather than frazil ice production. Instead, the difference in snowfall conditions provided a good opportunity to examine the effect of snow on the sea ice structure and surface heat balance at the early growth stage. We intend to estimate it quantitatively as a case study through the sample analysis and a thermodynamic ice-growth model.

6.2. Gas exchange process at the ice-free water surface

Recent CO_2 flux measurements on sea ice indicate that sea ice is an active component in gas exchange between ocean and atmosphere (Delille *et al.*, 2014). In this campaign, we tried to set up and measure the CH_4 flux on sea ice in addition to the CO_2. A LI-COR 8100-104 chamber was installed within 1 m×1.5 m artificial pool with float (Figure 15a) from 12:00 LT to 16:00 LT 27 February 2019. A chamber was connected to a LI-8100A soil CO_2 flux system (LI-COR Inc.) for CO_2 and Ultraportable Greenhouse Gas Analyzer (Los Gatos Research) for CH_4 concentration within chamber. The CO_2 and CH_4 flux (mmol C m^{-2} day^{-1} for CO_2 and μmol C m^{-2} day^{-1} for CH_4) (positive value indicates CO_2 and CH_4 being released from ice surface to air) was calculated based on the changes of the CO_2 and CH_4 concentrations within the headspace of the chamber (Figure 15b). This chamber deployment was also examined over the snow and after removing snow at site C2 at same time period (12:00 LT to 16:00 LT) at 26 and 27 February, respectively. These measurements were training and test for MOSAiC.

For CO_2 flux, the mean (and standard deviation) values within the pool were –0.9±0.9 mmol C m^{-2} day^{-1} (n=12) and the magnitude of negative flux was higher than those measured over the snow (–0.6±0.3 mmol C m^{-2} day^{-1}) (n=7) and the sea ice after removing snow (–0.8±0.3 mmol C m^{-2} day^{-1}) (n=11) at site C2. For CH_4 flux, the mean (and standard deviation) values within the pool were +34.9±9.4 μmol C m^{-2} day^{-1} (n=12) and magnitude of positive flux was higher than those measured over the snow +0.1±0.9 μmol C m^{-2} day^{-1}) (n=7) and the sea ice after removing snow (+0.7±1.7 μmol C m^{-2} day^{-1}) (n=11) at site C2. These results suggested that the ice-free surface acts as sink for CO_2 and source for CH_4 because CO_2 and CH_4 concentration would be low and high with respect to that in the atmosphere, respectively (DIC/TA for CO_2 and CH_4 concentration measurement were under process and analysis). The results obtained during this campaign will become comparison data with respect to the data that will be obtained during MOSAiC.

Acknowledgments

We would like to express heartfelt thanks to Saroma Research Center of Aquaculture and Napal Kitami for their support in conducting the field work. This work was supported by the Japan Society for the Promotion of Science (17H04715, 17K00534, 18H03745, 18KK0292, and 18F18794), the Grant for Joint Research Program of the Institute of Low Temperature Science, Hokkaido University, the Grant for Arctic Challenge for Sustainability, and the Grant for the Global Environmental Research Coordination System from Ministry of the Environment of Japan in FY2017, and the EU FP7 BISICLO project. This paper is a contribution to the SCOR Working Group 152–Measuring Essential Climate Variables in Sea Ice (ECV-Ice) and Biogeochemical Exchange Processes at Sea-Ice Interfaces (BEPSII).

References

Delille, B., Vancoppenolle, M., Geilfus, N.-X., Tilbrook, B., Lannuzel, D., Schoemann, V., Becquevort, S., Carnat, G., Delille, D., Lancelot, C., Chou, L., Dieckmann, G. S. and Tison, J.-L. (2014): Southern Ocean CO_2 sink: the contribution of the sea ice. *J. Geophys. Res. Oceans*, **119**, 6340–6355, doi: 10.1002/2014JC009941.

Fierz, C., Armstrong, R. L., Durand, Y., Etchevers, P., Greene, E., McClung, D. M., Nishimura, K., Satyawali, P. K. and Sokratov, S. A. (2009): The international classification for seasonal snow on the ground. Tech. Rep., 90 pp., IHP-VII Technical Documents in Hydrology No. 83, IACS Contribution No.1, UNESCO-IHP, Paris.

Kuchiki, K., Aoki, T., Niwano, M., Matoba, S., Kodama, Y., and Adachi, K. (2015): Elemental carbon, organic carbon, and dust concentrations in snow measured with thermal optical and gravimetric methods: Validations during the 2007–2013 winters at Sapporo, Japan. *J. Geophys. Res.*, **120**, doi: 10.1002/2014JD022144.

Liu, Y, Saitoh, S. I., Maekawa, K., Mochizuki, K. I., and Tian, Y. (2018): Impact of short-term climate effects and sea ice coverage variation on Japanese scallop aquaculture in Saroma Lake, Japan. *Aquacul. Res.*, **49**(5), 1752–1767, doi: 10.1111/are.13630.

Miller, L. A., Fripiat, F., Else, B. G. T., Bowman, J. S., Brown, K. A., Collins, R. E., Ewert, M., Fransson, A., Gosselin, M., Lannuzel, D., Meiners, K. M., Michel, C., Nishioka, J., Nomura, D., Papadimitriou, S., Russell, L. M., Sørensen, L. L., Thomas, D. N., Tison, J.-L., van Leeuwe, M. A., Vancoppenolle, M., Wolff, E. W. and Zhou, J. (2015): Methods for Biogeochemical Studies of Sea Ice: The State of the Art, Caveats, and Recommendation. *Elementa-Science of the Anthropocene*, **3**, 000038, doi:10.12952/journal.elementa.000038.

Mundy, C. J., Ehn, J. K., Barber, D. G. and Michel, C. (2007): Influence of snow cover and algae on the spectral dependence of transmitted irradiance through Arctic landfast first-year sea ice. *J. Geophys. Res.*, **112**, C03007, doi:10.1029/2006JC003683.

Nomura, D., Takatsuka, T., Ishikawa, M., Kawamura, T., Shirasawa, K., Yoshikawa-Inoue, H. (2009): Transport of chemical components in sea ice and under-ice water during melting in the seasonally ice-covered Saroma-ko Lagoon, Hokkaido, Japan. *Estu., Coast. Shelf Sci.*, **81**, 201–209, doi: 10.1016/j.ecss.2008.10.012.

Nomura, D., Yoshikawa-Inoue, H., Toyota, T. and Shirasawa, K. (2010): Effects of snow, snow melting and refreezing processes on air–sea-ice CO_2 flux. *J. Glaciol.*, **56**(196), 262–270, doi:10.3189/002214310791968548.

Nomura, D., McMinn, A., Hattori, H., Aoki, S. and Fukuchi, M. (2011): Incorporation of nitrogen compounds into sea ice from atmospheric deposition. *Mar. Chem.*, **127**, 90–99, doi: 10.1016/j.marchem.2011.08.002.

Perovich, D. K. and Grenfell, T. C. (1981): Laboratory studies of the optical properties of young sea ice. *J. Glaciol.*, **27**, 331–346, doi: 10.3189/S0022143000015410.

Roukaerts, A., Nomura, D., Deman, F., Hattori, H., Dehairs, F. and Fripiat, F. (2019): The effect of melting treatments on the assessment of biomass and nutrients in sea ice (Saroma-ko lagoon, Hokkaido, Japan). *Polar Biol.*, **42**, 347–356, doi: 10.1007/s00300-018-2426-y.

Shirasawa, K. and Leppäranta, M. (2003): Hydrometeorological and sea ice conditions at Saroma-ko lagoon, Hokkaido, Japan. In: Report Series in Geophysics. University of Helsinki, Finland No. 46, 161–168.

Shirasawa, K., Leppäranta, M., Saloranta, T., Kawamura, T., Polomoshnov, A., Surkov, G (2005): The thickness of coastal fast ice in the Sea of Okhotsk. *Cold Reg. Sci. Technol.,* **42**, 25–40, doi: 10.1016/j.coldregions.2004.11.003.

Tanikawa, T., Hori, M., Aoki, T., Hachikubo, A., Kuchiki, K., Niwano, M., Matoba, S., Yamaguchi, S. and Stamnes, K. (2014): In situ measurements of polarization properties of snow surface under the Brewster geometry in Hokkaido, Japan, and northwest Greenland ice sheet. *J. Geophys. Res. Atmos.*, **119,** 13,946–13,964, doi:10.1002/2014JD022325.

Vancoppenolle, M., Meiners, K. M., Michel, C., Bopp, L., Brabant, F., Carnat, G., Delille, B., Lannuzel, D., Madec, G., Moreau, S., Tison, J.-L. and van der Merwe, P. (2013): Role of sea ice in global biogeochemical cycles: emerging views and challenges, *Quaternary Sci. Rev.*, **79**, 207–230, doi: 10.1016/j.quascirev.2013.04.011.

Wongpan, P., Meiners, K. M., Langhorne, P. J., Heil, P., Smith, I. J., Leonard, G. H., Massom, R. A., Clementson, L. A. and Haskell T. G. (2018): Estimation of Antarctic land-fast sea ice algal biomass and snow thickness from under-ice radiance spectra in two contrasting areas. *J. Geophys. Res.-Oceans*, **123**, 1907–1923. doi:10.1002/2017JC013711.

Figure caption

Figure 1 (double column size).
Location map of the Sea of Okhotsk (a), Saroma-ko Lagoon (b), study site within the lagoon (c), and sea ice site coordination during SLOPE2019 (d).

Figure 2 (single column size).
Time series of air temperature (a) and wind speed (b) at Saroma-ko Lagoon (red) and the weather station in Tokoro (blue) (Figure 1c).

Figure 3 (single column size).
Photograph of MR-40 (a), CNR4 (b), FieldSpec FR (c), under-ice irradiance sensor measuring the light transmits through snow, sea ice, and is absorbed by sea ice algae (d). The irradiance sensor was installed through the borehole (e), and the above-ice sensor and under-ice while the temperature of the drilled core was measured in concert (f). Photograph of STS-VIS (g) and STS-VIS in the water (h).

Figure 4 (double column size).
Vertical profile of temperature (a), salinity (b), brine volume fraction (c), carbonate chemical parameters such as dissolved inorganic carbon (DIC) (d) and total alkalinity (TA) (e), and chl. *a* concentrations (f) within sea ice and snow at site C2 at 23, 25, and 27 February 2019. The picture in f shows the bottom ice section of the ice core at site C2. The vertical thin-section photographs of the sea ice core at site C2 at 25 February 2019 (g).

Figure 5 (single column size).
Photographic image of ice algae community assemblage for bottom ice section of the ice core from site C2. Cell counting for ice algae community assemblage was examined with a microscope (IMT-2, Olympus) 10× oculars and 40× objective.

Figure 6 (single column size).
Vertical profiles of snow parameters obtained from snow pit work at 24 February 2019 at site T1. The ds and hi are snow depth and sea ice thickness, respectively. The characters used to indicate snow form are in accordance with the snow classification scheme of Fierz *et al*. (2009). For snow grain size, statistics of minimum, maximum and medium (number within brackets) are indicated. Two dimensions of grain size were defined: one half the length of the major axis of dendrites or cluster of aggregated grains (r_1) and one-half the branch width of dendrites, which is half of the width of the narrower part of broken crystals or the radius of each spherical particle (r_2). Snow impurities has three values, OC, EC, and dust, respectively.

Figure 7 (single column size).
Time series of downwelling planar irradiance from different instruments (MR-40 and CNR4 above the ice surface and STS-VIS under the ice surface at about 5 m depth) (a). Time series of surface albedo diagnosed from MR-40 and CNR4 (b).

Figure 8 (single column size).
Spectral albedos for snow covered- and -free sea ice, respectively. θ_0 is solar zenith angle.

Figure 9 (double column size).
Inter-comparison of transmitted irradiance measurements from STS-VIS (grey) and TriOS RAMSES (black) sensors. Note that $z_{Ice\text{-}T}$ and z_{Ramses} are sensor positions and were measured from the air–ice interface.

Figure 10 (single column size).
Spectral transmittance measured by TriOS RAMSES ACC UV/VIS during SLOPE2019.

Figure 11 (single column size).
Schematic view of upper-water thermodynamic experiment (a) and an aerial photograph of the site (b). The photo was taken by an air drone.

Figure 12 (single column size).
Mean vertical profiles of the entire CTD observations for temperature (a) salinity (b) density anomaly σ_T (c), and chl. *a* concentration. A blue solid line in (a) shows the freezing point, determined from the mean salinity profile in (b).

Figure 13 (single column size).
Vertical turbulent heat flux measured by the eddy-covariance system (a). Temperature variation in the upper 2 m, recorded by the thermistor chain (b). Horizontal current velocity at depths of 3, 5, and 7 m (c). The length and direction of arrow indicate current speed and direction. The horizontal axis represents the local time. In panel (a), the upward heat flux is shown by positive sign, and the downward is vice versa.

Figure 14 (single column size).
Photographs of pool experiments for the whole site to examine the effects of snow on the sea ice structure at the early growth stage (a), where a white circle denotes a monitoring camera, and ice sampling (b).

Figure 15 (single column size).
Photograph of the CO_2 and CH_4 flux chamber system at an artificial pool site to compare the gas exchange process over the sea ice (a). Example of the temporal variation in CH_4 concentration in the chambers installed over the snow at 13:53 LT 27 February 2019 (b).

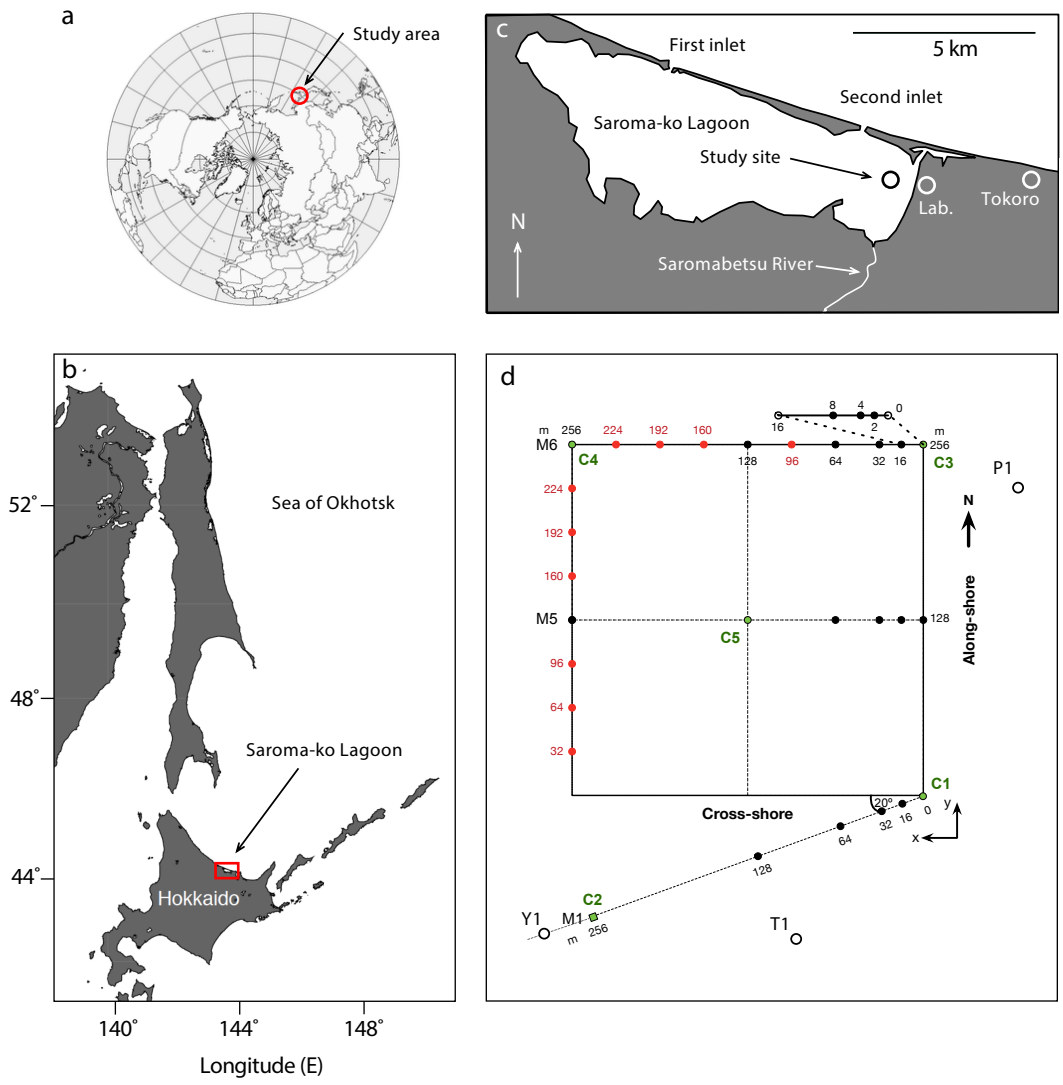

Figure 1

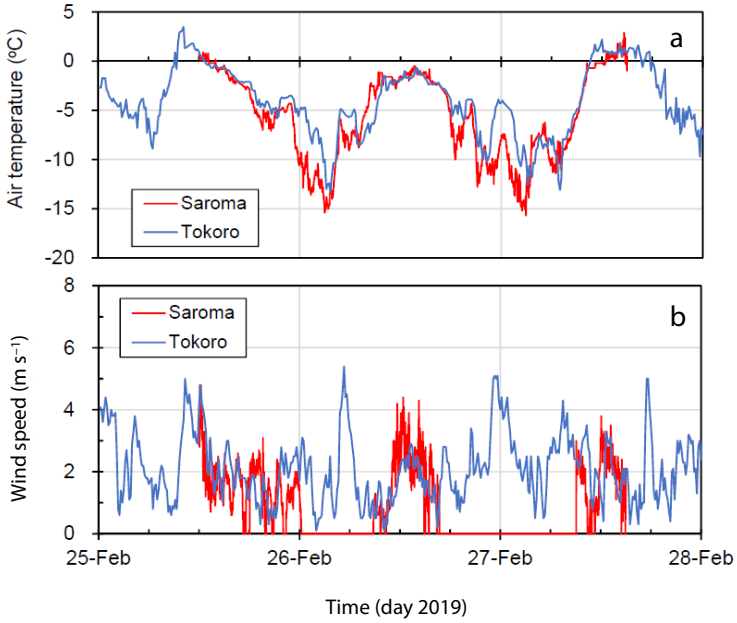

Figure 2

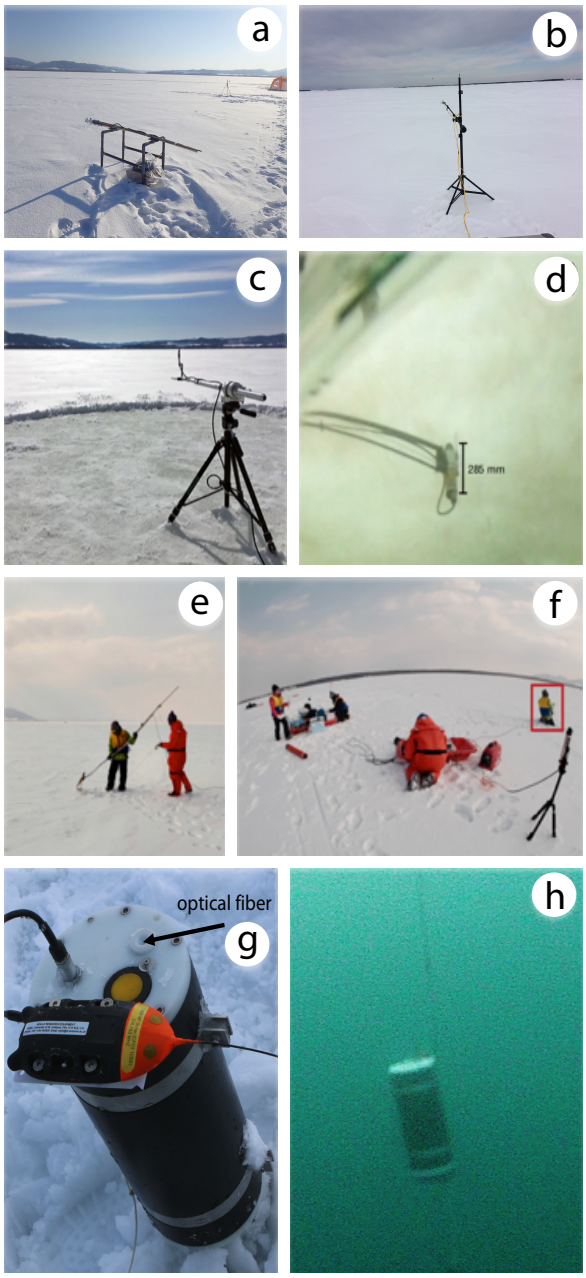

Figure 3

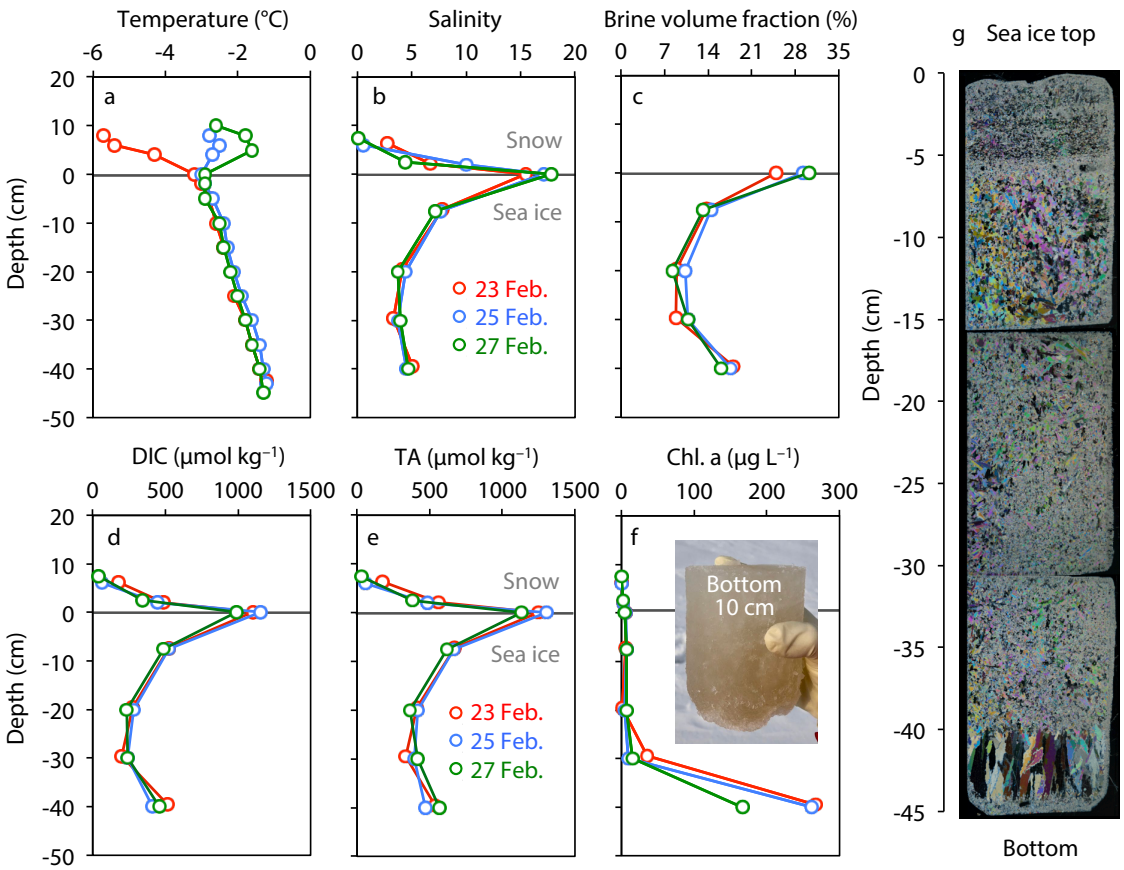

Figure 4

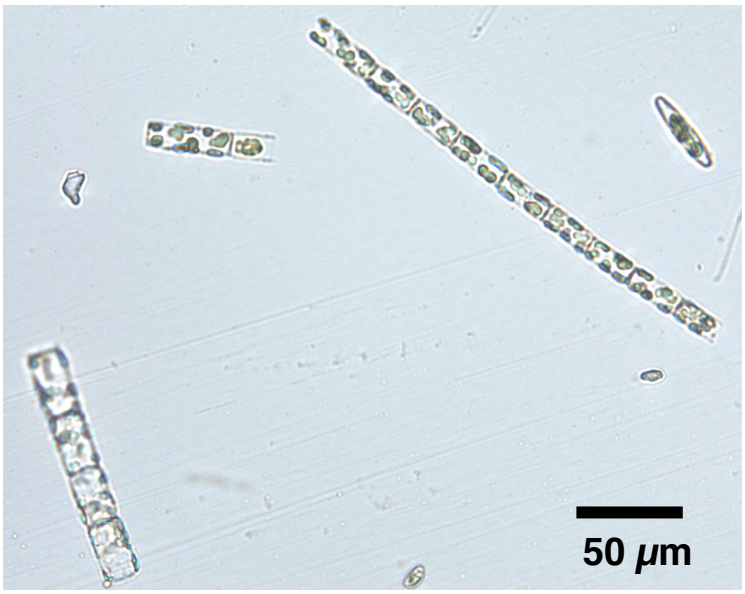

Figure 5

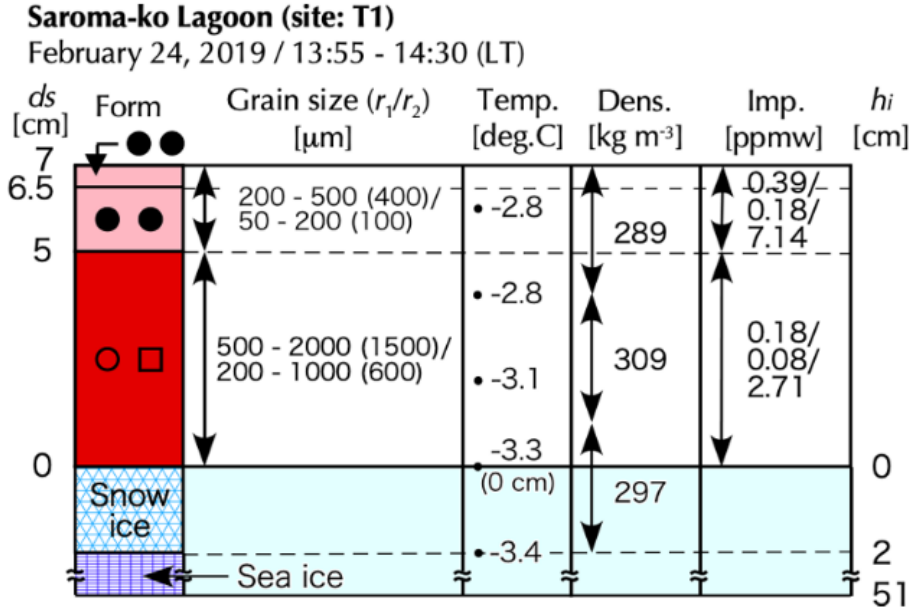

Figure 6

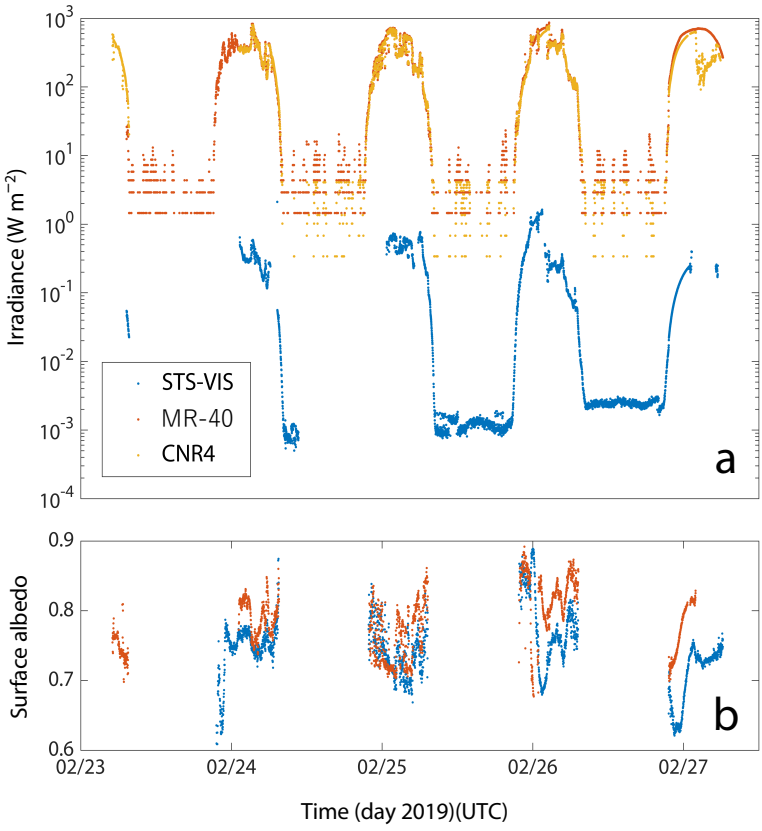

Figure 7

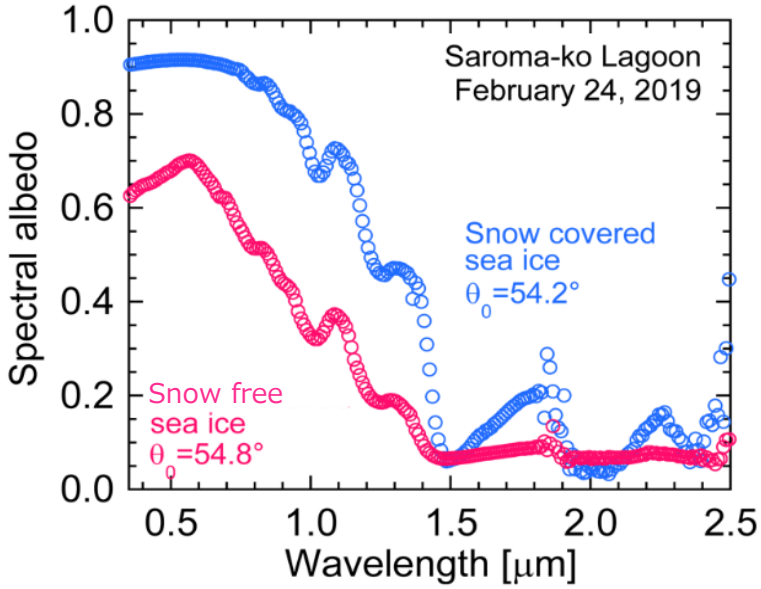

Figure 8

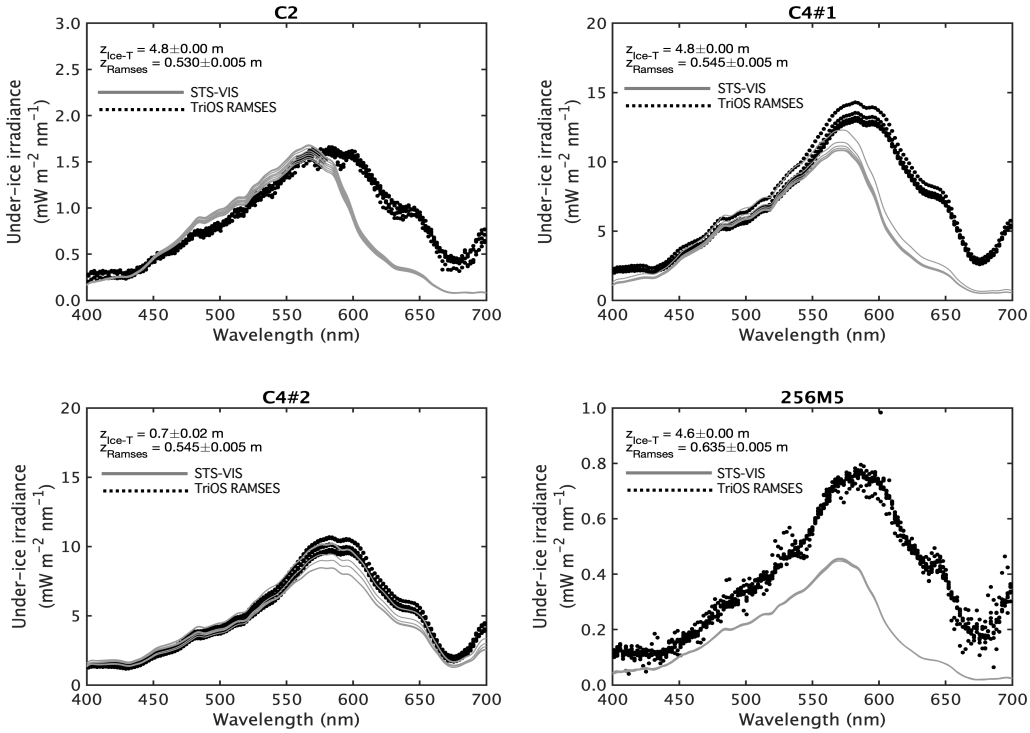

Figure 9

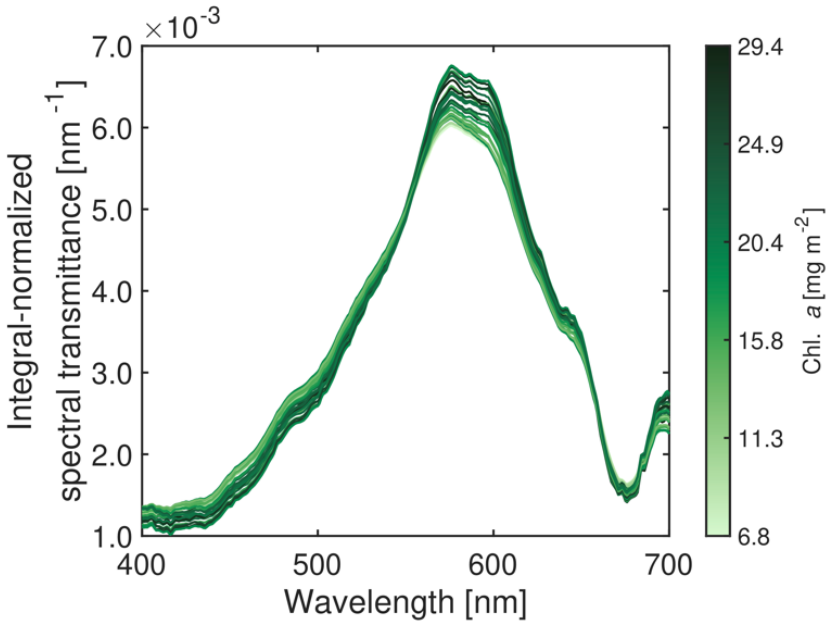

Figure 10

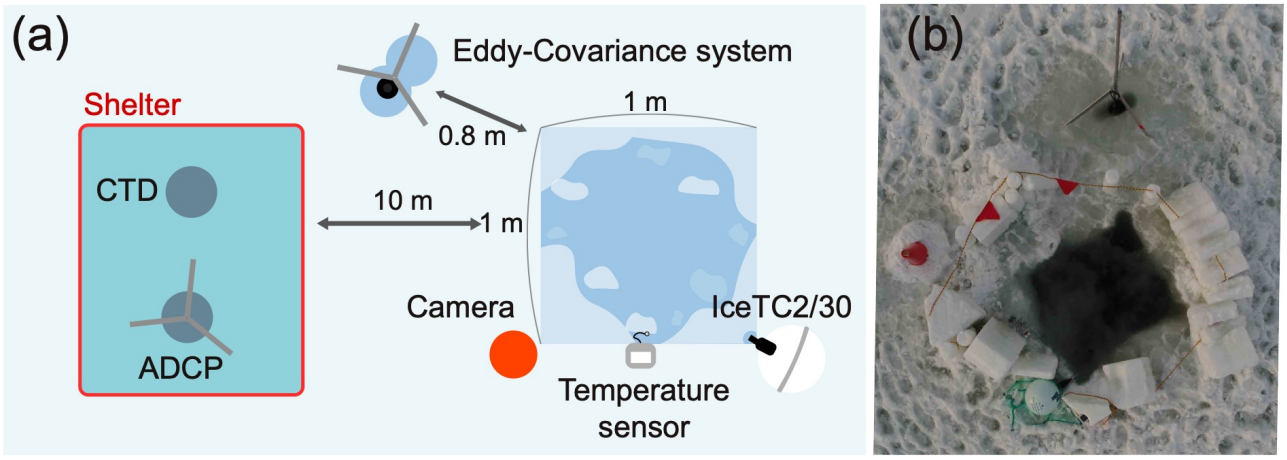

Figure 11

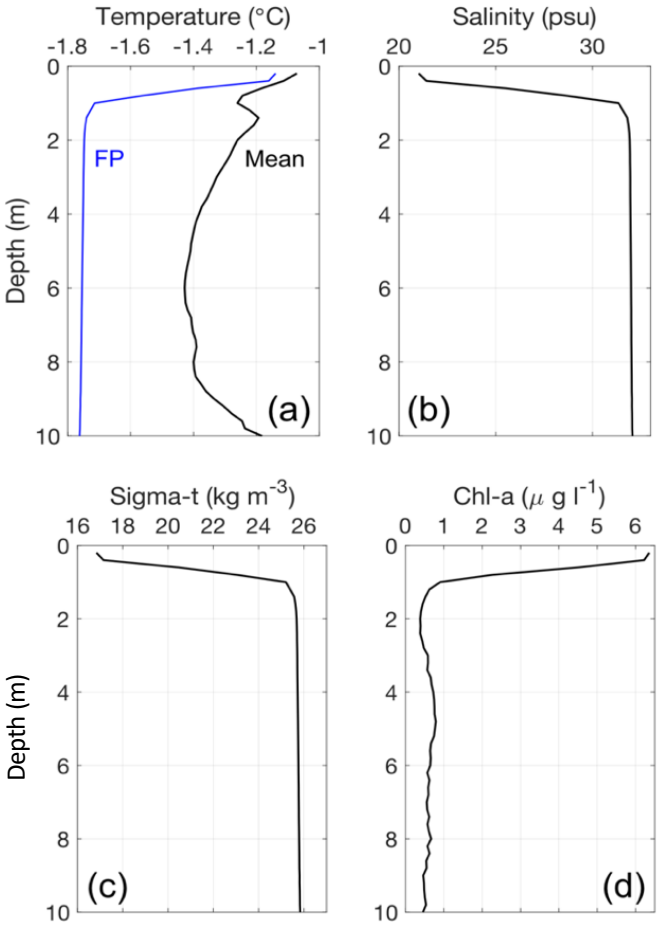

Figure 12

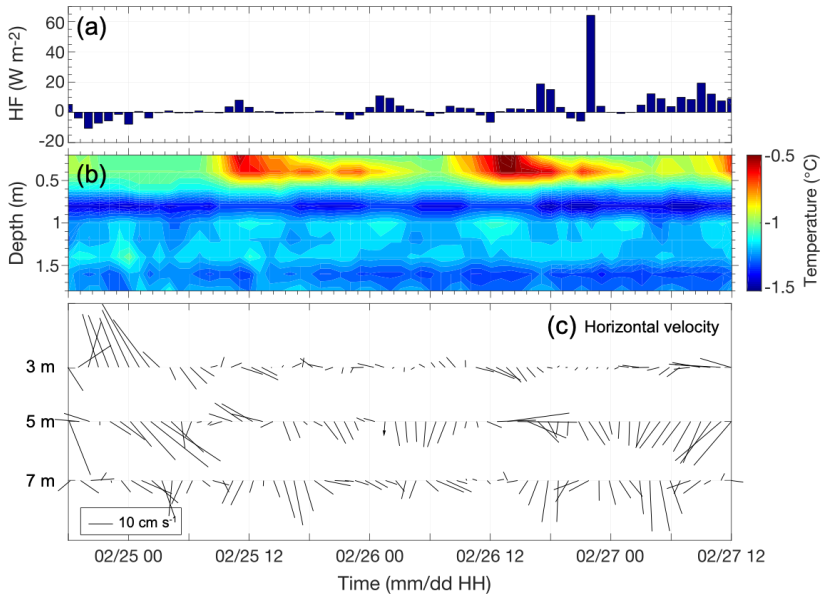

Figure 13

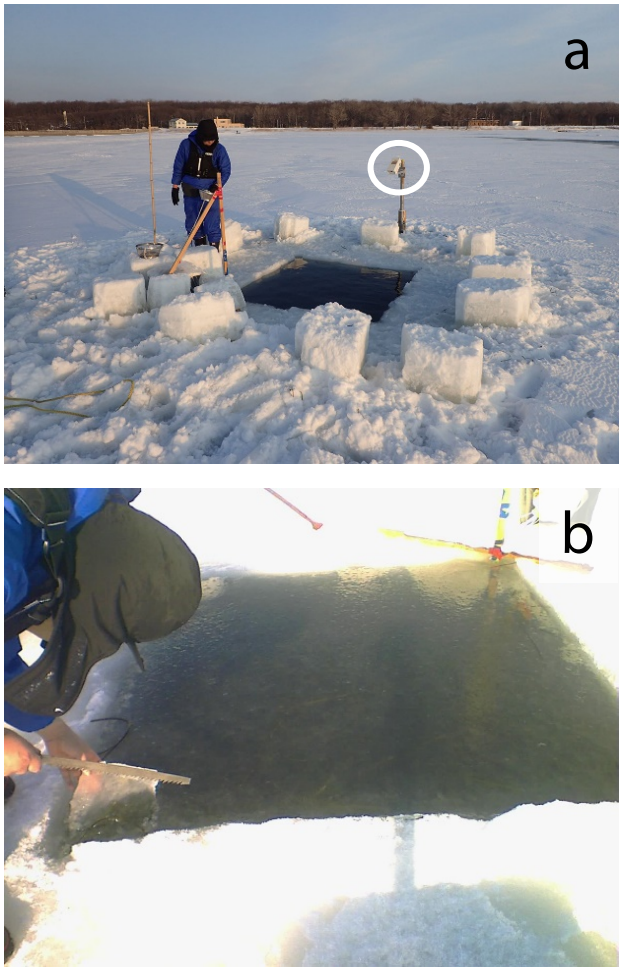

Figure 14

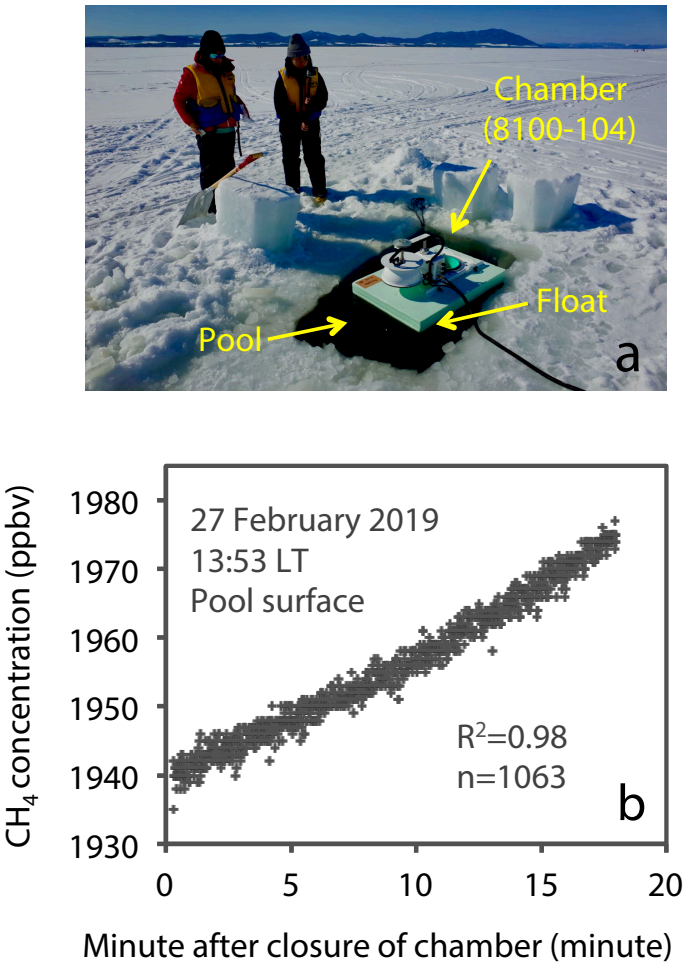
Chamber
(8100-104)
Float
Pool
a
27 February 2019
13:53 LT
Pool surface
R2=0.98
n=1063
b
CH4 concentration (ppbv)
1980
1970
1960
1950
1940
1930
0
5
10
15
20
Minute after closure of chamber (minute)

Figure 15

Lebrun Marion – Thèse de doctorat – 2016-2019

De l'interaction entre banquise, lumière et phytoplancton arctique

Résumé :
Nos connaissances sur les mécanismes gouvernant la croissance du phytoplancton dans les régions englacées arctiques présentent de nombreuses lacunes. Une des sources majeures d'incertitudes est liée aux interactions entre banquise, lumière et phytoplancton arctique.
L'objectif de cette thèse est de mieux comprendre ces interactions, de révéler les sources principales d'incertitude dans les modèles du système Terre pour pouvoir, à l'avenir, mieux contraindre les modèles quant à ces interactions.
Dans cette thèse j'étudie d'abord les mécanismes d'évolution de la saisonnalité de la banquise arctique, principalement en lien avec le forçage solaire. J'étudie ensuite l'impact de la banquise sur le rayonnement transmis à la surface de l'océan et enfin comment la lumière transmise à la surface des eaux englacées arctiques interagit avec le phytoplancton.
Je montre d'abord que la période d'eau libre arctique est majoritairement contrôlée par le cycle solaire et par les échanges thermodynamiques entre océan et atmosphère durant l'été. Selon les projections climatiques, elle devrait augmenter et se décaler vers l'automne.
J'évalue ensuite le schéma de transfert radiatif du modèle d'océan, NEMO, dans la zone de banquise arctique à partir d'une analyse de donnée in situ. Je montre que le rayonnement transmis sous la banquise est aujourd'hui fortement sous-estimé, en raison notamment d'une surestimation de l'atténuation par la neige et par les premiers centimètres de l'océan couvert de banquise.
Je définis, enfin, un diagnostic pour décrire le cycle saisonnier de la lumière disponible dans la zone de glace, et j'étudie son impact sur le phytoplancton simulé par le modèle biogéochimique, PISCES. Il reste néanmoins, de larges incertitudes pour comprendre la relation entre ce diagnostic et la croissance du phytoplancton, notamment en raison de la non-linéarité entre lumière disponible et croissance du phytoplancton ainsi que des incertitudes liées à la physiologie du phytoplancton arctique.

Mots clés : Océan Arctique, glace de mer, biogéochimie marine, modèles du système Terre, transfert radiatif, thermodynamique

About interaction between Arctic sea ice, light and phytoplankton

Abstract:
Large weaknesses remain considering our understanding of the drivers of phytoplankton growth in Arctic sea ice zone, especially due to large uncertainties in the interactions between sea ice, light and phytoplankton.
The aim of this PhD thesis is to better understand these interactions and to highlight the main uncertainties considering these interactions in Earth System Models to better constrain them.
I study the impact of solar shortwave radiation on the Arctic sea ice seasonal cycle, the impact of sea ice on transmitted light field to the upper ocean and finally, the influence of available light on the phytoplankton in Arctic sea ice zone.
I first show that the ice-free period is mainly led by the solar irradiance cycle and by the ocean-atmosphere thermodynamic exchanges during summer. It is consequently projected to extend into fall in the future.
Then, I evaluate the radiative transfer scheme in the ocean model NEMO, in arctic sea ice zone, based on an in-situ data analysis. I show that NEMO largely underestimates the transmitted shortwave radiation in ice-covered waters, especially due to the overestimation of the snow and the first level of the ocean attenuation.
I finally define a diagnostic to describe available light seasonality in the sea ice zone and I study the impact of this diagnostic on simulated phytoplankton in the bio-geochemistry model PISCES. However, large uncertainties remain in the study of the relation between this diagnostic and the phytoplankton growth. This is especially due to the non-linearity between available light and phytoplankton growth and also due to the lake of knowledge about the phytoplankton physiology.

Key words: Arctic Ocean, sea ice, marine bio-geochemistry, Earth System Model, radiative transfer, thermodynamic